Giagkoulovits, Christos (2018) *A fully integrated CMOS microelectrode system for electrochemistry.* PhD thesis.

https://theses.gla.ac.uk/39018/

Copyright and moral rights for this work are retained by the author

A copy can be downloaded for personal non-commercial research or study, without prior permission or charge

This work cannot be reproduced or quoted extensively from without first obtaining permission in writing from the author

The content must not be changed in any way or sold commercially in any format or medium without the formal permission of the author

When referring to this work, full bibliographic details including the author, title, awarding institution and date of the thesis must be given

Enlighten: Theses
https://theses.gla.ac.uk/
research-enlighten@glasgow.ac.uk

University of Glasgow

A Fully Integrated CMOS Microelectrode System for Electrochemistry

Christos Giagkoulovits

A Thesis submitted to

School of Engineering

University of Glasgow

in fulfilment of the requirements for the degree of

Doctor of Philosophy

December 2018

Abstract

Electroanalysis has proven to be one of the most widely used technologies for point-of-care devices. Owing to the direct recording of the intrinsic properties of biochemical functions, the field has been involved in the study of biology since electrochemistry's conception in the 1800's. With the advent of microelectronics, humanity has welcomed self-monitoring portable devices such as the glucose sensor in its everyday routine. The sensitivity of amperometry/ voltammetry has been enhanced by the use of microelectrodes. Their arrangement into microelectrode arrays (MEAs) took a step forward into sensing biomarkers, DNA and pathogens on a multitude of sites. Integrating these devices and their operating circuits on CMOS monolithically miniaturised these systems even more, improved the noise response and achieved parallel data collection. Including microfluidics on this type of devices has led to the birth of the Lab-on-a-Chip technology. Despite the technology's inclusion in many bioanalytical instruments there is still room for enhancing its capabilities and application possibilities. Even though research has been conducted on the selective preparation of microelectrodes with different materials in a CMOS MEA to sense several biomarkers, limited effort has been demonstrated on improving the parallel electroanalytical capabilities of these devices. Living and chemical materials have a tendency to alter their composition over time. Therefore analysing a biochemical sample using as many electroanalytical methods as possible simultaneously could offer a more complete diagnostic snapshot.

This thesis describes the development of a CMOS Lab-on-a-Chip device comprised of many electrochemical cells, capable of performing simultaneous amperometric/voltammetric measurements in the same fluidic chamber. The chip is named an electrochemical cell microarray (ECM) and it contains a MEA controlled by independent integrated potentiostats. The key stages in this work were: to investigate techniques for the electrochemical cell isolation through simulations; to design and implement a CMOS ECM ASIC; to prepare the CMOS chip for use in an electrochemical environment and encapsulate it to work with liquids; to test and characterise the CMOS chip housed in an experimental system; and to make parallel measurements by applying different simultaneous electroanalytical methods. It is envisaged that results from the system could be

combined with multivariate analysis to describe a molecular profile rather than only concentration levels.

Simulations to determine the microelectrode structure and the potentiostat design, capable of constructing isolated electrochemical cells, were made using the Cadence CAD software package. The electrochemical environment and the microelectrode structure were modelled using a netlist of resistors and capacitors. The netlist was introduced in Cadence and it was simulated with potentiostat designs to produce 3-D potential distribution and electric field intensity maps of the chemical volume. The combination of a coaxial microelectrode structure and a fully differential potentiostat was found to result in independent electrochemical cells isolated from each other.

A 4 x 4 integrated ECM controlled by on-chip fully differential potentiostats and made up by a 16 × 16 working electrode MEA (laid out with the coaxial structure) was designed in an unmodified 0.35 µm CMOS process. The working electrodes were connected to a circuit capable of multiplexing them along a voltammetric measurement, maintaining their diffusion layers during stand-by time. Two readout methods were integrated, a simple resistor for an analogue readout and a discrete time digital current-to-frequency charge-sensitive amplifier. Working electrodes were designed with a 20 µm side length while the counter and reference electrodes had an 11 µm width. The microelectrodes were designed using the aluminium top metal layer of the CMOS process.

The chips were received from the foundry unmodified and passivated, thus they were post-process fabricated with photolithographic processes. The passivation layer had to be thinned over the MEA and completely removed on top of the microelectrodes. The openings were made 25 % smaller than the top metal layer electrode size to ensure a full coverage of the easily corroded Al metal. Two batches of chips were prepared, one with biocompatible Au on all the microelectrodes and one altered with Pd on the counter and Ag on the reference electrode. The chips were packaged on ceramic pin grid array packages and encapsulated using chemically resistant materials. Electroplating was verified to deposit Au with increased roughness on the microelectrodes and a cleaning step was performed prior to electrochemical experiments.

An experimental setup containing a PCB, a PXIe system by National Instruments, and software programs coded for use with the ECM was prepared. The programs were prepared to conduct various voltammetric and amperometric methods as well as to analyse the results. The first batch of post-processed encapsulated chips was used for characterisation and experimental measurements. The on-chip potentiostat was verified to perform alike a commercial potentiostat, tested with microelectrode samples prepared to mimic the coaxial structure of the ECM. The on-chip potentiostat's fully differential design achieved a high 5.2 V potential window range for a CMOS device. An experiment was also devised and a 12.3 % cell-to-cell electrochemical cross-talk was found. The system was characterised with a 150 kHz bandwidth enabling fast-scan cyclic voltammetry(CV) experiments to be performed. A relatively high 1.39 nA limit-of-detection was recorded compared to other CMOS MEAs, which is however adequate for possible applications of the ECM. Due to lack of a current polarity output the digital current readout was only eligible for amperometric measurements, thus the analogue readout was used for the rest of the measurements.

The capability of the ECM system to perform independent parallel electroanalytical measurements was demonstrated with 3 different experimental techniques. The first one was a new voltammetric technique made possible by the ECM's unique characteristics. The technique was named multiplexed cyclic voltammetry and it increased the acquisition speed of a voltammogram by a parallel potential scan on all the electrochemical cells. The second technique measured a chemical solution with 5 mM of ferrocene with constant potential amperometry, staircase cyclic voltammetry, normal pulse voltammetry, and differential pulse voltammetry simultaneously on different electrochemical cells. Lastly, a chemical solution with 2 analytes (ferrocene and decamethylferrocene) was prepared and they were sensed separately with constant potential amperometry and staircase cyclic voltammetry on different cells. The potential settings of each electrochemical cell were adjusted to detect its respective analyte.

Author's Declaration

Unless otherwise acknowledged, the content of this Thesis is the result of my own work. None of this material has been submitted for any other degree at the University of Glasgow or any other institution.

Christos Giagkoulovits

Acknowledgements

This thesis would not have been possible without the support, encouragement and guidance from many people in my life. My gratitude cannot be expressed in these few lines of text but it is a good start.

First and foremost, I would like to thank my supervisor, Professor David Cumming for the opportunity he gave me to work all the way through a full and truly rewarding project. His support and patience in all matters I had to face during the past 4 years of my PhD has been unprecedented. He has given me the inspiration and guided me through a unique creative process. I am also particularly grateful to my dear office friend and unofficial second supervisor Dr. Mohammed A. Al-Rawhani for sharing his experience on integrated circuit design with me and the countless hours he has kindly devoted to my academic development. His support has not only been technical but also moral and I feel lucky I encountered such a positive person during my research work. I would also like to thank my flatmate Dr. Boon Chong Cheah for his patience and his helpful contribution to develop fabrication processes in the cleanroom. He has also aided me in my understanding of biochemistry as well as given me valuable life lessons.

I would like to extend my thanks to all members of the Microsystems Technology Group. In particular, Dr. James Grant for his technical help and cleanroom insights he offered me for the design and fabrication of my device. His response has always been extremely prompt and scientifically complete. I am indebted to Dr. Christopher Martin for training me in the cleanroom and teaching me how to make smart moves in the research environment. Thanks to Dr. James Beeley and Dr. Luiz Gouveia for introducing me to the design of systems with mixed components. Many thanks should also go to Claudio Accarino for helping me plan characterisation strategies. I would also like to thank Kirsty Rew for supporting me through dark times.

Special thanks should go to a group of friends. Thanks to my good friends Georgios Drosos Skotis and Charalambos Klitis for their good company during work and beer hours as well as the support they showed me through our common

journeys. I would also like to thank Francesco Mirando for his cheerful chats and for letting me use his Raman equipment.

I am also grateful to every single member of the James Watt Nanofabrication Centre, without them my work would not have progressed. I would like to extend my thanks to people inside and outside the academic community for their contribution. Thanks to Dr. Corrie Farmer of the Kelvin Nanotechnology Ltd for his input on lift-off processes. Thanks to Professor Leroy Cronin and Dr. Christophe Busche for lending me their equipment and some early discussions on electrochemistry.

I wish to express my appreciation to the Engineering and Physical Sciences Research Council (EPSRC) for the financial support of this project.

I would also like to thank all of my friends in Greece who have wished me well and believe in me. Especially George Lamprakis who has been calling me doctor before I even started my PhD.

Heartfelt thanks to my mentor and parental figure, Professor Konstantinos Psychalinos for helping me reach everything I have conquered so far.

Finally, my deepest gratitude to my parents Kostas and Eleni as well as my sister Sofia for their endless love and support throughout my whole life. Thanks for being the sturdiest rock one could wish to lay on and regain their power. I would have never achieved my goals without your help.

Publications

Journal Paper

1. C. Giagkoulovits, B. C. Cheah, M. A. Al-Rawhani, C. Accarino, C. Busche, J.P. Grant and D. R. S. Cumming, "A 16 × 16 CMOS amperometric microelectrode array for simultaneous electrochemical measurements," IEEE Trans. Circuits Syst. I Regul. Pap., 2018.

Conference Papers

1. C. Giagkoulovits, M. A. Al-Rawhani, B. C. Cheah, C. Martin, C. Busche, L. Cronin and D. R. S. Cumming, "Hybrid amperometric and potentiometric sensing based on a CMOS ISFET array," in 2017 IEEE SENSORS, 2017, pp. 1–3.

2. M. A. Al-Rawhani, B. C. Cheah, C. Giagkoulovits, A. Shakoor, B. Nagy, J. Beeley and D. R. S. Cumming, "Wide-range optical CMOS-based diagnostics," in 2017 IEEE International Symposium on Circuits and Systems (ISCAS), 2017, pp. 1–4.

Competitions

1. C. Giagkoulovits, "Chemical camera chip", Three minute thesis competition, 2015. [Online]. Available: https://youtu.be/fmLTMafkxZY. [Accessed: 29-Jan-2018].

Oral Presentations

1. C. Giagkoulovits, "Fabrication on CMOS redox microarray", James Watt Nanofabrication Centre (JWNC) user meeting, 2015.

Poster Presentations

1. C. Giagkoulovits and D. R. S. Cumming, "A 16 x 16 CMOS Multimodal Redox Microelectrode Array", Multicorder IAB Meeting, 2017.

2. C. Giagkoulovits and D. R. S. Cumming, “A 16 x 16-pixel CMOS Redox Microarray Imager”, Multicorder IAB Meeting, 2016.

3. C. Giagkoulovits and D. R. S. Cumming, “A 16 x 16-pixel CMOS Microelectrode Redox Camera Array”, Multicorder IAB Meeting, 2015.

Table of Contents

List of Figures

List of Tables

List of Acronyms

1-D	1 dimensional
2-D	2 dimensional
3-D	3 dimensional
ADC	analogue-to-digital converter
ADE	analogue design environment
AFM	atomic force microscopy
ALS	alternating least squares
ANN	artificial neural network
ASCII	american standard code for information interchange
ASIC	application specific integrated circuit
BEM	boundary element method
CAD	computer-aided design
CDS	correlated double sampling
CE	counter electrode
CMFB	common-mode feedback loop
CMOS	complementary metal oxide semiconductor
CMRR	common-mode rejection ratio
CPGA	ceramic pin grid array
CPU	central processing unit
CSA	charge-sensitive amplifier
CV	cyclic voltammetry

DAC	digital-to-analogue converter
DmFc	decamethylferrocene
DNA	deoxyribonucleic acid
DPASV	differential pulse anodic stripping voltammetry
DPV	differential pulse voltammetry
DRC	design rule checker
e-beam	electron beam
ECM	electrochemical cell microarray
EDL	electrical double layer
E-field	electric field
ESD	electrostatic discharge
Fc^0	ferrocene
FDM	finite difference method
FEM	finite element method
FOM	figure of merit
FSCV	fast-scan cyclic voltammetry
FVM	finite volume method
GOx	glucose oxidase
GUI	graphical user interface
HDL	hardware description language
HMDS	bis(trimethylsilyl)amine
HRP	horseradish peroxidase

i to *F*	current to frequency
I/O	input-output
IA	instrumentation amplifier
IC	integrated circuit
ICP/CVD	inductively coupled plasma chemical vapour deposition
IHP	inner Helmholtz plane
ISE	ion-selective interface
ISFET	ion-selective field effect transistor
JWNC	James Watt nanofabrication centre
Labview	laboratory virtual instrument engineering workbench
LAPV	large amplitude scan voltammetry
LCECA	liquid chromatography electrochemistry array
LOD	limit of detection
LSV	linear sweep voltammetry
LVS	layout versus schematic
MEA	microelectrode array
MIM	metal-insulator-metal
MOSFET	metal oxide semiconductor field effect transistor
NADH	dihydronicotiamide adenine dinucleotide
NHE	normal hydrogen electrode
NI	National Instruments

nMOS	negative-channel metal oxide semiconductor
NMP	N-Methyl-2-pyrrolidone
NPP	normal pulse polarography
NPV	normal pulse voltammetry
OHP	outer Helmholtz plane
OTA	operational transconductance amplifier
PCA	principal component analysis
PCB	printed circuit board
PCRe	principal component regression
PDMS	polydimethylsiloxane
PET-G	polyethylene terephthalate glycol-modified
PGA	pin grid array
PLS	partial least squares regression
PMMA	poly(methyl methacrylate)
pMOS	positive-channel metal oxide semiconductor
POC	Point-of-Care
polysilicon	polycrystalline silicon
RE	reference electrode
redox	reduction and oxidation
RNPP	reverse normal pulse polarography
RPV	reverse pulse voltammetry
RTL	register-transfer level
SAM	self-assembled monolayer

SAPV	small amplitude scan voltammetry
SCE	saturated calomel electrode
SECM	scanning electrochemical microscopy
SECPM	scanning electrochemical potential microscopy
SMBG	self-monitoring of blood glucose
SNR	signal-to-noise ratio
SWV	square wave voltammetry
$TBAPF_6$	tetrabutylammonium hexafluorophosphate
TCQN	tetracyanoquinodimethane
TMAH	tetramethylammonium hydroxide
TTF	tetrathiafulvalene
VLSI	very large scale integration
WE	working electrode

1 Introduction to the Research

1.1 Introduction

This chapter describes the motivations of the conducted research in terms of technology and applications. The general aim and key objectives are identified and lastly an outline of the thesis is provided.

1.2 Motivation

The fundamental element upon which electrochemistry is based upon is the electrochemical cell. After its first realisation by Allesandro Volta [1] in a voltaic pile (an early battery), a more thorough examination by Michael Faraday [2] set the basic principles for electrolysis by determining that for every chemical reaction there is a current associated that flows through electrodes in an electrochemical cell. Since those observations were made, a number of advancements have been made in the broad field of electrochemistry. Electrochemical cells which are divided into galvanic or electrolytic cells are being used in numerous applications in everyday life and for scientific purposes. In galvanic cells current is conducted when electrodes are connected at the expense of spontaneous chemical reactions, in electrolytic cells an external voltage is applied at which expenditure chemical reactions are imposed. One of the fields, where both electrochemical cell types have been used, is electroanalysis which studies the electrical behaviour of chemical systems to analyse their composition. Electroanalysis has been used as a tool to investigate chemical and biological processes through direct sensing of their ionic characteristics. Many important applications have been developed in the field such as portable devices for self-monitoring of blood glucose (SMBG) [3], genome sequencing [4], electronic noses [5], food safety tests [6] and many more.

The recent miniaturisation of the electrode sensing elements of an electrochemical cell into microelectrodes in the early 1970's has resulted in an enhancement in sensitivity towards smaller concentrations of biomarkers. Responsible for the sensitivity enhancement is their small size that changed the mass transfer rate as it became dependent on the electrode geometry, and also reduced undesirable impedance phenomena by the ion charges [7]. Their

arrangement into a microelectrode array (MEA) turned the sensitive transducers into arrayed devices with a microscale spatial resolution at a low manufacturing cost [8]. MEAs were the first electroanalytical devices to be miniaturised and they have been applied in the popular fields of amperometry (current sensing) such as biosensing of metabolites and microorganisms, immunosensing and DNA sensing [8] and potentiometry (potential sensing) such as brain-machine interfaces to monitor brain activity [9], [10], retinal implants [11] and others. The field of amperometry/voltammetry offers the MEA various methods to sense biochemical compounds of different characteristics. The amperometric MEAs' strength lies in the use of functionalisation layers on the microelectrodes for the detection of selective biomarkers. Having many sensing sites on a small platform it is only logical to make parallel measurements. However, the capabilities of substrates with insulated metal tracks for parallelised recording were limited and the circuit instrumentation was large and bulky.

The advent of the complementary metal oxide semiconductor (CMOS) technology that was initially used in the microprocessor industry [12], enabled the very-large-scale integration (VLSI) of circuits on a silicon substrate. CMOS is one of the most mature available technologies and a dominant pole for the demands of today's research. Advantages of the technology are high performance in terms of speed and accuracy, high signal-to-noise ratios (SNR), a reduced production cost relative to other chip technologies and low power consumption [13]. Integrating amperometric MEAs with circuits monolithically on CMOS not only miniaturised the systems into portable devices but it also improved the noise performance as the circuits were in close proximity to the microelectrodes and weaker signals could be detected. The CMOS MEA devices exhibited characteristics of parallel data collection and their function was easily controlled through a digital interface by the software [14]. Their integration with microfluidics led to Lab-on-a-Chip devices which are used as diagnostic tools in low sample volumes [15].

Nevertheless, the technology has not yet passed the threshold to make a platform capable of performing truly parallelised sensing not only with selective functionalisation of microelectrodes but also with many electroanalytical methods that perform independent measurements in parallel. Parallelisation is an important aspect in biochemical studies as a sample's composition changes

over the course of measurements, especially in amperometry/voltammetry which interacts with the analysed medium. Furthermore, studies with multivariate computational analysis have shown that when data from seemingly unrelated measurements are combined they can provide results otherwise undetectable or incomprehensible to the researcher [16]. A CMOS platform that can produce many independent results from a biochemical sample under analysis simultaneously would provide data to determine its composition more effectively.

In this study, a CMOS Lab-on-a-Chip device that integrates many individual electrochemical cells in the same fluidic chamber to perform concurrent independent amperometric/voltammetric measurements, named an electrochemical cell microarray (ECM), was developed. The core of the device was a CMOS ASIC that features a functionalisable MEA connected to an array of integrated independent potentiostats. The ASIC was designed in a 350 nm technology from ams AG [17]. It will be demonstrated that to develop effective autonomous electrochemical cells attention needs to be given to the design of both the electrode structure and the circuits. The system developed here can benefit many biochemical applications that require parallelisation of electroanalytical measurements. The employment of multiple electroanalytical methods and the detection of multiple analytes simultaneously were the focus of this work. The results that the system produces, even from one biomarker, can be used to deconvolute or clear measurements of a biochemical mixture through multivariate analysis and determine its composition. With automated functions and a portable housing setup the Lab-on-a-Chip ECM could be used as a powerful diagnostic point-of-care (POC) device.

1.3 Aims and Objectives

The main aim of this research is to implement a CMOS ECM with independent electrochemical cells that can perform multiple concurrent electroanalytical measurements in a single fluidic container. A list of the specific objectives is presented as follows:

- To simulate different electrode structures and potentiostat designs and find the best combination to be used as a wholly independent electrochemical cell in an array format.

- To design the circuits and the layout of an integrated ECM with the investigated electrodes and on-chip circuits and simulate its operation using an unmodified commercial CMOS process. The design of the readout circuits needs to be compatible with the potentiostat design. The finished design will be taped out to a foundry for fabrication.

- To modify the inherent CMOS chip aluminium metal layer with electrochemically inert, biocompatible and biofunctionalisable microelectrode materials. To package and encapsulate the chip in order to make it waterproof and prepare a chemically resistant microfluidic container for chemical and biological experiments.

- To prepare an experimental setup to house the encapsulated ASIC and software programs that can control and analyse the results of the system. The programs need to be able to drive the potentiostats individually with different electroanalytical methods and represent the results of each method in its appropriate format.

- To test and characterise the electrical and electrochemical behaviour of the ECM system. The electrochemical cross-talk between electrochemical cells is an important figure of merit to characterise the efficiency of the chip to make multiple simultaneous measurements independently.

- To perform electroanalytical measurements simultaneously on the multiple electrochemical cells of the ECM and demonstrate the device's capabilities to conduct independent analysis on the chemical sample media.

1.4 Thesis Outline

The remainder of this thesis is divided into 6 chapters and a brief description of each one of them is provided as follows:

Chapter 2 is a review of the literature relevant to the development of a CMOS electroanalytical Lab-on-a-Chip device with a MEA capable of performing multiple simultaneous electrochemical analysis.

Chapter 3 presents the theory for the operation of electrochemical cells in electroanalysis. An overview of electrochemical cells and the equations that govern their function is presented. An electrical equivalent model of the interface at electrodes is then described. Finally, electroanalytical methods and cross-talk in MEAs are reviewed.

Chapter 4 describes the approach to establish an independent operation of electrochemical cells on the same platform. An investigation of microelectrode structures and the potentiostat design through simulations with electrical models is presented. Based on the simulations the design of the ECM ASIC is described focusing on the potentiostat design, multiplexing of the microelectrodes and the readout system.

Chapter 5 provides details of the post-processing fabrication and encapsulation procedures that were followed to make the unprocessed CMOS chip ready for use in electrochemical and biological experiments. The production of test microelectrode samples as reference devices is also explained.

Chapter 6 describes the whole system's development and operation to advance the ASIC into a functional ECM that produces independent concurrent electroanalytical results. The system was characterised electrically and electrochemically, the cell-to-cell cross-talk was measured and the ECM was compared with CMOS MEAs found in the literature. Lastly, experiments that demonstrate the system's capability to perform amperometric/voltammetric measurement in parallel and for more than one electroactive compounds of interest are presented.

Chapter 7 summarises the conclusions of the research and provides some suggestions for future work.

1.5 Summary

The motivation of this work was provided by an explanation of where CMOS MEAs stand in the field of electrochemistry and a description on the room for improvement. This also included the identification of potential applications for the technology to be developed. Moreover, the aims and objectives were identified and an outline of the thesis was presented. The next chapter will be a review of the literature relevant to this study.

2 Literature Review

2.1 Introduction

The previous chapter described the motivation for this study along with the aim and objectives. This chapter focuses on a review of the literature relevant to the development of a CMOS Lab-on-a-Chip electrochemical cell microarray (ECM) capable of performing simultaneous electrochemical methods independently. A background of the field of electroanalysis and its use in biochemistry is first provided to showcase the available technologies for an ECM system. The chapter focuses on amperometry/voltammetry, the fields of application of miniaturised electrodes and the means to prepare them for biochemical sensing. The progress of MEAs into CMOS Lab-on-a-Chip devices towards Point-of-Care products with a focus on the integrated circuits is then discussed to identify components that assist to the making of an ECM. The chapter then moves on to review existing computational methods that could potentially combine complex results of an ECM to extract new data. Finally, an overview of simulation methods for electrochemical investigations is given to distinguish a suitable one for the development of independently controlled neighbouring subsets of electrodes.

2.2 Electrochemical Studies and Applications

One of the pioneers of electrochemistry, Michael Faraday commented "on Becquerel's process for extracting metals by voltaic means: "Who would not have been laughed at if he had said in 1800 that metals could be extracted from their ores by electricity or that portraits could be drawn by chemistry." (Aug. 20. 1847.)" [18]. After some early observations by Galvani [19], electrochemistry evolved rapidly as a field of study with the introduction of the electrochemical cell in the form of a battery by Allesandro Volta at the end of the 18th century [1]. Divisions of the field into the sectors of galvanic cells (i.e. the battery) and electrolytic cells (i.e. water splitting), and the work of Faraday and Humphry Davy established the use of terms such as the "electrode" and the "ion" [2].

Further studies helped push theoretical chemistry forward, even though electrochemistry's strength lies mostly in its new scientific discoveries and industrial applications. The range of applications varies from synthesis and

material treatment to energy management and analytical techniques. Electrosynthesis and its variations are used for the rapid production of organic and inorganic compounds, important in pharmaceuticals and other sectors. Electrowinning, electrorefining and electrodeposition as well as metal corrosion protection are used mainly to extract and manipulate metals. Energy conversion between the chemical and electrical phase using batteries and the recently revisited fuel cells has advantages such as portability and zero carbon emissions. Special attention has been recently drawn to the field of bioelectrochemistry with cochlear and retinal implants that stimulate nerves. One of the most successful bioelectrochemical branches is electroanalysis. The field of electroanalysis examines the composition of chemical or biological samples by their electrical response. It has been traditionally used in the industry for quality control with e.g. potentiometric titration that measures a sample's composition by checking its potential [20]. Emerging electroanalytical techniques such as scanning electrochemical microscopy (SECM), a scanning probe microscopy technique, and impedance spectroscopy [21], have also appeared.

2.2.1 Electroanalysis in Biochemistry

Living beings are advanced electrochemical machines, their functions can be analysed and controlled by electrochemistry. Electroanalysis and three of its sectors, namely: potentiometry, conductometry and amperometry/voltammetry have recently found application in the biochemical and medicinal disciplines, with many novel technologies emerging to reinvent medicine on a personal level. To analyse an electrochemical system, one studies processes such as the electrical charge transfer across an interface of different conducting phases such as a metal and ions in a liquid sample. Electroanalysis is not performed on single electrode-electrolyte interfaces but systems, called electrochemical cells. A simple electrochemical cell consists of two metals in a chemical phase [22]. From the electroanalytical methods shown in Figure 2.1, the marked sectors of potentiometry and voltammetry have been the most prominent due to their simple instrumentation setups. Miniaturised versions of the sensing elements from both sectors have recently been explored.

Potentiometry is a measure of the ionic concentration through the ions' accumulated charge. Charges are oriented on non-electrically-conductive

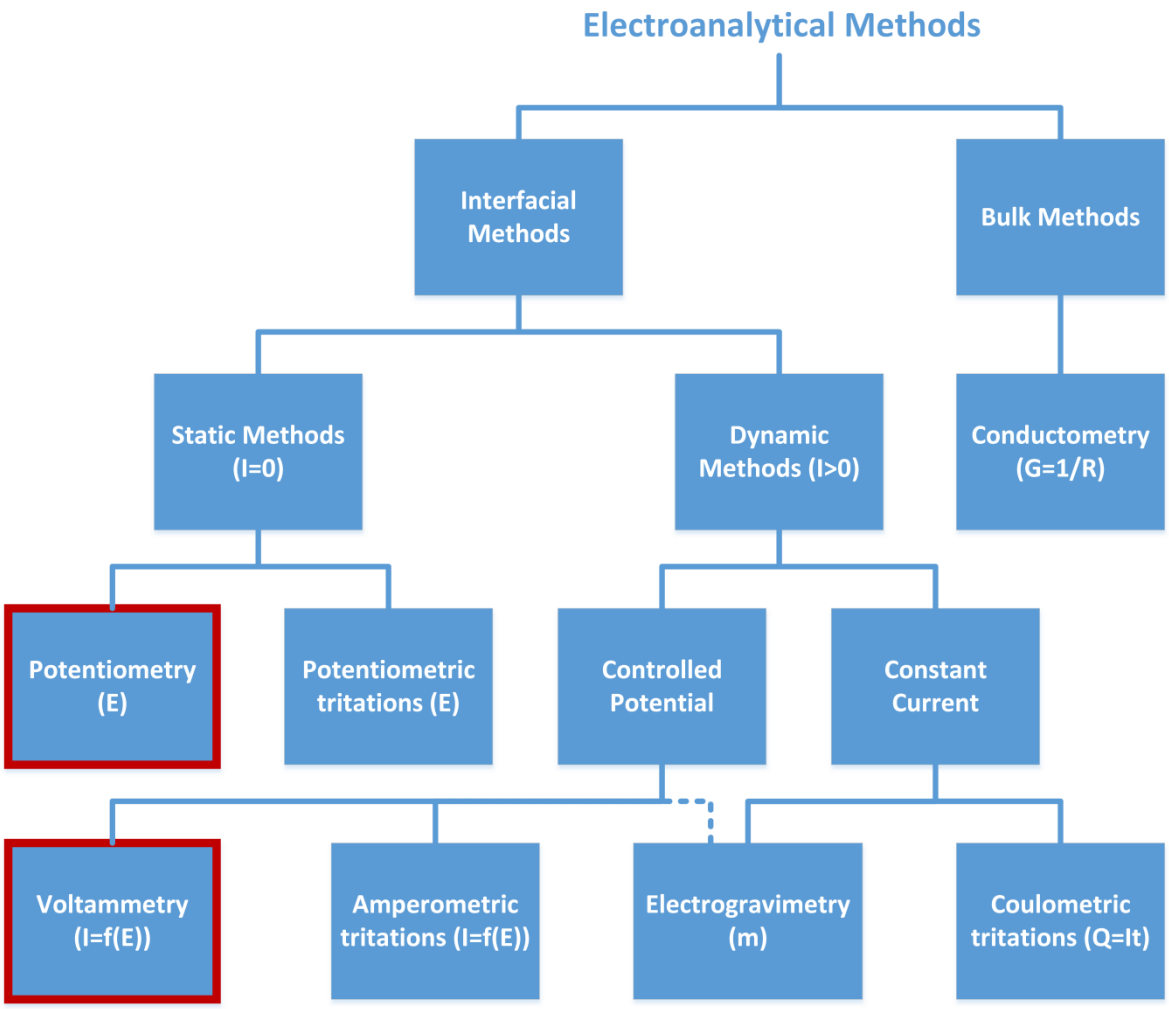

Figure 2.1: The classification of electroanalytical methods. The figure was adapted from [23].

electrodes inducing a change in voltage which is measured by a high impedance voltammeter. This voltage corresponds to the chemical solution's concentration of a certain type of ions. However, potentiometric electrodes are ion selective, meaning that the electrode's material composition also determines the level of voltage change. The pH sensitive glass electrode is one of the most recognisable ion-selective electrodes (ISEs) used in potentiometry for bioelectrochemical sensing. In this example the electrode is made of non-electrically-conductive silica coated with a Na^+ rich hydrogel. A layer of H^+ ions forms on the surface of the ISE and affects the measured potential that is used to determine the pH of the chemical solution [24]. Other potentiometric examples include liquid/polymer membrane ISEs sensitive to certain compounds of interest. These ISEs have been used as gas sensing electrodes (e.g. for CO_2 and NH_3 sensing), the gases are diffused in a liquid phase through semi-permeable membranes and sensed by the ISEs [25]. The addition of an additional biorecognition element in the polymer membrane can construct potentiometric biosensors when e.g. an

enzyme is coupled in the membrane [26], [27].

ISEs have been miniaturised to ion-selective field effect transistors (ISFETs) [28]. The SiO_2 layer of the FET device is used as a H^+ ion sensitive electrode that modulates the transistor current. As with their large scale counterparts the use of other sensing layers than SiO_2 might be better ISEs for H^+ ions (e.g. Ta_2O_5) so later versions had the sensitive layer altered. ISFETs are compatible with CMOS technology which later resulted in arrays of ISFETs [29], the technology can control and provide results from large numbers of transducers. A commercial success of an ISFET array was its application for deoxyribonucleic acid (DNA) non-optical genome sequencing [4].

Amperometry/voltammetry measures the current measured from induced reduction and oxidation (redox) reactions between ions in the chemical solution and conductive electrodes. For known electrode dimensions the concentration is measured directly from the current magnitude and it can reach down to the pA level (for miniaturised versions) [30]. The reactions are caused by a potential that is applied on the electrode where they occur, named a working electrode (WE), in respect to another electrode in the solution, called a reference electrode (RE). Amperometry uses a fixed potential while voltammetry uses a modulated one and measures current as a function of the potential change [31]. A method worth mentioning is fast-scan cyclic voltammetry (FSCV) which uses a high potential scan rate (operating frequency) and has advantages over conventional voltammetric techniques for its ability to detect analytes (compounds of interest) with a high temporal resolution [32]. Amperometric and voltammetric methods will be further explained in Section 3.4.

The first bioanalytical instrument (an electrode) was made by Clark [33] and it detected oxygen amperometrically. A Pt electrode was covered by a semi-permeable polymer membrane that allowed only oxygen to diffuse and get reduced due to an application of a voltage difference between the Pt WE and a AgCl RE. More recent versions of Clark's electrode are still being used [34]. Apart from oxygen, amperometric methods are able to readily quantify other electroactive biochemical compounds such as dopamine, serotonin, ascorbic acid and NO using redox reactions [35]. Another common application is the detection of heavy metals using stripping analysis which first electroplates the heavy metal

on the WE and its concentration is determined by oxidising this layer [8]. Biosensors for non-electroactive compounds of interest can also be manufactured by the addition of processes (e.g. enzymatic processes) that involve an electroactive product which can be detected amperometrically. The first biosensor was made in 1962, using a Clark electrode combined with an enzyme (glucose oxidase (GOx)) bound on the gas permeable membrane of the former, to make a glucose sensor [36]. An extensive use of enzymes catalysing reactions has been applied in amperometric biosensors with the enzymes usually trapped in polymers covering the electrodes. However, these systems suffer from interferents that become oxidised along with the analyte (e.g. O_2) thus electroactive compounds which become oxidised at a lower voltage, called mediators (e.g. ferrocene), started to be used alongside enzymes to transfer the exchange of charges from the enzyme to the electrode [37]. Furthermore, membranes have been used not only to immobilise enzymes but to also selectively block electroactive interferents from affecting measurements, similarly to ISEs [38].Other functionalisation methods include antigen-antibody or aptamer immunoassays where an electroactive element (e.g. ferrocene) or an enzyme is bound on antigens to make them amperometrically detectable when they bind on the functionalised electrodes, as well as on nucleic acid “targets” to detect DNA sequences [30], [38], [39].

The characteristics of potentiometry and amperometry/voltammetry are compared in Table 2.1. The main advantage of using potentiometry as an electrochemical method opposing to amperometry/voltammetry is that it minimally influences the chemical system’s behaviour. However, its response depends on the properties of materials involved and on the temperature variations [40]. Amperometry/voltammetry is a method capable of analysing a broader range of compounds of interest (analytes) than potentiometry using the same setup of electrodes at a different imposed potential. Although voltammetry pertruds the chemical solution under analysis more information can be extracted by its results. The measured current provides information about redox reactions and other electrochemical processes (e.g. mass transfer) as it is ploted as a function of the imposed voltage in what is called a voltammogram. Functionalisation of amperometric electrodes is a more direct process, especially post-fabrication of the electrodes, either by electropolymerisation or

	Potentiometry	Amperometry/Voltammetry
Output	Voltage	Current
Electrodes	Usually non-electrically-conductive	Electrically-conductive
Method	Non-interacting with the chemical/biological sample	Interacting and altering the chemical/biological sample composition
Selectivity	Electrode materials are inherently selective only to certain types of ions	More broad spectrum of analytes can be sensed but it is possible to narrow selectivity
Measurement	Intrinsic open circuit potential defined by the chemical composition of the chemical solution focused on one analyte.	Charge-transfer at voltages defined by more than one analytes in the chemical composition. In voltammetry more information about ion kinetics, the solution composition, the formal potential and interactions may be extracted as the current is measured as a voltage function.
Sensitivity	The voltage sensitivity is dependent on the theoretical (Nernstian) response as well as the material composition of the sensing layer.	Dependent on the electrode size and material
Biochemical functionalisation	Can be functionalised with polymers. The measured by-product of e.g. an enzyme reaction has to be compatible with the selectivity of the electrode material.	Direct functionalisation of Au electrodes with thiol chemistry. Electropolymerisation offers a wide selection of sensing layers to be entrapped in a polymer.

Table 2.1: Comparison table between characteristics of potentiometry and amperometry/voltammetry.

thiol chemistry that forms self-assembled monolayers (SAMs) of biorecognition elements on Au electrodes. One of amperometry's/voltammetry's main advantages is its ability to provide better measurements as the transduction elements (electrodes) are miniaturised, opposing to potentiometric sensors whose performance is better in larger sizes [41]. In amperometry/voltammetry the current magnitude reduces for smaller electrodes but the diffusion rate

increases, leading to higher mass transfer thus an ability to sense analytes at lower concentrations (if the correct instrumentation to read currents that might be in the nA-pA range is used) [7].

Comparison between the two methods showed that amperometry/voltammetry was an ideal choice for the development of a system with regions for independent analysis which can readily identify more than one substances with minimal or without functionalisation. In this work, the placement of multiple amperometric/voltammetric instrumentation together to perform many experiments simultaneously was seeked out. The use of smaller electrodes called microelectrodes was considered beneficial, more information on the choice of materials and the fields of application are provided in the next section.

2.3 Electrodes

The electrodes and their material selection is an important attribute of amperometric/voltammetric systems. These systems often employ a third electrode, called a counter electrode (CE) which acts as a current source while the RE is still used as a node for the potential difference on the WE to be controlled. In this three-electrode system each electrode is not necessarily fabricated with the same material. The CE has to be larger than the total area of the WEs to provide enough current for the operation of the system. It is fabricated by inert, stable materials that do not react or alter their surface chemistry such as carbon and noble metals, like Pt, Pd or Au. The RE may be constructed by different materials and architectures. All of these different REs' common characteristic is that they have to exhibit a stable potential reference independent of the chemical solution's composition. The most common RE which has an inherent voltage (named a standard potential E^0) of zero by convention is the normal hydrogen electrode (NHE). The NHE's operation is based on the conversion of H^+ to $H_2(g)$ and vice versa depending on the reaction occurring at the WE, its potential remains stable in any case. Its structure is made of a platinised Pt wire in a 1 M HCl solution with $H_2(g)$ being bubbled at a 1 atm pressure. Due to the NHE's complex structure other topologies were investigated, one of them is the saturated Ag/AgCl RE. The Ag/AgCl standard potential is 222 mV versus the NHE standard potential. It is made of a Ag wire

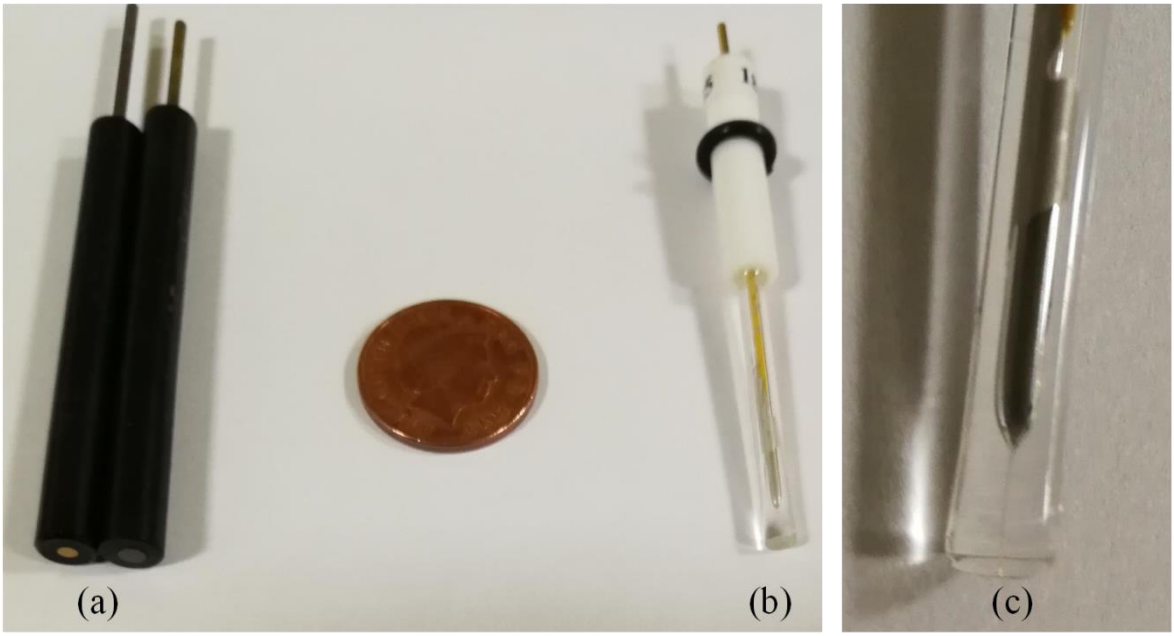

Figure 2.2: (a) A 2 mm Au and a 3 mm glassy carbon electrodes, (b) a 25 μm Au ultramicroelectrode and (c) its detail of the thin wire ending to to sensing area.

coated with a thin AgCl layer and contained in a 3.5 M KCl or NaCl solution with a junction an electrochemical solution under analysis through a semi-permeable membrane. The simpler portable setup of a Ag/AgCl electrode has made it a popular choice in labs, especially for miniaturised systems [42].

The WEs that are the system's transducer and they are fabricated by the most versatile selection of materials depending on the sensing requirements. One example is Au being used as a biosensing electrode material as it is a noble metal that is not only chemically inert and biocompatible but it also serves as a covalent bonding site for thiol-based self-assembled monolayers (SAMs). Another common material is carbon, due to its capability to be modified with biorecognition elements and has a wide potential range. A 2 mm Au and a 3 mm glassy carbon electrodes are shown in Figure 2.2(a). Pt and Pt black (a rough surface Pt layer that increases the active area) are also very common materials mainly due to their catalytic effects on H_2O_2 [31], [43]. Lastly, one of the increasingly adopted WE materials are conducting polymers [43], [44]. Conducting polymers offer attractive characteristics for biosensing such as selectivity over specific analytes and the possibility to incorporate enzymes as well as proteins and other biorecognition elements. The polymers are electrodeposited on the microelectrode sites using monomers and common voltammetric methods. In order to include the enzymes, they can be entrapped along with redox mediators (e.g. ferrocene) during electrodeposition or they can

be adsorbed on the surface of the polymer. Common conductive polymers are polypyrrole, polyaninline and polyphenylene [45]. More details on the theoretical background to select materials for each electrode type are given in Section 3.2.2.

2.3.1 Microelectrode Arrays

The ultramicroelectrode, an electrode of a diameter in tens of microns, started to attract attention in the 1960's as it demonstrated a better response when compared to large scale electrodes. A 25 μm Au microelectrode as well as a detail of its thin Au wire reaching the conductive surface is shown in Figure 2.2(b) and (c), respectively. One of the most important features of the ultramicroelectrode is a high mass transport that enables the electrode to reach steady state conditions faster than its large scale counterparts. Another beneficial attribute is a lower Ohmic (iR) drop due to the solution resistance between the CE and the WE lowering the desired potential difference applied between the chemical solution and the WE (a common problem in electrode configurations further explained in Section 3.2.3). Last but not least, its small size makes it a good candidate for use in portable devices [7].

Potentiometry and amperometry/voltammetry have found use in the form of miniaturised sensors in a 2-dimensional (2-D) grid array format. The miniaturisation led to an increase in the amount of data per unit area, in the sensitivity of individual sensors as well as to dedicated applications. Arrays of sensors can also facilitate averaging of measurements to counter for individual

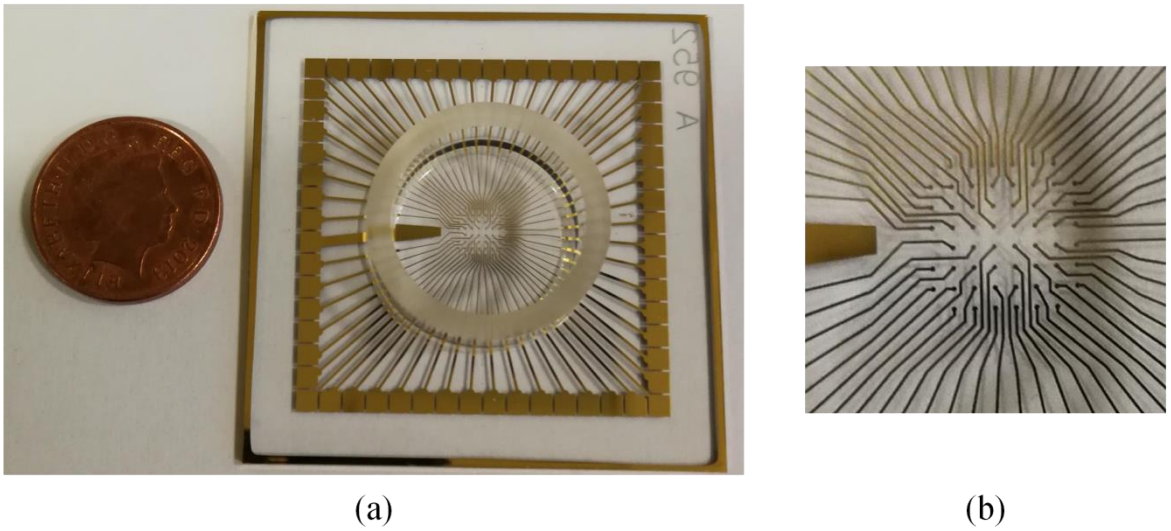

(a) (b)

Figure 2.3: (a) An 8 x 8 Au 100 μm microelectrode array on a glass substrate and (e) its detail showing the microelectrodes and its internal TiN RE.

sensor defects. Following the success of the single transducer, the ultramicroelectrode, microelectrode arrays (MEAs) have become the most versatile and established of the electrochemical arrays. An 8 x 8 Au 100 μm microelectrode array and its detail featuring the microelectrodes and an internal TiN RE are shown in Figure 2.3(a) and (b), respectively. Owing to their simplicity and wide range of choices in terms of their geometry and material selection they have become the dominant miniaturised and parallelised electrochemical tool.

Electroanalysis is the evident field of operation for MEAs. However, their parallel direct interaction with compounds and tissues allowed them to become an essential tool in many physiological applications too. They have been used in the study of the activity of electrogenic cells (cardiac and neural tissues), by reading the potential or current signals of ions generated by the depolarisation of cell membranes called “action potentials” [14]. Furthermore, monitoring electrogenic cell interaction across a 2-D plane is possible with MEAs. MEAs come in different shapes and material composition, planar or recessed electrodes are easy to fabricate and they have been used to monitor extracellular activity (mostly potential changes) as well as in electroanalysis. Whereas protruding electrodes (the Utah array [10]) or needle-like silicon nanowires have been used to penetrate the cell and monitor intracellular activity [46]. The technology has also been used in cortical implants for retinal, auditory and cognitive stimulation and recording, as well as in the ever so growing field of brain machine interfaces [47].

The main application of MEAs and interesting for this study is in electroanalysis, although the potentiometric electrodes were the first to be implemented, MEAs have mainly found application in amperometry/voltammetry. The metal electrodes can be used without any modification to detect a range of analytes, from heavy metals to oxygen. Depending on the target analyte(s), there is a range of metals that have been used for the fabrication of microelectrodes. All the applications mentioned in Section 2.2.1 have been applied to MEAs. As an example, thiol-modified oligonucleotides complementary to RNA strands of pathogenic microorganisms were immobilised on interdigitated microelectrodes (electrodes in an interleaved structure) in separate compartments on an MEA in [48]. The electronics used with MEAs that record signals from redox reactions

are responsible for the parallelised capture of events and when integrated they offer extended capabilities on top of the existing technology, as it will be analysed in Section 2.5.2. As it was mentioned in the previous sections many of the biochemical processes that can be recorded on electrodes and MEAs use electroactive materials as redox mediators to transfer electrical charge to the electrodes or as redox labels for non-electroactive components, such as antigens. A very common electroactive material often used for such applications is ferrocene, its origins and use are explained in the next section.

2.4 Ferrocene and its use in Electrochemistry

2.4.1 Origins

Organometallics are chemical compounds that consist of organic and metallic counterparts with metal-carbon bonds. The compounds have found application in synthetic chemistry as redox agents for the homogeneous catalysis of polymeric reactions and in pharmaceuticals as well as in stoichiometric studies. Organometallic compound analysis mainly commenced in the 1950's with the discovery of ferrocene (Fc^0) [49] and later other compounds that included transition metals. Their investigation produced several stable compounds that can be used as organic reagents that assist the formation of carbon bonds. Advances in electroanalytical chemistry go hand in hand with the analysis of organometallic compounds. One of the components necessary for the latter was circuits made of opamps (potentiostats) capable of driving three-electrode systems, which made the use of low polarity (non-aqueous) solvents possible as it corrected the *iR* drop. Another component was the discovery of the analytical importance of voltammetric techniques in the analysis of compounds compared to dc methods that were used before. Lastly another advancement was, the abandonment of classical electrodes, such as the mercury electrode, that were replaced by solid electrodes (e.g. Pt) which were benign and better candidates for the potential range to shift to more positive potentials and facilitate the study of anodic processes (e.g. Fc^0 oxidation).

Although the importance of REs was shortly discussed in Section 2.3, the physical electrode's composition sometimes vary between laboratories and the problem becomes even more apparent to non-aqueous solvents when the potential of

reference electrodes is not stable. A solution to circumvent this issue was to use a reversible compound as a redox internal standard (calibrant) to relate to the reduction and oxidation potentials of any other investigated electroactive compounds. The internal standard characteristics needed were a one-electrode charge transfer and a stable standard potential that was not affected by different chemical solutions. Due to its stability and the fact that the Fe metal centre was sandwiched inside two large organic rings, Fc^0 was deemed as an ideal candidate and it has been used as the golden internal standard for non-aqueous electroanalysis. Later studies indicated that there might be a possibility Fc^0 to interact with some chemical media, thus a compound with ring substituents, such as decamethylferrocene (DmFc), is considered to improve the interactions in chemical solutions [50].

2.4.2 Use in Biochemistry

In biochemical applications an undesired interference by accompanying electroactive species present in the chemical media with lower redox potentials than the analyte is observed as it was mentioned in Section 2.2.1. When enzymes are used, the substrate (e.g. glucose) is metabolised, the enzyme gets oxidised or reduced and an electroactive by-product of this reaction is sensed to determine the substrate concentration. An example is O_2 and H_2O_2, the co-substrate and product of the oxidase group of enzymes which are both electroactive. These compounds have a high redox potential thus other electroactive metabolites such as uric and ascorbic acid get oxidised and affect the resulting current, shown as interferents in Figure 2.4(a). To lower the range of the necessary potentials and sense the metabolic reaction, stable reversible electroactive compounds with a lower redox potential that do not interact with other chemical species in the solution, are often used as charge “shuttles”. Owing to its stability, high equilibrium constant *K* (i.e. fast electrode kinetics) and wide use, Fc^0, its derivatives (that have different formal potentials to each other) and the water soluble ferricyanide $[Fe(CN)_6]^{4-}$ anion found in salts are often used as redox mediators. There are several methods of mediator application; the simplest form is the introduction of the mediator compound in the bulk chemical solution. One approach is to use the mediator to change the redox state of an electroactive (co-)substrate (e.g. O_2). Otherwise, the mediator either performs a reduction or oxidation process of the electroactive

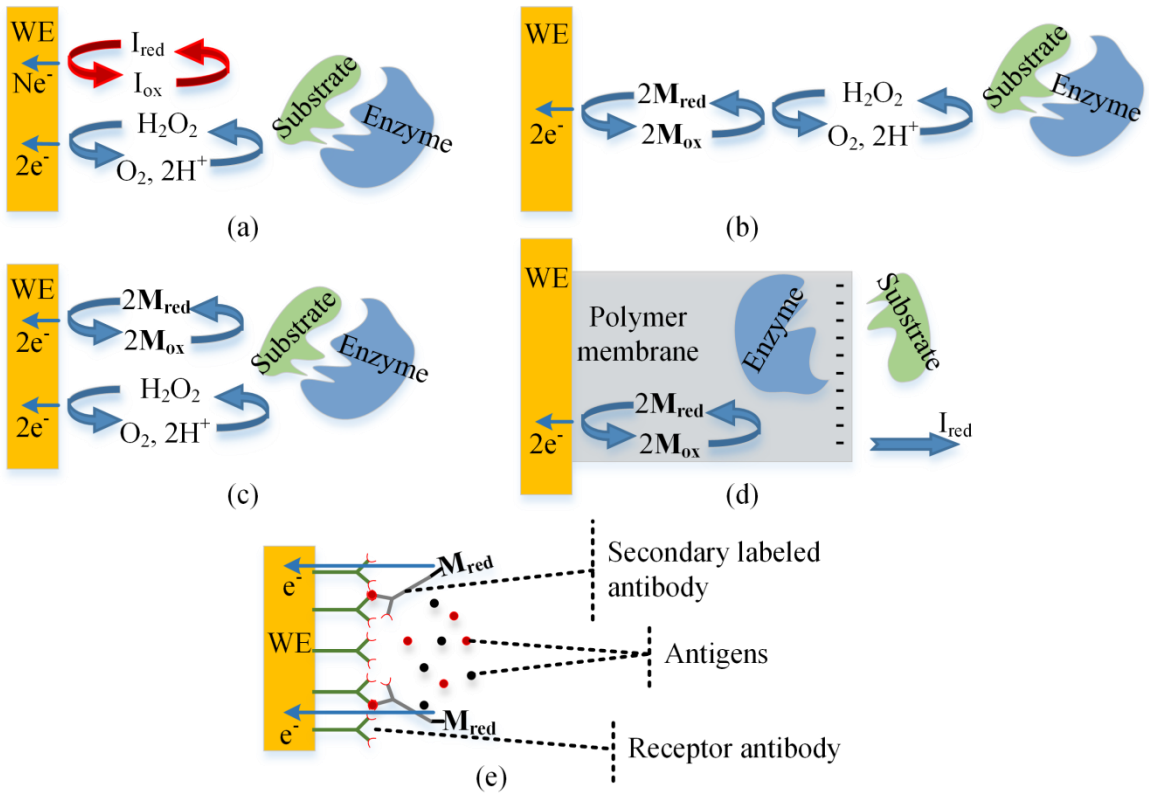

Figure 2.4: Detection of metabolic reactions and immunoassays. I_{red} and I_{ox} are the reduced and oxidised forms of interferents, respectively. M_{red} and M_{ox} are the reduced and oxidised forms of a redox mediator, respectively. Sensing of a metabolic reaction through (a) oxidation of the H_2O_2 product, (b) charge-transfer to the product through a redox mediator, (c) competition of the mediator and the regular product to transfer charge, (d) entrapment of an enzyme and mediator in a polymer membrane and direct charge-transfer through the mediator. (f) An immonuassay with an amperometric sandwich methodology, the redox label is tagged on a secondary antibody.

metabolised product (instead of a co-substrate) depending on their relative electronegativity or it competes with the inherent electroactive compound that changes the redox state of an enzyme, as shown in Figure 2.4(b) and (c) respectively. The reaction occurs close to the electrode where the mediator diffuses. If the mediator oxidises the other compound, the mediator's reduced form returns to the electrode to become reoxidised thus the current magnitude increases according to the substrate concentration. Another advantage by the use of certain mediators such as Fc^0 is the fast heterogeneous charge transfer assisted by the redox reactivity of the compound with the selected WE material when compared to the electroactive product. A more sophisticated approach is mediators to be encapsulated in water insoluble polymer membranes (or immobilised with other methods) with or without the enzyme to isolate any interference by other electroactive compounds, as shown in Figure 2.4(d). The polymer also acts as a negatively charged barrier to biological interferents. When the enzyme is casted in the polymer of the modified electrode, the

substrate and products pass through but the electron transfer is moved by the mediator and it is no longer dependent on mass transfer and kinetics. Apart from Fc^0 other mediators are organic dyes such as methylene blue, phenazines, methyl violet, Prussian blue, tetracyanoquinodimethane (TCNQ), N-Methyl-2-pyrrolidone (NMP), benzoquinone, tetrathiafulvalene (TTF) and others [37].

Last but not least, due the advantageous characteristics and its easily identifiable faradaic response Fc^0 is also used as a redox label bonded on target oligonucleotide strands or secondary antibodies of sandwich assays for genome sequencing or immunosensors. A DNA probe sequence or antibodies are stranded on the electrode surface and due to a close proximity of the two, current magnitude is enhanced when DNA sequences hybridise or when an immunoassay forms a stable complex, as shown in Figure 2.4(e) for the immunoassay case. A more direct approach doesn't use Fc^0 as a label but rather as an electroactive reactant abundant in the chemical solution and identifies the binding of moieties by a conductivity change in the current induced by the organometallic [30], [51], [52].

2.5 CMOS Technology

Even though electrochemical arrays are powerful tools, especially for electroanalytical applications, one of the advantages of arranging sensors in matrices is a parallel signal acquisition. External instrumentation is limited to its number of inputs and it is not sensitive enough for low concentration detection mainly due to several sources of interference on the signal path. Integrating transducers and electronics monolithically was shown to improve the performance of MEAs. The integration of many instrumentation hardware for the application of separate amperometric/voltammetric methods on the microelectrodes of an MEA to make an electrochemical cell microarray (ECM) seek for a technology capable of high integration. CMOS is an ideal candidate as such a technology, widely applied in the electronics industry.

The integration of a large number of electronic devices onto the same silicon die, made possible by the advent of CMOS very large scale integration (VLSI), has literary changed the way the world interacts with computational machines for nearly the past half-century. The commencing point was the development of the

MOSFET in 1960 by Kahng of Bell labs [53], a device that controls the flow of current through modulation of a channel of charge carriers (inverse layer). The discovery was followed by the first transistor switch by Wanlass et al. [54] made of an nMOS and a pMOS. An nMOS is a device with n-doped contacts on a p-type substrate and a pMOS is the p-doped equivalent, the devices are complementary hence the technology is called complementary MOS or CMOS. Later through innovative photolithographic techniques and the planar transistor, Fairchild Semiconductors created the first planar integrated circuit (IC) and MOS commercial device [55]. These techniques, described in the next paragraph, have been used for the development of CMOS VLSI devices by major foundries.

The fabrication starts with a polished single crystal silicon wafer, which has been doped most often with a p-type impurity, this case will be assumed for the rest of the description of the process. The next step involves the formation of n-wells by growing a SiO_2 layer (which is removed at the end of the step) and then etching it selectively over the desired areas to be implanted with donor atoms. Using similar photolithographic fabrication steps, a high resistance polycrystalline silicon (polysilicon) gate is formed, insulated from the substrate by a thin SiO_2 layer. Afterwards n- and p-type doping creates contacts to the substrate, the drain and source areas are defined, while the oxide layer ensures the donors do not reach the channel area, as it is shown in Figure 2.5. Aluminium metal is then used to interconnect the fabricated MOSFETs and other structures (e.g. resistors and capacitors). Due to the complexity of VLSI devices several metal layers insulated by a dielectric are needed. The final steps include the formation of a passivation layer (e.g. Si_3N_4) for the chip's protection against moisture and contamination. The passivation layer is etched over the pads to

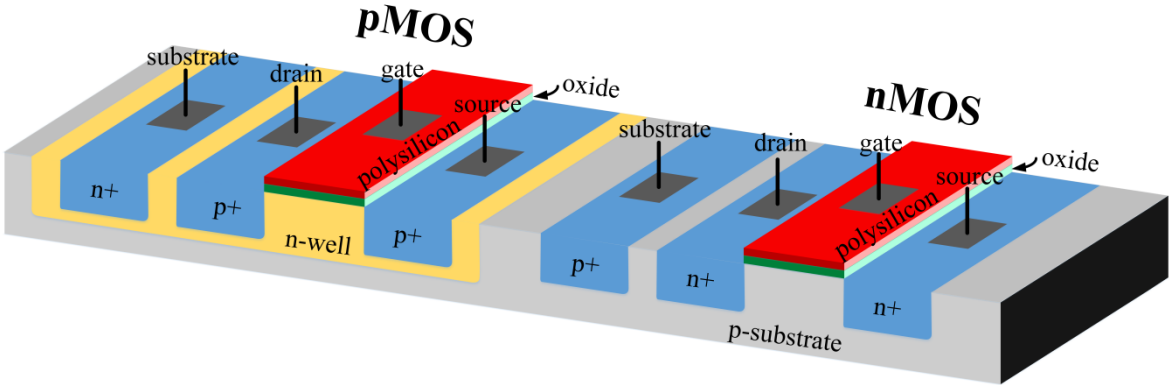

Figure 2.5: The CMOS structure.

enable connection to external instruments via bonding wires [13].

Using the explained IC fabrication techniques, employees from Fairchild Semiconductor founded Intel that made the first commercial microprocessor, which has ever since found use as the central processing unit (CPU) of personal computers [12]. As Intel's Gordon Moore predicted, the number of transistors per chip has been doubling every one and a half years [56] which was popularised by Caltech's professor Carver Mead as "Moore's law". Nowadays CMOS technology is pushing the boundaries down to the nanoscale where quantum phenomena start to dominate over macroscopic effects.

2.5.1 CMOS Instrumentation for Microelectrode Arrays

CMOS VLSI is now the prevalent application specific integrated circuit (ASIC) technology owing to its scalability to smaller feature dimensions leading to more devices per μm^2, low power consumption and low fabrication cost characteristics. Even though digital circuits have been in the spotlight due to their computing capabilities, analogue circuits are also of great importance as natural signals belong in the analogue realm. The majority of ICs are mixed-signal (analogue and digital), using the analogue part to interact with the environment (e.g. wireless and optical transceivers), while it is interconnected with digital electronics monolithically. Such practices offer CMOS VLSI integrated sensor devices the advantages of high signal-to-noise ratios (SNR), parallel data collection, miniaturisation of bulky large scale equipment to portable dimensions, precisely reproducible devices, high speed and low cost devices [13].

In order to operate MEAs and in essence any type of electroanalytical instrument, they have to be included as a part of an electrical circuit. As mentioned in Section 2.2.1, electroanalysis is conducted in environments made of conductive (usually metallic) and chemical parts. Electrochemical cells, electrode interfaces and ion formations are explained in detail in Chapter 3, this section will be focused on the circuits that control such an arrangement. Even though electrode systems can be controlled by circuits as simple as a power supply unit, research on these interfaces has led to instrumentation that controls and records electrochemical events more accurately.

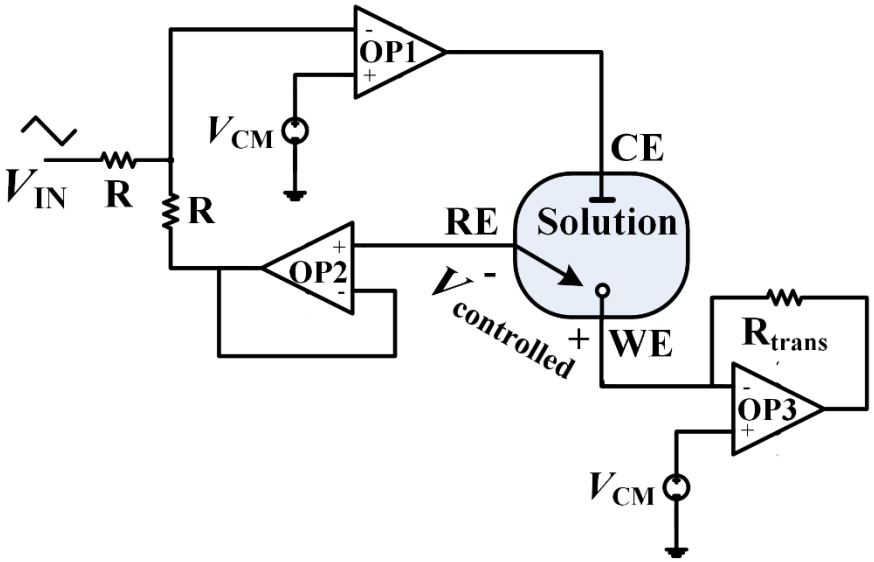

Figure 2.6: Standard design of a potentiostat circuit [31].

A potentiostat, shown in Figure 2.6, is an instrument that is able to control a three-electrode system. These systems consist of three electrodes, namely counter, reference and working electrode (CE, RE and WE respectively). The advantage of a three-electrode arrangement is that it achieves a displacement of the conductive path in the chemical solution to the control of a certain potential difference value in the same solution. The CE and WE are used to apply voltages on the electrode-electrolyte interface, redox reactions develop due to these external forces. When operated in potentiostatic mode, a signal is applied on the potentiostat inputs, which in turn takes into account the chemical solution between the CE-WE path to adjust the potential that will appear on the RE to maintain $V_{controlled} = V_{WE} - V_{RE}$ equal to the input signal and compensate for an Ohmic (iR) drop by the electrolyte and electrode impedance. The current from redox reactions is measured at the WE. In galvanostatic mode which in not used in the scope of this study, the input signal adjusts a current drain on the WE, while the RE is used to measure the potential induced by this current that develops on the WE $V_{controlled} = V_{WE} - V_{RE}$ [31].

A circuit design of a potentiostat, which is often adopted, is depicted in Figure 2.6. OP1 is called the control amplifier and it is connected as an inverting amplifier and an adder, this way it is possible to control the voltage appearing on the RE, independently of the variable chemical solution load, through a feedback loop. A second stage is often used as a gain booster after OP1. OP2 is connected as a voltage follower; the purpose of this opamp is to act as a buffer

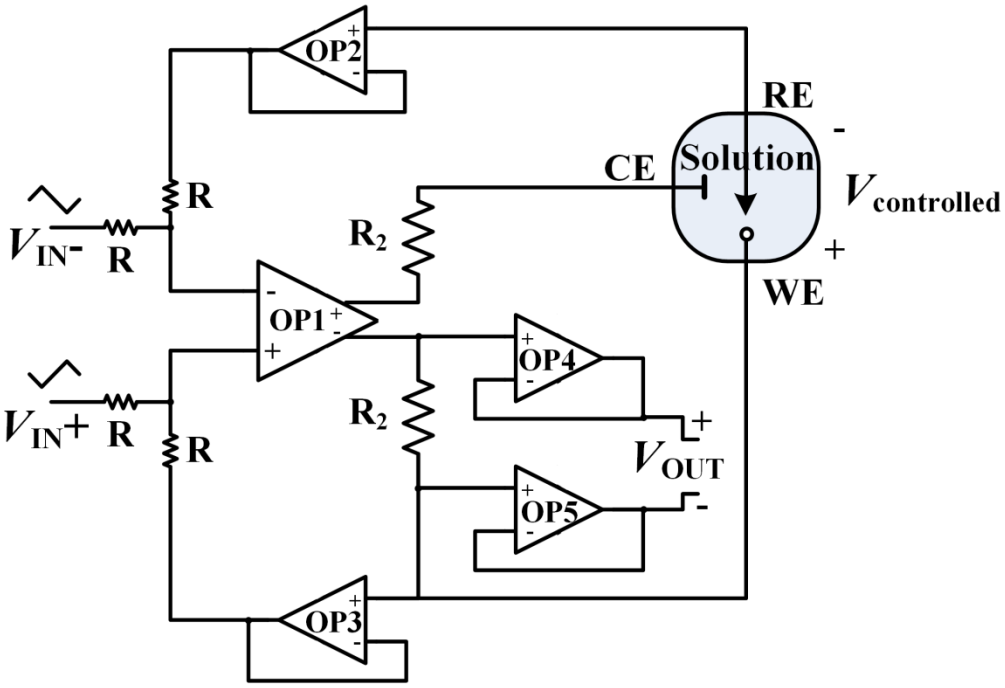

Figure 2.7: A fully differential potentiostat. The figure was adapted from [57].

for the RE voltage and prevent any current to flow through the RE, as it is connected to a high impedance input of the opamp. The last opamp, OP3 is connected as a transimpedance amplifier to keep the WE at virtual ground (V_{CM}) and measure the redox reaction current.

Although CMOS technology offers many advantages for more sensitive and parallelised measurements, it has power supply voltage constraints. Special potentiostat designs can compensate for these constraints. Martin et al. implemented a fully differential potentiostat [57], [58] which is depicted in Figure 2.7. A fully differential opamp (OP1) was used in this design to control the CE and the WE independently and a source follower (OP3) was added at the WE. This way the output voltage swing (and dynamic range) was doubled which is beneficial for the low power supply voltage of integrated CMOS processes. The common-mode noise rejection ratio (CMRR) was also increased. Instead of a current follower, the redox current was read by the OP4 and OP5 buffers as a potential difference across R_2. The power consumption increased compared to the standard potentiostat design by the use of more integrated opamps. Other attempts to increase the power supply voltage range were made by Ahmadi et al. [59] and Wang and co-workers [60]. The former attempt used just one opamp and current mirrors to increase the potentiostat's dynamic range, the design suffered from the ability to attain negative $V_{controlled}$ potential values. The latter

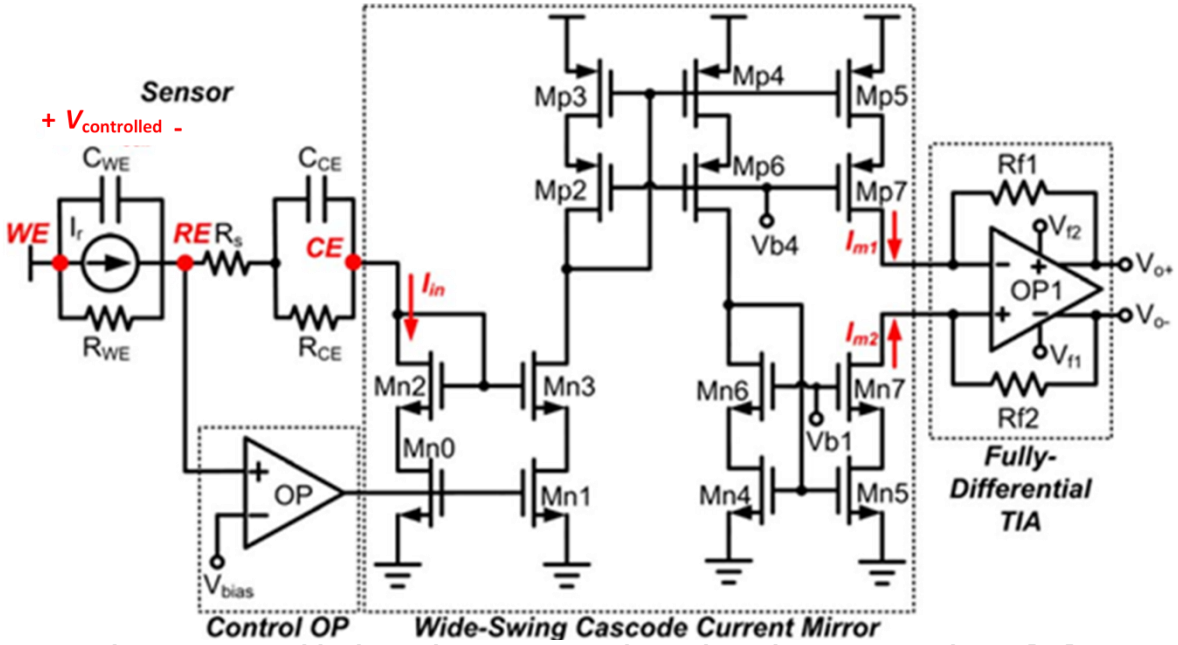

Figure 2.8: : A wide dynamic range potentiostat based on current mirrors [60].

attempt demonstrated an improved current mirror design suffering from the same issue and a fully differential transimpedance amplifier only to improve distortion, as shown in Figure 2.8. Other circuits designed to drive microelectrodes include a capacitor that is discharged on a pair of interdigitated electrodes for redox cycling between them [61]. A similar approach demonstrated by Ayers et al. takes advantage of circuit integration on the same

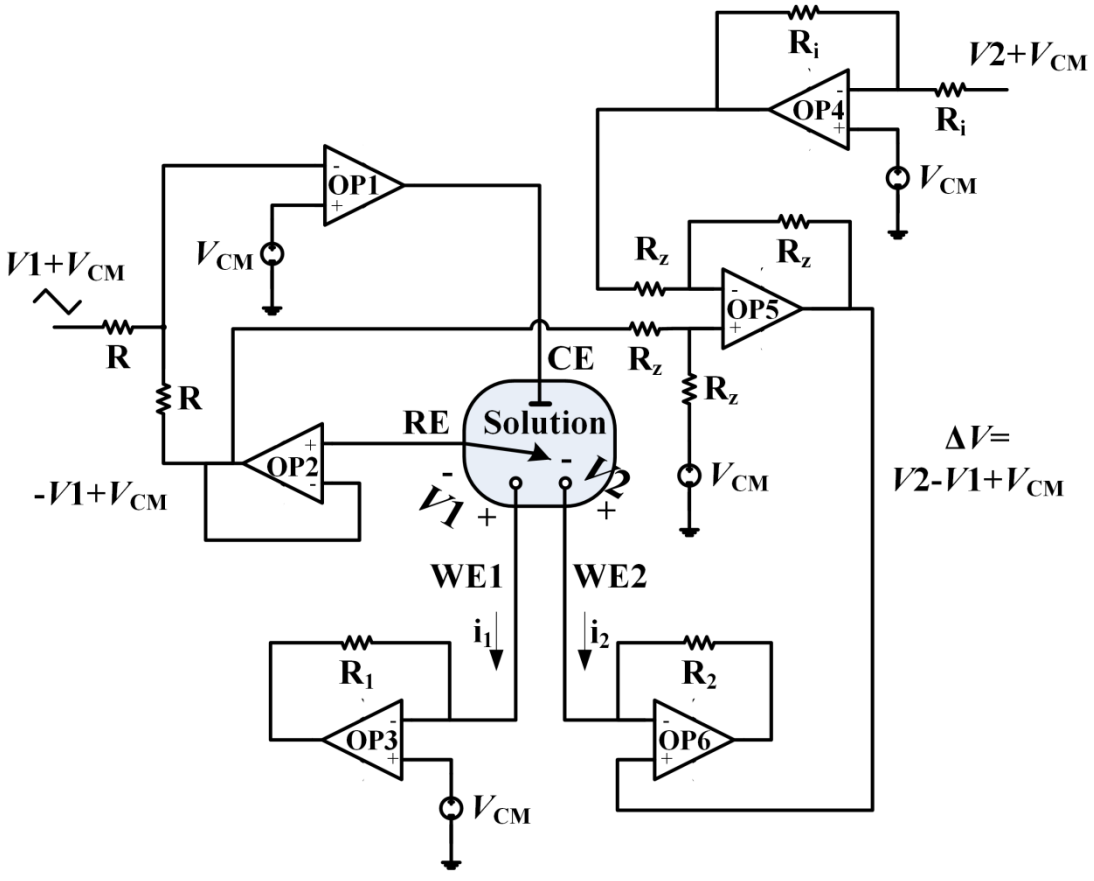

Figure 2.9: A bipotentiostat circuit design. The figure was adapted from [31].

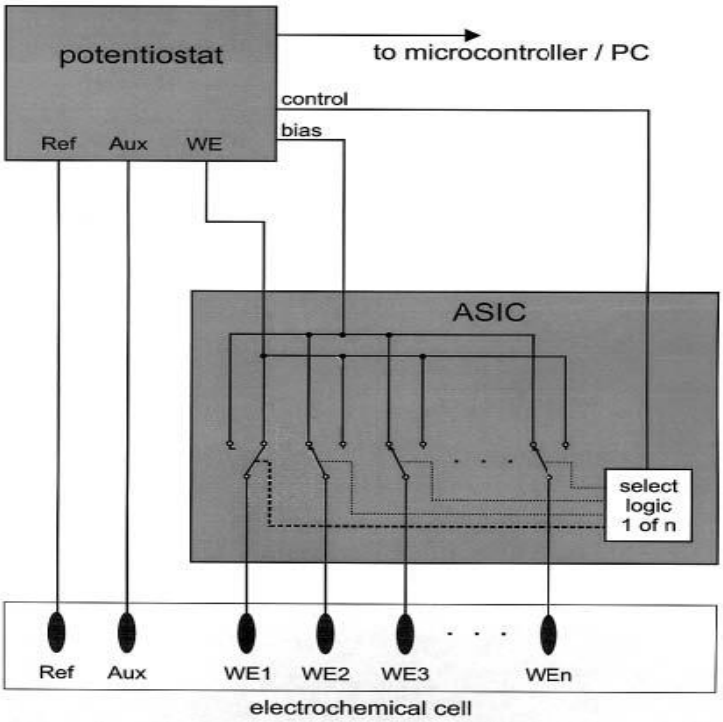

Figure 2.10: Multielectrode array multiplexing circuit [63].

chip by the use of a common part of the opamp on all readout electrode circuits [62].

Certain applications require the control of more than one electrode independently. A known device that is able to control a second WE's potential in respect to the potential of the RE is called a bipotentiostat and is shown in Figure 2.9. The potential of WE2 is changed independently but its voltage range is limited by the initial potential setting of WE1 since its voltage level is changed by $\Delta V = V2 - V1$ [31]. Extending this concept to more than two electrodes is of particular interest for microelectrode arrays, which can access and control all of the electrodes simultaneously. Taking advantage of the CMOS mixed signal capabilities, a potentiostat multiplexer that can be used with a bipotentiostat has been presented by Hintsche et al. [63]. Considering the simple case of using an ordinary potentiostat, Figure 2.10 demonstrates the circuit's advantage to keep electrodes that are not used at a bias potential. This feature is responsible for maintaining the microelectrodes' kinetics stable all through an amperometric/voltammetric measurement. The use of CMOS transmission gates and multiplexers is compatible with VLSI logic as it minimises the number of potentiostats required to control the microelectrode array.

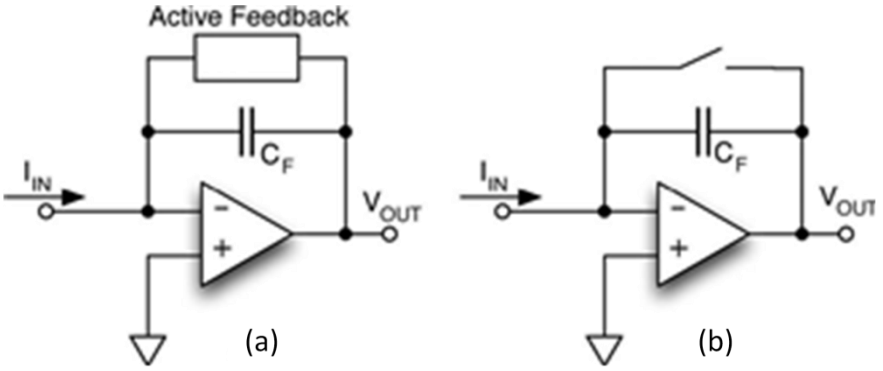

Figure 2.11: CSA using (a) a continuous time and (b) a discrete time implementation [64].

The integration of miniaturised electrodes on CMOS offers electrochemical advantages explained in Section 2.3.1 but it also reduces the noise as the overall transducer impedance becomes smaller. These features can be combined with low noise CMOS integrated amperometric readout circuits to further enhance noise suppression. Amperometric readout circuits' important features are a wide bandwidth, a large current range and bidirectional current conversion [43]. The common circuit used for this purpose is a transimpedance amplifier, as the one used in Figure 2.6, however the resistor required for the current to voltage conversion is a major thermal noise source depending on its size. The CMOS approach to this problem is to use a capacitor in its place to make the opamp act as a charge-sensitive amplifier (CSA). A CSA has two different implementations, a continuous time one that uses a low noise active feedback to set the bias voltage and a discrete time one that employs current integration, sampling and discharging steps, as shown in Figure 2.11(a) and (b), respectively [64]. The continuous-time approach has been reported by Ferrari et al. [65], using a low pass filter and a CMOS active high impedance stage to act as a feedback. The approach results in a lower noise figure especially at higher frequencies but care must be taken to match the feedback poles and zeros. The discrete-time approach has been adopted more often, owing to it being relatively undistorting. The input current charges the capacitor C_F until a voltage threshold is reached, sensed by a comparator (not shown), which activates a switch to reset the capacitor to a common mode potential. The timed comparator pulses are used to calculate the integrated current in a current to frequency (*i* to *F*) format [66], [67]. Another approach more suitable for bidirectional currents includes the charge of the capacitor for a predetermined time and the use of a known reference current drain and source to discharge it depending on the polarity, as shown in Figure 2.12(a). The discharging time is ΔΣ

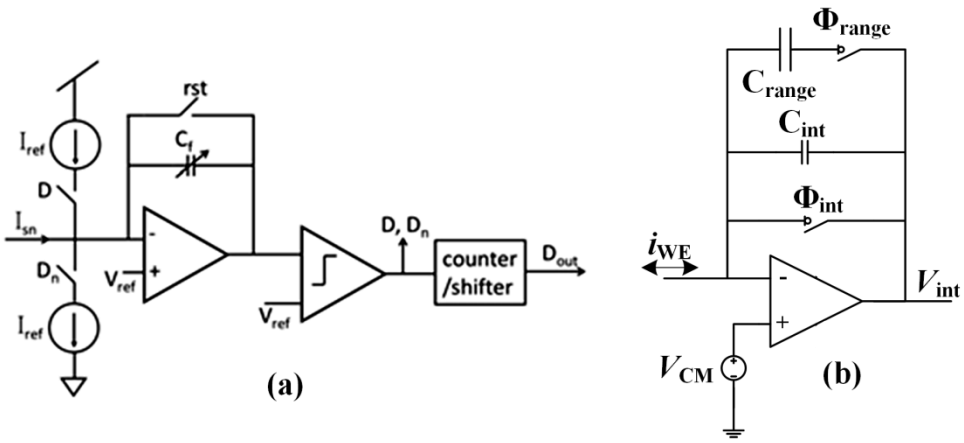

Figure 2.12: Discrete time (a) ΔΣ current integration ADC [43] and (b) extended range current integration [68] circuits.

modulated and it can be measured to calculate the total discharged current [43]. The current range was also shown that it can be expanded by the use of an extra capacitor (C_{range}), which can be selectively activated to increase the capacity value when needed, as shown in Figure 2.12(b) [68]. The discrete-time approach may suffer from thermal noise depending on the capacitor size as well as clock feedthrough and charge injection originating from switching. To improve the performance of these readout circuits, a correlated double sampling (CDS) method is often included in the design. CDS takes two measurements, one that is the input current and another one that samples the switching noise and then subtracts it to acquire a value closer to the noise-free input current. An example of a CDS design is shown in Figure 2.13, where the two clocks are inverted. The use of a current conveyor with an operational transconductance amplifier (OTA) has also been reported for current to voltage conversion [69].

CMOS potentiostats and current readout circuits are essential components with advantages such as high performance and the use of samples at low concentrations (achieving better sensitivity). They are used with MEAs to make integrated amperometric/voltammetric systems. However, each CMOS MEA is

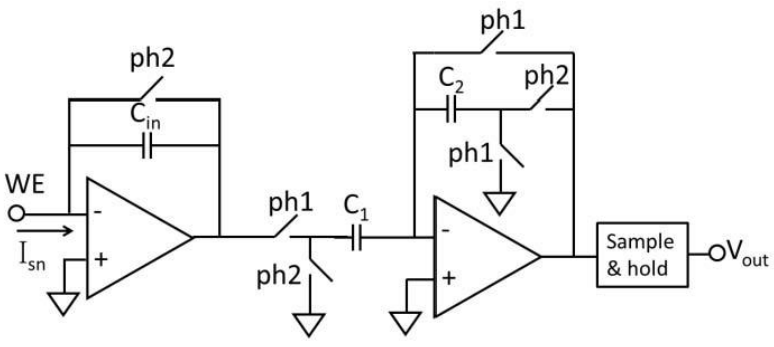

Figure 2.13: A correlated double sampling design for a CSA [43].

designed for a specific target application, thus the use of these components and the chip's architecture vary significantly. To construct a CMOS ECM, the integration of multiple potentiostats would make their respective microelectrodes to be controlled in an independent manner rather than change an offset as in multipotentiostatic designs. From the reviewed designs, the fully differential potentiostat [57], [58] is particularly interesting because of its wider dynamic range in CMOS and its 2 independent feedback loops that could be both readjusted while maintaining the desired $V_{controlled}$. Furthermore, controlling a set of WEs with the same potentiostat while at the same time avoiding voltage fluctuations, with a multiplexing scheme as in Figure 2.10, would also be beneficial to be integrated along with the other circuits. For current readout a resistor is the simplest failsafe converter. However, a more sophisticated readout design, more sensitive and compatible with digital logic could prove valuable for a portable system. A combination of the CSA shown in Figure 2.11 with additions to account for the current polarity changes in voltammetric measurements and extend the current range for a wider concentration range, as shown in Figure 2.12(a) and (b) respectively, could offer smaller current readings. The circuits to be included in systems need to be arranged in a chip architecture, several CMOS MEA architectures are presented in the next section.

2.5.2 CMOS Amperometric Microelectrode Arrays

The use of MEAs on CMOS takes an array of electrodes on a substrate and integrates it monolithically with mixed signal circuits to make integrated multi-transducer devices towards a Lab-on-a-Chip. These devices benefit from electronic interface circuits in close proximity to microelectrodes. Considering the microelectrode's advantages in terms of steady state analysis, sensors with improved noise performance can be built. The microelectrodes' inherent small size matches perfectly with CMOS VLSI to make dense amperometric microarrays that are capable of addressing many sites in parallel [14]. The resulting systems offer a high spatiotemporal resolution at a low unit cost and are easily controlled to perform many different functions. As it was mentioned in Section 2.3.1, MEAs have numerous applications on several fields of study. This section will focus on applications related to amperometry/voltammetry.

Hwang et al. presented a MEA with a simple readout regime where the CE and

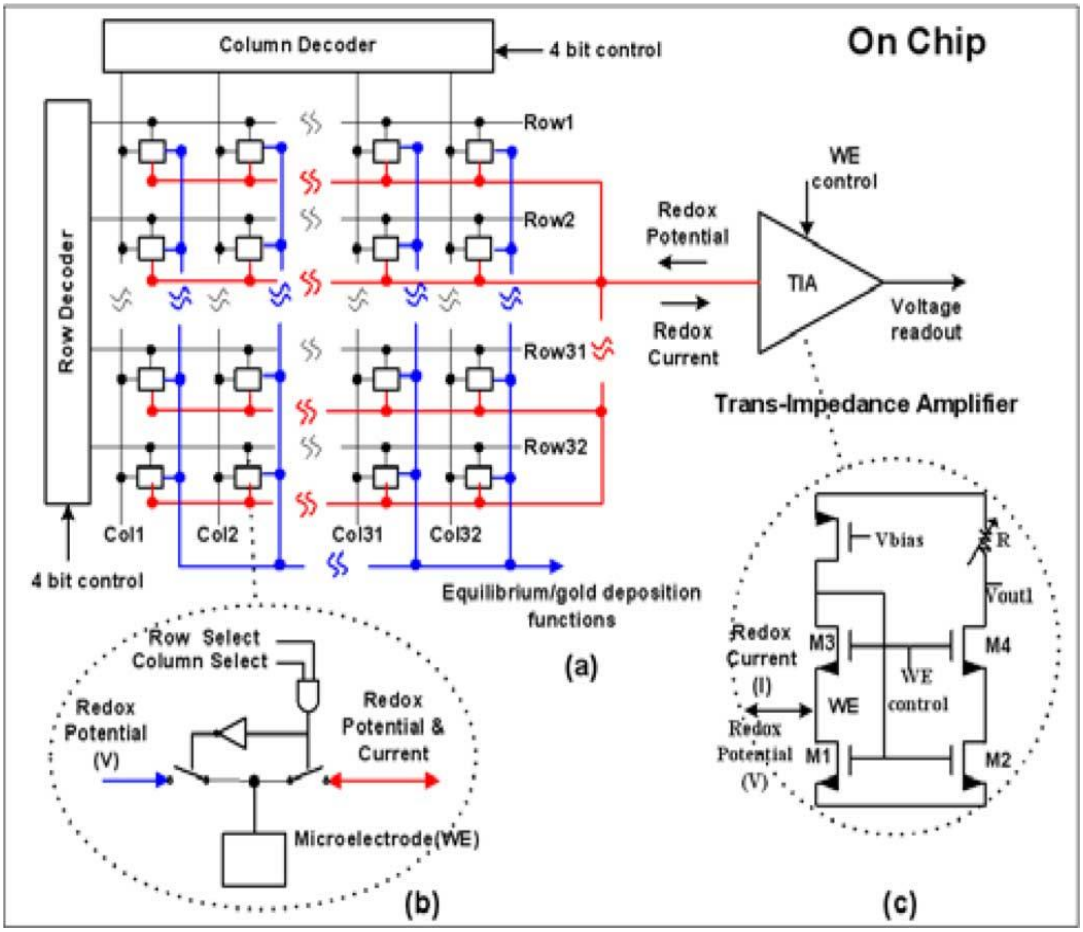

Figure 2.14: A CMOS MEA with (a) a multiplexing approach, (b) each switch selected whether the microelectrode would be connected to a bias redox potential or (c) an on-chip simple transimpedance amplifier [70].

RE were external and the WEs were addressed sequentially to be read by a simple wide range transimpedance amplifier. Following the example of [63] (Figure 2.10) electrodes that were not read were kept at an equilibrium potential. The same switch served for gold deposition functions, as shown in Figure 2.14 [70]. Another CMOS MEA that was presented by Kuno et al. used the same biasing multiplexing scheme [71]. In that work CEs were patterned as rings that surrounded each of the WEs while an external potentiostat was used to control all CEs as one and read the WEs' current sequentially. The ring structure ensured a steady state performance by the WEs as it controlled the diffusion (the movement of molecules from regions of higher concentration to regions of lower concentration to reach an equilibrium) layer shape, an important aspect in MEA designs that limits chemical cross-talk between WEs. Nonetheless the system resembled more a regular MEA than an integrated device as the chip only consisted of a single current converter and addressing circuits. A CMOS integrated MEA with a temperature sensor was demonstrated in [44] where the

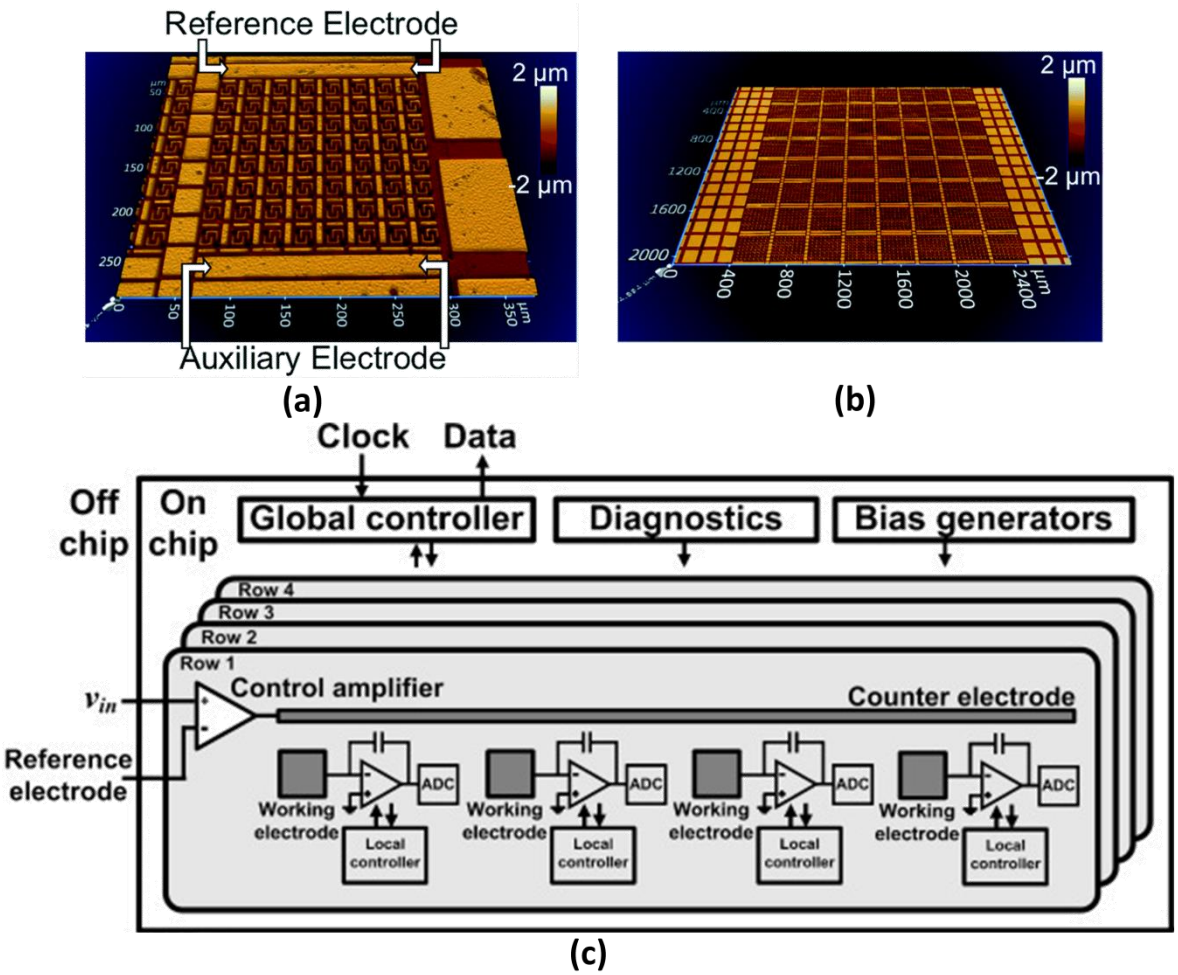

Figure 2.15: Modular integrated CMOS MEAs. (a) A subarray of microelectrodes with its own CE (auxiliary electrode) and RE and (b) the complete array [72]. (c) A CMOS amperometric system with on-chip potentiostats and readout circuits [73].

potentiostat and current readout circuits were integrated for each microelectrode row. Three different readout circuits were integrated on this system, two that were simplified discrete-time ΣΔ converters and a current conveyor. The system also had the capability of a connection to microfabricated biofunctionalised polypyrrole microprobe arrays with an enzyme to correlate catalysed and non-catalysed measurements.

Designing amperometric CMOS ASICs in a modular architecture has advantages over the power management, the required integrated instrumentation circuits and the scalability of subsequent versions. The design of circuits that drive a set of microelectrodes can be operated independently and only meet the requirements of a small subset of microelectrodes than the whole array. Modular potentiostats can be repeated as many times as it is required by the number of microelectrodes. A modular CMOS system that was presented by Wydallis et al. comprised of a single potentiostat that could multiplex through multiple on-chip

128 microelectrode subarrays, each with its own CE and pseudo-RE (a RE made of a material with a predictable yet varying potential according to the electrochemical conditions), as shown in Figure 2.15(a) and (b). The MEA was used to image norepinephrine diffusion gradients. The interdigitated microelectrodes required a reported 1 s readout for each subarray, resulting in a total 64 s readout time for the 8 K MEA [72]. A simple modular 16 × 12 CMOS MEA for neurotransmitter sensing that used a two electrode arrangement (local RE and CE) with a current conveyor at each WE to set its potential and record the current was presented in [66]. Although the ASIC was made to set 4 different voltages at the WEs independently, the feature was not experimentally verified. Another modular system by Levine et al. [52], [73] demonstrated an array of potentiostats driving subarrays of WEs and local CEs per subarray, as shown in Figure 2.15(c). The potentiostats were able to function in parallel and the reactions at the electrodes were recorded by on-chip discrete-time CSAs. The modular design relaxed the demands in power per potentiostat. That work has led to applications of biofilm employment and spatial imaging [74], [75]. However, when a shared RE is used [52], [70], as in this case, the potential is controlled on the RE but it is delocalized from the WEs, leading to V_{WE} vs V_{RE} voltage fluctuations. A similar work demonstrated by Li et al. [76] employed 4 three-electrode systems that engulfed each WE and had a waveform control electronic circuit integrated. Each electrode subset had its respective integrated potentiostat and a discrete-time CSA readout with CDS.

Integrated systems for DNA genotyping using amperometric transduction have also been presented. A system that was based on the charged-capacitor driver principle explained in [61] in Section 2.5.1 was developed by Schienle et al. [77]. The aforementioned ASIC by Levine et al. [52], [73] was shown that it can be functionalised with oligonucleotides (small DNA fragments) “probes” that hybridise with ferrocene-modified DNA “targets”. Ferrocene was sensed by FSCV to determine the bound “targets’” surface coverage as a method to identify for DNA mutations. In another work, a commercial CMOS MEA, shown in Figure 2.16(a), used with the Electrasense™ system, was initially developed by CombiMatrix and now a spinoff company called CustomArray. The MEA features individual functionalisation of each of the 12,544 microelectrodes with oligonucleotides using another instrument called the CustomArray B3™

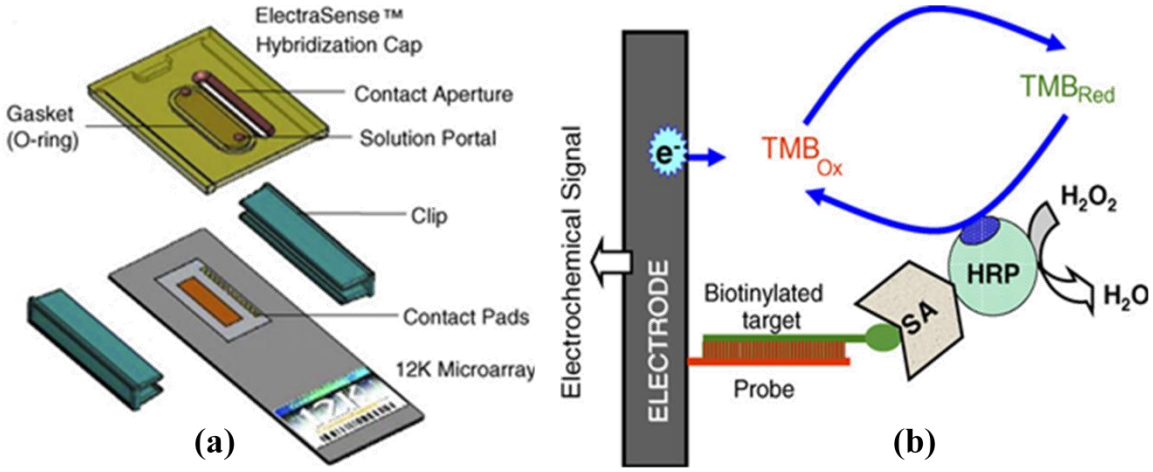

Figure 2.16: The ElectraSenseTM (a) CMOS chip with its packaging and (b) its principle of operation [78].

functionalised electrodes hybridise with horseradish peroxidase (HRP) labelled DNA "targets". HRP metabolises a redox mediator that is amperometrically sensed by the corresponding microelectrodes at close proximity, as shown in Figure 2.16(b) [78]. Each electrode was addressed to record its output data sequentially, resulting in a reported 25 s readout time. Nevertheless, faster systems presented here with parallel readout outputs promise higher throughput, which is a desirable characteristic for automated microarrays.

The amperometric CMOS MEAs that have been presented so far were limited to differentiate microelectrode sensing with surface functionalisation. In order to sense electroactive compounds with different redox potentials, systems that employ individual control over each electrode potential are emerging. A single

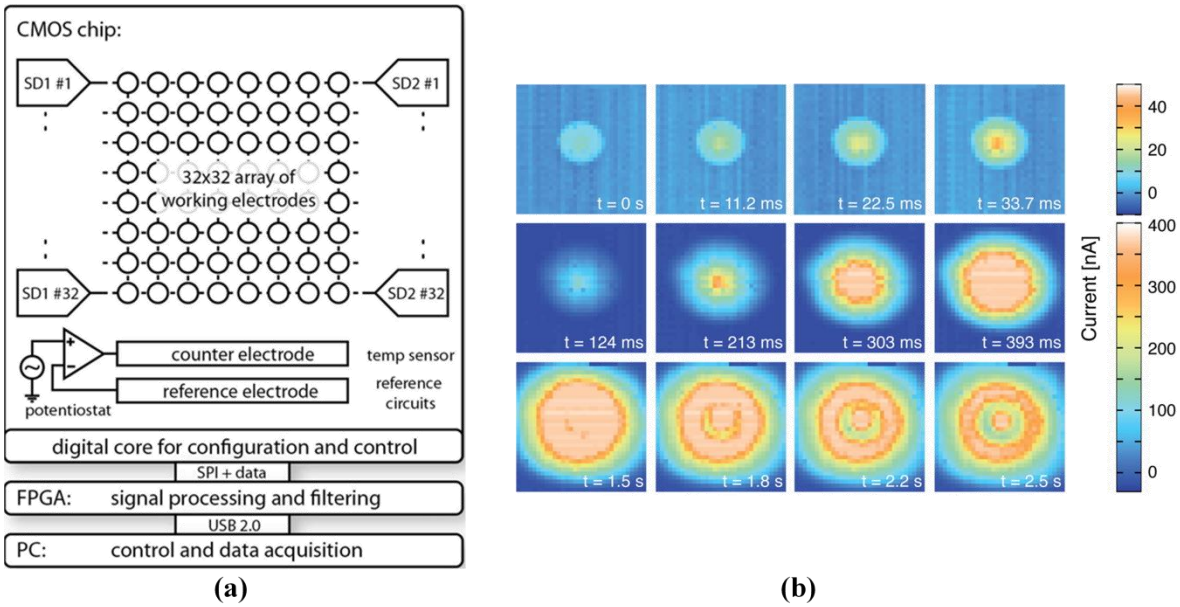

Figure 2.17: (a) The block diagram of a multipotentiostatic MEA and (b) video frames recorded by the MEA as an amperometric imager from a single droplet of H_2O_2 [79].

potentiostat in a multipotentiostat format was chosen by Rothe et al. [79] with a common CE and RE in a CMOS MEA. The WEs' potential could be connected to 4 different voltage levels, using an architecture shown in Figure 2.17(a). The MEA also served as an amperometric imager to monitor the diffusion of analytes, as shown in Figure 2.17(b). This chip was used in a subsequent work with microfluidic chambers [80] measuring 2 analytes simultaneously. However, as it was mentioned in Section 2.5.1 the different WE potential ranges set by a multipotentiostat (or bipotentiostat) are limited as they are dependent on each other and the RE. Massicotte et al. [81] presented a simple two electrode current integrating bipotentiostat, shown in Figure 2.18, for constant potential amperometry. 5 microelectrodes were separately microfabricated and functionalised with permiselective polymers for the detection of dopamine and activated with a glutamate dehydrogenase enzyme for the detection of glutamate. That system was capable of setting two different potentials on each electrode type and performed simultaneous detection of both analytes. The system focused only on low current density applications but if it was integrated with an MEA monolithically it could make a CMOS ASIC towards microarray applications.

Many different applications and system level design approaches were presented on CMOS amperometric MEAs. These devices were shown that they can be modular to save power and employ multiple potential levels, while they demonstrate applications from genotyping to neurotransmitter detection. From the CMOS MEAs presented in this section, the concepts of placing potentiostats in a modular architectures as in Figure 2.15 [52], [72], [73] and employing different potential settings in different subsets of electrodes as presented in Figure 2.17(a) [79] could be combined to make an electrochemical cell

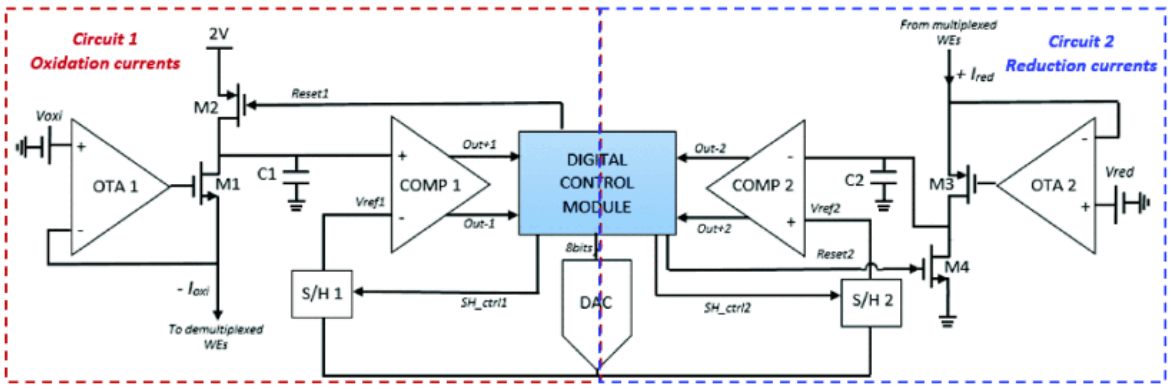

Figure 2.18: A simple bipotentiostat based on a CSA [81].

microarray (ECM) CMOS ASIC. From the review of CMOS MEAs it became evident that in order to achieve isolated electrode subsets the operating circuits are not the only aspect that needs special attention but also the geometrical structure of the electrodes themselves. Surrounding the subsets with CE rings [71], [76] is an architecture that shows an improvements to the control of the diffusion of reactants between microelectrodes. The ASICs presented in this section showed many different applications and possibilities for commercialisation, however flexibility on the functionalisation of an integrated MEA would offer many possibilities for different applications. A switching architecture similar to the one presented in Figure 2.14(a) and (b) [70] could be integrated in the ECM to bypass integrated potentiostats and other circuits depending on the operation that would need to be performed.

The methodologies presented in this section to develop ASIC MEAs do not only differ on the design aspect but also on the fabrication approach. The materials being used for CMOS fabrication have not been prepared to work in wet chemical environments. In order to enable the use of advanced ASICs as presented in this section with integrated microelectrode surfaces active to biochemical operations, post-processing fabrication steps are necessary.

2.5.3 Post-processing Techniques

The CMOS amperometric ASICs presented in the previous section have properties that enhance the capabilities of MEAs. One of the steps to make the advantageous monolithical integration of the MEAs capable to work with chemicals is to protect the intrinsic CMOS interconnections Al metal from corrosion by chemicals. Another aspect of post-processing is the protection of pads and bonding wires from coming in contact with conductive liquids and mechanical stresses. Lastly, a fluidic container is required to handle the liquid solution used with the MEAs and lead towards a Lab-on-a-chip device [43].

Post-CMOS Fabrication

In order to use CMOS technology as a substrate for a MEA, the original CMOS fabrication layers need to be post-processed. The top-metal layer can be exposed from the passivation layer either by the foundry or by post-processing

etching. After this initial step, the Al formed microelectrodes need to be altered. Several methods have been demonstrated to deposit materials inert to electrochemistry on a CMOS surface and prevent corrosion on the Al metal layer. One method is to perform electroless plating of a chemically inert conductive material directly on the electrodes [70]. Electrodeposition of metals or polymers is also another option that is common in regular MEAs but it was only recently explored on CMOS as it requires control of the electrodes' to be plated potential [44], [82]. The most common method compatible with CMOS fabrication is photolithography, which provides accurate control of the dimensions and smoother surfaces but it entails access to a cleanroom facility. Pyrolysing photoresist is a common method to create carbon working microelectrodes [83]. Photoresist is also used as a temporary patterning layer that is used to shape a wide range of deposited materials via several methods such as sputtering and thermal vapour deposition [83]. The photolithographic steps that have been reported vary, metals were deposited directly over the Al electrodes [67], [72], [77] or the Al top-metal layer was first removed to expose the CMOS intrinsic tungsten vias [52], an adhesion layer such as Ti was used. Another approach was to move the electrode area away from the top-metal layer by the use of chemically inert metal tracks and covered it with an extra passivation layer [44], [71], [76], [79].

The complexity of the RE's structure to exhibit a stable potential independent of the chemical solution's composition has made its miniaturisation a separate matter. The most common CMOS post-processing fabrication material is Ag, trying to follow the standard Ag/AgCl RE performance. However, the Ag/AgCl RE is normally kept in a solution that contains KCl with a semi-permeable membrane to maintain an equilibrium of ions and protect the electrode's surface composition. The miniaturisation of a non-degradable encapsulated electrode is challenging, methods to confine the electrode include the use of hydrogels, heterogeneous polymers or a glass layer. Sometimes an unchlorinated Ag electrode or other materials are used to serve as quasi-REs (or pseudo-REs) that adequately follow the Ag/AgCl RE behaviour.

Packaging

The successful incorporation of CMOS ASICs into a Lab-on-a-Chip format requires the addition of a microfluidic packaging. After post-processing CMOS ASICs are bonded on a carrier for interconnection with large scale components. The standard carriers, such as a PGA (pin grid array), have dies placed in a cavity creating a vertical step. Other carriers that are levelled better include printed circuit boards (PCBs), silicon wafers, polydimethylsiloxane (PDMS) and hardened epoxies. Only the active area of the sensors must be in contact with liquids, the bonding wires and pads area must be encapsulated. Each carrier has characteristics that enable different encapsulation methods. Having a relatively flat surface is a condition that enables the patterning of microfluidics through photolithographic techniques. However, to make flat surfaces large enough to be handled several steps that either increase the cost or that are not always replicable are required. Recently a method that used an epoxy to incorporate the CMOS die followed by photolithographically patterned metal extensions of the pads was presented [84]. The metals were protected with a biocompatible polymer named parylene-C. Parylene-C (poly(monochloro-p-xylylene)) is a polymer that can be deposited through chemical vapour deposition (CVD) into thin films and it offers inertness in chemical environments, a conformal coating presenting a pinhole-free layer with a uniform thickness and acts as a moisture, chemical and dielectric barrier [85]. Even though in that example parylene was a good insulator, when used to coat wire bonds and pads of electroanalytical CMOS chips it can prove challenging to be removed from the active area. Regular photolithographic techniques cannot be followed after wire bonding due to the complex packaged structure, thus non-trivial methods such as patterning with a PDMS block [85] or expensive laser micromachining [86]. It has also been reported that when covering wire bonds the polymer's mechanical integrity can become fragile over time [43], [86]. An elastomer called polydimethylsiloxane (PDMS) is usually surface bonded on flat surfaces to form microfluidic structures, it has also been reported as an encapsulating candidate using several layers to construct the microfluidic structures [87]. Another silicone elastomer (Silastic 9161 RTV) with a wax mould to protect the active area was used to form the microfluidic container [88]. Although, elastomers might absorb solvents and are not as chemically resistant as epoxies, thus the latter have been extensively used to form microfluidic containers [43], [84]. Epoxies must be carefully

selected for their viscosity characteristic to flow evenly over the wire bonds. However, epoxies can cause mechanical stresses to wire bonds and might not have a good adhesion to the CMOS die after being cured [43].

Many techniques have been presented for the preparation of a CMOS ASIC towards a Lab-on-a-Chip device. Every technique has its own advantages and disadvantages; the choice of the correct technique depends on the targeted application. Some CMOS Lab-on-a-Chip devices are reviewed in the next section to demonstrate applications where these devices can promote fully integrated systems.

2.5.4 CMOS Lab-on-a-Chip Devices

The progress of microfluidics as well as the reviewed preparation and encapsulation of CMOS chips made possible for the development of Lab-on-a-Chip devices, which are capable of performing complex lab procedures on a portable platform using low volume samples. These portable diagnostic tools are a potential candidate for affordable global health in developing and other countries [89] by the means of early diagnosis for epidemiological control. The use of CMOS on a Lab-on-a-Chip benefits from on-chip sensor signal acquisition and processing circuits. These devices use several sensing technologies for a variety of lab procedures [15], some examples of electroanalytical devices are presented in the next paragraph.

One of the first examples of the use of a potentiometric array with a microfluidic chamber to monitor electrogenic cells using a CMOS Lab-on-a-Chip device was demonstrated by Eversmann et al. in 2003 [90]. Heer et al. later developed a Pt CMOS MEA with a microfluidic chamber that both actuates and senses electrogenic cell activity with on-chip circuits. On the commercial side of CMOS Lab-on-a-Chip devices, the potentiometric DNA sequencing CMOS electrochemical microarray by Thermo Fischer Scientific [4] is one of the best examples. In the mentioned examples microelectrodes have been used as sensors or actuators in many cases, as the use of MEAs expands over a large area of applications as explained in Section 2.3.1, their CMOS versions along with microfluidics is a promising technology for Lab-on-a-Chip applications [43]. Lab-on-a-Chip devices aim for use as personalised diagnostic instruments for home

environments or for low-budget portable instrumentation in laboratories or hospitals. These applications are summarised as Point-of-Care devices, some examples of electronic commercially available products are presented in the next section.

2.6 Commercial Electroanalytical Point-of-Care Devices

Electroanalytical along with other non-electrochemical instruments have been used as diagnostic devices aiming at the general public. They exhibit attractive characteristics such as rapid results acquisition as well as an ease of implementation and use. The aim of these devices is to address individual needs based on a personal profile by diagnostic readings. These readings are provided by genomics that are based on mapping an individual's genome, proteomics that study the change of proteins in cells, leading to changes of a person's phenotype, and metabolomics that measure small molecule concentrations which have an inter-individual variability due to environmental and genetic factors. The use of such devices leads to the application of personalised medicine, to decide on a healthcare strategy based on individual needs [91], [92].

Many electroanalytical POC devices have been developed and commercialised pointing towards personalised medicine. Their complexity, ease of use and throughput vary, but some products have been proven to be very efficient for the improvement of personal healthcare quality. An electroanalytical technique combined with mixture separation is called liquid chromatography electrochemistry array (LCECA), a method that has been widely investigated in metabolomics [92]. Another amperometric device is the glucose biosensor that is broadly used in self-monitoring of blood glucose (SMBG), a point-of-care technology whose product development has been improving version after version, an example by Bayer is shown in Figure 2.19(a). Acquiring results rapidly along with the small blood volume requirement made the SMBG a successful preventative technology for diabetes implications [3]. Following the success of SMBG, multi-analyte electrochemical devices have been produced to provide for better, low-cost and rapid healthcare at home and intensive care units. One example is the i-STAT, a portable POC device that attaches to cartridges with several analyte variations, shown in Figure 2.19(b), now owned by Abbott

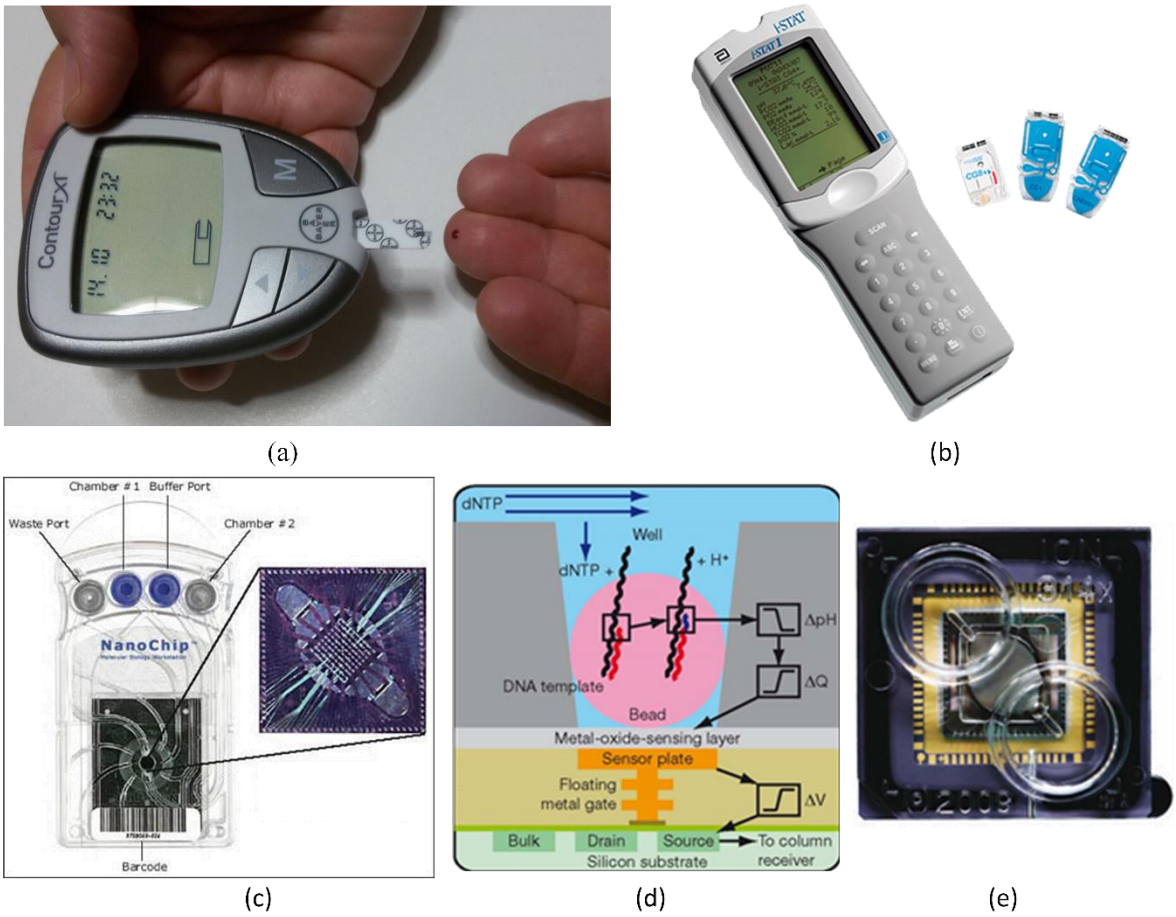

Figure 2.19: POC devices. (a) A self-monitoring blood glucose system. (b) The i-STAT handheld device and cartridges [97]. (c) Nanogen's Nanochip cartridge [98]. (d) Thermo Fischer Scientific ISFET array DNA sensing principle and (e) the CMOS chip with a microfluidic channel [4].

Laboratories [93]. The system comprised of an electronics part and multiple electrodes that can be used in all three modes of electroanalysis, depending on the application [94], [95]. Cross-contamination between different tests using the same sample media was avoided by the use of semi-permeable and polymeric membranes on the transducers of the i-STAT cartridges [95], [96].

The combined measurement of multiple biomarkers using the same sample media has applications not only in clinical chemistry but also in industrial online monitoring and environmental sensing. This type of measurement offers advantages such as reduced cost, high throughput, improved accuracy in the detection of diseases, reduction of the factor of human errors and a multitude of potential applications. The first notion of detecting multiple biomarkers on the same platform was by Ekins in 1989 [99], commencing the field of microarrays ever since it has found use in genomics [100], proteomics [101] and recently metabolomics [102]. The microarray technology multiplexes the detection of

several characteristic substances in an array format, its detection methods are usually chemical or optical. There are two successful microarray implementations using commercial electrochemical transducers. One is the Nanochip by Nanogen Inc, a microarray that was used for DNA sequencing [103]. The platform was made of a combination of a microelectrode array and fluorescent optical detection, the cartridge is shown in Figure 2.19(c). Detection was enabled as follows: each oligonucleotide "probe" (a small DNA fragment) known in prior was bound to microelectrodes selectively by the application of a potential difference at user defined sites on the matrix. A hybridisation step matched several fluorescent DNA "target" that were introduced and washed successively to determine "target-probe" match optically. The other one is the ion chip by Ion Torrent (now Thermo Fischer Scientific), an ISFET array-based microarray for fast non-optical DNA sequencing. In this paradigm DNA fragments were bound on magnetic beads that were centrifuged into ISFET containing wells to place a bead per well. Four different nucleotides were then introduced and washed in a successive fashion. Bound DNA polymerase joined the nucleotide when it matched into the emerging double stranded product, resulting in the release of a proton that was sensed potentiometrically [4], as shown in Figure 2.19(d). The result was a fast and reliable CMOS compatible DNA microarray, shown in Figure 2.19(e), which is able to sequence multiple DNA fragments simultaneously. Electroanalytical microarrays are an advantageous technology due to their direct analyte sensing and easy implementation. In this section the advantages of using multiple methods and analyse different biochemical compounds using one platform were proven as attractive features for commercial applications. The possibilities of applying such features on CMOS electroanalytical ASICs and how they can improve on their analysis power is presented in the next section.

2.7 Simultaneous Multiple Measurements

POC devices exhibit a trend towards multiple measurements for personalised medicine. In amperometric/voltammetric systems the plethora of independent measurements, even for the same analyte, can be combined through multivariate data analysis to construct models that interpret medical diagnostic properties of interest, a field often described as chemometrics [16], [104]. As it was mentioned in Section 2.5.2 CMOS MEA examples of multiple measurements

have started to emerge. However, these attempts were mainly focused on detecting more than one analyte by functionalising the microelectrodes. Other research that can be found in the literature detected either multiple biomarkers simultaneously or used multiple methods to detect more than one clinically important features. Both of these techniques are reviewed in the following sections.

This study aims at the development of a system that can employ several amperometric/voltammetric methods on subsets of microectrodes in the same fluidic container, an electrochemical cell microarray (ECM). The section demonstrates results acquired from several methods could be used in conjuction with computational techniques to provide more accurate or not even previously detectable results. It also reviews the background of techniques to selectively prepare electrodes to sense different analytes and distinguish between many compounds with computational methods. These techniques demonstrate the steps that can follow after the preparation of the ECM to make new types of measurements that could make the system a POC device for the analysis in a mutlitude of areas.

2.7.1 Multiple Analyte Techniques

Physical Functionalisation

The functionalisation of electrodes with bio-recognition materials is a step towards selective biosensing and the development of multiple analyte sensors. These materials include SAMs to construct immunoassays, thiol-modified DNA oligonucleotide genotyping assays as well as enzymatic biosensors [8]. In a work using a CMOS ASIC, a hanging drop microfluidic structure that detected microtissue activity was presented that had the electrodes functionalised with enzymes entrapped in hydrogels [80], as shown in Figure 2.20(i). A different approach was reported by Lin et al. that used surface adsorption to modify carbon nanotube electrodes with 3 enzymes and needed a microfluidic system to keep the electroactive products separated. The electrodes were operated by an external multipotentiostat at two different potentials for H_2O_2 and dihydronicotinamide adenine dinucleotide (NADH) sensing [105].

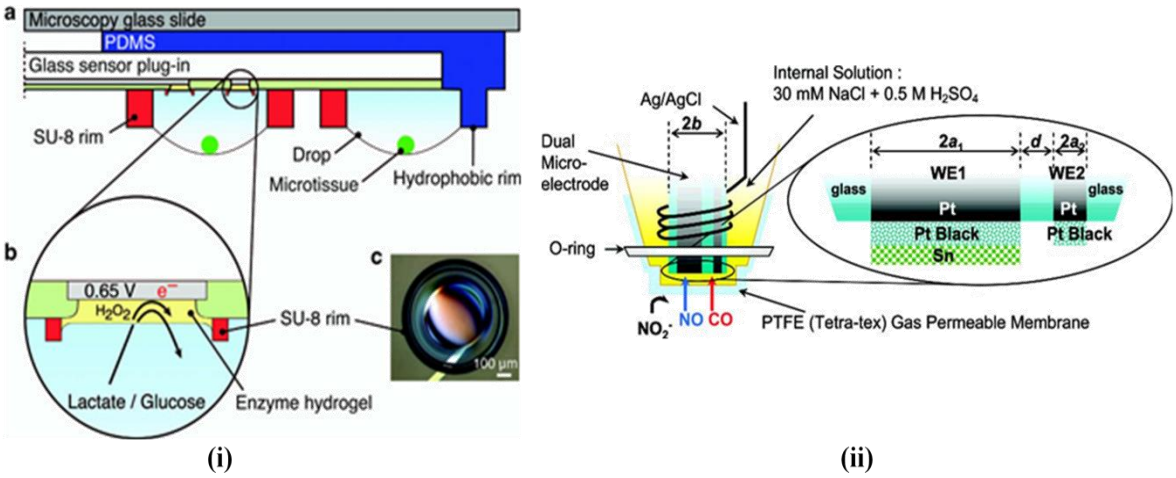

Figure 2.20: Surface functionalised electrodes (i) (a) in a hanging drop network (b) using enzymes trapped in hydrogels. (c) A picture of the hydrogel deposited on a microelectrode [80]. (ii) The electrodes were coated with Pt black or Sn to detect NO and CO respectively [106].

Selective analyte detection is not only possible through enzymatic bio-recognition elements but also with materials that are either selective towards specific analytes or catalyse them. An example for the detection of NO and CO for mouse kidneys used Pt black and Sn surface modified electrodes, shown in Figure 2.20(ii), and a bipotentiostat [106]. A combined approach uses both enzymatic biosensors and selective materials to modify the microelectrodes. This approach was demonstrated in neurotransmiter sensing in two papers, sensing glutamate with the enzyme glutamate oxidase and NO (controlled by a bipotentiostat) [107] or dopamine [108] by the use of permiselective polymers. The latter concurrent detection arrangement was also demonstrated with a slightly different topology in [81]. Carbon nanotubes were used as the microelectrode material and a mediator was incorporated with the enzyme to increase the sensitivity, controlled by a bipotentiostatic CMOS ASIC.

Except for the selective functionalisation of electrodes that usually uses amperometric techniques to distinguish analytes, bare metal or other material electrodes that enhance the signal can be used with voltammetric methods. Voltammetric methods have the advantage of scanning the potential to detect analytes that do not share the same redox potential, even on the same electrode. Electroactive biomarkers and medicines were detected simultaneously in a cyclic voltammogram by separating their current peaks through the use of pyrolytic carbon or carbon nanotube layers on the electrodes. [109]–[111]. However, normal voltammetric techniques require a certain amount

of time to complete, depending on the scan rate. Being a rapid technique, FSCV can be used to that end. The technique was used to detect two neurotransmitters' concurrently as well as the effect drugs had on their in-vivo concentrations [112]. The neurotransmitters redox potentials were identical but voltammograms after the addition of stimulants indicate the readings were independent. Even though these techniques have successfully detected the targeted analytes, cases of convoluted data still exist. Apart from physical separation of mixed compounds of interest, exhaustive computational methods have come to the aid of the modern electrochemist, as explained in the next paragraph.

Computational methods

In all voltammetric methods if the analytes' redox potentials are close to each other, the resulting plot might not be easy to distinguish between analytes for a researcher thus signal enhancing materials are often used. For computing software however the task is not as demanding. The use of multivariate analysis in chemometrics involves the statistical analysis of electroanalytical data to predict the concentration of analytes. The process starts with calibration by the collection of data to model current-concentration maps that are then used to determine the concentrations of analytes in mixtures. Two methods have been used towards this goal. The so called one-way method deconvolutes the signals to their components and performs calibration on the individual analyte's peaks in order to find their concentrations. Examples of this method are the Kalman filter, Fourier transform to the frequency space and the wavelet transform. Even though scientifically important results have been demonstrated by this method, it requires prior knowledge of the number of analytes and it assumes a one-to-one contribution by these electroactive materials to the recorded voltammogram. The two-way method on the other hand, considers the voltammograms as a complete collection of data and analyses them as such. This multivariate approach also takes into account interfacial and other non-predefined phenomena. The two-way method is performed through several approaches, such as principal component regression (PCRe), partial least squares regression (PLS) and artificial neural networks (ANNs) which is a machine learning method. Chemometrics have been used for the filtering of interferents and noise in single analyte measurements, the deconvolution of analytes in

mixed compounds as well as the qualitative determination of e.g. beverages [104], [113]. The importance of the use of amperometric electrode arrays with multivariate analysis for the development of “electronic tongues” was described by Krantz-Rülcker et al. [114]. They demonstrated an application of an electrode array that analysed the water sample quality with normal pulse polarography (a voltammetric technique) on electrodes of different materials followed by principal component analysis (PCA). Ni et al. presented that the use of another voltammetric technique called differential pulse voltammetry (DPV) with a combination of PCRe and PLS could determine the concentrations of individual analytes in mixtures of glucocorticoids or pharmaceuticals (paracetamol and phenobarbital) [115], [116]. Recently, the CMOS integration of multivariate PCRe signal analysis of FSCV signals was presented to result in a system for the accurate and rapid measurement of dopamine [117]. The system acquired cyclic voltammograms every 100 ms from an external microelectrode to determine dopamine levels on a rat’s forebrain and stimulated the brain with another pair of electrodes to maintain the concentration within certain limits. The chemometrics ASIC was used to subtract the background current and interference caused by pH changes, as shown in Figure 2.21.

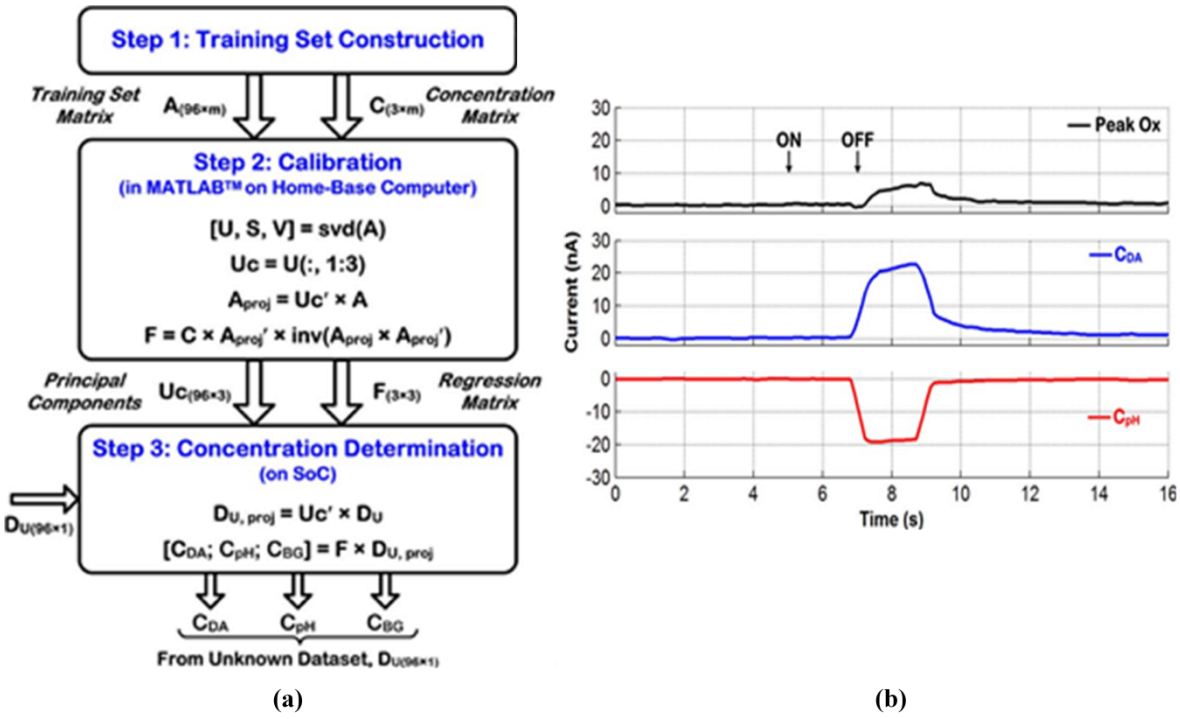

Figure 2.21: The neurochemostat a chemometrics CMOS ASIC for the control of dopamine levels. (a) The PCRe method to distinguish between dopamine levels and the interferents of pH and FSCV background current. (b) An FSCV without any analysis (black) and the deconvoluted components after the analysis [117].

2.7.2 Multiple Voltammetric Method Techniques

The power of multivariate analysis in chemometrics is not only limited to data acquired by a single electroanalytical method or even by a single type of sensor. The very nature of the statistical analysis supports a calibration step using data from different sources. This feature facilitates the use of seemingly unrelated techniques which were not self-sufficient to determine the composition of unknown compounds and construct models that reach the successful analysis of data. Grabarić et al. studied successive complex compounds of Cd(II) ligand metals by performing higher order multivariate analysis of voltammograms collected via several voltammetric methods (DPV, normal pulse polarography (NPP), reverse normal pulse polarography (RNPP) and differential pulse anodic stripping voltammetry (DPASV)) [118]. The combined data from all methods were analysed using PCA combined with alternating least squares (ALS). The results were compared to established "hard modelling" techniques which were based on theoretical descriptions of the system and exhibit a very similar performance. A similar work that used glycine complexes and the voltammetric techniques: DPV, NPP and RNPP was presented in [119]. Chemometrics have also been used with biomarkers and separation of overlapping current peaks. Cukrowska et al. resolved the redox peaks of adenine and cytosine (found as DNA bases or components of coenzymes) by the use of ANNs on either DPV or linear sweep voltammetry (LSV) [120]. The voltammograms before the analysis present wide current peaks that overlap and hydrogen influences the measurements. The ANN proved to be a valuable tool for the electrochemical analysis of these biologically significant analytes. In another work the combination of voltammetric methods through multivariate analysis was shown to be crucial to categorise varieties of teas voltammetrically. In this case PCA was used to analyse large and small amplitude scan voltammetry (LAPV & SAPV respectively) as well as staircase voltammetry, as shown in Figure 2.22. Best results were observed from the combined analysis of LAPV and staircase voltammetry [121]. If applied to an integrated system, the use of computational analysis with concurrent multiple techniques can lead to systems that are able to analyse a wide range of variables performing minimal pre-treatment of the device.

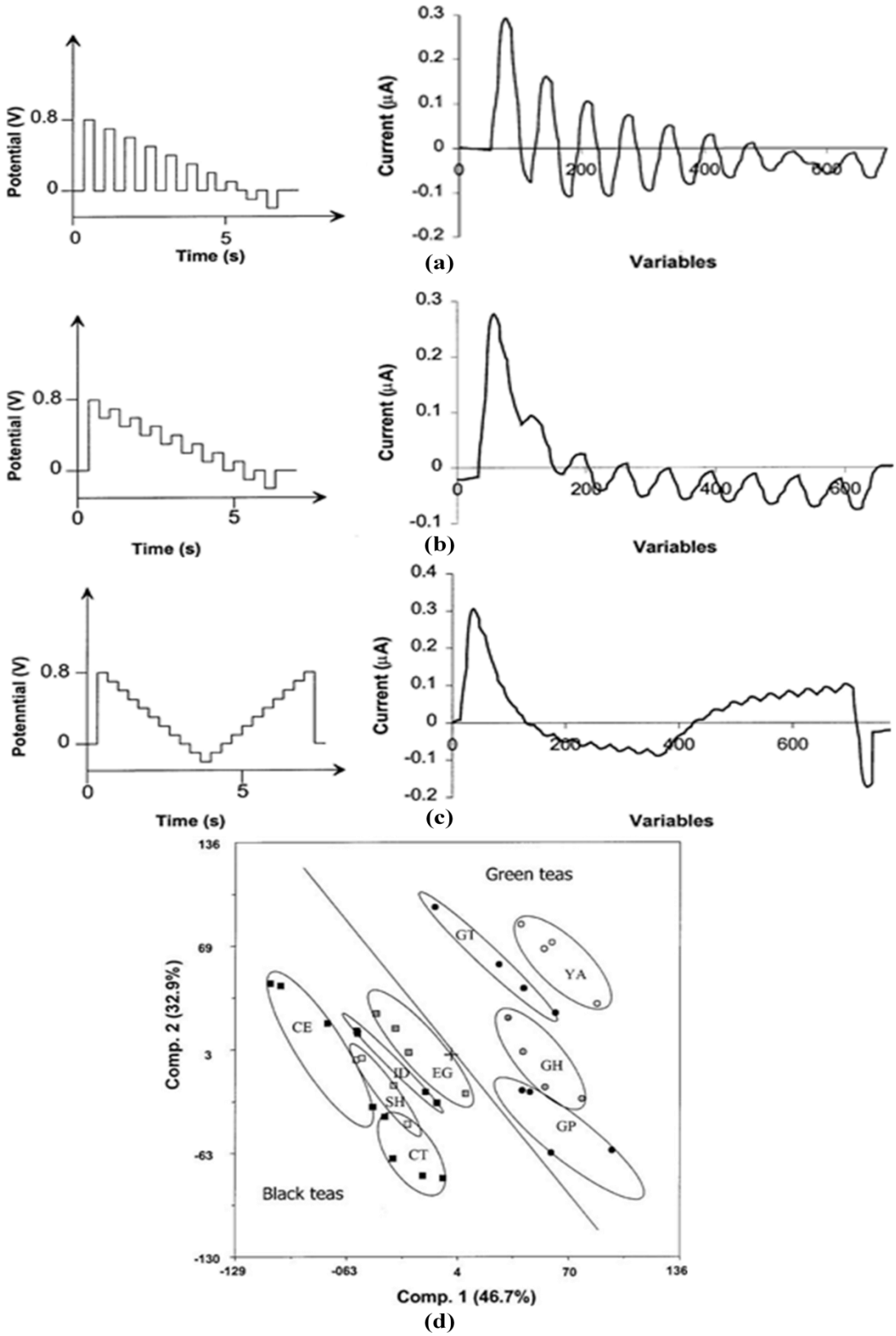

Figure 2.22: Multivariate analysis using tea voltammograms. On the left hand side the operational signals are shown and on the right hand side the resulting signals by the use of (a) LAPV, (b) SAPV and (c) staircase voltammetry. The measurements are plotted against variables (measuring points) instead of time as samples were taken every 300 ms. (d) An example of combined analysis using all three method data is shown [121].

Research on the simultaneous use of FSCV and other techniques has recently been reported in the literature. An example is the use of constant potential

amperometry and FSCV, taking advantage of the small diffusion layer spread caused by the high scan rates [122]. This research was conducted on non-integrated pyrolysed photoresist microelectrodes. However, the electrical cross-talk has not been quantified in these studies [122], [123]. Another system that included a patch clamp and carbon-fibre microelectrodes for iontophoresis and FSCV in a rat's brain was presented by Kirkpatrick et al. [124]. Recently the concurrent measurement of ascorbate with FSCV and neural recordings were shown in [125] by the use of single nanotube modified carbon-fibre microelectrodes. Electrical cross-talk was observed between methods in [124], [125]. FSCV is a good candidate to be used in a multimodal system as it can measure rapid changes and intermediate chemical compounds. However, the need to remove background current and signal distortion by the Ohmic drop as explained in Section 3.4.2 are drawbacks of the method [126], [127].

The research that was reviewed in this section demonstrates the advantages of chemometrics and multivariate analysis, especially when they were used in conjunction with MEAs or parallelised measurements. In order to improve on these remarks, systems that employ multiple electroanalytical methods in a closed environment might be a possible path to enhanced analysis of measurements. To build novel MEA systems, electrode configurations need to be investigated. One way to estimate the response of electrochemical setups is through numerical simulations using computational software, as explained over the next section.

2.8 Electrochemical Simulation Methods

Computational methods in electrochemistry are not only used for statistical (multivariate) analysis. The construction of models in that case is based on on-site experimental measurements. Other models that describe the physical phenomena in an electrochemical setup are constructed through the theoretical study of electrochemistry, often referred as "hard modelling". These models, which have been developing for decades, are used in simulation programs to predict and study the behavioural response of the described electrochemical setups e.g. new MEA geometries in a chemical solution. Digital simulation became widespread by the advent of computers and their ability to perform computations in large datasets. In order to design a simulation to represent

space, various methods can be used. The investigation to construct a CMOS ECM entails not only the design of circuits but also microelectrodes and how they interact in an electrochemical environment. The digital simulation of electrode subsets and how their structure affects the overall system performance can provide useful information for this study. The most prominent numerical techniques, some of which are used in commercial packages, are described over the next paragraphs.

The electrochemical realm is governed by phenomena regarded as diffusion, convection (the movement of the solution), migration (movement of molecules as a result of an electric field) and chemical reactions. These phenomena are described by partial and ordinary differential equations. When they are transferred into space they can be approximated into a discrete form in order to be solved by numerical methods. Several methods have been used to approximate the set of differential equations; most of them are based on the finite difference method (FDM) and apply to 1 dimensional (1-D) problems. For higher dimensions problems are solved individually for each dimension, a depiction of the method into a grid of points is shown in Figure 2.23(a). Taylor expansion is used to approximate the differential equations between points in these methods. Another popular method was Feldberg's box method which is a finite volume method (FVM) that uses Fick's law to describe the flux in and out of a box of a set volume in an arrangement of concomitant boxes, as shown in Figure 2.23(b). The most recent methods that are used for 2-D & 3-dimensional (3-D) cases are the finite element method (FEM) and the boundary element method (BEM). These methods are oriented towards an integral form of the partial differential equations and are able to solve complex geometries as they can function in discontinuities and complex boundary conditions. The FEM uses nodes in a mesh with defined algebraic solutions of the differential equations, depending on the density of the grid the FEM can provide detailed simulation of an electrochemical nature, a depiction of an FEM grid is shown in Figure 2.23(c). The BEM only requires the modelling of boundary surfaces thus the computational effort is lower and it is considered a more accurate method, as shown in Figure 2.23(d). However, the BEM lacks of detailed simulation and often a combination of the two methods is chosen[128]. Another method that was first explored by Horno [129] is the network method. This method translated

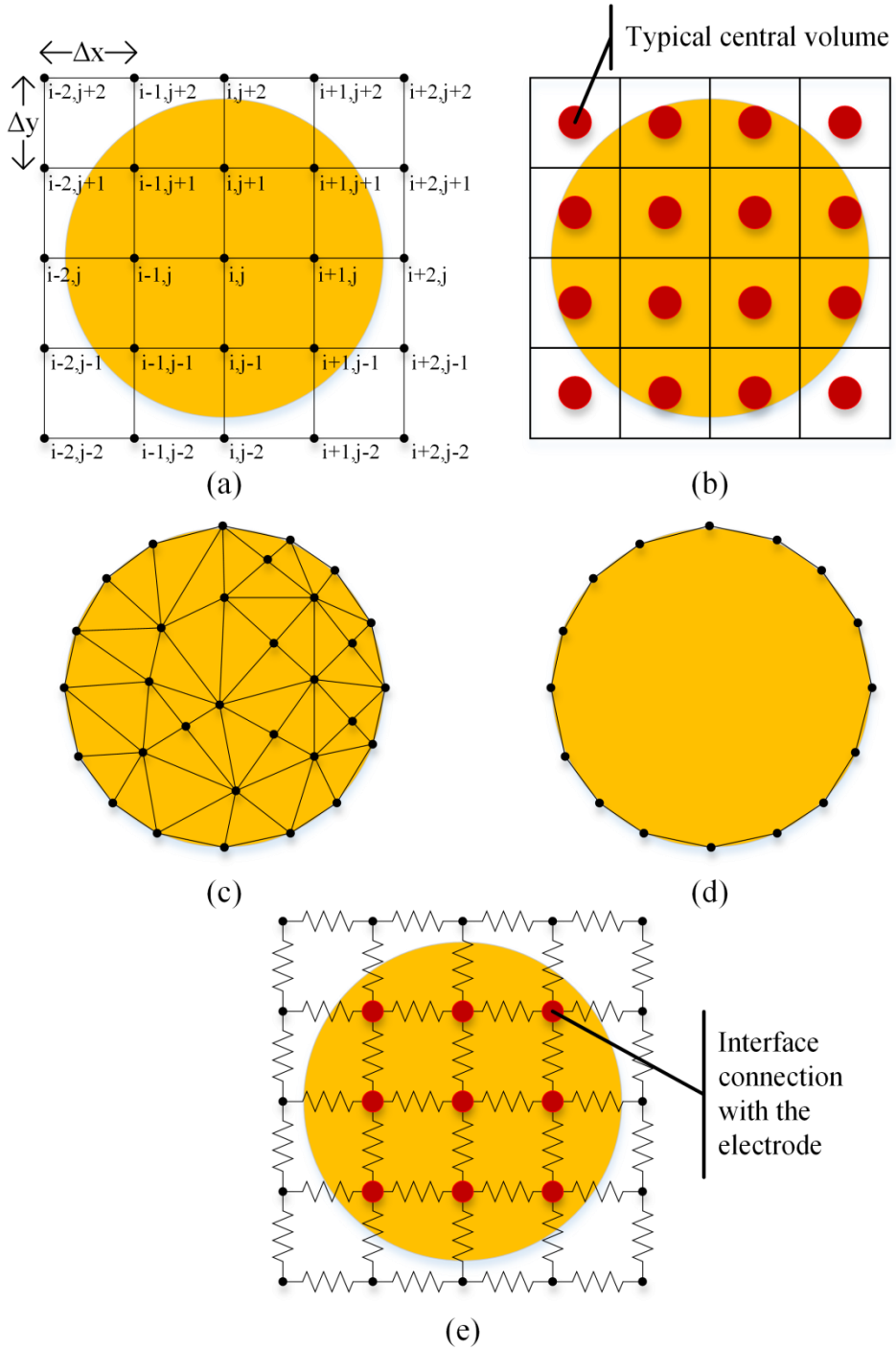

Figure 2.23: Schematic representation of a round electrode and the constructs that need to be developed to simulate it in (a) a finite difference method, (b) a finite volume method, (c) a finite element method, (d) a boundary element method and (e) a resistor grid method.

the system of electrochemical equations into an electrical circuit in the form of a network to be solved by electrical simulation software such as PSPICE and HSPICE. Even though the method has not been adopted widely, it commenced the concept of using electrical software for electrochemical simulations as shown in the next paragraph [130].

Coles et al. presented a method that used a resistor mesh with values based on the solution's conductivity to simulate the potential distribution in wall-jet

electrodes [131], a representation of the method is shown in Figure 2.23(e). In a consecutive publication they demonstrated the generation of potential maps by successive simulations of a 3-D resistor mesh in SPICE that resembled the electrolyte conductivity of a channel-electrode flow cell [132]. The electrode-electrolyte interface was modelled as a simple diode with an adjustable limiting current. A backward-implicit difference method was used with different limiting currents to reproduce a Tafel slope and simulate for mass transfer from SPICE data. A similar 2-D resistor mesh approach was adopted by Hung et al. to simulate the effect of the electrode surface structure in MEAs for visual prosthesis applications [133]. The electrode-electrolyte interface at the surface was modelled by elements of capacitive and resistive impedance in parallel, connected to the mesh of resistors. Potential and current maps were produced by HSPICE simulations. The resistor mesh method is a promising technique, especially if combined with modern IC simulation tools such as Cadence.

Numerical methods are the most widely recorded methods for electrochemical simulations, the commercial package COMSOL uses a combination of FEM and BEM in its Multiphysics package. There are several examples in the literature of these methods being used to model the modulation of the potential, electric field (E-field), current or diffusion by the exploration of electrode geometries in MEAs. Simulations of the media in a large scale electrode matrix used in conductometric experiments was demonstrated in [134]. The electrode potential maps were simulated using the BEM and they were verified by measurements of an experimental setup. The configuration of electrodes at different potentials simultaneously was explored and potential maps were generated. In epiretinal prosthesis a technique named current focusing used surrounding electrodes to

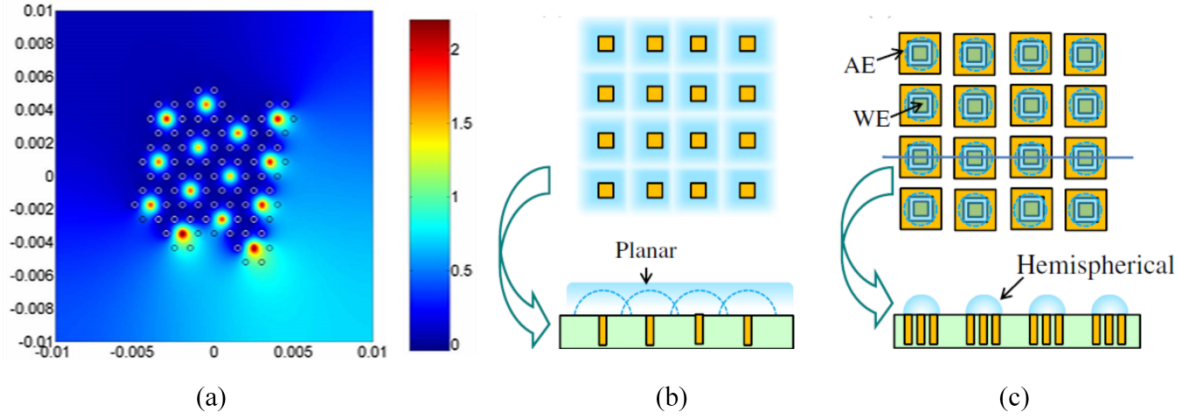

Figure 2.24: (a) Potential map of stimulating electrodes with surrounding return electrode rings [135]. (b) The diffusion layers with a conventional MEA and (b) with local CE rings [71].

form isopotential islands around a current injecting stimulating electrode. In [135] a finite difference method was used to simulate the potential distribution of concurrent current injecting electrodes, as shown in Figure 2.24(a). Khalili Moghaddam et al. used the FEM to simulate the E-field distribution of the surrounding structure. Overlapping E-field layers from neighbouring structures were noted as a source of electrical cross-talk and the need for their spatial control was indicated [136]. Flores et al. used HSPICE to define the boundary conditions and COMSOL to simulate the effect of surrounding electrode groups operating simultaneously on the E-field in 3-D [137]. The results were experimentally verified and a current leakage limitation was recorded. For electroanalytical applications it has been stated that the distance between WEs affects the diffusion layer shape and type [138], [139]. When the WE pitch is above a certain value the diffusion layers do not overlap and they remain independent. Using the COMSOL Multiphysics package, it was recently proved by Hasegawa et al [71], [140] that CE rings around the WE assist for the confinement of the diffusion layers of these pairs, as shown in Figure 2.24(b) and (c). Therefore chemical cross-talk among WEs in the MEA was reduced. This approach can lead to more dense MEAs at the same performance standards.

2.9 Summary

Electroanalysis is a field traditionally involved in biochemistry. From its sectors amperometry/voltammetry appears to be the most efficient in making a platform with many analytical regions due to its ability for selective imposition of charge-transfer to different ions. Implementing such an analytical device with microelectrodes in a MEA format not only would prepare it for portable applications but it would also enhance its response towards lower concentration sensing. It was shown that the integration of MEAs in CMOS technology has revolutionised the production, accuracy and sensitivity of these devices. Plenty CMOS MEA circuit designs and ASIC architectures have been found in the literature. The design of the bipotentiostat [31] inspired the development of a CMOS MEA capable of applying many amperometric settings on subsets of microelectrodes [79]. Modular architectures can make for independent subsystems on-chip rather than changing the offset as a bipotentiostat [52], [72], [73]. Similarly the use of fully differential potentiostats [57], [58] in a modular architecture can auto-adjust the voltage of subsets of electrodes for

many voltammetric methods to coexists in a chemical solution as simulations indicated in Chapter 4 and results verified in Chapter 6. From simulation methods presented in this chapter the use of a resistor mesh in electrical simulation software appears as a method to investigate both electrochemical interactions and integrated circuits. A coaxial geometrical arrangement of electrodes was shown to limit the diffusion over individual WEs [71], [140], the electrical response of such an arrangement and its electrical isolation with other electrode subsets is explored in Chapter 4. Creating an ECM that can perform many independent amperometric/voltammetric experiments can provide simultaneous results not previously possible but techniques for their analysis have already been reported to interpret similar data. Results presented in Chapter 6 show exhibit a possibility for computational methods to be used for a their combinatory analysis. As it was explained, the use of ferrocene has many implementations with biorecognition elements that could be applied in a CMOS MEA and it has been used as a calibrant for organic electrochemistry, thus it will be used for the verification of the system developed in this study. In the next chapter the theory of electrochemical cells and electrode kinetics will be explained. This theory will be used in the rest of the chapter in simulations for the cross-talk between electrochemical cells. Based on these simulations the design of the ASIC will be presented.

3 Theory

3.1 Introduction

The previous chapter reviewed the literature aiming at applications and design approaches for the development of a CMOS integrated independent electrochemical cell microarray (ECM) made of microelectrodes. This chapter describes the theory and operation of electrochemical cells in electroanalytical applications. First the terminology and equations that govern electrochemical systems are explained. More specifically the relation between the increase of the potential energy to the induced electrical current according to the ionic concentration is discussed. The processes that govern this relation mainly occur at the interface between the electrode and the solution which is described and modelled on an established theoretical basis as an electrical circuit equivalent. The chapter then provides an overview of the wide range of electroanalytical methods and the cross-talk phenomena that can be found in MEAs. Finally, tactics to reduce this cross-talk through physical design and chemical means are provided.

3.2 Electrochemical Cells

The movement of charge is the main effect that is monitored when investigating electrochemical phenomena. Particularly interesting is the charge accumulation or charge transfer at the interface of materials of a different nature (called phases) i.e. an electrode (called an electrical phase) and an ionic solution (a chemical phase). Electrochemical phenomena cannot be studied at a single interface but a collection of phases that construct a conducting path, called an electrochemical cell. An electrochemical cell is a closed system which consists of two or more electrodes immersed in a chemical solution. Those electrodes are named anode and cathode only by the type of ions that populate around them. If anions (negatively charged ions i.e. the oxidized form of a compound) populate around an electrode it is called an anode. Equally cations (positively charged ions i.e. the reduced form of a compound) populate the cathode [5]. The words anion and cation originate from the Greek words άνω (áno) and κάτω (káto) which mean, “up” and “down”, respectively. These terms refer to the charge movement direction of electrons from anions to the electrode (“upwards” and

away from the ion) at the anode. And from the electrode to the cations ("downwards" and towards the ions) at the cathode.

The reason why certain types of ions populate different electrodes is divided in two different cases that make two types of electrochemical cells. The first case is found in a galvanic cell which has the structure of a battery, as shown in Figure 3.1(a). In a galvanic cell the electrodes are made of different materials which have their own electronegativity (a measure of the ability of an atom of a material to attract electrons). The electronegativity of each electrode attracts a certain type of ion which charges the electrode to become a positive or a negative electrode. Thereof the electrical and chemical phases of a galvanic cell dictate the potential difference between electrodes, called an open circuit potential. Potentiometry is based on galvanic cells to sense the concentration of analytes (compounds of interest) through changes in the potential. If the electrodes of a Galvanic cell were connected to an external load spontaneous reactions would occur converting chemical energy to electrical energy with an electron flow from the the negative electrode (cathode) to the positive electrode (anode). The other case is found in electrolytic cells in which electrodes can be even from the same material composition and they are connected to an external power source that applies a voltage, as shown in Figure 3.1(b). The applied voltage value is set greater than the inherent open-circuit potential of the system. The voltage source forces the electrodes to attain a

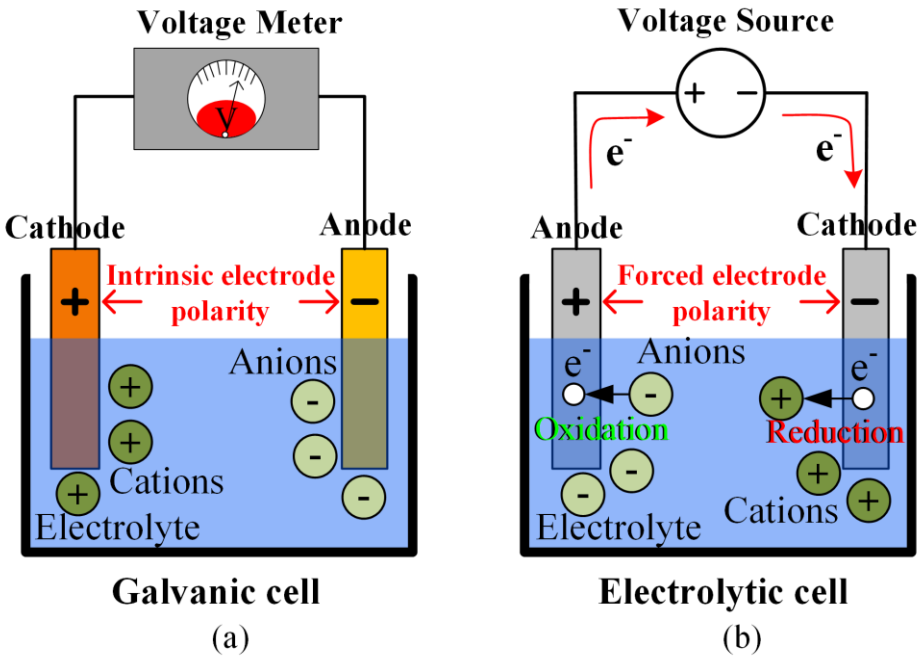

Figure 3.1: Illustration of (a) a galvanic cell and (b) an electrolytic cell.

certain polarity and chemical reactions occur at the expense of electrical energy. The ion types that are attracted around the electrodes are opposite to the polarity of the electrode in this case. However, the electrode names only depend on the type of ions that populate around them, thus in this case the anode and cathode have opposite signs than in a galvanic cell [31]. Amperometry/voltammetry is conducted in an electrolytic cell setup. A microelectrode array in a chemical solution with its driving potentiostat is essentially an electrolytic cell.

The chemical solution consists of: a solvent (usually a liquid that is capable of dissolving chemical species e.g. H_2O), a supporting electrolyte e.g. NaCl (a chemical compound that when dissolved in a suitable solvent or when fused becomes an ionic conductor) to reduce the chemical solution resistance and the analyte (the chemical compound of interest like H_2O_2). The solvent breaks the bonds of salts and results in an ionic solution of positive and negative charges. In the simple case of a two-electrode cell such as the ones shown in Figure 3.1, the system is comprised of two half-reactions that occur on each of the electrodes. An example of a pair of half-reactions is:

$$\begin{cases} H_2O_2(aq) \rightarrow 2H^+(aq) + O_2(g) + 2e^- \\ Na^+(aq) + e^- \rightarrow Na(s) \end{cases} \quad (3.1)$$

In the first of these reactions the analyte of interest (H_2O_2) is involved and in order to monitor it the current or the potential is measured at that electrode, called the working electrode (WE). The potential of the WE is always referenced to that of the other electrode, called the reference electrode (RE) which material is chosen so that it maintains a stable composition in order for that half-part of the cell to be standardised. More details on the choice of WEs and REs are given in Section 3.2.2. The magnitude and sign of the potential that appears at an electrode-electrolyte interface is a measure of the energy and direction of charge-transfer between the electronic states of the metal and the ions accumulated in the electrolyte phase at the surface of the electrode [22]. The direction of the current is a confusing parameter in electrochemical cells, a convention is always made for the definition of the sign. In this work the direction of current from the electrode to the electrolyte (an anodic or

oxidation current), as shown on the anode of Figure 3.1(b), is considered as positive. Accordingly a cathodic or reduction current is considered as negative.

The potential difference that can be measured between the electrodes is subject to the thermodynamics and kinetics of the electrochemical cell. In order to study the system thermodynamically, an essential concept that needs to be defined first is that of reversibility. There are three types of reversibility in electrochemical systems. Chemical reversibility relates to the reversibility of the chemical reactions if the driving force changes its direction. Some reactions are irreversible, depending on how accompanying compounds in the chemical solution might affect the reverse reaction as well as on the time scale of the experiment. The processes might also be chemically reversible for a short period of time. Another type is thermodynamic reversibility. The concept is based on infinitesimal changes of a driving force to a system at thermodynamic equilibrium. A system is thermodynamically reversible if it can transition from one state to another through a path of infinitesimal steps at equilibrium. In reality these steps would require a very accurate and long transition. The third type of practical reversibility is a more realistic approach. The applied changes are considered reversible when they are slower than the processes that preserve the equilibrium. Practical reversibility employs a perspective of real-life situations on both chemical and thermodynamic reversibility.

In electrochemistry one is interested in how the equilibrium is maintained at induced reactions. Faraday was one of the first researchers whose work was on the characterisation of electrochemical processes. Processes of oxidation and reduction where the current is relative to the amount of ionic reactions are defined as Faradaic. These processes obey Faraday's law:

$$Q = \frac{mzF}{M} \text{ or } N = \frac{Q}{zF} \tag{3.2}$$

where m is the mass of the substance, Q is the charge that passed through, M is the molar mass, F is Faraday's constant, z is the valency number of ions of the substance (electrons transferred per ion) and N is the number of moles. The rate of a reaction can be found by: *Rate* (mol/s) = $\frac{dN}{dt} = \frac{i}{zF}$. Other processes such as adsorption, desorption, mass transfer (migration, diffusion, convection) and

charging of a layer of ions (electrical double layer) that forms a capacitor can also occur in an electrochemical system and they are denoted as non-Faradaic. These processes change the distribution of ions inside the solution and when studied they provide information on the system's composition. Faradaic processes were also studied later by other researchers. The Nernst equation and the Butler-Volmer model (explained in Sections 3.2.1-3.2.2) are part of these studies and they require the reactions to be at equilibrium, such a behaviour at the electrode is called Nernstian. In a typical system the charge-transfer reactions are processes faster than mass transfer, thus while the concentrations of reactants at the electrode are considered to be at equilibrium the reaction rate is dominated by mass transfer. In order to diminish the effects from mass transfer, a supporting electrolyte at a much higher concentration than the analyte is used to prevent migration and the solution is not disturbed mechanically to prevent convection effects [31]. The theoretical basis that describes charge transfer across an interface as well as a description of the redox potentials at which reactions occur are explained in the next sections.

3.2.1 Redox Potential and Potential Windows

One of the most important thermodynamic theoretical expressions used in electrochemical cells that was introduced in the previous section is the Nernst equation. In an electrochemical cell the half-reactions at the two electrodes may be described by:

$$\begin{aligned} Ox_1 + z_1e^- &\Leftrightarrow Red_1 \\ Ox_2 + z_2e^- &\Leftrightarrow Red_2 \end{aligned} \tag{3.3}$$

where Ox_i and Red_i represent the oxidised and reduced state of the chemical species i, respectively. z_i is the number of electrons that participate in an occurrence of the reaction for species i. Both electrodes half-reactions constitute the system reaction:

$$v_1Red_1 + v_2Ox_2 \Leftrightarrow v_2Red_2 + v_1Ox_1 \tag{3.4}$$

where v_i is the stoichiometric number for species i. The electromotive force of the cell taken as the potential difference between the electrodes according to this reaction is:

$$E_{cell} = \frac{1}{zF}\left(v_1\mu_{Red_1} + v_2\mu_{Ox_2} - v_2\mu_{Red_2} - v_1\mu_{Ox_1}\right) \quad (3.5)$$

where E_{cell} is the electromotive force (equilibrium cell potential), where $z = z_1v_1 = z_2v_2$ and μ_i is the chemical potential for species i. The term in the brackets on the right of equation (3.5) matches to the Gibbs free energy of a reaction, according to:

$$\Delta G = -zFE_{cell} \quad (3.6)$$

where ΔG is the Gibbs free energy. Therefore the standard Gibbs free energy is:

$$\Delta G^0 = -zFE^0{}_{cell} \quad (3.7)$$

where $E^0{}_{cell}$ is the standard equilibrium potential. The thermodynamics laws for Gibbs free energy in a chemical system give:

$$\Delta G = \Delta G^0 + RT\ln K = \Delta G^0 + RT\ln\frac{a_R^{v_R}}{a_O^{v_O}} \quad (3.8)$$

where R is the gas constant, T is the absolute temperature, K is the equilibrium constant and a_R, a_O are the activities of the reduced and oxidised species respectively. The Nernst equation is derived by the substitution of the ΔG and ΔG^0 terms in equation (3.8) and becomes:

$$E_{cell} = E^0_{cell} + \frac{RT}{zF}\ln\frac{a_O^{v_O}}{a_R^{v_R}} = E^0_{cell} + \frac{RT}{zF}\ln\frac{\gamma_O C_O^*}{\gamma_R C_R^*} \quad (3.9)$$

where γ_i is the activity coefficient and C_i^* is the bulk concentration of species i in the solution. The standard potential $E^0{}_{cell}$ is the measure of the electromotive force of an electrochemical cell under a 1 atm pressure and 1 M concentration of

ionic species at 25 °C that does not take into account thermal effects and the diffusion potential. The equation (3.9) can be rewritten as:

$$E_{cell} = E^{0'}_{\text{cell}} + \frac{RT}{zF}\ln\frac{C^*_{\text{O}}}{C^*_{\text{R}}} \tag{3.10}$$

where $E^{0'}_{\text{cell}}$ is the formal potential, defined as:

$$E^{0'}_{\text{cell}} = E^{0}_{\text{cell}} + \frac{RT}{zF}\ln\frac{\gamma_{\text{O}}}{\gamma_{\text{R}}} \tag{3.11}$$

The standard potentials of several electroanalytical compounds have been measured, tabulated and archived in the literature [31]. The use of the formal potential has the advantage of incorporating the activity coefficients of the redox species as well as other components included in the solution within the term. It is often a simpler and the preferred notation as repeatable compositions will give the same result. The known redox potential values of the compounds are organised in tables and they are used as a reference to determine the composition of a chemical solution and help estimate the presence of new compounds. The Nernst equation is a very useful expression that is used to find the concentration of reduced and oxidised species from the potential value and vice versa. However, the equation is only valid for fully reversible reactions when the system is in equilibrium. The shift of a redox potential can also provide information on the system. The redox potential determination of an electroactive compound depends on the solvent, supporting electrolyte and the material of the electrodes used in an electrochemical cell. These components can decompose at certain potentials set in an electrolytic cell. In order to keep them inert an electrolytic cell needs to be operated over a certain voltage range, called a potential window. For example, water has a potential window that ranges from −1.4 V to 1.4 V, meaning that if amperometry/voltammetry was performed at voltages outside this voltage range the solvent (water in this case) would be decomposed. The solvent's decomposition overshadows the charges from the analyte's redox reactions and creates an unstable chemical environment for analysis. That voltage range is specific for metals of the platinum group that catalyse the hydrogen evolution reaction as normally the

oxygen-evolution reaction ($2H_2O(l) \rightarrow O_2(g) + 4H^+(aq) + 4e^-$) occurs at E^0_{cell} = 1.23 V vs NHE (normal hydrogen electrode) [31], [22], [141]. Limiting the potential window around the formal potential of the analyte of interest prevents the development and interactions with undesired compounds that can limit the current response from the analyte at the working electrode. The kinetic charge-transfer characteristics of the electrode-electrolyte interface are explained in the next section.

3.2.2 Electrode Kinetics

The choice of materials and the underlying function of electrodes are important attributes that need be explained for the operation of a MEA to be understood. Each electrode used in an electrochemical cell has features that dictate its use as a working electrode (WE) or a reference electrode (RE) in a two-electrode system. The electrode-electrolyte interface consists of several layers of charges that are part of an ionic capacitor between the electrode and ions, called the electrical double layer. Charges that appear at the electrode phase due to the applied potential (E) cause the rearrangement of ions in the electrolyte phase so that the charge densities cancel each other and act as a capacitor (between the electrolyte and the electrode). However, this capacitor's size is not defined in the electrolyte phase and it is dependent on E thus an average value is used to approximate its value. The formation of the electrical double layer will be further explained in Section 3.3.1. The application of E causes a charging current of the ionic capacitor to flow along with charge-transfer currents. The passage of charge through an electrode-electrolyte interface is termed as a heterogeneous reaction (between the different electrical phase of the electrode and the chemical phase of the solution) in contrast to reactions that occur in the solution between ions termed as homogeneous reactions.

When an electrolytic cell is at equilibrium, an equilibrium potential (E_{eq}) set by the charge coordination of ions around the electrode is maintained. To induce charge transfer the system needs to be biased at a potential that exceeds E_{eq} according to $\eta = E - E_{eq}$, where η is termed as an overpotential. The process is called polarisation as the system is disturbed by the change of the potential and the ends of the ionic capacitor attain a polarity before electrons transfer between the two phases and a new state of equilibrium is reached again. If no

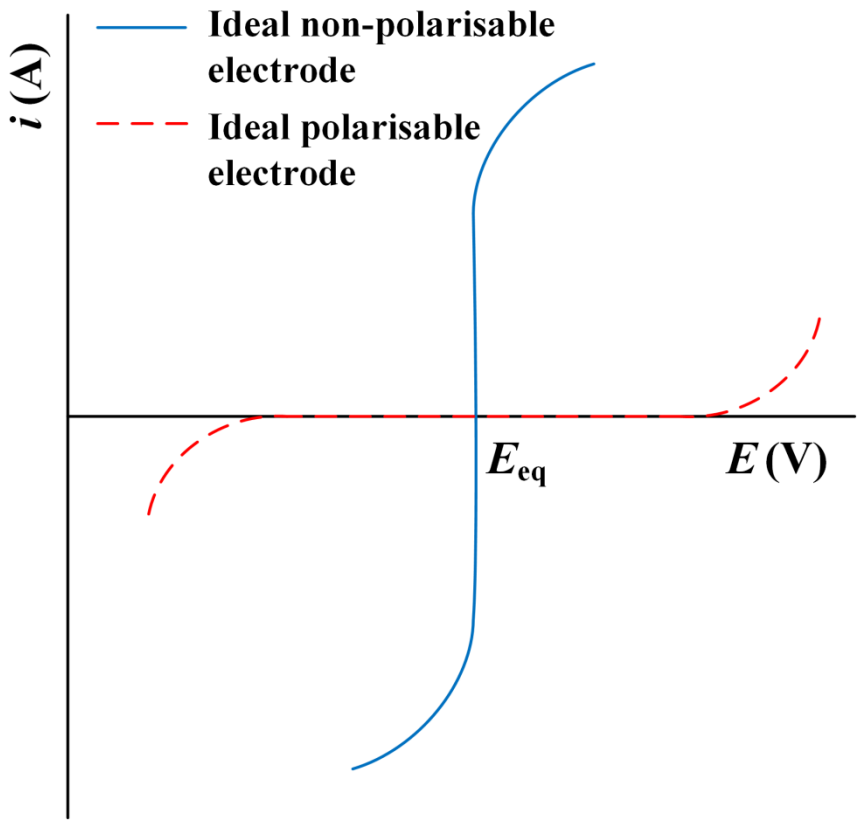

Figure 3.2: i-E curves of real electrodes that approach the performance of an ideal polarisable electrode and an ideal non-polarisable electrode.

charge-transfer is assumed to occur at the electrode then it is called an ideal polarisable electrode. An ideal polarisable electrode does not allow Faradaic behaviour of charge-transfer, making it essentially a non-conductive electrode for redox reactions. Even though such electrodes do not exist in reality, there are electrodes that approach this behaviour for certain potential windows and an infinitesimal amount of current passes through, as shown in Figure 3.2. Ideal polarisable electrodes are suitable for the stimulation and recording of potentials in potentiometric experiments. On the contrary, an ideal non-polarisable electrode is a highly conductive electrode that maintains its potential no matter the amount of current that passes through, as shown in Figure 3.2.

REs usually approach the behaviour of ideal non-polarisable electrodes as the current does not influence their behaviour and they can be used as standards for the characterisation of electrochemical systems. There is a wide availability of REs, selectively chosen depending on them being appropriate for the electrochemical system under observation. E.g. the Ag/AgCl RE can be easily manufactured and has a smaller temperature coefficient than the saturated

calomel (SCE) RE. In many cases REs are kept in saturated electrolyte solutions with semi-permeable membranes to keep the charge density of ions at the electrode surface at an essentially standard value. The REs potentials have been characterised and tabulated with their corresponding potential, which can be found in the literature. When standard REs (i.e. in non-aqueous solvents) cannot be manufactured, quasi-REs are used instead. In order to calibrate quasi-REs against a standard RE, a known reaction that exhibits Nernstian behaviour in most systems such as the ferrocene/ferrocenium (Fc^0/Fc^+) redox couple is used. In the scope of this work an ideal non-polarisable electrode would be a good candidate as a WE. However, other factors such as the biocompatibility limit the choice to noble metals such as Au that do not oxidise and have a response that lies somewhere in between the two electrode types.

In amperometry/voltammetry the output of the electrolytic cell is the current which is a result of redox reactions between the analyte and the electrode that occur due to the imposed potential difference. In order to describe the relation of the induced current to the electrolytic cell overpotential the Butler-Volmer equation is used. The equation accounts for charge-transfer exchange net currents induced by a change over the equilibrium potential. Its expression is:

$$i = i_0 \left[\frac{C_O(0,t)}{C_O^*} e^{-\frac{azη}{U_t}} - \frac{C_R(0,t)}{C_R^*} e^{\frac{(1-a)zη}{U_t}} \right] \tag{3.12}$$

where z is the number of electrons being transferred per reaction, $C_i(0,t)$ is the surface concentration of species on the electrode (at $x = 0$), x is the distance from the electrode, a is the transfer coefficient of the reaction, $U_t = RT/F$ is the thermal potential and i_0 is the equilibrium exchange current calculated by $i_0 = AFk^0 C_O^{*(1-a)} C_R^{*a}$, where k^0 is the standard rate constant [142]. The exchange current i shows the magnitude of either anodic or cathodic currents and how it increases exponentially in relation to the overpotential changes, as shown in Figure 3.3 (where the equilibrium potential is maintained at $\eta = 0$ V as expected). The transfer coefficient (a) is a measure of the symmetry of the energy barrier between oxidation and reduction reactions. For well stirred solutions, the bulk (in the volume of the electrolyte away from the electrode)

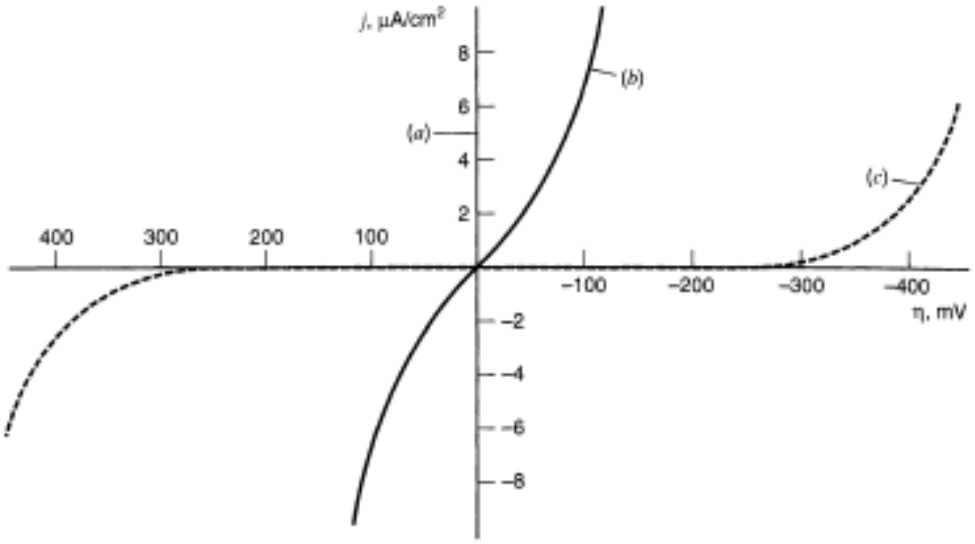

Figure 3.3: Current-overpotential curves for different values of the equilibrium exchange current density. (a) $j_0 = 10^{-3}$ A/cm^2, (b) $j_0 = 10^{-6}$ A/cm^2 and (c) $j_0 = 10^{-9}$ A/cm^2 [31].

and surface concentration become identical (so that $C_i(0,t)/C_i = 1$, where i is the species state) and equation (3.12) simplifies to:

$$i = i_0 \left[e^{-\frac{azn}{U_t}} - e^{\frac{(1-a)zn}{U_t}} \right] \tag{3.13}$$

Even though the Butler-Volmer equation is not going to be derived in the context of this work, it is a result of the Nernst equation and Faraday's equation [143]. At equilibrium the net current flowing through the interface is zero, meaning that the anodic and cathodic currents are equal and the equation equals to i_0. The value of i_0 is linked to the activation energy required by the overpotential to start the reaction. In Figure 3.3 the exchange current density j_0 (the normalised value of the exchange current that takes into account the surface area of the electrode) is plotted against the overpotential (η). It is shown that for low values of j_0 the overpotential needs to attain very high values to overcome the inertia of internal kinetics and cause the current density to increase, the observed behaviour is closer to an ideal polarisable electrode. As j_0 increases the current responds acutely to small changes of the overpotential, behaviour indicative of a non-polarisable electrode. Other effects that have an influence on the current such as mass transfer will be explained in Section 3.3 [31].

3.2.3 The Three Electrode Cell – A Potentiostat

For amperometric/voltammetric experiments the current that is measured as a result of the applied potential depends on the heterogeneous processes as described in Section 3.2.2 and other effects such as the electrical double layer. However, in the simple case of a two-electrode system using non-polarisable electrodes at both ends, the effects of thermodynamics can be neglected. In that case the applied potential does not only cause kinetic effects but also a potential drop from the solution, resulting in a smaller value actually being applied at the two ends of the electrode-electrolyte interface. This potential (*iR*) drop is essentially an Ohmic drop caused by the passage of current on the solution resistance. For an applied potential $E_{applied}$ by e.g. a power supply unit the distribution of the potential can be expressed as:

$$E_{applied} = E_{eq} + \eta + iR \tag{3.14}$$

the magnitude of the *iR* drop depends on the distance between the electrodes as well as the solution conductivity, as shown in Figure 3.4(a).

In order to compensate for the *iR* drop a three-electrode system is often used. In this arrangement, a third electrode named a counter electrode (CE) is added to the system, as shown in Figure 3.4(b). The potential is applied between the CE and the WE, while the RE is connected to a high impedance node so that practically zero current passes through it. The RE is placed in close proximity to the WE to have a negligible *iR* drop. The open circuit potential of the RE is

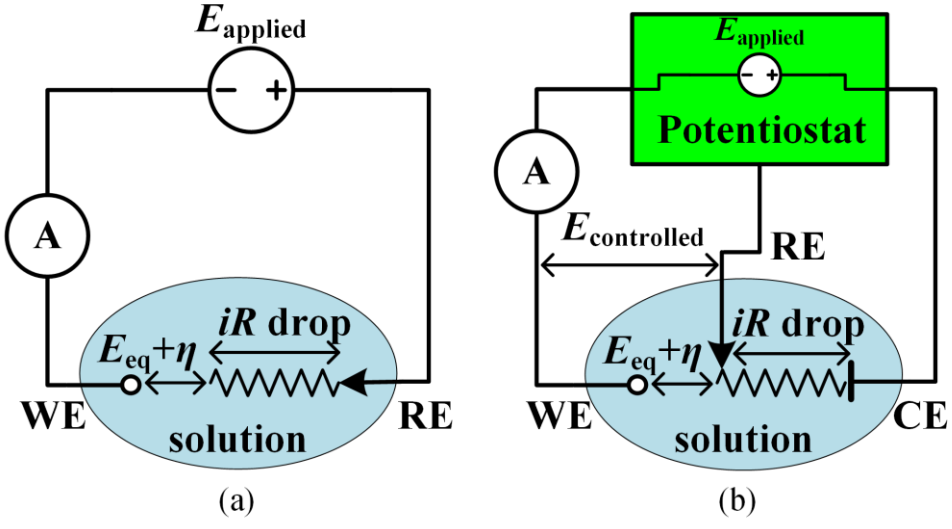

Figure 3.4: The potential distribution in (a) a two-electrode and (b) a three-electrode system.

maintained and the potential between the WE and the RE ($V_{WE\ vs\ RE}$), defined as $E_{controlled}$ for the context of this work, is controlled through a feedback loop. The CE acquires an excessive potential value in order to maintain $E_{controlled}$ through the chemical solution's resistive behaviour. The CE is chosen to be made of an inert material as it is important not to contaminate the solution with any decomposable products or alter the potential control of the electrochemical cell. The CE has to source a large amount of current and should have a minimal effect on the WE potential. This implies that it should have larger dimensions and placed relatively further away from the WE. To control such an electrochemical setup a potentiostat is used. Some examples of potentiostats were reviewed in Section 2.5.1. Nevertheless, unless the RE is exactly at the surface of the WE not all potential drop is compensated and a small amount still remains. In the next section the phenomena that appear at the electrode-electrolyte interface that can be interpreted as electrical components in an electrical model are discussed.

3.3 The Electrode-electrolyte interface

As discussed in Section 3.2 the interface, where different phases interact, is a very important component of an electrochemical cell that is studied for Faradaic and non-Faradaic processes. All the phenomena studied in voltammetry are explained by the theoretical analysis of the electrode-electrolyte interface that is provided in this section. The electrode-electrolyte interface is responsible for the development of a potential at an electrode as it is the collection of charged species accumulated and arranged according to electrochemical thermodynamics and kinetics [141]. The current that is measured at the electrode is a consequence of several processes that occur at this interface. The electrical double layer is accountable for non-Faradaic phenomena of charging currents to an equivalent capacitor made of the arrangement of ions and charges at the electrode phase. Apart from the electrical double layer, it was mentioned in Section 3.2.2 that for the electrode to overcome the equilibrium state of zero net current a certain overpotential needs to be applied. However, charge transfer is not the only factor that affects the total overpotential value. Other factors are:

1. Mass transfer which includes diffusion (movement of molecules as a result of a concentration difference), migration (movement of molecules as a result of an electric field) and convection (the movement of the solution). However, for undisturbed solutions and a supporting electrolyte at a high concentration only diffusion of reactants is influential.

2. Chemical reactions (homogeneous and heterogeneous) that occur before or after charge transfer reactions.

3. Surface reactions, including crystallisation, adsorption and desorption.

A schematic representation highlighting these processes and the order in which they occur is shown in Figure 3.5. The total overpotential is a sum of the overpotentials that relate to these processes according to $\eta = \eta_{ct} + \eta_d + \eta_{rxn} + \eta_c$, where η_{ct}, η_d, η_{rxn} and η_c are the overpotentials caused by charge-transfer, diffusion of reactants, chemical reactions and surface reactions, respectively. For a small value of the overpotential above the equilibrium ($\eta \ll E_{eq}$) it will be dominated by the charge-transfer process η_{ct}, the current will obey the current-overpotential equation (3.12). For higher values of the overpotential ($\eta \gg E_{eq}$) the diffusion of reactants may become a limiting factor and the net current will become saturated at a level defined by the value of η_d. In the case where mass transfer of reactants is slower than the charge-transfer process, the available ions are not enough to increase the Faradaic current and it plateaus. The

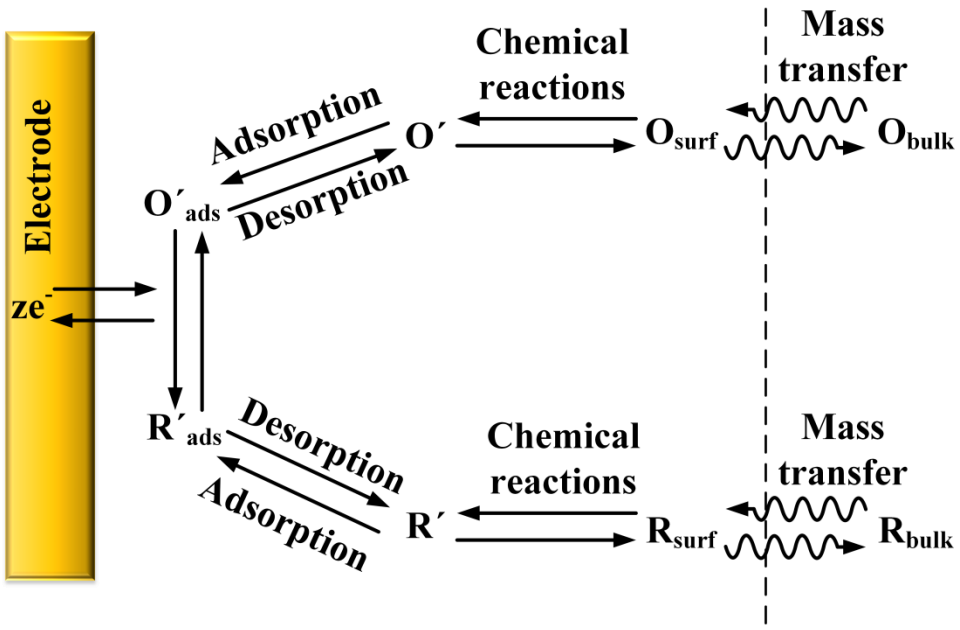

Figure 3.5: Processes at an electrode-electrolyte interface. Figure adapted from [31].

overpotentials can also be represented by impedances that relate to the amount of excess potential needed for these processes.

The most prominent phenomena that occur at the electrode-electrolyte interface are presented in the next sections. The elements derived from these phenomena model the electrochemical behaviour in chemical solutions. These elements were used to construct an electrical model that combines processes of reaction rates and mass transport as it was shown by Randles in his 1947 paper [144]. The electrical model of an electrode is an important component in the scope of this thesis, that was used for electrical simulations of the electrochemical microarray.

3.3.1 The Electrical Double Layer

At the boundary of two homogeneous environments (electrode-solution) layers of charges develop to make up an electrified interface. An electrolytic cell like the one previously presented in Figure 3.1(b) is made up of such interfaces between its electrodes and the chemical solution. An example of a two electrode electrolytic cell made up microelectrodes and the way in which charges are organised in the solution and on the electrodes is shown in Figure 3.6. Closest to the surface of an electrode, the inner layer is made up of solvent dipoles which orientate according to the distribution of charges that are present on the other side of the same electrode. The solvent dipoles are accompanied by non-

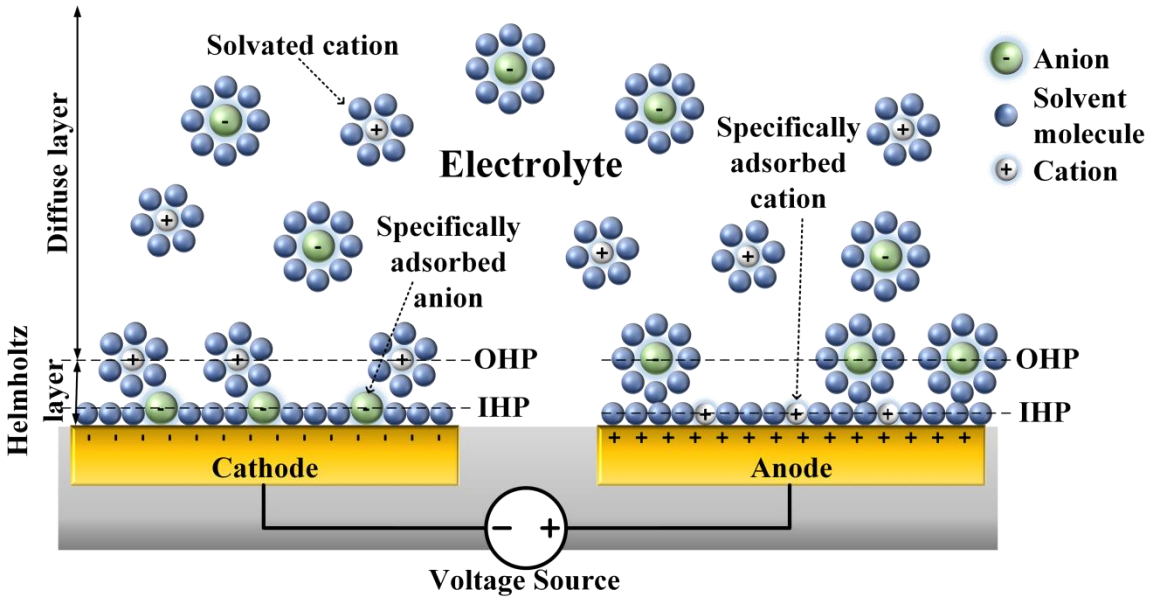

Figure 3.6: The electrical double layer in a two electrode electrolytic cell made of microelectrodes.

solvated ions that get specifically adsorbed interspersed at the surface of the electrode via chemical means, the locus of this plane is called the inner Helmholtz plane (IHP). Following the IHP, a layer of solvated ions with countercharges to the existing charge distribution populate an area further away from the electrode called the outer Helmholtz plane (OHP) to complete the chemical capacitor. The OHP ion distribution does not depend on their chemical properties but it obeys only long-ranged electrostatic forces thus the ions are non-specifically adsorbed. In Figure 3.6 it is illustrated that the ions which populate the OHP have a countercharge to the electrode charge, e.g. the cathode is negatively charged and cations populate this locus. Thermal effects cause ions beyond the OHP to create an ionic cloud in a diffusion layer which combined with the OHP has a total charge opposite to the one developed by the IHP and the electron charge density of the electrode. The description of this arrangement of charges describes the formation of an electrical double layer at each of the electrodes, which can be explained as an ionic capacitor, the size of which is also variable and it depends on the potential magnitude.

The first to model the electrical double layer at the boundary of an electrode (as the naming of the planes suggests) was Helmholtz [145]. The Helmholtz-Perrin model [145], [146] suggested an electrostatic approach over the formation of the electrical double layer. The electrode-electrolyte interface was viewed as a molecular capacitor with exactly opposite electrostatic charges at two ends, defined by the electrode surface and the OHP. The model assumed that the solvent dipoles at the IHP served as the dielectric between the parallel plates and neglected the presence of the specifically adsorbed ions. The Helmholtz capacitance expression is:

$$C_{\mathrm{H}} = \frac{\varepsilon_0 \varepsilon_r A}{d_{\mathrm{OHP}}} \tag{3.15}$$

where ε_0 is the permittivity of free space, ε_r is the relative permittivity of the electrolyte, A is the surface area of the electrode and d_{OHP} is the distance of the OHP from the surface of the electrode.

Even though the Helmholtz-Perrin model described the charging behaviour of the electrical double layer, it did not take into account the influence of the

potential magnitude on the capacitance value as it had been experimentally verified previously. In order to account for the mobility of ions, a model that viewed the distribution of charges in the solution as a reconfigurable arrangement influenced by the combined thermal and electrical forces was developed by Gouy and Chapman [147], [148]. This model was based on a statistical approach and it described an exponential decay of the charges away from the electrode surface proportionally to the electric potential and the concentration of charges. The Gouy-Chapman model replaced the static ionic layer of countercharges with a diffusion layer. The potential in that diffuse region was described by:

$$V(x) = U_0 e^{\left(-\frac{x}{L_D}\right)} \tag{3.16}$$

where U_0 is the potential at the surface of the electrode (at $x = 0$), x is the distance from the electrode and L_D is the Debye length. The Debye length is a reference point that characterises the distribution of charges within the diffusion layer. It can be viewed as a measure of the electrical double layer distance as it is approximately: $d_{OHP} = 1.5L_D$. The Debye length expression is:

$$L_D = \sqrt{\frac{\varepsilon_r \varepsilon_0 U_t}{2n^0 z^2 e}} \tag{3.17}$$

where $n^0 = C^* N_A$, is the number concentration of ions in the bulk solution (N_A is Avogadro's constant) and e is the elementary charge of one charge carrier (i.e. an electron). The Debye length shows the dependence of the potential on the concentration and thermal effects.

Equation (3.16) is derived by the expression of the charge density per cross-sectional area moving away from the surface of the electrode:

$$\sigma_d = -\sqrt{8\varepsilon_0 \varepsilon_r k_B T n^0} \sinh\left(\frac{zU_0}{2U_t}\right) \tag{3.18}$$

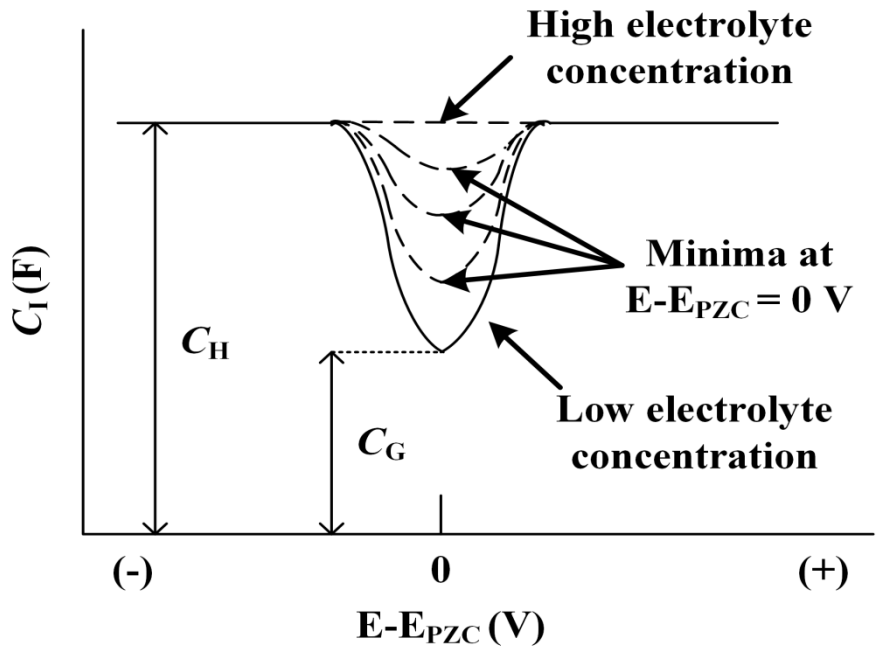

Figure 3.7: The expected behaviour of the interfacial capacitance according to the applied potential in respect to the zero charge potential (E-E_{ZPC}) and concentration. The figure was adapted from [31].

where k_B is Boltzmann's constant. The charge density at the electrode area is $\sigma_e = -\sigma_d$, the derivative of this density in respect of the potential at the electrode results in the differential capacitance C_G according to:

$$C_G = \frac{d\sigma_e}{dU_0} = \underbrace{\frac{\varepsilon_0 \varepsilon_r A}{L_D}}_{\text{molecular capacitor}} \underbrace{\cosh\left(\frac{zU_0}{2U_t}\right)}_{\text{thermodynamic effects}} \tag{3.19}$$

The capacitance comprises of two terms that contribute to its final value. The first term ($\varepsilon_0\varepsilon_r/L_D$) is linear and describes the molecular capacitor at the Debye length, the second term is hyperbolic and accounts for thermodynamic effects of the solvated ions in the chemical solution.

Even though the Gouy-Chapman model offered an improved estimation for the effect of the diffusion layer on the capacitance, it is limited as the value shows an exponential increase when high potential settings were applied. The reason was that ions were considered as points of charge that could approach the electrode at its surface. The phenomena that were described in the Helmholtz model such as the solvent dipoles in the IHP and the finite size of ions establish that this model is more applicable at higher polarisation settings and at higher concentrations. In order to create a model of the capacitance that would be

more accurate for a wide range of potentials and concentrations, Stern combined the two aforementioned models into one [149]. He considered the capacitors to be connected serially and both contribute with their representation of the electrical double layer to the interfacial capacitance C_I according to the electrochemical cell characteristics:

$$\frac{1}{C_I} = \frac{1}{C_H} + \frac{1}{C_G} \tag{3.20}$$

Each term dominates the equation at different settings. A plot demonstrating the behaviour of the interfacial capacitance of the electrical double layer against the applied potential, with respect to the zero charge potential (E_{PZC}), with the electrode charges being zero at equilibrium is shown in Figure 3.7. When the electrical potential is increased or the electrolyte is at a high concentration the U_0 term of equation (3.19) becomes significantly larger than U_t thus the C_G term of equation (3.20) attains a high value. In these cases the charges are arranged as the Helmholtz-Perin model suggests. On the other hand for smaller potential perturbations around the equilibrium potential the thermal potential governs the C_G value and a thermal hyperbolic behaviour becomes apparent in Figure 3.7 exhibiting a stronger effect at low concentrations. In most chemical solutions the interfacial capacitance will attain a value as the one drawn with dotted lines, depending on the applied potential its magnitude will change [31], [150].

Although specifically adsorbed non-solvated ions were not included in this model of the capacitance, it still provides a comprehensive understanding of the electrode-electrolyte interface. This basic model is adequate for the description of the electrical double layer, to be included in the simulations of this work.

3.3.2 Faradaic Impedance

The Faradaic impedance is the collection of phenomena that are responsible for a net current due to polarisation. The terms: charge-transfer resistance and diffusion impedance form the components of Faradaic impedance and together they account for a heterogeneous charge-transfer behaviour. These Faradaic phenomena can be considered as parallel processes to the interfacial

capacitance of the electrical double layer, thus the impedances can be included in a model as elements connected in parallel.

3.3.2.1 Charge-transfer resistance

The interfacial capacitance of the electrical double layer that was discussed in the previous section is responsible for the non-Faradaic currents. However, when the applied potential attains a value close to the formal potential, $E^{0'}$, of the electrochemical cell, charge-transfer Faradaic phenomena are responsible for the largest part of the readout current magnitude. The behaviour of the charge transfer phenomena on different types of electrodes and the equations that govern them were explained in Section 3.2.2. Using the linear approximation of the exponential terms according to $e^x = (x + 1)$, the Butler-Volmer equation described by expression (3.13) can be further simplified for small overpotential values to:

$$i = i_0\left(-\frac{\eta z}{U_t}\right) \tag{3.21}$$

The use of small overpotential values causes the electrode to remain at equilibrium and ensures a reversible behaviour. Furthermore, the magnitude of i is expected to be smaller than i_0. These characteristics enable a normal electrode to almost behave as a non-polarisable one.

The charge-transfer resistance R_{ct} related to the charge-transfer portion of the overpotential η_{ct} can be extracted by $-i/\eta$ which is the negative reciprocal of the current-overpotential plot that was shown in Figure 3.3. Using equation (3.21) this part of the Faradaic impedance is expressed as:

$$R_{ct} = \frac{U_t}{z i_0} \tag{3.22}$$

The charge-transfer resistance depends on thermodynamics and the exchange current density which is an indication of the system's mobility. When the i_0 value is small it means that the system has a limited movement of ions. For a small i_0, R_{ct} is maximised and consequently the system relies mostly on the

parallel interfacial capacitance that will explain the current response. On the other hand, when i_0 is maintained at very high levels the system is highly mobile and R_{ct} is minimised leading to the behaviour of an ideal non-polarisable electrode [31].

3.3.2.2 Diffusion impedance

Apart from the charge-transfer resistance, the Faradaic impedance also consists of a term that represents the effect of slow diffusion processes that govern the movement of ions to or from the electrode under the influence of a low frequency ac signal. The potential drop by the Faradaic impedance is $E = iR_F + q/C_F$, for $i = I\sin(\omega t)$, where R_F and C_F are the Faradaic resistance and capacitance respectively, I is the current magnitude and ω is the angular frequency of the applied signal. Differentiating the potential drop for small changes, transforms the equation to:

$$\frac{dE}{dt} = (R_F I\omega)\cos(\omega t) + \left(\frac{I}{C_F}\right)\sin(\omega t) \tag{3.23}$$

For a system with reduced and oxidised species $E = E$ [i, $C_O(0,t)$, $C_R(0,t)$]. Using the Nernst equation, Fick's second law for diffusion and the rate of reaction the derivative of the potential drop can assist in finding the individual terms of the Faradaic impedance as:

$$\frac{dE}{dt} = (R_{ct} + \frac{\sigma}{\sqrt{\omega}})I\omega\cos(\omega t) + I\sigma\sqrt{\omega}\sin(\omega t) \tag{3.24}$$

and $\sigma = \frac{U_t}{z^2 e N_A A}\left(\frac{1}{\sqrt{2D_O C_O^*}} + \frac{1}{\sqrt{2D_R C_R^*}}\right)$, where D_i is the diffusion coefficient of species i.

From equations (3.23) and (3.24) the Faradaic impedance can be identified as:

$$\begin{cases} R_F = R_{ct} + \dfrac{\sigma}{\sqrt{\omega}} = R_{ct} + R_w \\ C_F = \dfrac{1}{\sigma\sqrt{\omega}} = C_w \end{cases} \tag{3.25}$$

where R_w and C_w are terms defined as the Warburg impedance. Replacing σ in the Warburg impedance elements and assuming only one dominant species, either at oxidation or reduction, they can be expressed as:

$$Z_w = \begin{cases} R_w = \dfrac{U_t}{z^2 e n^0 A \sqrt{2\omega D}} \\ C_w = \dfrac{z^2 e n^0 A}{U_t} \sqrt{\dfrac{2D}{\omega}} \end{cases} \tag{3.26}$$

The Warburg impedance is related to mass transfer processes of diffusion under the influence of a relatively rapidly alternating signal which is relative to many voltammetric techniques used in this work. However, the Warburg impedance is solved only for a certain frequency thus the impedance value would be a simplistic representation of reality.

As charge-transfer processes precede diffusion, R_{ct} and Z_w can be placed in that order as electrical elements connected in series. As it was stated in the beginning of this section the Warburg impedance, which is related to the diffusion of reactants, is only significant at a low frequency modulating signal because at higher frequencies Z_w does not form fast enough and charge-transfer phenomena dominate. Another factor that is important for the observation of current related to the Warburg impedance diffusion is the speed at which electrochemical reactions of reactants in the system occur (related to i_0). Therefore if i_0 is large the Warburg impedance will dominate over R_{ct} and the Faradaic impedance will be modulated in respect of $1/\sqrt{\omega}$. If i_0 is small charge-transfer phenomena become more significant and dominate over the Z_w [31], [151].

3.3.3 Spreading Resistance

Another element that is included in the electrode-electrolyte interface is the resistive path seen from the electrode to the conductive solution. This element is called spreading resistance and it is a consequence of the spreading current from the electrode to the solution or vice versa. As it was explained in Section 3.2.3, the electrolyte acts as a resistive path that causes an *iR* potential drop that induces a deviation from $E_{applied}$ seen from the working electrode. Even

when the three electrode setup is used to reduce the Ohmic drop, a finite potential drop still remains. It was shown by Newman [152] that the Ohmic drop is mainly found at the vicinity of the electrode for a small disk electrode. To account for all the spreading resistance, R_s, of an electrode, it is calculated with the assumption that the counter electrode is at an infinite distance away from the working electrode. For the purposes of calculations the current is assumed to be anodic thus the overpotential at infinity is essentially zero. The size of R_s depends on the surface area as well as the surface shape as the way the resistive path will be formed depends on the geometry of the electrode. For a disk electrode in a homogeneous solution the current density at the surface of the electrode for $z = 0$ (distance) is $j = 2\eta_0 / \pi\rho\sqrt{\alpha^2 - r^2}$ where η_0 is the overpotential at the surface of the electrode, α is the electrode radius, r is the distance from the axis of symmetry and ρ is the resistivity of the electrolyte [152]. To find the total current one can calculate the integral of the area in radial coordinates as:

$$i = \int_0^{2\pi} \int_0^{a} j r dr d\varphi = \frac{4a\eta_0}{\rho} \tag{3.27}$$

Thus the spreading resistance is:

$$R_s = \frac{\eta_0}{i} = \frac{\rho}{4a} \tag{3.28}$$

The calculations of R_s close the electrode surface vary proportional to equipotential lines that follow the electrode geometry. Expression (3.27) estimates for all the spreading current hence the derived resistance R_s is the total spreading resistance. For a planar rectangular electrode, often employed in microfabrication, the spreading resistance can be calculated by:

$$R_s = \frac{\rho}{\pi l} \ln\left(\frac{4l}{w}\right) \tag{3.29}$$

where w and l are the electrode width and length, respectively [153].

3.3.4 Electrochemical Circuit Equivalent Model

The collection of impedances explained in previous sections make up for the basic description of electrochemical behaviour in electrical terms. In a work that was initiated by Randles in 1947 [144], the most popular model where these elements are connected together is shown in Figure 3.8. The electrode as depicted in the circuit diagram is the connection point between the electrolyte and the electronic circuits that control an electrochemical cell. Although an

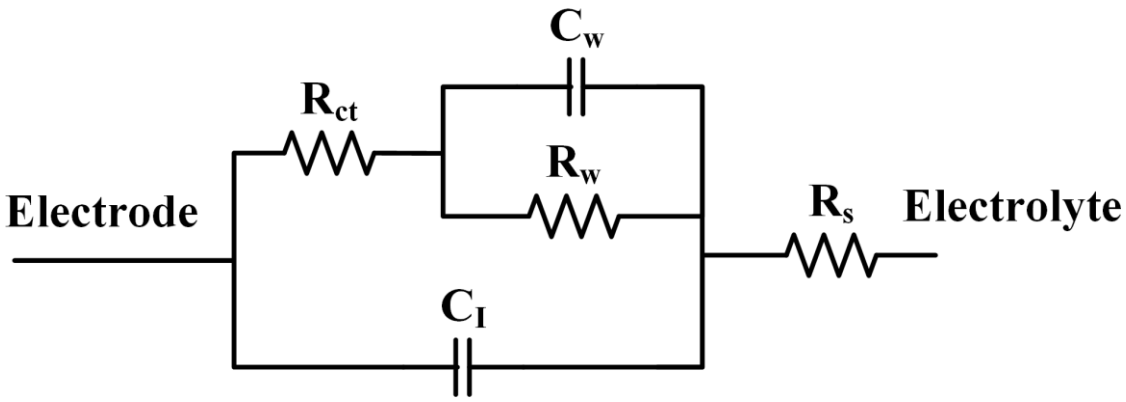

Figure 3.8: An equivalent circuit model for the electrical behaviour of the electrode-electrolyte interface

electrode has parasitic impedances of its own, they are not included in the model as they are considered negligible compared to the electrode-electrolyte interface impedances. The interfacial capacitance C_I that was described in Section 3.3.1 is connected in parallel with the Faradaic impedance as they are parallel phenomena. The Faradaic impedance consists of the charge-transfer resistance R_{ct} and the Warburg impedance R_w and C_w as explained in Section 3.3.2. Lastly, these parallel phenomena are all connected in series to the spreading resistance R_s that follows and represents the spreading current in the electrolyte.

The equivalent circuit model cannot provide the exact current response in respect of $E_{applied}$ of an actual electrochemical cell, that varies $E_{applied}$ according to an electroanalytical method e.g. cyclic voltammetry (CV). However, due to the accurate representation of the electrochemical processes this equivalent circuit provides a current response with the same amplitude and phase angle as the real-life electrode in an electrochemical environment. There have been other models in the literature that describe electrochemical processes more accurately or account for more complex conditions but this simple electrical

model is suitable for electrical simulations and within the scope of this work. Using the electrical model of an electrode-electrolyte interface an electrical circuit that represents a potentiostat connected to a three electrode electrochemical cell was drawn. An illustration of the potentiostat connected

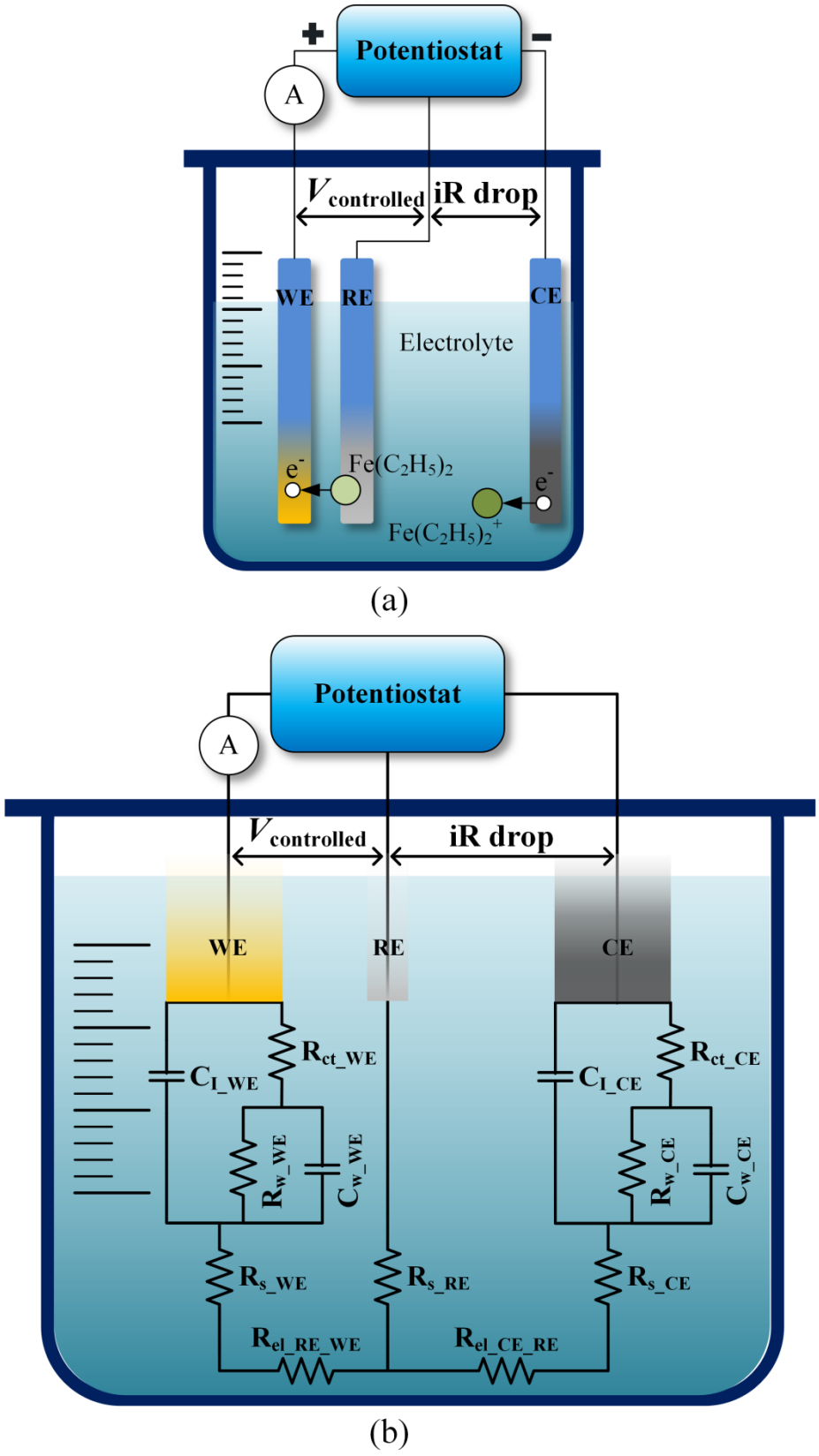

Figure 3.9: (a) Illustration and (b) an electrical circuit that represent a potentiostat connected to a three electrode system.

with the three electrode cell having the CE set as an anode and the WE as a cathode as an example configuration and the electrical circuit that corresponds to that setup are shown in Figure 3.9(a) and (b) respectively. The CE and WE are represented with models as the one shown in Figure 3.8 that includes all the processes that occur in an electrode-electrolyte interface. The RE only reads the potential that reaches in its spatial coordinates after an *iR* drop by $R_{el\_CE\_RE}$ which is the resistance of the electrolyte for the distance between the CE and RE, an effect that was already discussed in Section 3.2.3. As it connected to a high impedance node at the potentiostat the RE has no charge transfer processes occurring at its surface. The only element of the electrode-electrolyte electrical model relevant to the RE is the spreading resistance of ions that appear on its surface for their charge to be recorded, as shown in Figure 3.9(b).

As in this simple case for a three electrode system the model of Figure 3.8 can serve as the building block that represents an elemental electrode to build geometrical electrical simulations of microelectrode structures that will be investigated in Chapter 4 to build the ECM. Theoretical models assist in the understanding of the fundamental behaviour of electrochemical cells. Nevertheless methods which are used in amperometry/voltammetry with electrolytic cells are equally important as results can be interpreted to study the chemical composition of the system under investigation as it will be explained in the next section.

3.4 Amperometric/Voltammetric Methods

Electrochemical cells can provide information on the chemical composition of the solution. In order to acquire such readings, there are several methods that use a power source and take readings of induced current or potential. The electrochemical field involved with the analysis of these data is termed as electroanalysis. The methods that are directly focused on the analysis of the current or the potential are sectors of electroanalysis called amperometry/voltammetry and potentiometry, respectively. Potentiometry and amperometry/voltammetry have both been used in biochemical applications to determine biomarkers and other biologically interesting characteristics. A review of these applications was presented in Chapter 2. Even though potentiometry is an easy to perform non-interacting technique, it requires ion-selective surfaces

which focus on the analysis of a specific analyte. On the other hand, in spite of interacting with the analysed compound amperometry/voltammetry's strength to analyse many compounds relies on its wider variety of methods that can be employed. The various methods are able to characterise complex processes as well as system attributes. Some of these methods will be presented in the succeeding sections.

3.4.1 Amperometry

Measurements of current performed using a controlled potential usually applied by a potentiostat belong to the category of amperometry and voltammetry. Amperometry is concerned with the application of a dc potential whereas voltammetry involves more dynamic measurements. Chronoamperometry's actuating signal is a potential step past the electroactive species redox potential while the current is monitored in an *i-t* diagram that is related to the concentration profile at the electrode. A method that applies the reverse potential step is the amperometric equivalent of current reversal potentiometry and it is denoted as double potential step chronoamperometry. Another technique that uses a constant potential is bulk electrolysis although it is concerned with exhaustive electrolysis of electroactive compounds for e.g. coulometry (charge measurement). Bulk electrolysis is mainly applied on large scale electrodes capable of electrolysing large concentrations of reactants in reasonable timescales.

3.4.2 Sweep Voltammetry

Voltammetry is concerned with the study of the current in relation to the known varying applied potential. Potential sweep methods use a linear function of voltage within the limits of a potential window in respect of time by a scan rate υ measured in V/s. The results can be plotted against time to result in a linear sweep chronoamperogram or in an *i-E* curve and the technique is referred as linear sweep voltammetry (LSV). If after the end of the forward potential scan a reverse one follows, as shown in Figure 3.10(a), the method is a potential sweep equivalent of double potential step chronoamperometry and the technique is called cyclic voltammetry. In the voltammogram (*i-E* curve) the thermodynamic and kinetic processes that occur in the system in the vicinity of the working

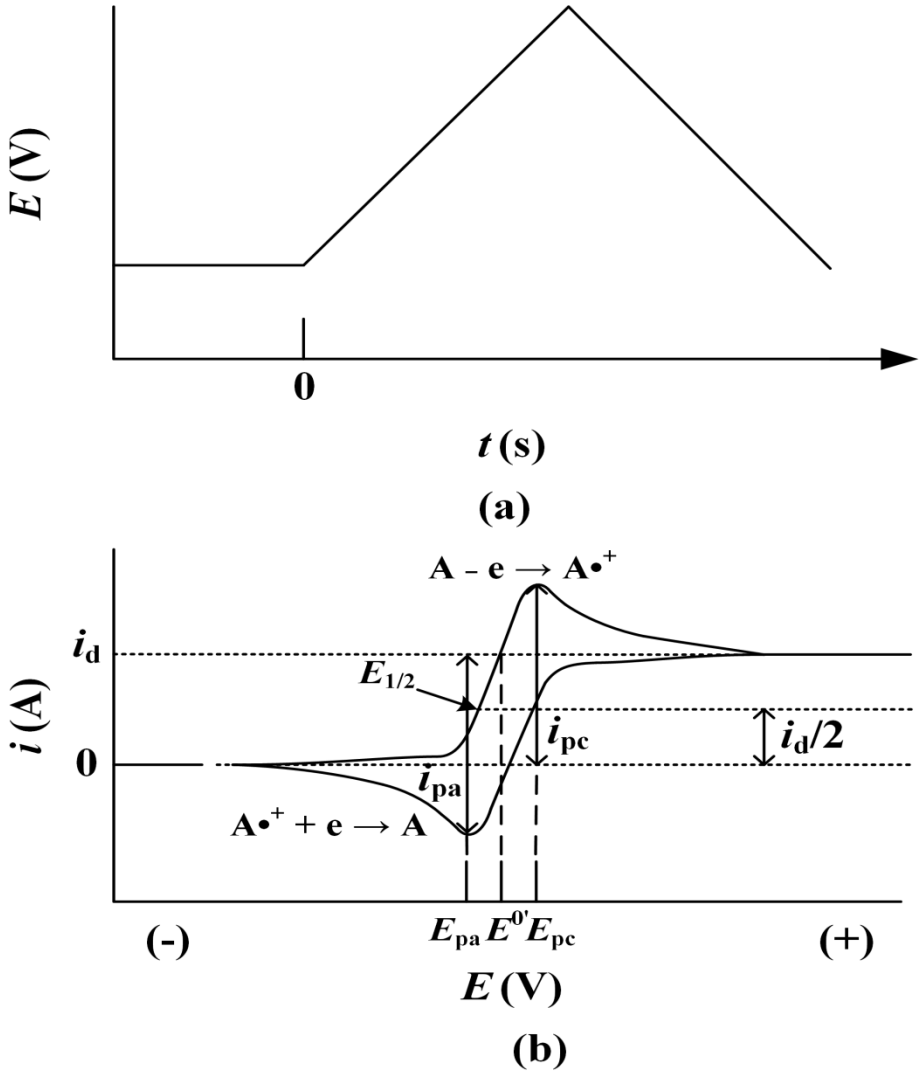

Figure 3.10: Cyclic voltammetry (a) driving signals and (b) the resulting voltammogram.

electrode in respect of the applied potential can be identified by their effect on the current shape. Scanning the electrode potential at voltages lower than the formal potential $E^{0'}$, charging currents appear and the electrical double layer develops until the electroactive species become oxidised (or reduced depending on the potential scan direction). At potentials higher than $E^{0'}$ the surface concentration reaches to a maximum and then depletes featuring a current peak and a plateau where the diffusion rate is maintained. For cyclic voltammetry at the reverse potential scan the reverse processes occur for the cation radical that was developed and concentrated at the electrode surface, as shown in Figure 3.10(b).

Voltammetry can provide information contained in the voltammogram that can be extracted by the curve analysis. Figure 3.10(b) will be used to explain the findings. The half-wave potential $E_{1/2}$ is the potential at which the diffusion current is at its half ($i_d/2$). Voltammograms are used to determine the formal

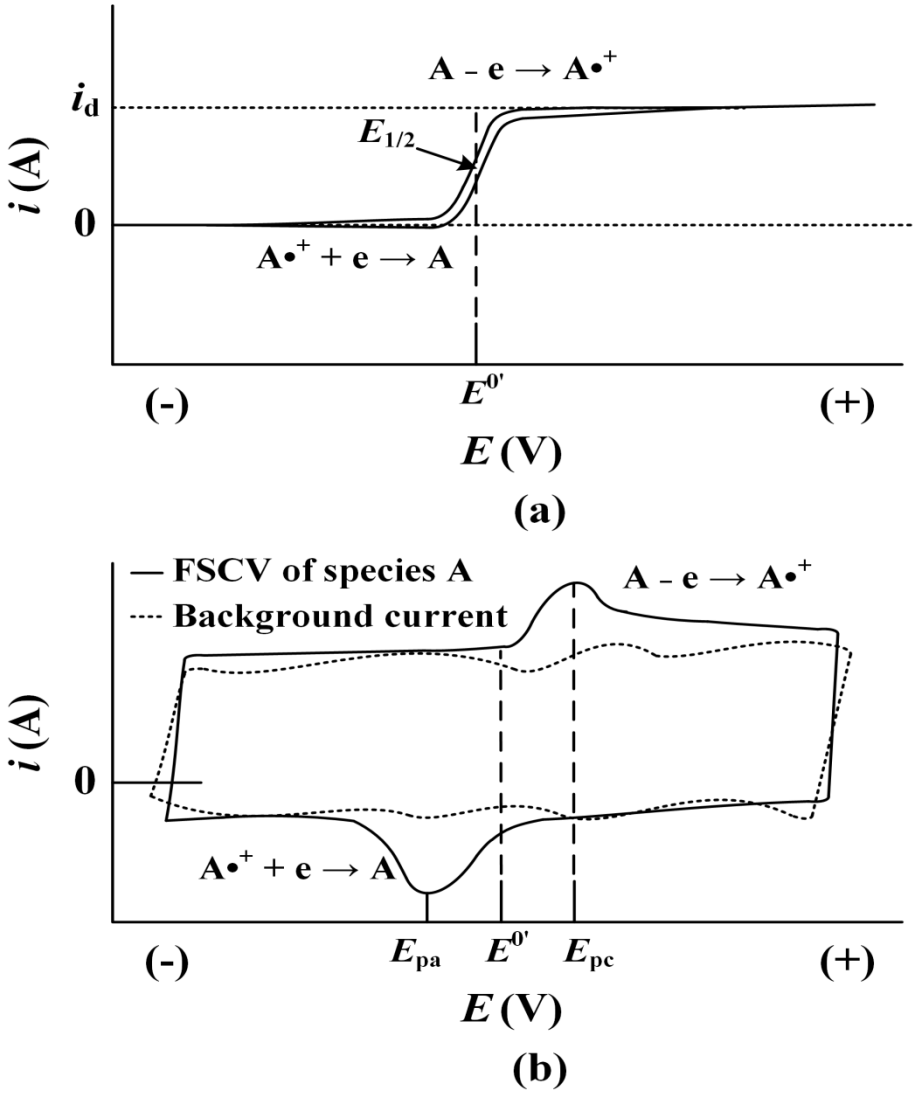

Figure 3.11: The resulting voltammogram of a microelectrode under the influence of (a) cyclic voltammetry and (b) fast-scan cyclic voltammetry.

potential $E^{0'}$ through $E_{1/2}$ which is a good measure, however $E_{1/2}$ might shift due to changes in the medium such as its acidity, the activity coefficients, adsorption on the electrode and the concentration of reduced and oxidised species. For sweeping methods $E_{1/2}$ can be found from the half-peak potential $E_{p/2} = (E_{pa} + E_{pc})/2$ which is used instead as the current exhibits a peak current i_p. The shape of the slope at $E_{1/2}$ can provide information on the reversibility of a system as Nernstian response exhibits a certain slope and anything different may suggest kinetic effects especially through techniques such as CV. The current plateau after the half-wave potential $E_{1/2}$ is the steady state current. The steady-state current can provide information on the electroactive compound's bulk concentration, its diffusion coefficient and the number of electrons in charge transfer (z).

When cyclic voltammetry is applied on microelectrodes a voltammogram changes and looks as shown in Figure 3.11(a). The mass transfer in this case is more than enough for the small amount that can be converted on the microelectrode thus the surface concentration does not deplete and current peaks are not evident as in Figure 3.10(b). The reason the voltammogram yields to a steady-state current after the $E^{0'}$ is reached is also that the diffusion rate is dependent on the electrode size. The high mass transfer rates result in a sigmoidal response that more accurately approximates the true $E_{1/2}$ value and the steady state current is an accurate measure of the solution's concentration of the analyte. Another different feature is the capability to use higher scan rates without non-Faradaic behaviour artefacts. The better performance lies in the microelectrodes' size which minimises the interfacial capacitance C_I as well as the uncompensated iR drop (R_u) which is proportional to the spreading resistance, leading to an overall smaller cell time constant R_uC_I. Moreover, the spreading resistance is also responsible for the inability of electrodes to be used in low conductivity chemical media as its magnitude increases dramatically, microelectrodes also have an advantage in such systems [31].

A recent addition to potential sweep methods made possible by microelectrodes is fast scan rate methods, with fast scan cyclic voltammetry (FSCV) being the most prominent one. The fast scan rates require larger charging currents for the electrical double layer and the resulting voltammogram is dominated by these residual currents rather than from the Faradaic processes, as shown in Figure 3.11(b). In order for FSCV to present a voltammogram that resembles Figure 3.10(b) an additional measurement of the background charging current without the presence of the analyte is first conducted which is then subtracted from the response voltammogram. Although microelectrodes are used a drawback of FSCV is that the extracted voltammograms are still susceptible to a potential distortion by the iR drop [127], [154]. The use of these techniques can monitor fast heterogeneous charge transfer reactions, limit the Debye length to the nanometre scale and enhance the chemical reversibility of otherwise irreversible reactions [155]. Additionally, size limited experiments can use these methods to increase the current magnitude of microelectrodes. FSCV has been used to monitor fast dopamine concentration changes in the brain and other diagnostically important applications presented in Chapter 2.

3.4.3 Pulsed Voltammetry

Apart from sweeping the voltage there is another group of voltammetric methods that produce *i-E* curves called sampled-current (or pulsed) voltammetry. In these methods the potential is not swept but it is rather an outcome of many chronoamperometric measurements recorded at multiple potential step settings. The results from these methods are sampled at a fixed time τ after the step and plotted against the potential. This approach is followed to eliminate the recording of charging currents and enable measurements at low analyte concentrations. Methods that are part of this group are staircase voltammetry, normal pulse voltammetry (NPV), reverse pulse voltammetry (RPV), differential pulse voltammetry (DPV) and square wave voltammetry (SWV). In this study a selection of these methods was used, namely staircase voltammetry, NPV and DPV.

In staircase voltammetry the potential is not swept linearly as in LSV and cyclic voltammetry but as a series of successive potential increments, as shown in Figure 3.12(a)(i). The resulting current from staircase voltammetry may be sampled at the end of each potential increment as in other sampled-current voltammetries but it would not have a major effect on the resulting voltammogram. The reason lies behind the potential increments that result in successive states of the diffusion depletion build-up that resembles its sweep method equivalents (CV). Staircase voltammetry can be considered as a CV run with a voltage sweep by a low ADC resolution. The discretised potential sweep can be a useful method for MEAs as microelectrodes can be multiplexed at every potential increment. The resulting voltammogram of staircase voltammogram is shown in Figure 3.12(a)(ii). If the driving potential is increased with small potential increments and a smoothing filter is applied on the resulting voltammogram, the results can become almost identical to CV.

Normal pulse voltammetry (NPV) is a voltammetric method in which the potential is changed as a series of pulses between a base potential (E_b) and incremental values of voltages, as shown in Figure 3.12(b)(i). The reason this method was developed was that the longer an electrode is held at potentials around $E^{0'}$ where Faradaic processes occur, the local concentration becomes depleted before a sensible result is attained. NPV's principle is to regenerate

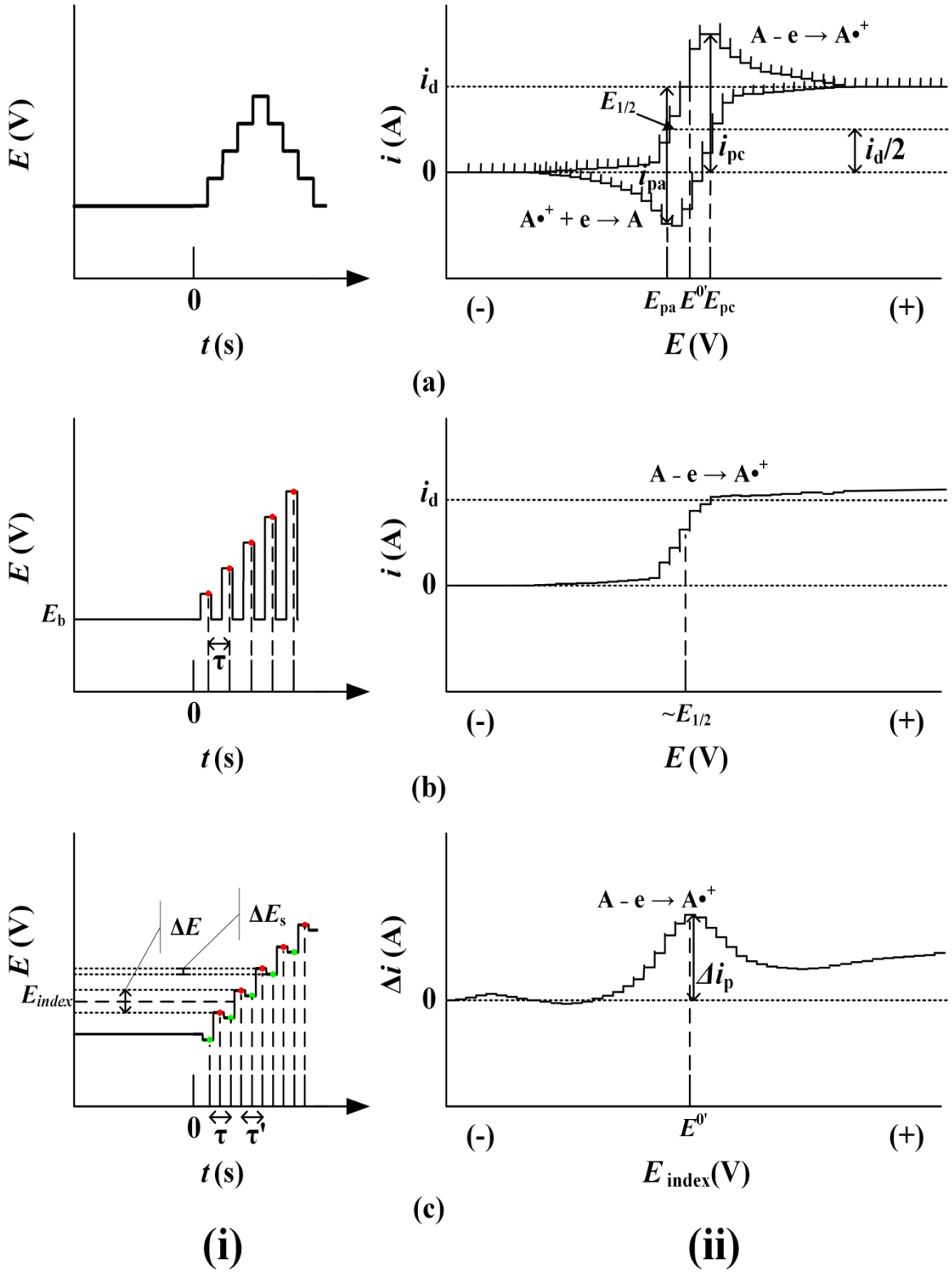

Figure 3.12: (i) Driving signals and (ii) the resulting voltammogram using (a) staircase voltammetry, (b) normal pulse voltammetry and (c) differential pulse voltammetry.

the diffusion layer at the WE, as for chemically reversible processes E_b is chosen to be sufficiently lower than $E^{0'}$ to return the reactants to back to their initial state. The current is sampled at the end of the voltage pulse increments at a τ time period where the Faradaic current to charging current ratio is best. The resulting voltammogram from NPV is shown in Figure 3.12(b)(ii). Charging

currents are almost eliminated with this method and the Faradaic response is enhanced, leading to a capability of lower concentration measurements. However, there are still background currents present from other electrode surface processes and the qualitative information that can be found are not the same as CV [31].

A method that can more accurately measure the Faradaic component of redox processes is differential pulse voltammetry (DPV). The difference of this method to NPV is that the pulses have a smaller controlled amplitude as the base potential (E_b) changes proportionally with every new pulse so that a ΔE_s potential difference between them is maintained, as shown in Figure 3.12(c)(i). In this case E_b serves more as a pre-electrolysis step rather than a regenerative process. The current is sampled at two different time intervals (τ and τ'), before the application of the pulse and at the end of it respectively. The current is plotted as the difference between the two samples, $\Delta i = i_2(n\tau') - i_1(n\tau)$, for every pulse against the voltage found at the half of every potential increment (E_{index}), as shown in Figure 3.12(c)(ii). The principle of DPV lies in the fact that background currents from charging and other processes can be removed by subtraction as ΔE has quite a small amplitude. The resulting voltammogram displays a peak-shaped current response that originates from the charge-transfer currents as information about the diffusion profile found in both samples is removed by subtraction. DPV is a method that can accurately measure lower concentrations of analytes by the peak current Δi_p referenced to the baseline before its appearance [31], [156].

As it was shown in Figure 3.11, microelectrodes exhibit improved performance in response to electrochemical methods, their advantages can be further exploited when arranged into arrays with a wide-range of applications. However, simultaneous readings from many of these electroanalytical transducers can potentially lead to undesirable cross-talk interactions, the amperometric cross-talk aspect will be explained in the next section.

3.5 Cross-talk in Microelectrode Arrays

MEAs and essentially any system that conducts electrochemical measurements on more than one electrode may suffer from interactions that are of chemical

and electrical nature. Chemical interactions may originate from the chemical properties of the compounds in the chemical media or by the thermodynamic and kinetic properties of their heterogeneous and homogenous charge-transfer. A source of chemical interference, when looking at a single heterogeneous reaction at the analyte formal potential $E^{0'}$, is the oxidation or reduction of other accompanying electroactive species at preceding formal potentials to $E^{0'}$. Another factor that reduces the sensitivity is fouling of the electrode surface usually by biological components in biochemical measurements. When an MEA aims at multiple analyte sensing as it was presented in Section 2.7.1 or even when a biological sample is used with a rich composition of electroactive compounds, cross-reactivity may become an issue [157]. Lastly, in MEAs microelectrodes form their individual diffusion layers according to the theory explained in Section 3.3, however an optimal WE pitch needs to be maintained to prevent their diffusion layers to overlap as it will be analysed in Section 3.5.1.

The other factor that influences electrochemical measurements is electrical interference. One source of electrical coupling (noise) is the wiring and circuits used to drive electrochemical cells and obtain the results. Environmental interference from sources of electromagnetic fields in close proximity to the electrochemical cells may also influence the recorded signals thus a Faraday cage is often used in these measurements. Last but not least, in MEAs electrical coupling may occur between microelectrodes through the chemical solution which acts as a short-circuit conductor as it will be explained in Section 3.5.2 [158].

3.5.1 Chemical Cross-talk

The advantageous characteristics of high mass transfer, sigmoidal current performance and a small interfacial capacitance (C_I) found in microelectrodes that were explained in Sections 2.3.1 and 3.4.2 occur when diffusion layers form a hemispherical shape around the electrode. However, if the scan rate is too fast or the WE pitch is too small, the diffusion layers change their shape. Although microelectrodes benefit from a hemispherical diffusion layer due to their small dimensions that increases mass transfer, at very high scan rates they behave as their large scale counterparts. When the scan rate increases, the

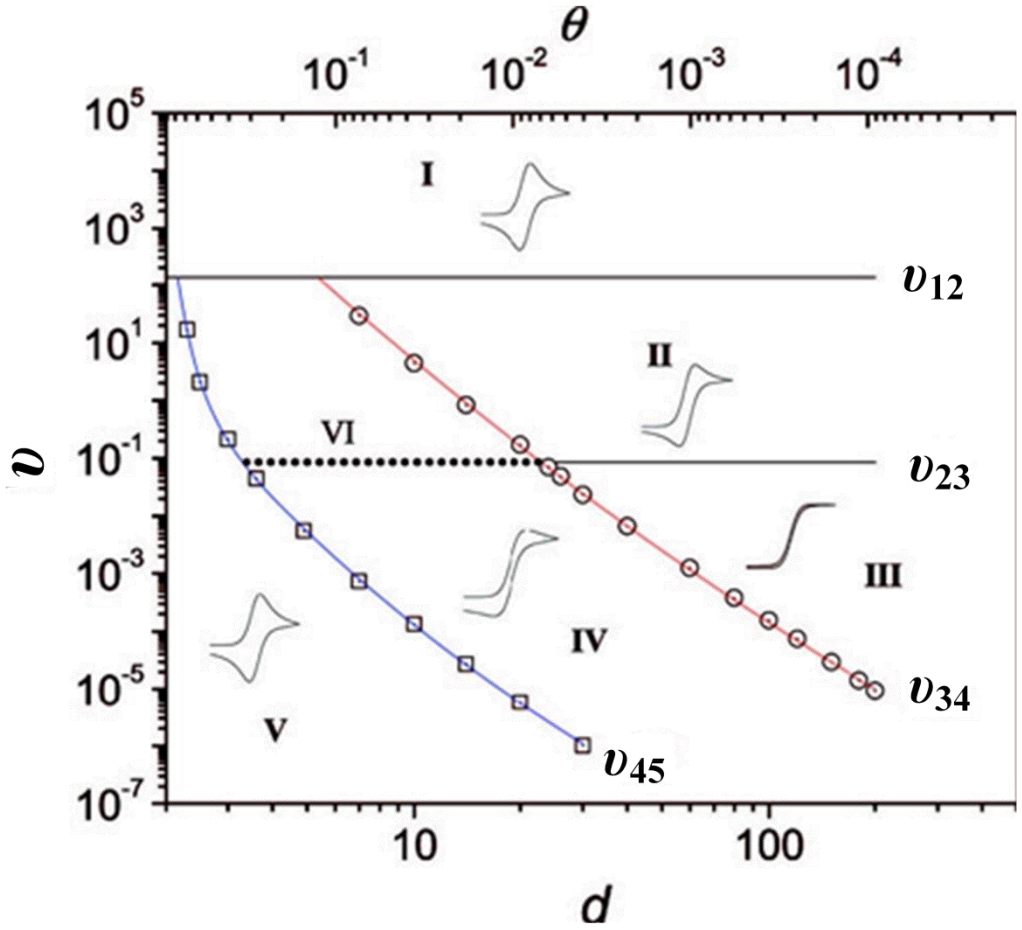

Figure 3.13: Diagram showing zone separation of cyclic voltammograms in respect of their pitch (*d* in units of *α* the electrode radius), the scan rate *υ* and the fraction of the active area in the array *θ*. I – V regions start from localised planar diffusion to a planar diffusion over the whole MEA as explained in the text. The borderlines υ_{12} - υ_{45} separate regions with a different response [139].

formal potential is reached faster thus reactions take place at the electrode-electrolyte interface more rapidly, however the rate of diffusion is not as fast to provide with new reactants and the diffusion length is more limited than for lower scan rates. In particular high scan rates induce a suppression of each microelectrode's diffusion profile to a planar or semi-hemispherical shape which make the response similar to a macroelectrode as reactants do not reach the electrode surface fast enough and charging currents are observed. However, in FSCV an additional measurement of the background charging currents is performed and removed from the final voltammogram. It has been exhibited by Zachek et al. and other groups that at high scan rates microelectrodes can be operated along with other electrochemical methods. The cross-talk was not quantified in these works and the experiments were conducted with specially prepared microfabricated electrodes [123], [122]. On the other hand at normal scan rates, if a certain ratio of the electrode size to pitch is not maintained, Nernst radial diffusion layers overlap and form a planar diffusion of the analyte

species over the whole MEA leading to a "shielding" effect that degrades the electroanalytical performance [8], [139]. The term that describes the performance degradation due to overlapping diffusion layers is called chemical cross-talk. The phenomenon was investigated by Guo and Linder using simulations and experimental observations. A guideline for the optimal working microelectrode centre-to-centre distance (d normalised in units of the electrode radius (a) with respect to the scan rate (υ) is shown in Figure 3.13. The optimal minimum value for a steady-state behaviour was reported as $d_{necessary} = 24a$. The optimal response of CV in a MEA is that of a sigmoidal response, as shown in region III of Figure 3.13 and explained in Section 3.4.2. This behaviour can assist for the better estimation of the half-wave potential $E_{1/2}$ as well as the concentration measurement of the analyte. The effect of the electrode position on the diffusive flux has also been shown by Zhang et al. through simulations and experiments. For the experimental setup, 5 μm sized WEs were spaced 7 μm away and around a central WE using separate microelectrodes. Measurements on the central WE exhibited a 40% decrease of the current magnitude compared to measurements on the surrounding WEs due to interferences by the surrounding electrodes [159].

Hesegawa et al. and Kuno et al. presented FEM simulations and experimentally showed that the geometrical arrangement of microelectrodes in a two-electrode system can prevent the formation of a planar diffusion layer. The geometrical pattern that was used in that work placed the CE in a surrounding ring structure around each WE. Unlike external counter macroelectrode that is often used in MEAs, a hemispherical profile that was contained inside the ring structure was observed in simulations. The WEs exhibited typical steady-state microelectrode behaviour at smaller distances ($d = 1.75a$) between them than the distances proposed by Guo and Linder, leading to an improved electrode density [140], [71].

3.5.2 Electrical Cross-talk

Apart from chemical sources of cross-talk, electrical signals also affect each other in the classical notation of cross-talk. It was theoretically investigated and experimentally verified by Anderson et al. that origins electrical cross-talk are electrical coupling between electronic elements integrated in MEAs or through a

conductive path along the chemical solution. The factors that were found to influence the electrical cross-talk were the electrode size (because an increase in the size results an increase in the interfacial capacitance but the resistance dropped), the gain of the amplifier used in the potentiostat and the size of the integration capacitor for discrete time CSA schemes that were introduced in Section 2.5.1. These current integrating circuits were investigated and the cross-talk was found to vary from less than 0.1 % to more than 10 % [160]. In another study, Yu et al. reported an electrical cross-talk using independent external potentiostats at different potentials for each WE but a quantifiable value was not provided [161].

Similar to chemical cross-talk, an approach that has been explored in order to minimise electrical cross-talk and improve isolation was the use of guard rings around the WE. [5], [12], [13]. As work on simulations of an electrode matrix of multiple voltage sources connected to electrodes in parallel has demonstrated, the potential distribution can be controlled and contained by the choice of geometrical arrangement [134]. In epiretinal prosthesis, a technique called current focusing, exhibited localized potential and electric field control [136], [135]. In that technique, the use of multiple concurrent current injection electrodes paired with local surrounding return electrode guards demonstrated an improved control over crosstalk between the pairs, when compared to the use of a distant delocalized common return electrode [135], [137]. This technique could be adopted into electroanalytical MEAs and is of particular interest in this thesis where the isolation among independently controlled microelectrodes is investigated.

Even though ring structures around each WE seem to be correct the chemical and electrical cross-talk phenomena, a structure is required to be investigated that is more appropriate for an electrochemical cell microarray. Such a structure that enables multiple electrochemical experiments simultaneously was investigated in this thesis. In this work, the potential distribution and electric field among independent electrochemical cells set at different potentials was investigated in simulations and it is presented in the next chapter. Furthermore, to account for both sources of cross-talk (chemical and electrical) an electrochemical cross-talk was measured which is a combination of both cross-

talk types, the measurement is presented in Chapter 6. This is a novel figure of merit, introduced to characterise a multiple electrochemical cell system for the first time. Apart from cross-talk another type of interference that was reported in this section was the influence of other compounds on the Faradaic response. Compounds that are used to counteract this issue and their use in electrochemistry are presented in the next section.

3.6 Summary

In this chapter, the theoretical background of electroanalytical processes and experiments was explained. The electrode-electrolyte interface was analysed to the processes that characterise it and these were modelled electrically. Although the model cannot provide the exact electrochemical response it does account for electrical characteristics and it is adequate for electrical response simulations conducted in this work. This model will be used as the building block to make electrical simulations of electrode geometrical arrangements in integrated circuit simulation software (Cadence) in Section 4.3. Furthermore, the significance of the potentiostat in electrochemistry to account for the *iR* potential drop due to the electrolyte resistance and its ability to perform various electrochemical methods with an electroanalytical importance were emphasised in this chapter. Amperometric and voltammetric methods were reviewed with emphasis to the ones that were used in this study in results found in Chapter 6. Sources of interference were identified in MEAs, electrical and chemical cross-talk was shown to affect measurement quality, this was taken into account in the geometrical design of the electrode pattern in Section 4.4 and the circuit design in Section 4.5. Lastly, in order to verify the effect of these approaches to the cross-talk between independently controlled electrochemical cells an experiment was devised to measure an electrochemical cross-talk figure of merit that is described in Section 6.3.4.

4 Electrochemical Cell Microarray Design and Simulations

4.1 Introduction

The previous chapter included the theoretical background of electrochemical cells in terms of equations, chemistry and methods used in these systems. This chapter explains how electrochemical cells can be operated simultaneously to perform separate electroanalytical measurements. First, the electrical model that was described in the previous chapter was incorporated in the integrated circuit software to simulate the potential and electric field distribution in a chemical solution using a 3-D resistor mesh as described in Section 2.8. The simulation investigated the effect of different electrode geometries on the independent function of neighbouring electrochemical cells. Based on the theoretical background and on information acquired by the simulations, the design of a 4 × 4 microarray of electrochemical cells integrated into a CMOS process is described. That chapter then describes the system-level design for the whole chip as well as the components of each integrated electrochemical cell. Each electrochemical cell consisted of control and readout electronics to operate a 4 × 4 working electrode (WE) subarray. Furthermore, the chip's design that enables for several modes of operation is also discussed. Lastly the physical layout of the circuits, the 4 × 4 WE electrochemical cell and the 16 × 16 WE ASIC is presented.

4.2 Computer-aided Integrated Circuit Design

As it was discussed in Section 2.5 the capabilities that CMOS VLSI provided with highly integrated reliable devices, has led to the development of ASIC's customised to the needs of individual applications. Computer-aided design (CAD) software has become an essential tool to the pipeline process of ASIC's from the electronic designer to the fabrication plant of a CMOS foundry. The automation of such tools has become all the more important in digital design by the needs of the modern consumer for more computing power. Specialised computer languages termed hardware description languages (HDL) have been developed to create register-transfer level (RTL) designs of digital electronic systems comprised of a very large number of digital circuits. Using a top-down approach

these high-level model designs can be translated into gate-level designs and finally be placed and routed into a physical design, all by automated software, to finally reach the manufacturer. However, in analogue and mixed-signal design the design process is more customised and a bottom-up design approach is followed. For analogue circuits models at the transistor and device level are used provided by the foundry. The models are constructed partly by equations that describe the behaviour of semiconducting structures and characterisation measurements. Following a set of requirements, the design engineer custom builds the circuits using these fundamental elements. The degrees of freedom for the designer are higher in this case where the available materials are organised by the foundry in drawing layers accompanied by their respective constraints. ICs cannot be tested on a breadboard for verification thus an accurate simulation that takes into account semiconductor physics and parasitic effects is necessary. An established software package used for these by major industrial corporations is Cadence [162], its individual components and their use will be explained in the next paragraph.

4.2.1 Integrated Circuit Design Flow

The design of an analogue or mixed-signal system (without complex digital units) commences with a set of requirements according to the desired application and the design process follows logical steps, as shown in Figure 4.1. These requirements determine the specifications of the circuit. Some hand calculations are required at this stage to find the transistor and other components sizes according to the specifications and the circuit diagram is drawn in Cadence Virtuoso schematic editor. The design is often split into different blocks and then connected and combined together into hierarchical blocks. Certain parameters can be set at this stage and the circuit can be simulated after its conversion to a netlist (a circuit description language) by the Cadence Virtuoso analogue design environment (ADE) an advanced version of the SPICE simulator developed by the University of California Berkeley [163]. The simulation results at this stage correspond to a typical response by each of the elements used in the circuit design. Parasitic and effects caused by their physical dimensions or placement are not taken into account. If the simulation results agree with the set requirements the process can continue to the physical design (layout) of the circuit. This process is usually repeated many times before the response is

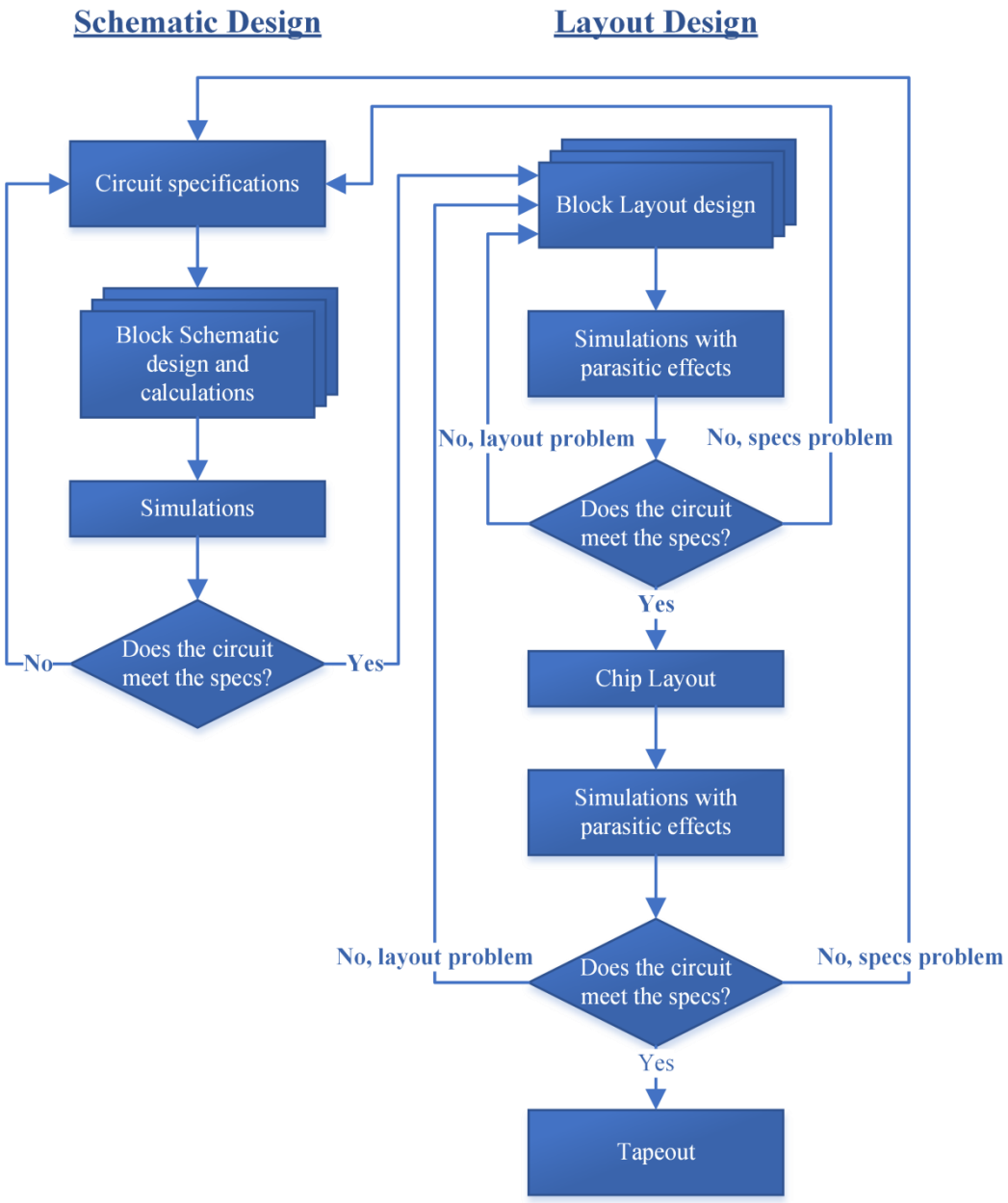

Figure 4.1: Flow diagram of the analogue design process.

matched. The physical design of the circuit blocks is prepared at this stage with Cadence Virtuoso layout suite, allowing the electronic designer to use layers that define photomasks of different steps in the fabrication process conducted at the foundry. Certain constraints have been set by the foundry for the chosen CMOS technology in this tool to follow their guidelines e.g. for dimensions and spacing. An embedded tool called design rule checker (DRC) is used to verify compliance with these requirements. After a successful run of the DRC a layout versus schematic (LVS) checker is used to verify that the physical layout corresponds to the original circuit diagram block. A tool named Quantus QRC is used for the parasitic extraction of resistances and capacitances by the physical design into a netlist. A second round of simulations with ADE follows using these

netlists, if the requirements are not met at this stage it falls in the designer's judgement to identify whether this is a layout or a specification problem. Finally, when the physical design of all the blocks is prepared and verified they are all combined in the chip layout. A final check versus a chip schematic is conducted and the system is simulated and compared to the specification for a last time before the design is sent for fabrication to the foundry (tapeout).

4.3 Simulation of the Electrochemical Cell Geometry

Simulations are needed to investigate the behaviour of ICs and electrochemical systems. The electrical simulation tools discussed in Section 4.2 were used to conduct simulations using the network method described in Section 2.8. The microelectrodes and the integrated potentiostat construct an electrochemical cell. The simulation setup of the electrodes in a chemical environment and the ICs were combined in Cadence to offer bidirectional information on both parts of the electrochemical cell. Even though specialised finite element analysis software for electrochemistry (e.g. COMSOL Multiphysics [164]) could be used for the simulation of the microelectrode structure, such an approach would neglect the contribution of the designed ICs in the electrochemical response. The simulation provided an insight in the electrode-electrolyte response and used a very close approximation to the real electrical load the integrated potentiostats needed to drive as well as how their WEs multiplexing affected the system's stability. The effect of multiple potentiostats being connected on the same electrical network was studied under these conditions. Furthermore, the electrochemical response that could be studied by this simulation enabled the investigation of a good geometrical design of electrodes to assist the MEA design so that it would operate as an electrochemical cell microarray (ECM) with an independent function per electrochemical cell. Concluding, these features lead to an approximate representation of the chemical environment's electrical response and a very good load model for the accurate design of the integrated circuits.

In this section the spatial potential distribution and the electric field pattern in the chemical solution are presented for two electrode geometries. The effect of the electrode geometries on the independent operation of electrochemical cells was investigated by placing two electrochemical cells next to each other. A

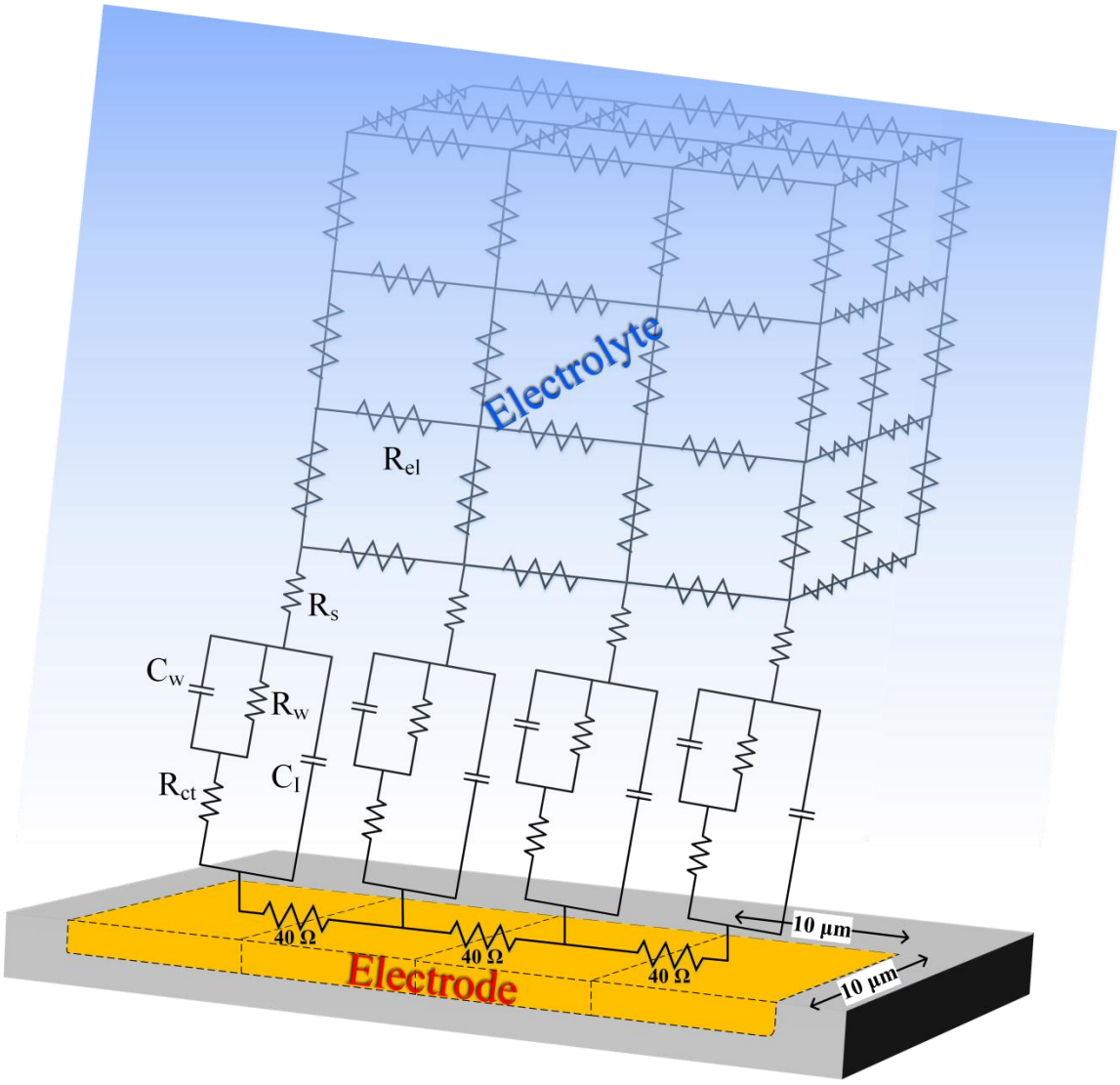

Figure 4.2: A visual representation of the impedance mesh structure used for the electrical simulation of the electrode arrangement.

simple example of 4 electrodes was used in each electrochemical cell of the microarray. The electrical equivalent of the electrode-electrolyte interface that was described in Section 3.3 was used. An electrical circuit described with 3-D spatial coordinates was constructed to simulate the electrical response of the electrode arrangement immersed in a chemical solution. Figure 4.2 shows the visual representation of the impedance mesh structure used for simulations of the electrode arrangement. The geometrical shape of the electrodes was divided into 10 × 10 μm^2 two dimensional elements (as flat surfaces) connected to each other with 40 mΩ/□ resistors as transmission lines (represented as 40 mΩ resistors in Figure 4.2) [165]. The value of the resistors was chosen following guidance of a typical sheet resistance of the top metal layer in a CMOS process,

as this is where the microelectrodes are typically designed in CMOS MEAs. Each of the 10 × 10 μm^2 elements was represented by an equivalent circuit model as the one shown in Figure 3.8. For elements that were part of the reference electrode (RE), only a portion of the model (the spreading resistance) was used as it was considered to be an ideal non-polarisable electrode. All the elements were connected to points of a resistor mesh that represented the electrolyte resistance of the chemical solution. The 3-D cubic mesh was made of resistors R_{el} for a solution volume of 200 μm × 200 μm × 90 μm. The electrolyte composition of the chemical solution assists in the value determination of $R_{el} = \rho_{el}/x$ where x is the grid size of the cubic lattice and ρ_{el} the electrolyte resistivity. The chemical solution was assumed to consist of 0.1 M tetrabutylammonium hexafluorophosphate ($TBAPF_6$) dissolved in acetonitrile. $TBAPF_6$ is a good supporting electrolyte commonly used in chemical solutions of non-aqueous solvents to reduce the solution's resistivity and prevent migration, which was explained in Section 3.2 that it is a source of non-Faradaic currents. The resistivity of this compound is ρ_{el} = 60.82 Ω·cm [166]. The x value chosen for these simulations was 10 μm, equal to the electrode element side length, thus

			10 × 10 μm^2 element	**20 × 20 μm^2 element**
Parameters	**Values**	**Impedance part**	**Values**	**Values**
ρ_{el}	60.82 Ω·cm	C_l	10.6 fF	42.3 fF
z	1	R_{ct}	39.1 MΩ	9.77 MΩ
U_t	26 mV @ 298 K	R_w	46.1 GΩ	11.5 GΩ
U_0	0.50 V	C_w	3.45 fF	13.8 fF
k^0 [167]	6.74 m/s	R_s	26.8 kΩ	13.4 kΩ
a [167]	0.6			
ε_r	37.5			
L_D	2.09 μm			
D_{Fc}	2.60 x 10^{-9} m^2/s			

Table 4.1: Parameters used for the calculation of the impedances of the electrode-electrolyte electrical equivalent model and each impedance part substituted values for a 10 × 10 μm^2 and a 20 × 20 μm^2 element.

R_{el} = 60.82 kΩ. An uncompensated iR drop that was defined in section 3.2.3 was considered negligible for the purposes of these simulations.

To construct a cubic mesh in a two-dimensional schematic circuit diagram each node was assigned a three-digit number corresponding to the XYZ coordinates of the point in the cubic mesh. The representation of the electrolyte was prepared with SPICE netlists containing resistors and capacitors. Due to the large number of nodes, a program was developed in C++ to create the netlist files. The program also allowed for the prospective change of the electrolyte composition. An additional program was developed that connected the electrode nodes of the electrode-electrolyte equivalent circuit to make transmission lines in the shapes of the electrodes. All these netlists were imported and modified in Cadence Virtuoso schematic editor to construct the chemical schematic block of the simulation. The size of the 200 μm × 200 μm × 90 μm volume was selected for the investigated electrode sizes and arrangements to fit in it. A larger volume was not considered as the complexity would be very high for Cadence Virtuoso ADE to simulate. The mesh ends were considered to be enclosed in an insulating electrically non-conductive container, thus the boundary conditions were considered to be infinite resistance nodes and they were not connected to any voltage source or any other circuit. The block was inserted as a symbol with input/output connections in another schematic diagram where input and power sources, opamps and transmission gate switches for the WEs were arranged as a simple potentiostat setup to construct an electrochemical cell for simulations. The source code of the programs and the schematic diagrams of the simulated electrochemical setup are provided in Appendices A and B, respectively.

The WEs had a square shape of 20 × 20 μm^2. Instead of a transmission line design it was deemed more appropriate to calculate a separate set of numerical values of a single 20 × 20 μm^2 element for these electrodes. The 10 × 10 μm^2 electrode elements impedances values were also calculated. Table 4.1 summarises the impedances values, their calculation is explained in this paragraph. The model calculations were made for a solution of the aforementioned composition with the addition of 10 mM of ferrocene and 10 mM of ferrocenium. First, the interfacial (Stern) capacitance C_I was estimated, breaking it down to its Helmholtz (C_H) and Gouy-Chapman (C_G) capacitance components (equation

(3.20)). For the calculation of C_G the dielectric constant of the electrolyte (ε_r) [168], the thermal potential U_t at 298 K and ferrocene's one electron valency were used. Another term of the Gouy-Chapman capacitance is U_0 which was assumed to be 0.50 V as an average potential and the Debye length was calculated using equation (3.17). Most of these terms were also used to calculate C_H. The electrical double layer thickness (d_{OHP}) value was estimated by the Debye length as $d_{OHP} = 1.5L_D$. The next component calculated was the charge-transfer resistance (R_{ct}) using equation (3.22). The equilibrium exchange current that needed to be calculated for this component to solve equation (3.22) was found using $i_0 = AFk^0C_O^{*(1-\alpha)}C_R^{*\alpha}$ [142] which was mentioned in Section 3.2.2. k^0 and a were calculated using experimental observations of ΔE_p in cyclic voltammograms of the aforementioned chemical solution using a large scale experimental setup [167]. The setup included a CHI600D commercial

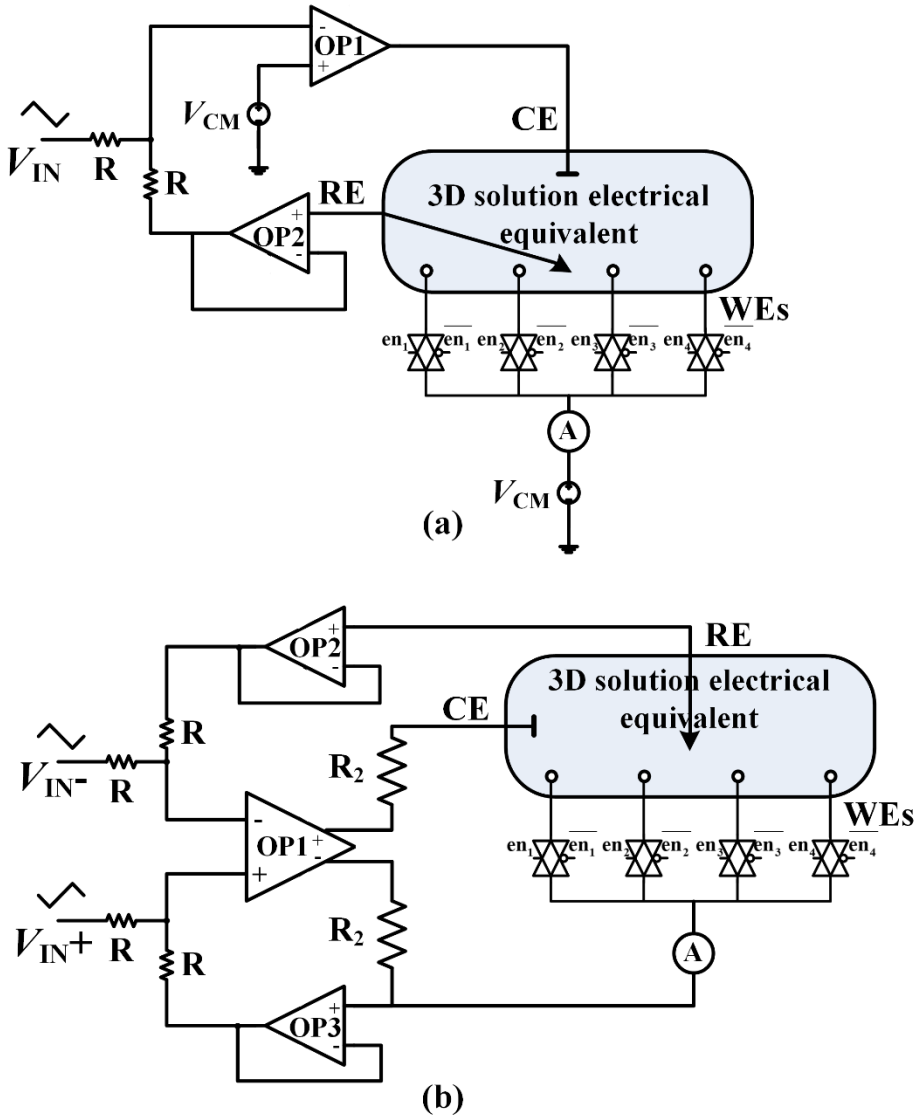

Figure 4.3: The electrochemical cell schematic setup used to simulate electrode arrangements with (a) a standard and (b) a fully-differential potentiostat design.

potentiostat from CH Intruments, a Pt wire as a CE, a Ag^{+}/AgCl quasi-RE (made by electrolysing a Ag wire in 3 M KCl) and a 3 mm glassy carbon electrode. For the calculation of the Warburg impedance (C_w and R_w), a typical value for the diffusion coefficient was used. In most of the electrochemical methods applied in this work, a varying signal was used. The frequency was set following the example of square wave voltammetry; for a scan rate of 1 V/s and a potential staircase shift ΔE_s = 1 mV the square wave frequency is f = 1 kHz. Lastly, ρ_{el} was used to calculate the spreading resistance (R_s).

After the model was built, it was included in an electrochemical cell setup with the schematic circuits designed with the CMOS technology models that were provided by the foundry. Several circuit implementations were tested on this setup, the one chosen was the simple circuit arrangement of Figure 4.3(a). It is similar to the standard potentiostat design presented in Section 2.5.1. The circuit was verified with transient signal simulations and it had the capability to multiplex between WEs. Electrode shapes and sizes were also tested on this setup to conclude to a size of the electrodes that complied with the current supply capabilities of the CMOS technology used in this work. Preliminary simulations with this setup exhibited low driving capabilities and an inability to adjust the electrical potential of independent electrochemical cells in the same chemical solution. This inflexibility led to the simulations setup of Figure 4.3(b) to be tested with the electrode geometries that made up the electrochemical cell microarray. This setup is similar to the fully differential potentiostat explained in Section 2.5.1. In order to view the potential distribution in the solution as a snapshot in space and time, the dc response of the simulations was stored as an ASCII file with the Cadence Virtuoso ADE. The file that described all the potentials at every single node of this schematic diagram was imported in programs that were developed and represented potential maps, current density vectors as well as electric field intensity maps in 2-D and 3-D formats.

A flowchart that represents the code that was developed to interpret the results is shown in Figure 4.4. After the file was selected through a “dialog box”, the ASCII file was scanned and the nodes’ and electrode-electrolyte element positions in space were identified by their naming. Values of the potentials were assigned to a 3-dimensional table. A gradient function was used to find the

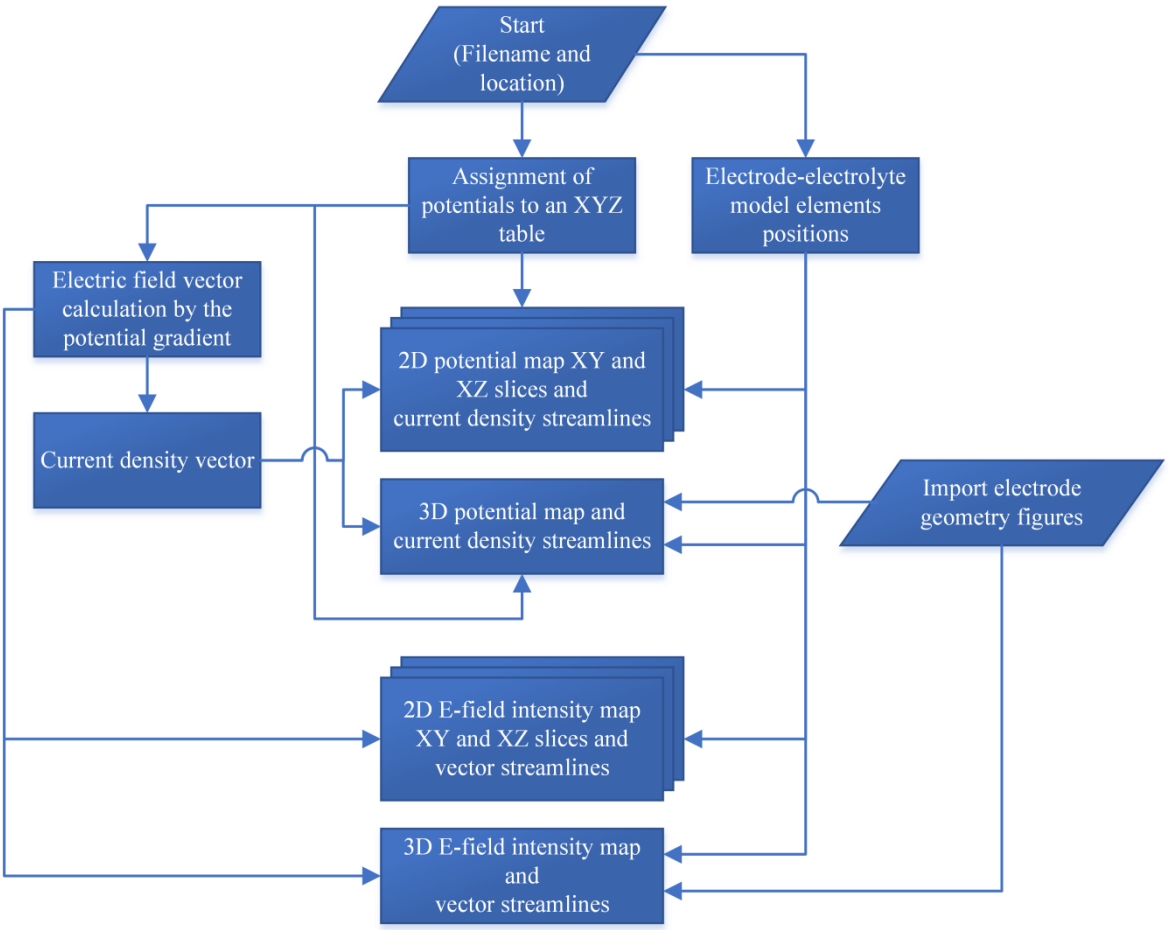

Figure 4.4: A flowchart describing the Matlab programs used to interpret the simulation results into potential distribution and electric field intensity maps with current density and electric field vectors.

electric field vector and the current density was found using the electrolyte's conductivity value. This data was then used to build the 2-D and 3-D space distributions of the simulated electrical response dependent on the circuit setup and the electrode geometry. The potential distribution was plotted against the working electrode potential (V_{WE}), since $V_{controlled} = -(V_{RE} - V_{WE})$, where $V_{controlled}$ is the controlled potential and V_{RE} is the potential at the RE. Due to the computing requirements and different case studies setups, the imaging process was split into separate programs in Matlab (provided in Appendix C.1) to represent all the results in a visually comprehensive manner. The most suitable electrode geometries for neighbouring electrochemical cells on a silicon substrate are discussed in the next sections.

4.3.1 Conventional Electrode Geometry

Using the setups shown in Figure 4.3, the electrode geometries were first simulated in a single electrochemical cell netlist to depict the spatial electrical

characteristics according to the geometrical shapes of the electrodes. The electric field intensity and the potential distribution were extracted by the aforementioned program in Section 4.3. A simple geometrical arrangement of the electrodes found in [52], [73] was first investigated and shown in Figure 4.4(a) where the electrodes are colour-coded. The CE and RE had a 10 μm width and the simulation was conducted for only a 4 WE arrangement as an indicative example. For this simulation V_{IN} was set at 0.65 V and V_{CM} at 1.65 V, resulting in an expected response of $V_{controlled}$ = 1 V. The resulting 2-D and 3-D potential maps were plotted against $V_{WE} = V_{CM}$. The first simulations exhibited a response of the potential distribution lower than the expected $V_{controlled}$ = 1 V. These simulation results indicated that the electrochemical simulations setup netlist of Figure 4.3(a) had limited driving capabilities. The results shown in Figure 4.5 were simulated by the simulation setup of Figure 4.3(b) which controlled the electrochemical cell adequately to attain the desired potential distribution at the electrodes. Each of the points shown in Figure 4.5(a) represent an electrode-electrolyte electrical equivalent connected to the electrolyte resistor mesh as explained in Section 4.3. They represent $10 \times 10\ \mu m^2$ electrode elements connected together with a typical 40 mΩ resistors to represent the metal sheet resistance and form the linear shapes of the CE and RE. WEs were single $20 \times 20\ \mu m^2$ elements. The element values were taken from Table 4.1.

As it can be observed in Figure 4.5(b) and (c), WEs placed close to each other as in the conventional design to fit them in the available space resulted in electric field intensity zones to overlap. Such an interaction has been recognized as a source of electrical cross-talk [136]. Analyte diffusion is also related to the electric field [31], as it was explained in Section 3.5.1; overlapping diffusion layers are responsible for chemical cross-talk among WEs. A planar diffusion layer that is observed in macroelectrodes can occur when placing microscale WEs in close proximity, diminishing the high current density characteristics of microelectrodes. Regarding the potential distribution, the CE was designed with a larger size than the WEs total area to be able to supply enough current and an electrical potential high enough to overcome the electrode-electrolyte interface impedance and the electrolyte *iR* drop. The simulations indicated that the use of potentiostats (either standard or fully-differential) regulate the potential so that it is defined around the RE. The potential distribution where these effects are

observed is shown in an XY plane at $z = 0$ µm and the 3-D chemical solution volume in Figure 4.5(d) and (e), respectively. These simulated results indicate a

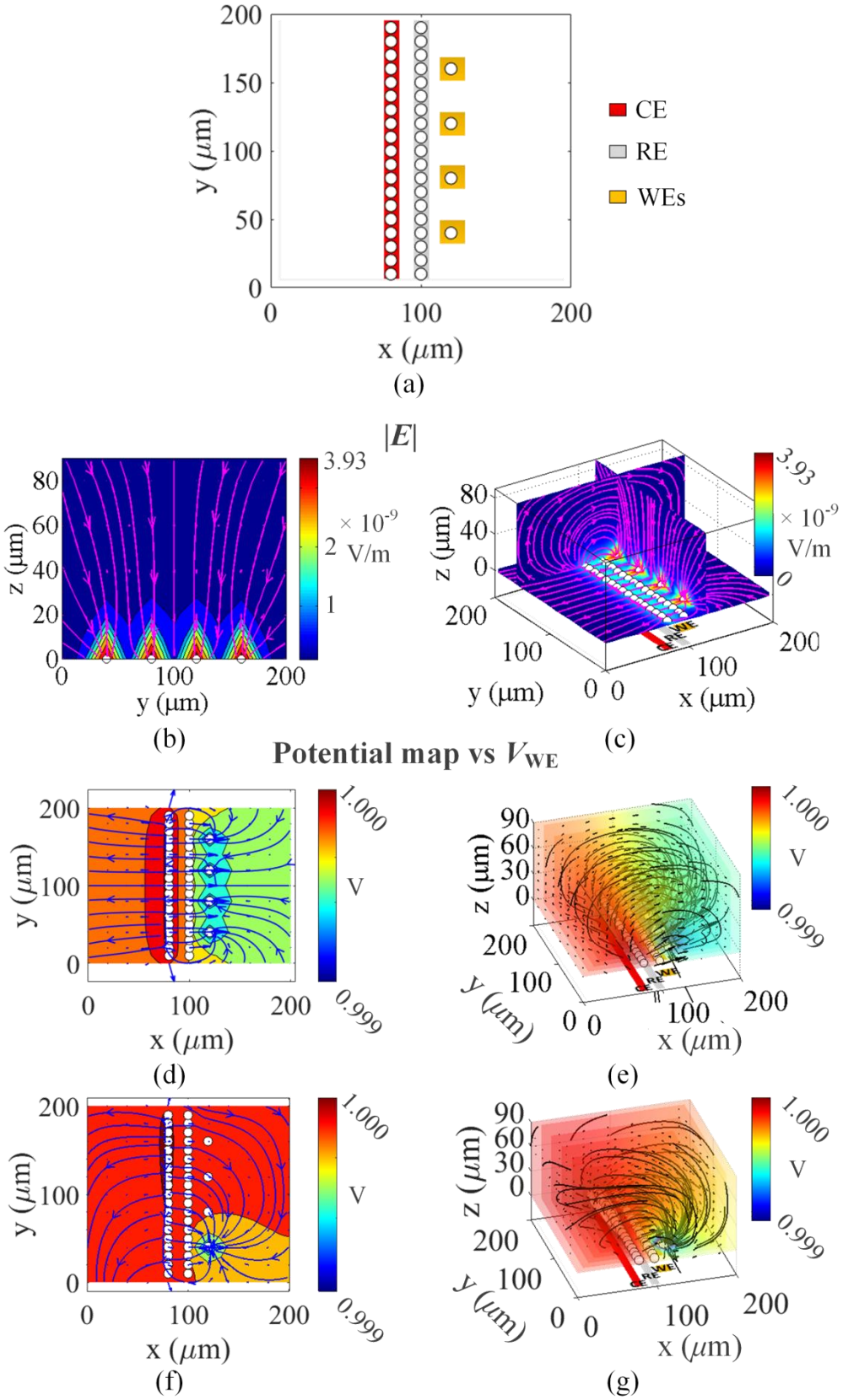

Figure 4.5: (a) A conventional electrode geometry pattern. The electric field intensity map and vectors of (b) an YZ slice at the WEs and (c) 3-D slices when all WEs were activated. The corresponding electric potential distribution and current density vector of (d) an XY slice at $z = 0$ µm and (e) the 3-D volume. The same potential distributions (f-g) when only 1 WE was activated.

division in two electrical potential regions. The electrode geometry lacked a barrier for charges to remain within the limits of the electrochemical cell. An uneven potential distribution around the very ends of the WE array compared to the inner ones can also be observed Figure 4.5(d). The electrode layout shape had an effect in the simulation of the electric field and current density, as they are also associated by:

$$\vec{J} = \frac{\vec{E}}{\rho} \tag{4.1}$$

The simulation indicated that the current (hence the charge movement) in this conventional geometry would flow as a cylindrical stream from the CE towards the WEs, as shown in Figure 4.5(d) and (e). A simulation of only one WE was also performed to test the electrical response with this geometry. The results are shown in Figure 4.5(f) and (g). The CE exhibited an uneven potential distribution with higher values at areas away from the WE.

4.3.2 Coaxial Electrode Geometry

In order to correct for the issues that were observed with the conventional geometry, a coaxial geometry that surrounds the WEs in coaxial RE and CE structures was developed, as shown in Figure 4.6(a). The pattern was designed so as to each WE would have an identical structure around it to maintain a consistent response from every WE of the electrochemical cell. The simulations were conducted with the CE enclosing a group of 4 WEs and the RE. Although using CE rings around every single WE would be a measure against intra-cell isolation, it was avoided to reduce capacitive coupling among the interconnections of these CE rings. The available space was used to place WEs at a distance to maintain the radial diffusion layers of each WE, as shown in Figure 4.6(b) and (c). In these simulation results the coaxial geometry demonstrated an inwards cycling current flow. Charges influenced by the electric field are more likely to follow a redox cycle within the cell than move to adjacent cells. Additionally, an equipotential area is observed in simulations of the coaxial layout. The area is defined in the vicinity of the RE and the surrounding CE act as a guard to it, as shown in Figure 4.6(d) and (e). As a result unlike the conventional electrode geometry, in the coaxial geometry the charges were

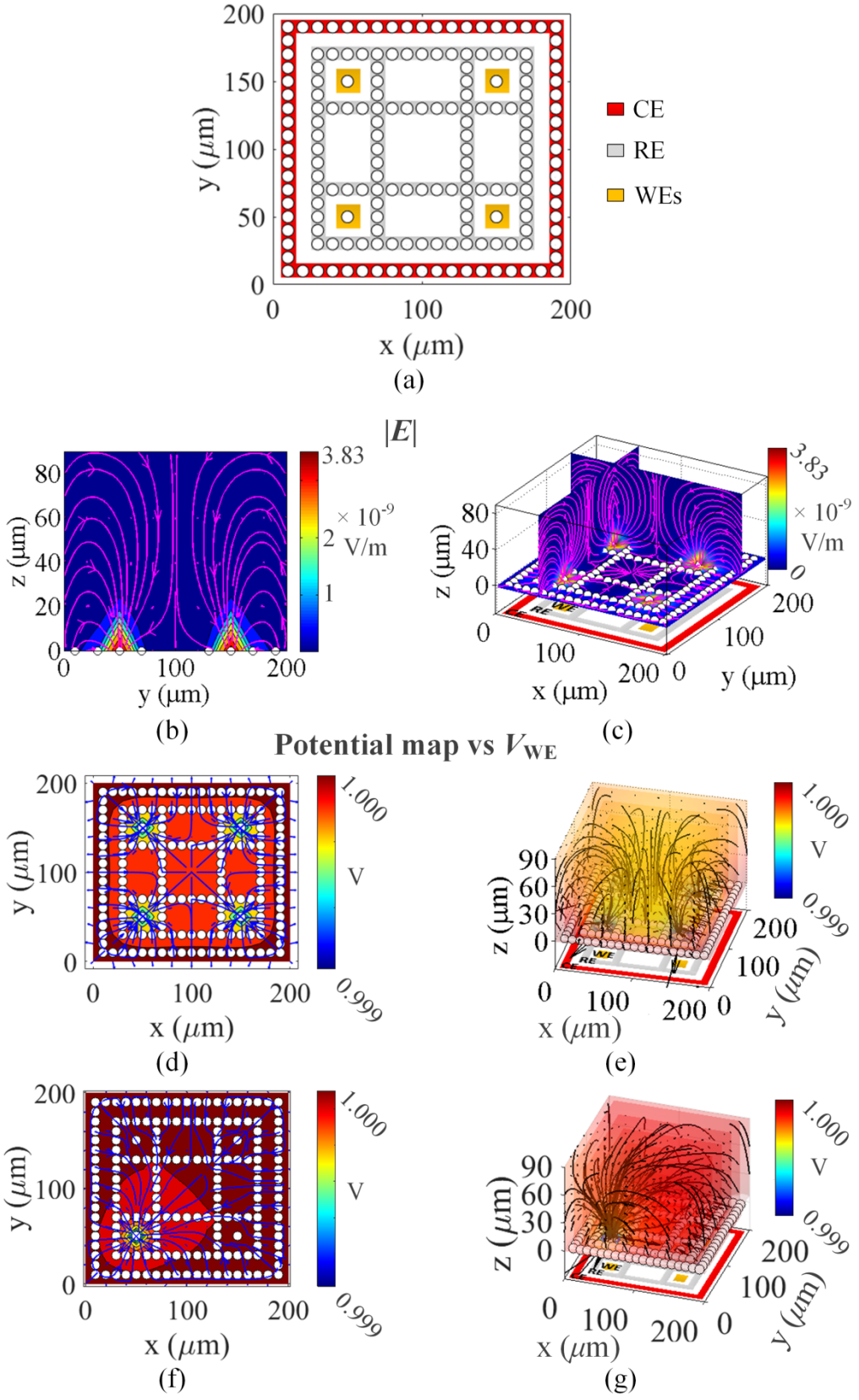

Figure 4.6: (a) A coaxial electrode geometry pattern. The electric field intensity map and vectors of (b) an YZ slice at the WEs and (c) 3-D slices when all WEs were activated. The corresponding electric potential distribution and current density vector of (d) an XY slice at *z* = 0 μm and (e) the 3-D volume. The same potential distributions (f-g) when only 1 WE was activated.

surrounded by an electric potential barrier. Another positive effect of the coaxial arrangement was that all the WEs had an identical potential distribution

around them, indicating that any variability that might be observed in forthcoming experimental results would not be an effect of the potential distribution but rather of chemical species' inhomogeneities in the solution. In the case of only one active WE, the coaxial design exhibited an even electric potential around the CE and the variance was similar to when all the WEs were activated, as shown in Figure 4.6(f) and (g). However, the voltage at the vicinity of the RE was not equal on its whole area thus activating all the WEs simultaneously was considered a better option in terms of stability.

4.3.3 Simulation consistency

The use of electrical simulation software to simulate electrochemical phenomena was a choice that offered a more complete setup for the better understanding of both the chemical environment and the circuits. However, it is not the usual route followed to extract information for electrochemical systems. Two sets of further simulations of the two electrode geometries were performed to verify the consistency of the simulation setup to deliver a good approximation of the processes in an electrochemical system orientated by the parameters of the chemical solution's composition. In the first set of simulations the supporting electrolyte concentration ($TBPF_6$) was considered to be altered to investigate if the response of the electrical potential distribution would change to follow what was expected by the effect of the concentration change on the physical properties of the chemical medium. In the second set of simulations the mesh step size was reduced, essentially to depict an enlarged simulation of a part of each electrode geometrical arrangement. To achieve a mesh step size reduction to 5 μm all the elements of the 3-D impedance structure were recalculated for this value as it will be further explained below. The amount of nodes of the electrical network had to be maintained for the software to cope with simulating the large number of electrical elements. Thus the part of the electrode geometry under investigation was slightly altered to follow the behaviour of the original arrangement for only 1 WE.

4.3.3.1 Supporting electrolyte concentration change

A change in the supporting electrolyte concentration does not have a major influence on the values of the electrode-electrolyte model elements. However,

the supporting electrolyte is important to maintain high conductivity in the chemical solution, which in turn prevents migration of reactants. Lowering the supporting electrolyte concentration leads to an increase of the solution resistivity and a higher potential difference between the microelectrodes is expected. That effect of a higher potential gradient is exactly the source of migration effects to the reactants which in electroanalysis is understood by the appearance of large non-Faradaic currents, as explained in Section 3.3. For the means of this simulation a 1 mM $TBAPF_6$ concentration was considered only to verify that the simulation would result in higher electric potential gradients. The resistor value of the 3-D cubic mesh and the spreading resistance of the electrode-electrolyte models were recalculated for the $TBAPF_6$ concentration change. For 1 mM $TBAPF_6$ the electrolyte resistivity is ρ_{el} = 60.82 Ω·m, thus the value of the resistor elements of the 3-D mesh was recalculated as R_{el} = 6.082 MΩ, the spreading resistance for the 10 μm × 10 μm and the 20 μm × 20 μm electrode-electrolyte models were recalculated as R_s = 2.68 MΩ

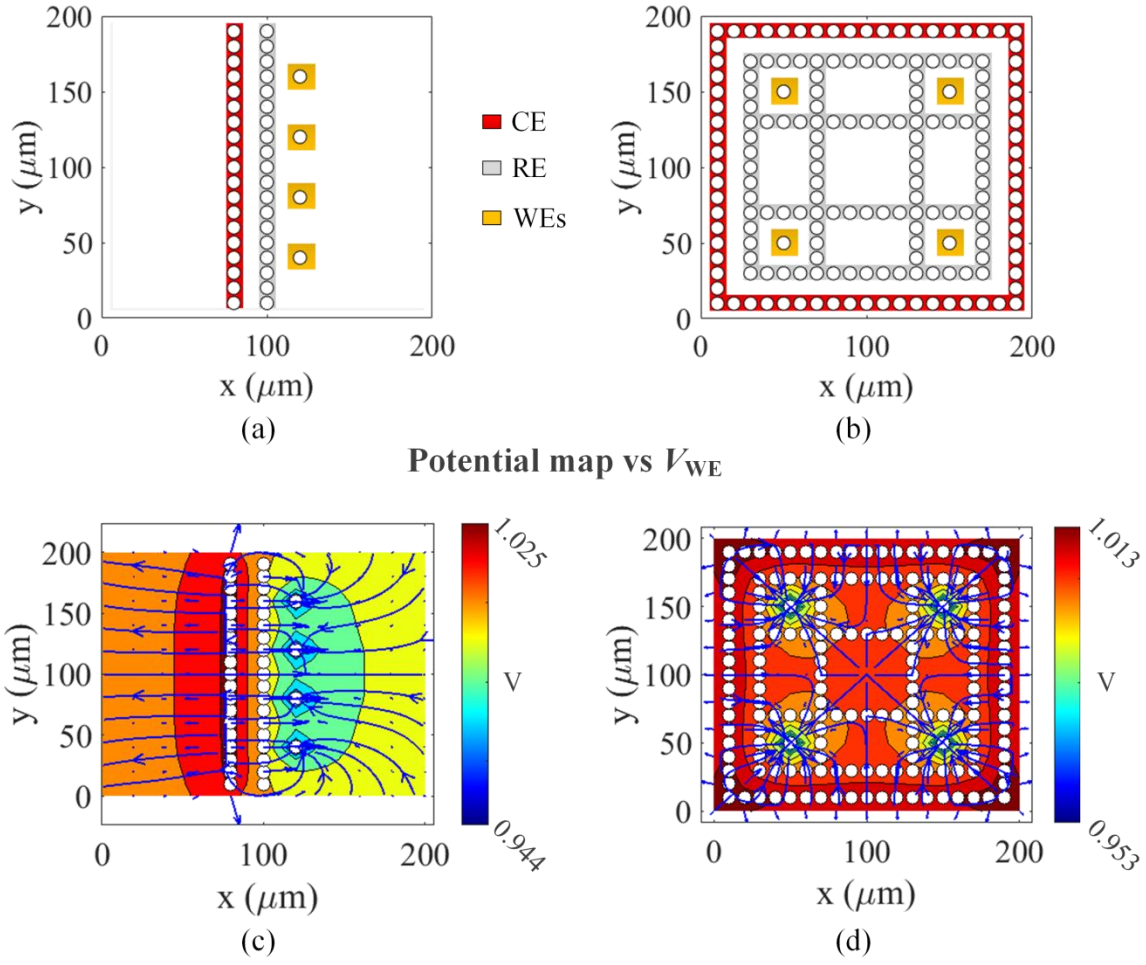

Figure 4.7: The a) conventional and b) coaxial electrode geometry patterns. The simulated electric potential distribution and current density vector for c) the conventional and d) the coaxial electrode patterns with all the WEs activated for 1 mM concentration of the $TBAPF_6$ supporting electrolyte.

and R_s = 1.34 MΩ respectively.

As it was expected the potential gradient increased in both electrode arrangements by the decrease of the supporting electrolyte's concentration, as shown in Figure 4.7. The range of electrical potential values has increased for both electrode geometries compared to Figure 4.5(d) and Figure 4.6(d). As it can be observed in Figure 4.7(c) the conventional geometry's potential range values are larger than the coaxial geometry's one, shown in Figure 4.7(d). The large potential variation caused by the low concentration of the supporting electrolyte induced a weak control over the potential of the RE as well as the uncompensated spreading resistance from the RE to the WE interface, as mentioned in Sections 3.2.3 and 3.4.2. For these reasons a relatively high concentration value of the supporting electrolyte is usually used, to ensure a low Ohmic drop between electrodes. This example was only simulated to verify the model's consistency. However, even in these conditions the coaxial geometry exhibited a better spatial control of the electrical potential as well as defined the potential distribution from all directions around the vicinity of the WEs, as illustrated in Figure 4.7(c) and (d). This simulation demonstrated that a controlled change in the model parameters led to a consistent response, according to the theory, from the electrochemical setup in the electrical simulation software. It also demonstrated a better control of the potential by the coaxial electrode as well as the reason why a relatively high concentration of the supporting electrolyte was used and a smaller Ohmic drop is observed in all other simulation figures.

4.3.3.2 Mesh step size reduction

After a change of an attribute was tested on the electrical software setup for the electrochemical simulation, the original parameters were used again but a complete change of all the impedances was attempted to move to a simulation with an increased accuracy over a smaller region of the electrode geometries. The mesh step size was reduced from 10 μm to 5 μm, meaning that the resistor elements of the mesh representing the electrolyte resistivity were changed to represent a 5 μm step in all directions, thus for ρ_{el} = 60.82 Ω·cm the new resistance was R_{el} = 121.64 kΩ. The electrode-electrolyte model two dimensional elements were corrected for a 5 μm × 5 μm area and the WE elements for a

			5 × 5 μm² element
Parameters	**Values**	**Impedance part**	**Values**
ρ_{el}	60.82 Ω·cm	C_l	2.65 fF
z	1	R_{ct}	156 MΩ
U_t	26 mV @ 298 K	R_w	184 GΩ
U_0	0.50 V	C_w	863 aF
k^0 [167]	6.74 m/s	R_s	53.7 kΩ
a [167]	0.6		
ε_r	37.5		
L_D	2.09 μm		
D_{Fc}	2.60 x 10^{-9} m^2/s		

Table 4.2: Parameters used for the calculation of the impedances of the electrode-electrolyte electrical equivalent model and each impedance part substituted values for a 5 × 5 μm² element.

10 μm × 10 μm area, connected together with 40 mΩ/□ resistors as transmission lines to construct the electrode geometry, as previously described in Section 4.3. The 10 μm × 10 μm electrode-electrolyte model element impedance components that were used were the same as in Table 4.1, the 5 μm × 5 μm elements along with the parameters used for their calculations are summarised in Table 4.2.

The electrode geometries are shown in Figure 4.8(a) and (b). The width of the CE and RE was kept at 10 μm and the WE side length at 20 μm, as for the original geometries. The points shown on the electrodes were quadrupled compared to the amount of elements fitted in the same length in the original simulation setups shown in Figure 4.5(a) and Figure 4.6(a) due to a half size reduction of the mesh step size. For the original geometries to be simulated with the reduced mesh step size a very large number of impedance elements would have to be used in the electrical simulation software which would be hard for the latter to handle. A smaller version of the geometries was devised, that demonstrated the same conceptual completeness as the original geometries. More specifically, as shown in Figure 4.8(a) only one WE was placed in the conventional geometry

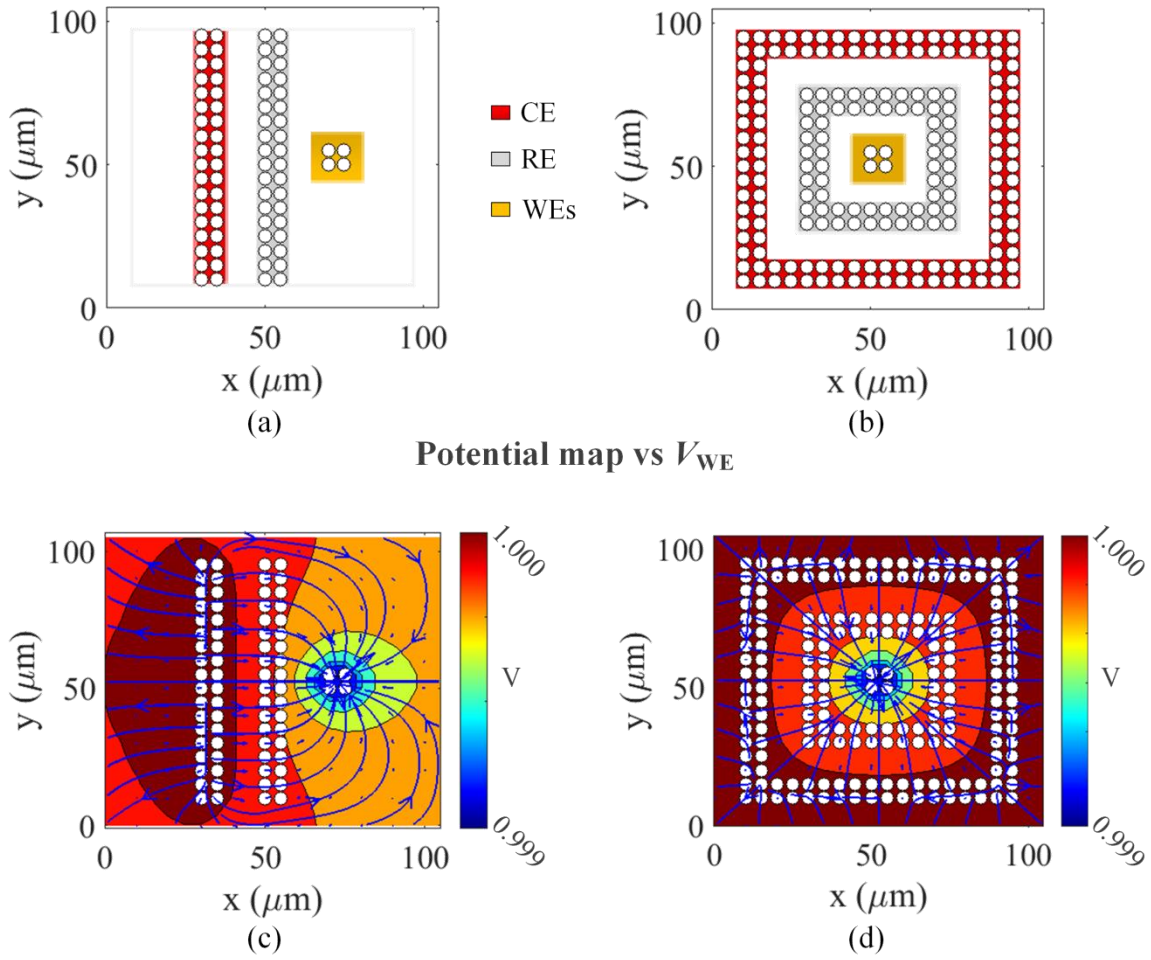

Figure 4.8: The amended a) conventional and b) coaxial electrode geometry patterns for a 5 µm mesh step size. The corresponding simulated electric potential distribution and current density vector for the amended c) conventional and d) coaxial electrode patterns.

pattern where two were originally designed to maintain symmetry and a direct comparison to the coaxial geometry of Figure 4.8(b). Likewise, the CE and RE structures were altered to surround only 1 WE.

The simulation results with the smaller mesh step size for the conventional and coaxial geometry are shown in Figure 4.8(c) and (d), respectively. The potential distribution was similar to the original geometries, as shown in Figure 4.5(d) and Figure 4.6(d). The range of potentials was equal to the original geometries, exhibiting a consistent response independent to the impedances used to construct the electrochemical model, as long as it is relied upon the electrochemical theoretical basis established in Chapter 3. The conventional geometry displayed a current flow that followed the cylindrical movement seen in Figure 4.5(d) and (e). The potential distribution of Figure 4.8(c) resembles more the one found in Figure 4.8(f) and (g) regarding to the fact that a single WE is turned on in both cases. The lack of nearby WEs by the design found in

Figure 4.8(a) led to the formation of an individual diffusion profile around the WE instead of a combined one. The coaxial geometry exhibited an inwards cycling current flow and a potential distribution that controlled the potential at the RE inside the region enclosed by the CE in a manner that resembled the result of Figure 4.6(d) and (e), as shown in Figure 4.8(d). This smaller version of the coaxial geometry, shown in Figure 4.8(d), demonstrated an equipotential region at the CE similar to its original counterpart. The investigation of a smaller mesh step size demonstrated a consistent response of the electrode geometries by the electrochemical simulation setup. The electrochemical simulation setup appears to be a good candidate for electrical investigations of electrochemical systems. Investigating the electrical effect on the electrode structures if they were to be repeated and controlled by independent potentiostats is described in the following section.

4.3.4 Independence of Adjacent Cells

The two microelectrode geometries were simulated to investigate the electrical response in a single electrochemical cell. To verify how these patterns would behave in an array format a new set of simulations was performed with two of these simple patterns placed side by side and operated by two independent driving circuits, (Figure 4.3). The patterns along with their corresponding potentiostats were meant to construct independent electrochemical cells in the same sample media. Both the standard and the fully-differential potentiostats were used to search for the best candidate. First, two cells of the conventional electrode geometry were simulated side by side, as shown in Figure 4.9(a). When the standard potentiostats were used, the WEs of both cells were connected to V_{CM} = 1.65 V. The desired result was the chemical solution residing on top of the electrodes of an electrochemical cell to attain a different electrical potential value in respect to the WEs potential. However, even for small differences of $V_{controlled}$ on the electrochemical cells ($V_{controlled1}$ = −0.15 V and $V_{controlled2}$ = −0.05 V) the simulated result showed a degraded electrical response, exhibiting potentials around 0.05 V vs V_{WE} ($V_{controlled}$ = −0.05 V), as shown in Figure 4.9(b). The standard potentiostats were competing to establish their configured electrical potential leading to the electrochemical cell configured at $V_{controlled1}$ = −0.15 V (left) to lower its potential response. The main reason for this behaviour was the low electrolyte resistivity which worsens the

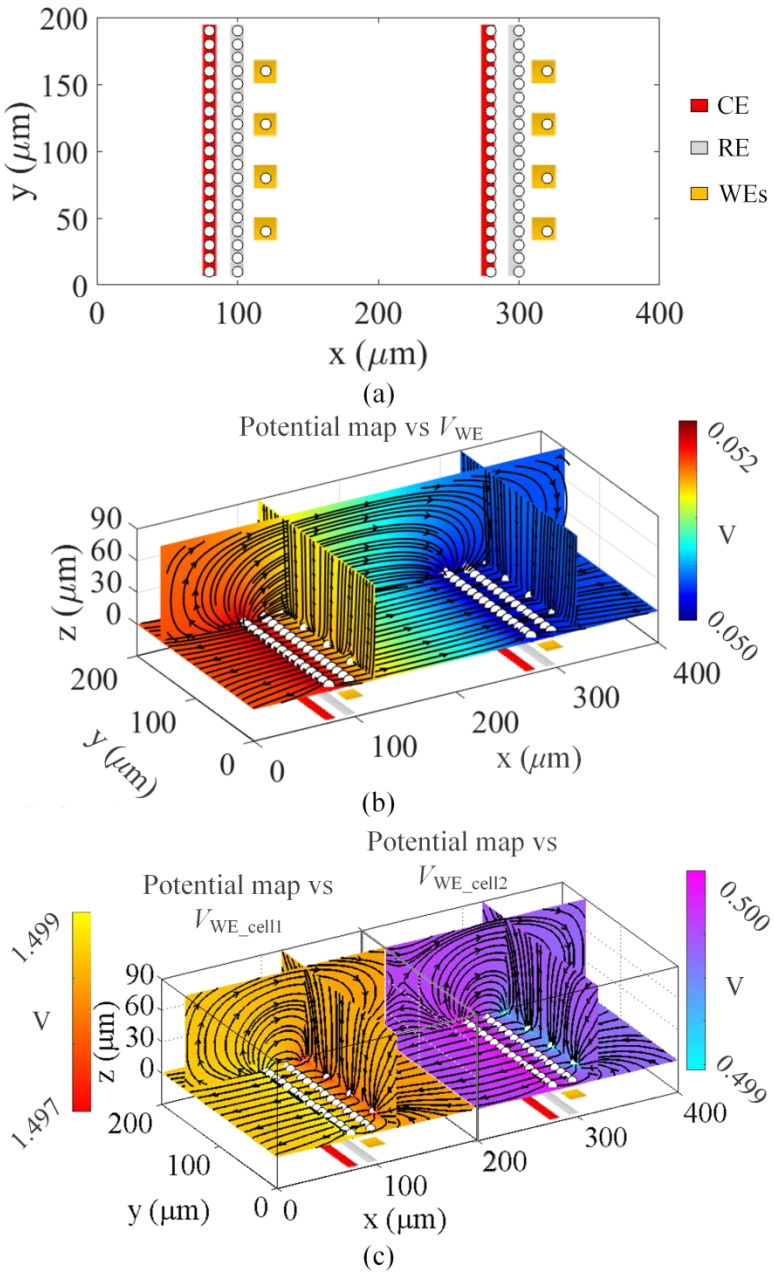

Figure 4.9: (a) Two electrode systems of the conventional geometry positioned side by side. The potential distribution of the chemical solution using (b) the standard potentiostat circuit and cell potential settings of $V_{controlled1}$ = −0.15 V and $V_{controlled2}$ = −0.05 V respectively and (c) the fully differential potentiostat circuit and cell potential settings of $V_{controlled1}$ = −1.5 V and $V_{controlled2}$ = −0.5 V respectively.

response. The current was mostly sourced to the CE of the adjacent cell and other transient simulations exhibited an unstable response. The fully differential potentiostat setup was then used to counteract on the defects of single-ended opamps and make stable systems independent of the chemical solution composition. Besides the advantages offered by the fully differential potentiostat that were explained in Section 2.5.1, the control opamp used in this design has the capability of auto-adjusting both CE and WEs electrical potential levels to achieve the desired $V_{controlled}$. The results using this potentiostat design

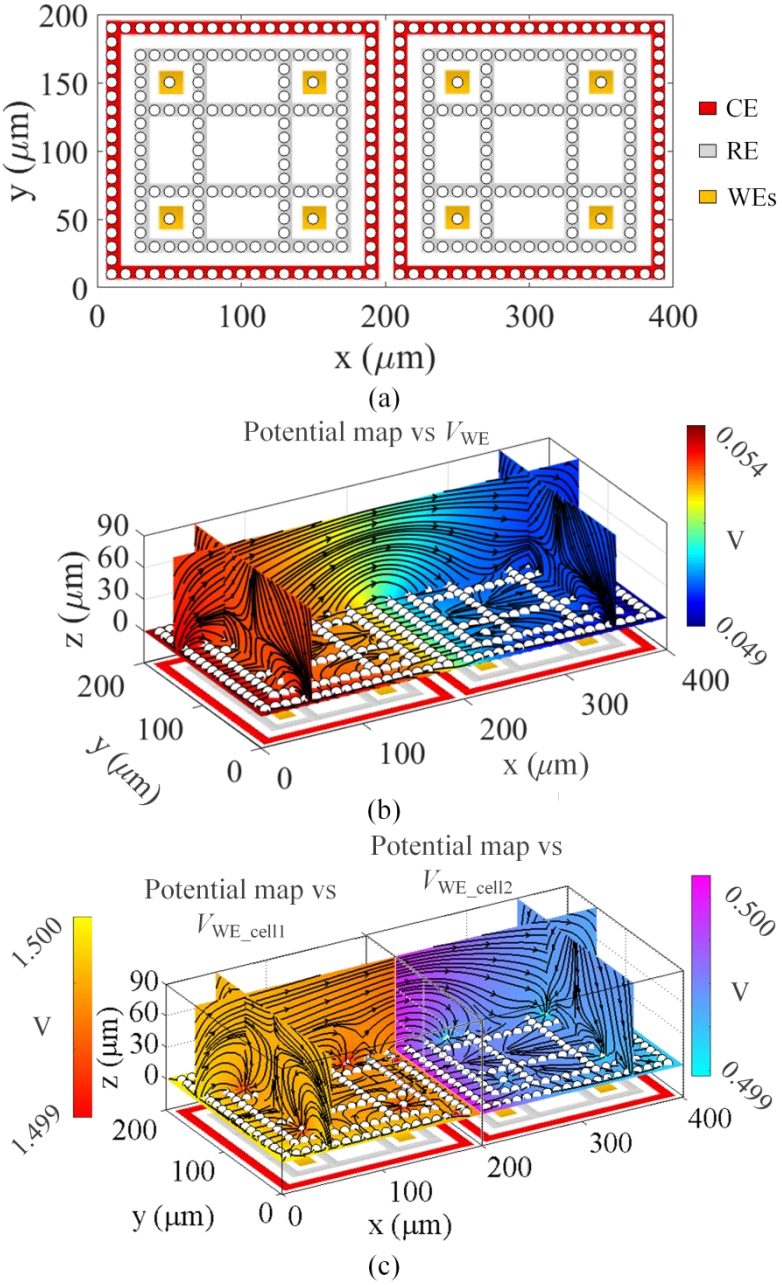

Figure 4.10: (a) Two electrode systems of the coaxial geometry positioned side by side. The potential distribution of the chemical solution using (b) the standard potentiostat circuit and cell potential settings of $V_{controlled1}$ = −0.15 V and $V_{controlled2}$ = −0.05 V respectively and (c) the fully differential potentiostat circuit and cell potential settings of $V_{controlled1}$ = −1.5 V and $V_{controlled2}$ = −0.5 V respectively.

are shown in Figure 4.9(c). The electrochemical cells were configured at $V_{controlled1}$ = −1.5 V and $V_{controlled2}$ = −0.5 V. The results are depicted against the WE electrical potential value of each cell since $V_{controlled} = -(V_{RE} - V_{WE})$. As it can be observed in Figure 4.9(c), the potential settings of each cell were regulated in the chemical solution. Although the electrodes auto-adjusted their potential values in respect to the chemical solution potential distribution, the electric potential varied more at cell1 (left) because cell2 (right) influenced its behaviour due to a lower potential setting. Moreover, an inter-cell leakage current from the CE of cell2 can be observed to affect the WEs of cell1.

The advantageous characteristics of the coaxial electrode geometry were tested with the design of adjacent cells simulation setup shown in Figure 4.10(a) and the same setups and electrical potential settings. As with the conventional electrode geometry when the standard potentiostat was used, the electrochemical cells could not regulate the potential distribution so that two different potential settings could be adjusted for the cells as it can be observed in Figure 4.10(b). The most successful combination of an electrode geometry and potentiostat architecture was that of the coaxial pattern and the fully differential potentiostat, as shown in Figure 4.10(c). The fully differential potentiostat was responsible for a distinct regulation of the potential distribution over each electrochemical cell by adjusting V_{CE} and V_{WE} accordingly. The microelectrode structure maintained a potential distribution around the RE to sustain a stable $V_{controlled}$. An inter-cell leakage current was mainly observed between CEs of the cells owing to a potential difference by the dissimilar potential settings of each cell. Surrounding the cell with a CE created a "shield" against leakage current that could affect the recording of current by the WEs. Owing to its coaxial nature, the geometry was deemed ideal to be used in an array and create independent electrochemical cell "islands" as it will be described in the next section.

4.4 CMOS Electrochemical Cell Microarray

The CMOS chip that was designed according to the simulations presented in the previous section was outsourced to ams AG, an established CMOS foundry that provides fabrication services and models for Cadence. The technology used in this work was a standard 4-metal 0.35 μm CMOS process biased at a 3.3 V power supply voltage. The process includes a mixed-signal design toolkit with libraries of analogue, digital and pad cells as well as some predesigned basic circuit blocks. After the design flow was completed, the design was outsourced to ams AG through the Europractice mini@sic multi project wafer service for fabless manufacturing. The service was provided at a reduced cost (5 % – 10 % of the full wafer cost). The chips were purchased as unpackaged dies that were later post processed in the James Watt Nanofabrication Centre (JWNC) located in the University of Glasgow [169].

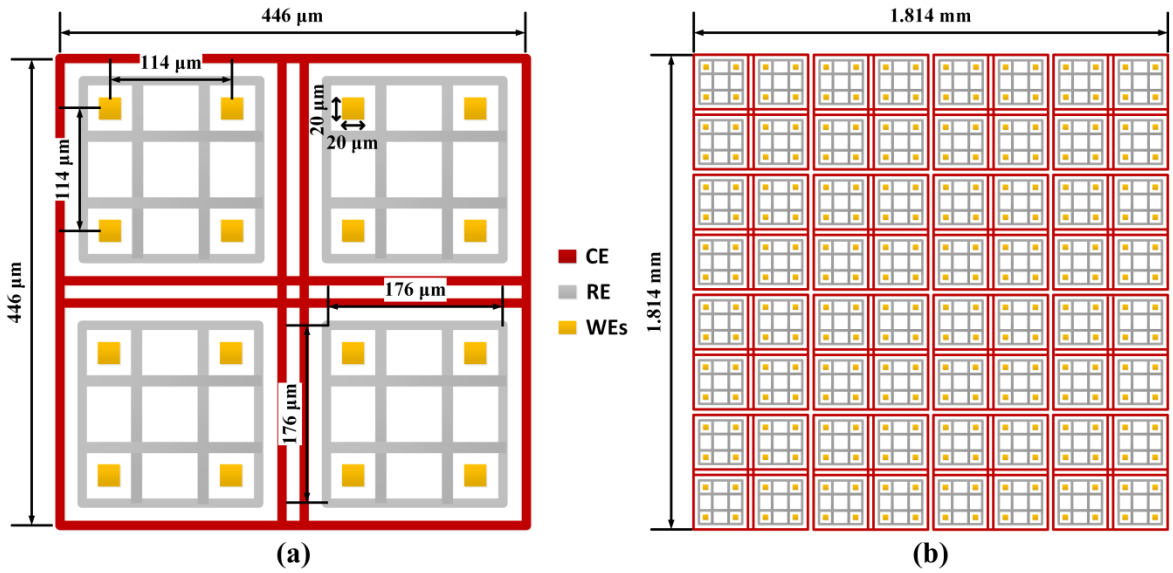

Figure 4.11: Microelectrode design of (a) one electrochemical cell and (b) repeated in a 4 x 4 array.

The simple coaxial electrode geometry that was presented in Figure 4.6(a) was expanded to include 16 WEs as presented in Figure 4.11(a). Local control of the electrodes was achieved by their integration with their respective electronic circuits on a CMOS chip. Each cell consisted of a sub-array of 16 WEs and a fully differential potentiostat [57] and it is controlled by distinct differential input signals. The electrode geometry was designed for the microelectrodes to be surrounded by the same structures as before in order to maintain a similar potential distribution as the coaxial ones presented in the previous section. The width of the CE and RE was 11 µm and the WEs side length was 20 µm. The patterns were repeated in a 4 × 4 array format maintaining a 114 µm WE pitch in all directions. The electrochemical cells had a 456 µm pitch and the active area of the whole array was 1.814 mm × 1.814 mm, as shown in Figure 4.11(b). To meet the requirements of this electrode geometry a design that included a fully differential potentiostat was used and it will be presented over the next sections.

4.5 Potentiostat Design

The potentiostat design along with WE multiplexing and functionalisation switches used in every single electrochemical cell is presented in Figure 4.12. The fully differential potentiostat was similar to the design shown in Figure 2.7 [57] using a folded-cascode fully differential control opamp (OP1) and 2 simple 2-stage differential amplifiers (OP2 and OP3). The current was converted with a

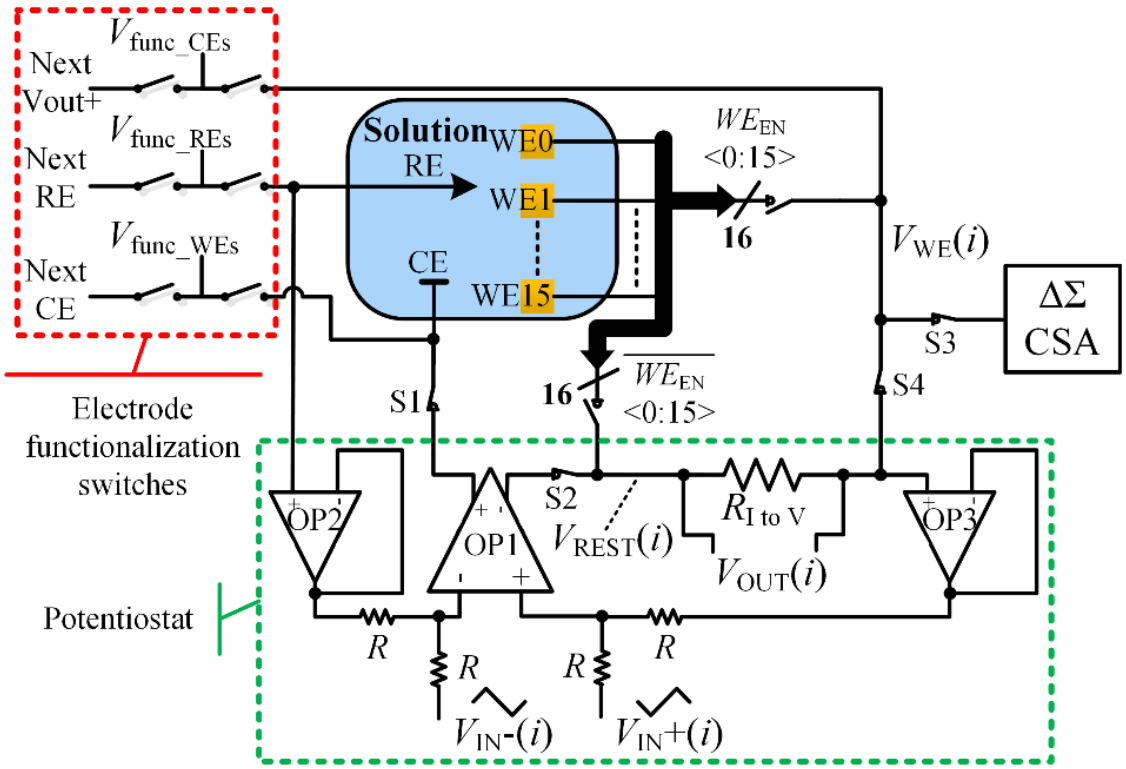

Figure 4.12: The fully differential potentiostat with the multiplexing WE circuit and functionalisation switches [170].

simple current to voltage resistor $R_{I\ to\ V}$ directly connected to ESD protected analogue pads. A high sheet resistance 200 kΩ polysilicon resistor per electrochemical cell was integrated on chip. Switches S1 and S2 were used to isolate the circuits from the electrodes and switches S3 and S4 to select the charge-sensitive amplifier (CSA) output. The design of the opamps, the functionalisation switches, the WE multiplexing circuit and the ΔΣ CSA are described in the next sections.

The presented system's operation is described as follows: Each potentiostat is operated by a pair of input signals, $V_{IN+}(i)$ and $V_{IN-}(i)$ that govern the control opamp's (OP1) operation. A feedback loop made up of the unity gain amplifiers (OP2 and OP3) regulates $V_{controlled} = V_{WE} - V_{RE}$ according to the input signals of the potentiostat. Electrochemical phenomena induced by the $V_{controlled}$ potential develop at the microelectrodes. The WEs are selected using a rolling shutter method with the WE_{EN} switches to multiplex them. The current associated with the electrochemical activity is sampled at the $V_{WE}(i)$. It is converted to an output potential at the cell's current to voltage resistor ($R_{I\ to\ V}$) or the ΔΣ discrete-time CSA. The output voltage or frequency changes indicate the degree of redox charge transfer occurring at the WE.

4.5.1 Fully Differential Amplifier

Advantages of a fully differential control opamp in the potentiostat design are to diminish common mode noise and an individual regulation of the CE and WEs potentials. As it was explained in Section 2.5.1 a fully differential potentiostat increases the output voltage swing and the dynamic range of the 3.3 V powered CMOS circuits allowing for wider potential windows hence a wider range of analytes [57], [58]. The simulations that were presented in Section 4.3 suggest that the feature is also essential to perform multiple voltammetric experiments in the same sample media simultaneously.

A folded-cascode fully differential opamp, shown in Figure 4.13, was used for the potentiostat design. A second stage was added to the design to enhance the output voltage swing and gain. The design benefits from a high dc gain, ideal for the low frequency signals used in electrochemical methods, a low input common mode noise and a wide bandwidth [57], [60]–[62], [81]. Two differential signals at an offset dc potential ($V_{DD}/2$ = 1.65 V) may be applied at the inputs. Depending on their relative potential difference the output voltages (V_{OUT+} and V_{OUT-}) would drive V_{CE} and V_{REST} of Figure 4.12 accordingly while biasing the transistors in the saturation region. A common-mode feedback loop (CMFB) would sense the outputs' common mode level using source followers to prevent

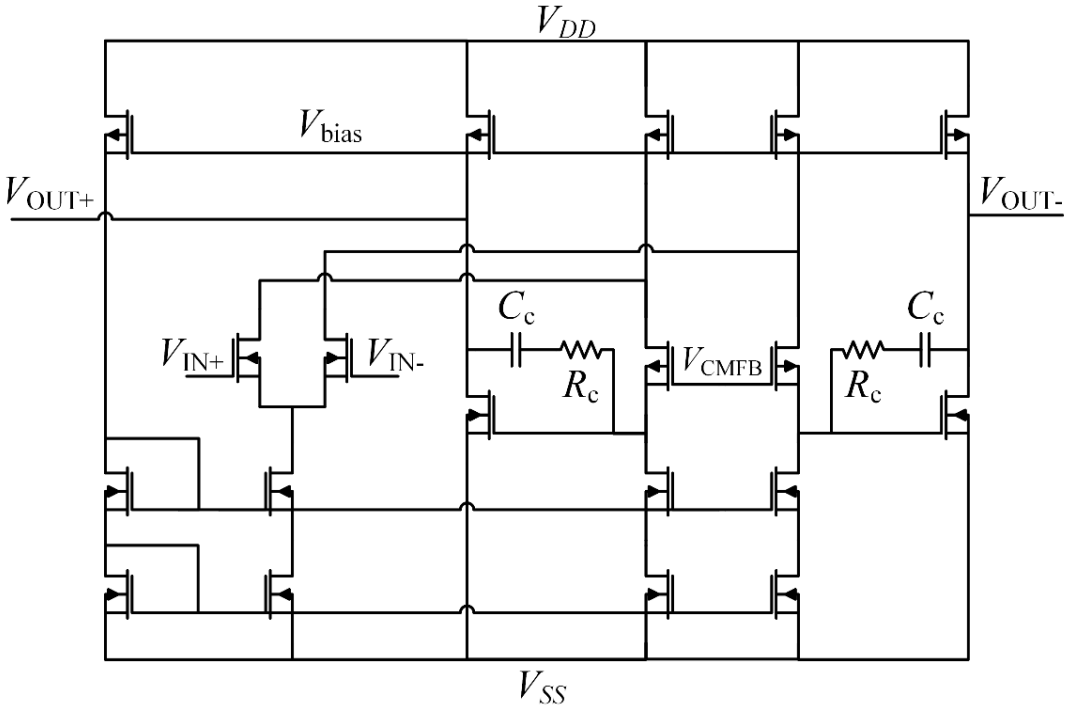

Figure 4.13: The folded-cascode fully differential opamp design [170].

resistive loading. The source followers outputs were connected to an integrated circuit of 500 kΩ coupled to 1 pF capacitors that sensed the output common mode signal. Polysilicon was used as the elements' material with the resistor exhibiting a high sheet resistance. The level was adjusted by an externally applied reference common mode voltage (V_{CM}) [13]. A single stage differential amplifier was used to adjust V_{CMFB} and complete the loop.

4.5.2 Bandwidth and Compensation

As the load that the control amplifier had to drive was both resistive and capacitive, compensation was necessary. Even though the folded cascode design offers a wide bandwidth, the addition of a second stage added a second pole that had to be compensated using a Miller compensation circuit. Moreover, switches that were added to choose the active WE required the opamp to be stabilised.

To design the control opamp to suit the needs of a potentiostat in a chemical solution it was simulated with the electrode-electrolyte models. A simpler version of the chemical solution model was used for the circuit to be simulated where the objective was to verify the electronic circuit design operation rather than the electrode geometries. In this case, the 3-D resistor mesh as well as information concerning the spatial locations of electrodes were not used as they

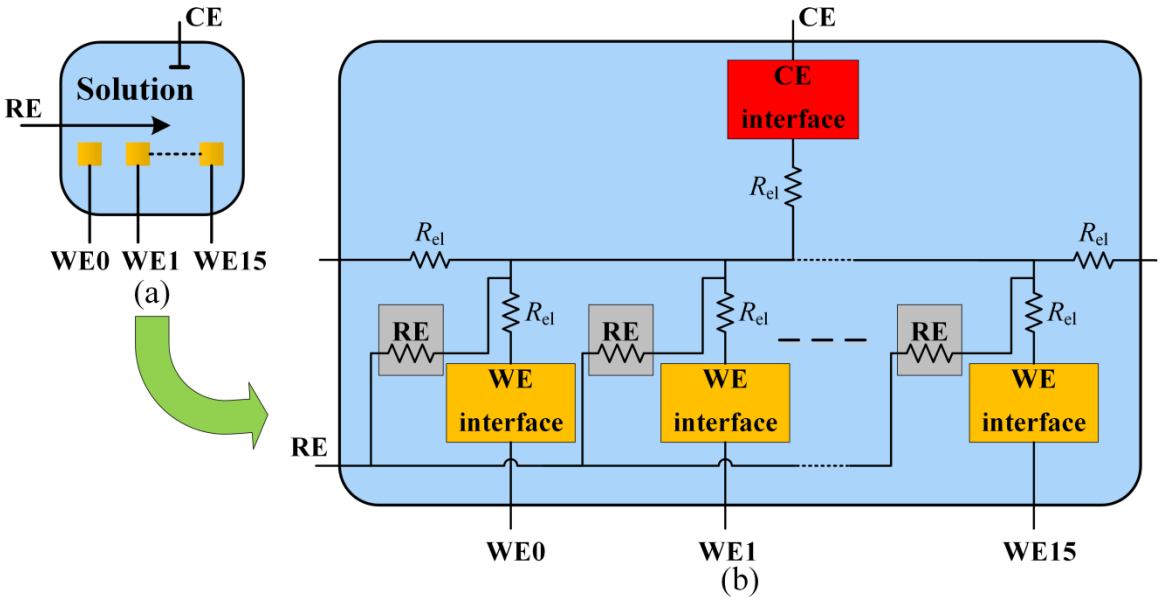

Figure 4.14: (a) A conceptual diagram and (b) the simplified electrical model describing the electrodes in the chemical solution lacking any spatial information of their locations.

3392 µm × 11 µm CE model impedances				
C_l	R_{ct}	R_w	C_w	R_s
3.95 pF	105 kΩ	124 MΩ	1.29 pF	406 Ω

Table 4.3: Impedance values calculated for the total area of a CE of an electrochemical cell.

led to rather long simulation times. If spatial information is neglected, the conceptual diagram of the chemical environment is presented in Figure 4.14(a). Electrically the electrode-electrolyte models of the electrodes were connected to each other with single R_{el} resistors symbolising a 10 µm length of electrolyte resistance, as shown in Figure 4.14(b). Additional resistive load of the order of the electrolyte's resistance could be removed as it did not have a major impact on the circuits' characterisation and reduced the simulation netlist size. The components in the electrode-electrolyte model of the WE interface were kept as in Table 4.1. The components for the CE interface were recalculated accounting for its whole surface area within an electrochemical cell, summarised in Table 4.3. The RE interface was only represented by a spreading resistance, calculated only for the square surface area that surrounded each WE. Each of these RE resistors were connected at nodes between the CE and each WE, as shown in Figure 4.14(b). That surface area was 164 µm × 11 µm and the spreading resistance was calculated as R_s = 4.83 kΩ.

The control opamp was designed using the parametric analysis tool of Cadence Virtuoso ADE in an open loop ac analysis. In Figure 4.15 the Miller compensating

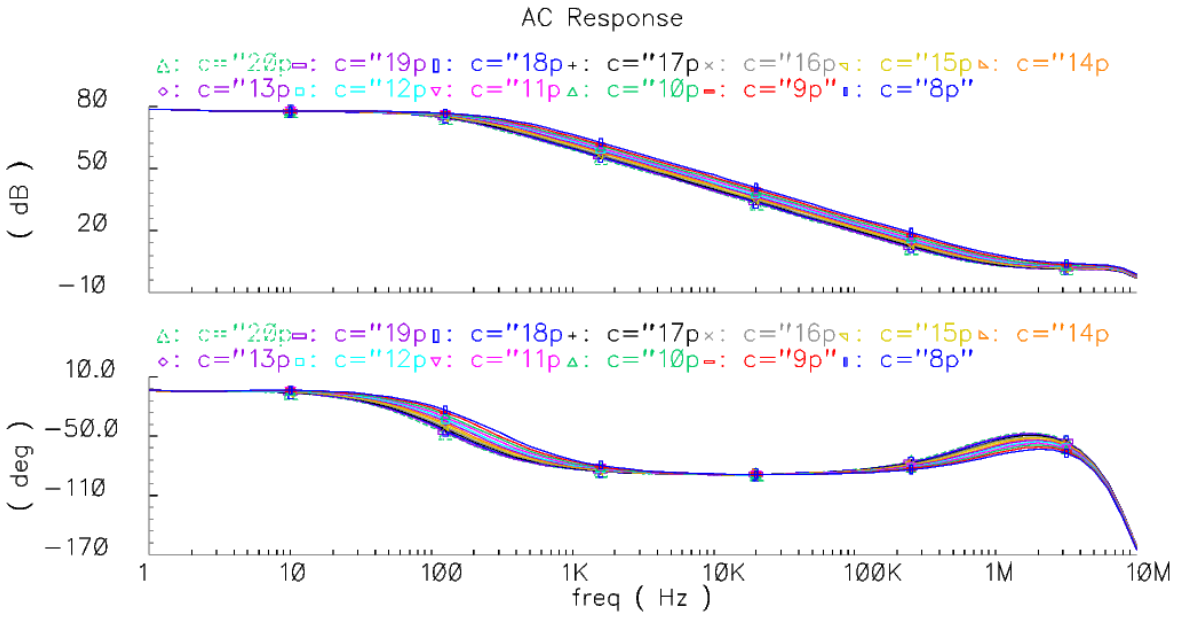

Figure 4.15: Bode plots of the folded cascode fully differential opamp for different C_c values.

capacitor's (C_c) value was changed to find a good compensation response. Initially the compensation values were: C_c = 15 pF and R_c = 10 kΩ but after the layout of the opamp block the simulated performance was better for C_c = 8 pF. The unity gain bandwidth recorded from the post-layout simulations was at 3.3 MHz with a phase margin of 110° and a dc gain of 77 dB. The designed opamp was also simulated for its stability with transient input signals and fast WE switching that introduced harmonic distortion. This performance was achieved at the expense of 940 μW power dissipation. Major contributors to the power dissipation are the compensation circuits and the stage of CMFB necessary for the correct operation of the fully differential opamp. The unity gain amplifiers' simulation indicated a a unity gain bandwidth of 29 MHz with a phase margin of 113° and a dc gain of 92 dB. Each of them exhibited a dissipation figure of 234 μW.

4.5.3 Multiplexing

An electrochemical cell of the array is comprised of its own subarray of WEs. Due to size limitations of the CMOS chip for the readout circuitry, the WEs of each subarray were multiplexed and the current of one WE was read at a time, using an approach that was first presented in [63], as shown in Figure 4.16. The WE selection was made with a 4 to 16 decoder (common for all the electrochemical cells) that was designed. Using the decoder, a transmission gate of the active WE was enabled (S0-S15) while the inverted signals were used to enable transmission gates that connected all the other WEs to V_{REST} $\left(\overline{\text{S0-S15}}\right)$, as shown in Figure 4.12 and Figure 4.16. An enable/disable switch and a switch that sets all the decoder outputs to the enabled state were added to the decoder for operations that required all or none of the WEs connected at the same node. Two readout methods were designed, a simple resistor for current to voltage conversion and a discrete-time current integrating (*i* to *F*) CSA [64]. Owing to its simplicity, the analogue readout of the resistor ensured for accurate readings. The digital *i* to *F* system is capable of recording currents of a lower magnitude, extending the range to a lower limit of detection (LOD). Each electrochemical cell was designed with its own analogue and digital output pads. To select the readout method of the array a pair of transmission gates (S_{int} and S_{trans})

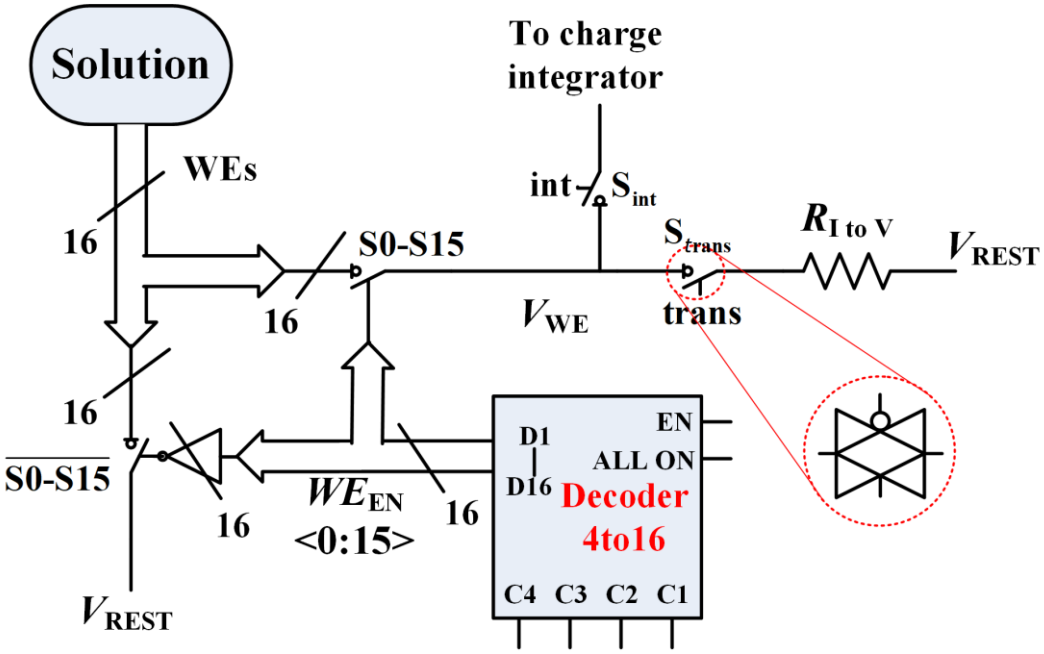

Figure 4.16: Multiplexing scheme for the WEs of an electrochemical cell and their connection to the two readout methods.

controlled by separate signals was placed at the WE connection point (V_{WE}), as shown in Figure 4.16.

The usual readout method of MEAs is each WE to be selected and the signals of an entire voltammetric experiment to be scanned. In this work the compensated design stabilised the potentiostat so that WEs of an electrochemical cell were multiplexed over segmented potential levels. A problem that may arise by the active multiplexing is the voltage at the WE surface to be perturbed therefore the analyte diffusion layer may be disturbed. Such problems were prevented and the current flow was sustained by connecting WEs whose currents were not read at V_{REST}. The small readout current magnitude changed the $R_{I\ to\ V}$ over only a few mV setting V_{WE} and V_{REST} at similar potentials. This small difference led addressed and non-addressed WEs to retain almost the same diffusion profiles.

4.5.4 Switches

The electrochemical cell microarray was designed to be a reconfigurable system by the introduction of switches to isolate or group parts of the array together. One part of these switches was placed at the outputs of the control amplifier to isolate the circuits' connection to the CE and WEs. When the switches are enabled by the Is_{EN} signal the S_{IS1} and S_{IS4} integrated switches (transmission gates) connect the outputs to ground while S_{IS2} and S_{IS3} act as high impedance

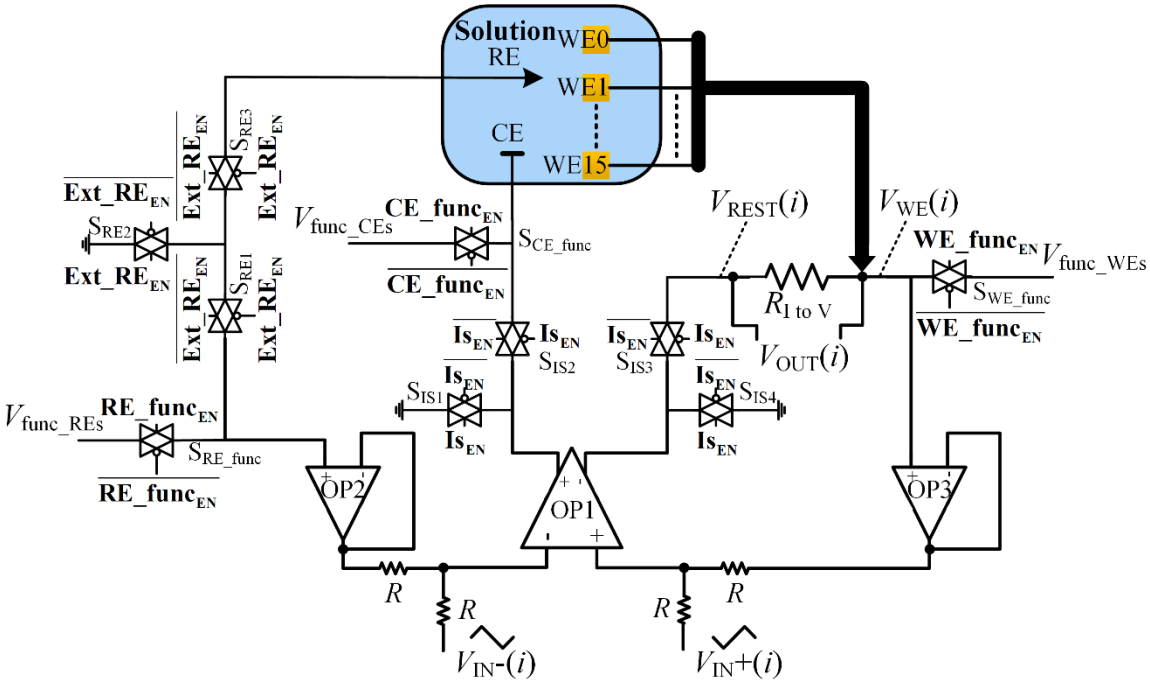

Figure 4.17: Isolation and grouping switches of the electrochemical cell microarray.

elements to the electrodes, as shown in Figure 4.17. After the isolation is ensured the chip can become functionalised (e.g. through electrodeposition) using a feature of the designed circuit. Voltages at nodes common to all electrochemical cells can be applied externally for the microelectrodes' functionalisation (V_{func_CEs}, V_{func_REs} and V_{func_WEs}), as shown in Figure 4.17. Each electrode type (CEs, REs or WEs) can be individually selected with transmission gates integrated in each cell (CE_func_{EN}, RE_func_{EN} and WE_func_{EN}). The V_{func} pins can also be used to operate the electrodes of the CMOS chip externally. The RE isolation switches were designed slightly different to have the option of connecting an external RE while using the integrated circuits. When the WEs are connected to V_{func_WEs} they are all short-circuited at V_{WE} as shown in Figure 4.17 using the ALL_ON decoder switch. Under normal operation of the ECM, the $func_{EN}$ control signals were turned off and V_{func} nodes were connected to ground.

4.6 Discrete-time Charge Sensitive Amplifier

The potentiostat design and the switching capabilities of the electrochemical cell were presented in the previous sections. One of the circuits that was included in every electrochemical cell for the readout of low current values was the charge integrating *i* to *F* CSA. The circuit was made of a discrete-time CSA implementation made of an OTA (OP1), a charging capacitor C_1 = 500 fF and an extra capacitor C_2 = 10 pF to extend the integrating range when necessary, as

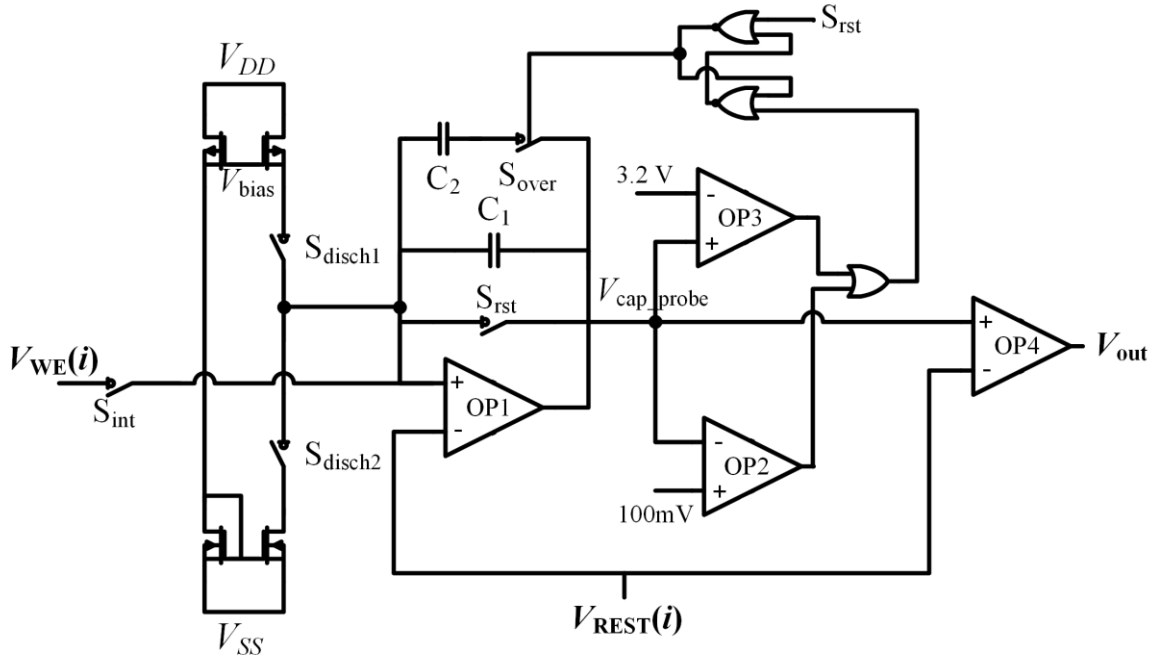

Figure 4.18: Discrete-time bidirectional ΔΣ charge sensitive amplifier with an extending range capacitor.

shown in Figure 4.18 [64], [68]. A pair of comparators (OP2 and OP3) were used to detect the limits of the charging capacitor set at a lower and upper threshold of 100 mV and 3.2 V respectively according to the power supply voltage headroom. If OP1 output potential exceeded the threshold in a charging cycle a NOR latch enabled the overcharging capacitor (C2) until the CSA was reset, as shown in Figure 4.18. The CSA was implemented with a circuit that detected the current polarity (described in Section 4.6.1) that enabled a reference current source or sink to discharge the capacitor back to $V_{REST}(i)$ of the corresponding potentiostat. The circuit architecture enabled for a ΔΣ modulated output by the integrated comparator (OP4), as explained in Section 2.5.1 [43].

A single-ended folded cascode amplifier was chosen as the discrete-time system amplifier. The reason why this design was selected was due to its high gain, wide dynamic range and rapid settling time necessary for switched capacitor readout systems [76], [171]. The opamp design was preferred over a telescopic design as it can adjust the common-mode voltage of the output to the input at the reset stages. Another advantage of this design for this application was its inherent higher speed compared to e.g. a two-stage opamp and the use of the integrating capacitor for its compensation [13].

4.6.1 Automation and Threshold

The circuit presented in Figure 4.18 is a simplified version of the design that was implemented for the bidirectional CSA. The digital logic behind the operation described above required a higher complexity to achieve a consistent output ΔΣ format independent of the current polarity and sampling of events at the correct part of the charging/discharging cycles. The signals controlling the charging/discharging steps of the digital logic are shown in Figure 4.19. The operation commences with a reset signal (S_{rst}) that resets the potential of C_1 at V_{REST}, using amplifier OP1. When this signal turns off the integration step starts for the duration of S_{int} − S_{rst}. The polarity of the current determines whether C_1 would be charged or discharged. After the integration step, a sampling step follows (S_{smpl}) to determine the polarity of the current. Lastly, according to the current polarity that was sensed the appropriate negative or positive reference current discharges or charges the capacitor(s) back to V_{REST} (named as a discharging step for the purposes of this description). Charging and discharging potentials of V_{cap_probe} for a 120 nA negative current (from the solution to the WE) for the first 100 µs and a 120 nA positive current for the next 100 µs are shown in the "cap_probe" signal of Figure 4.19.

The digital logic designs that used these signals to induce the required behaviour are shown in Figure 4.20. Latches were used to sample events as a fast clock's

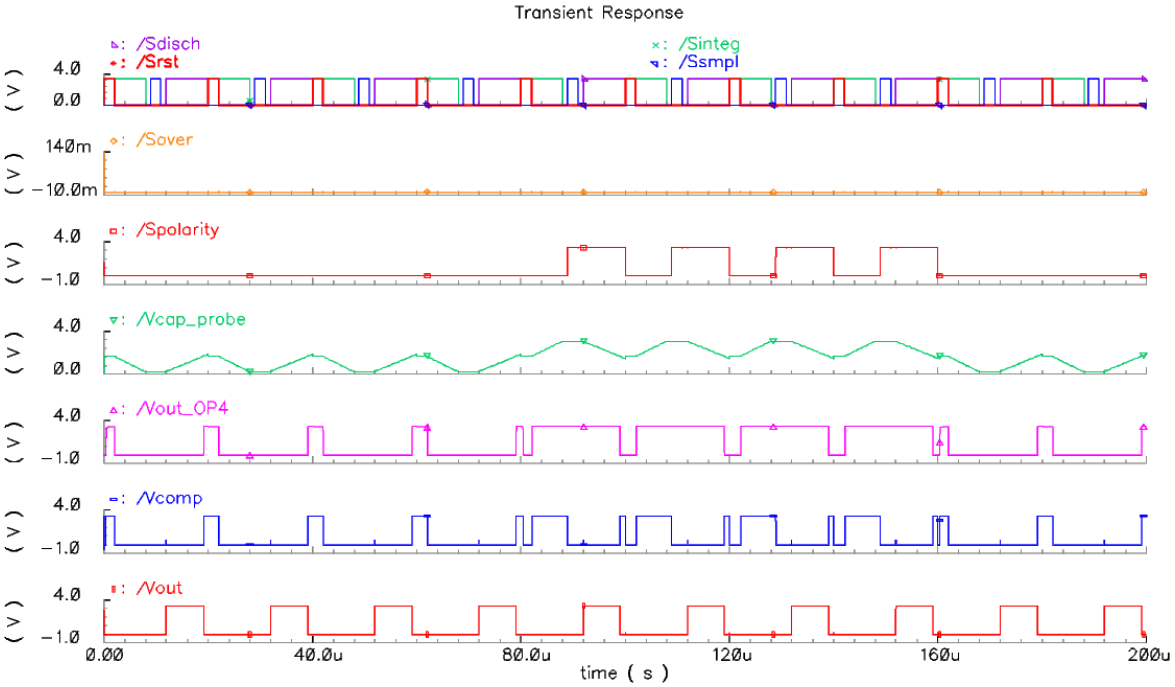

Figure 4.19: Discrete-time CSA circuit control and output signals.

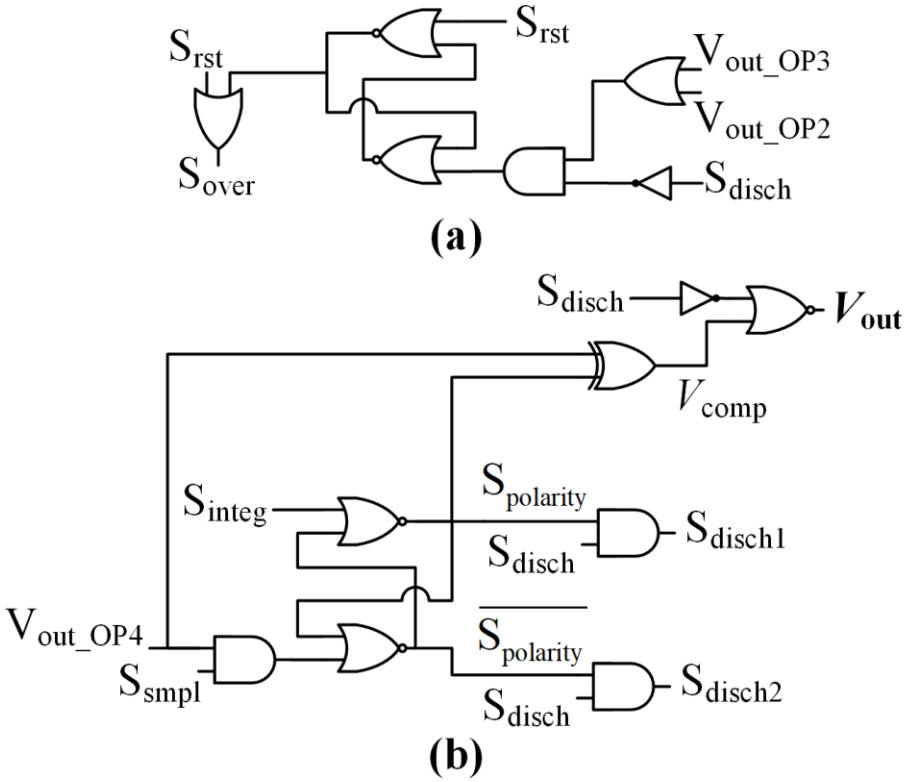

Figure 4.20: Digital logic circuits for (a) the sampling of an excessive charging step and (b) the detection of the current polarity followed by a logic that ensures the representation of the output results always in the same format.

rising edge is not required in these circuits (as in i.e. flip-flops). Figure 4.20(a) depicts a detailed version of the NOR latch power supply threshold circuit shown in Figure 4.18. An AND gate was added to ensure that the extending range capacitor is not disabled during the discharging step and a NOR gate to reset it along with C_1. In Figure 4.20(b) the current polarity circuit is presented. First, the output of OP4 comparator is sampled to determine whether the WE current charged or discharged the capacitor(s). The output of the latch for a negative and a positive WE current is shown in Figure 4.19. Depending on the result either S_{disch1} or S_{disch2} is enabled at the S_{disch} control signal and the appropriate reference current source switch of Figure 4.18 is turned on. At the discharging step when the capacitor(s') potential reaches V_{REST} the comparator output V_{out_OP4} exhibits a rising edge for a negative current and a falling edge for a positive current, as shown in Figure 4.19. This result is changed to attain always a rising edge (V_{comp}) using an XOR gate with the $S_{polarity}$ signal, as shown in Figure 4.20. To shape the output (V_{out}) as ΔΣ modulated pulses, a NOR gate was used that outputs S_{disch} with a modulated pulse width ending at V_{comp} rising edge. The circuits make for a discrete-time CSA with an extended current range that reconfigures itself according to the polarity.

4.7 Electrochemical Cell Assembled Design

The complete CMOS chip overview comprised of all the components described in the previous sections is shown in Figure 4.21. The system is controlled by 16 independent pairs of analogue inputs for an equal number of electrochemical cells. Each of these 4 × 4 WE subarrays organised as electrochemical cells have a differential voltage output from the two ends of the output current converting resistor and a digital output from the discrete-time CSA. One digital output grouping all of the overcharging outputs of the CSA with a 16-input OR gate was used to notify for a possible adjustment in the integration and discharging steps duration. The electrochemical cells are structured each with their own potentiostat and an independent set of on-chip microelectrodes. The array is controlled by common addressing signals enabling the same WE in each subarray as well as the same control signals for current integration. A set of control signals that could be used to isolate or group electrodes that was explained in Section 4.5.4 was applied to all the electrochemical cells of the array. The grouped on-chip microelectrodes were connected to pins (V_{func_CEs}, V_{func_REs} and

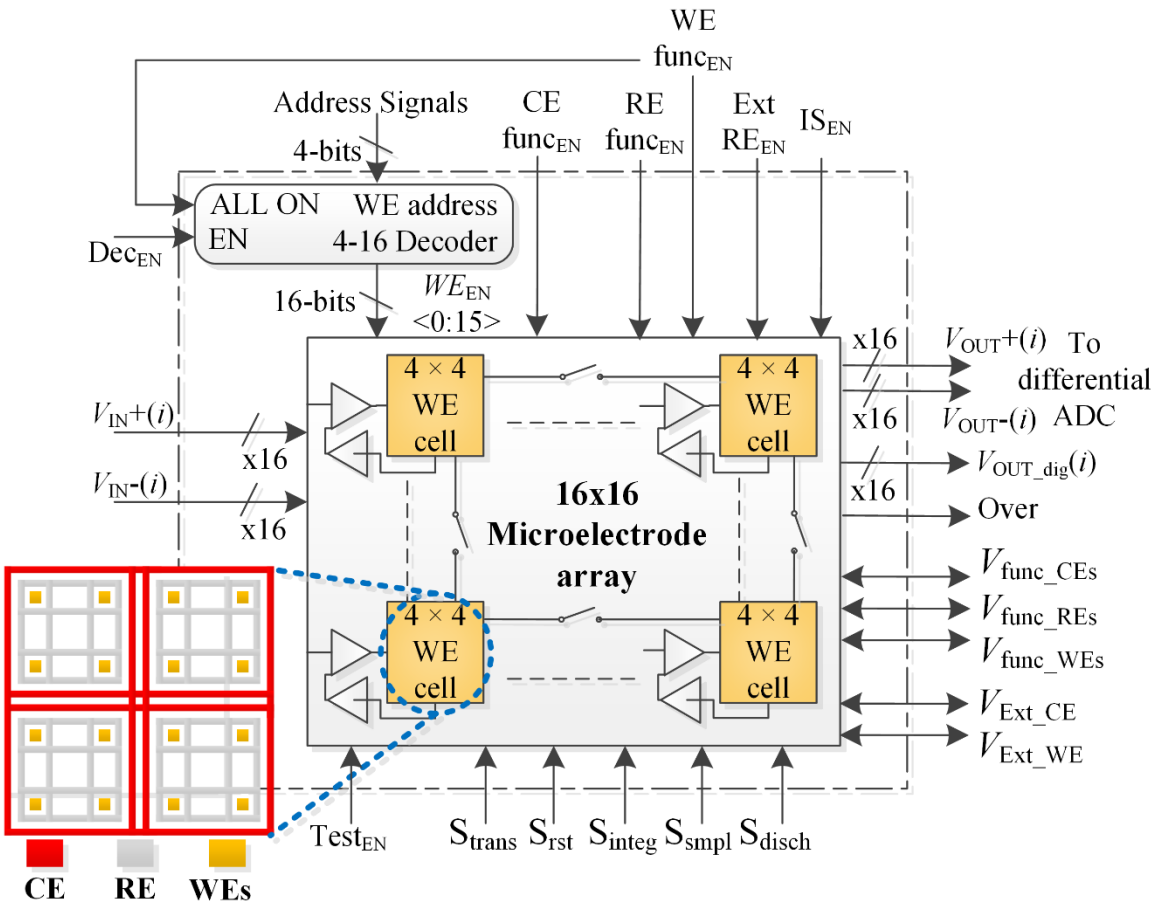

Figure 4.21: CMOS chip overview of the electrochemical cell microarray with input/output, subarray architecture and microelectrode geometry details [170].

V_{func_WEs}) that could be connected to external equipment and perform several operations for the characterisation and functionalisation of the chip. Another set of switches were added in one of the electrochemical cells that connected the internal circuits of its potentiostat to pins (V_{Ext_CE} and V_{Ext_WE}) enabled by the $Test_{EN}$ control signal shown in Figure 4.21.

4.7.1.1 Modes of operation

The way the control and enable switches are combined together can configure the system for different modes of operation:

- In the analogue mode the current to voltage transduction switch (S_{trans}) and the reset switch of the current integration circuit (S_{rst}) are enabled.

- In the digital mode the control signals sequence is as described in Section 4.6.1 while S_{trans} is enabled when S_{integ} is off in order to prevent V_{WE} (Figure 4.16) from floating on a high impedance node.

- In an internal circuits test mode the $Test_{EN}$ and Ext_RE_{EN} switches connect the internal circuits of one potentiostats to the V_{Ext_CE}, V_{Ext_WE} and V_{func_REs} pins to be connected to external loads.

- In characterisation mode the circuit isolation switch (Is_{EN}) is turned on and the appropriate switches are controlled to characterise e.g. the $R_{i\ to\ v}$ resistors of each potentiostat.

- The same isolation switch (Is_{EN}) is used when the on-chip microelectrodes are grouped together with the $func_{EN}$ control signals for functionalisation, electroplating or external driving purposes. For electroplating and functionalisation purposes the Ext_RE_{EN} signal is turned on when the focus is not on the on-chip REs to isolate them.

4.8 CMOS Electrochemical System Physical Layout

The circuit diagrams to make the system of electrochemical cells was the first step towards the realisation of the electrochemical cell microarray. The physical layout and its design considerations to materialise the ideas on a silicon

substrate using CMOS technology is explained in this section. Part of this layout is the geometrical arrangement of microelectrodes formed in the shape defined in Figure 4.11 on the top (fourth) metal layer of the 0.35 μm technology. More details on the layouts of circuits of the potentiostat, the electrodes and the final layout of the whole chip, shown in Figure 4.22, are described in this section.

The use of a standardised CMOS fabrication technology entails studies conducted by the foundry to make a set of rules that improve yield in the fabricated devices. As it was mentioned in Section 4.2 this ruleset is included in the technology libraries that are embedded into Cadence. The rules include a minimum width for each layer, a minimum spacing between geometries of the same or other layers, constraints on the overlapping of layers, minimum density and other constraints. These rules are set due to the processing capabilities of photolithographic steps used in the fabrication process. All these rules were taken in consideration when designing the chip layout.

4.8.1 Electrochemical Cell Layout

The microelectrodes and circuits layout of the electrochemical cell is shown in Figure 4.22. Although the MOSFETs and basic impedance elements were provided by ams AG, the circuits and their layouts used in this chip were mainly custom designed except for digital gate designs that were supplied in the ams AG library files. Placing the circuits on a common silicon substrate entails interference phenomena from unwanted signal paths to devices. The problem originates mainly from high-frequency digital signals that perturbate the substrate potential. To address this issue guard ring structures were designed around sensitive parts of analogue circuits and digital cells. The structure is made of low impedance doped contacts to the substrate (or the doped wells for pMOS transistors) that connect to power signals, V_{SS} or V_{DD} for charge carriers to escape before they corrupt sensitive signals. The initial layout of the electrochemical cell was designed with the circuits placed under the microelectrodes as one block. Although this design was more compact, post-layout simulations indicated capacitive coupling of sensitive signals with the wide metal electrode geometries. The potentiostat and most of the circuits of the electrochemical were placed on the sides while only WE multiplexing switches were kept under their corresponding microelectrodes, as shown in

Figure 4.22. Another common issue in CMOS fabrication is device mismatch which is particularly important for the common mode signals of amplifiers. Mismatch can be caused by process variations, process gradients, a systematic

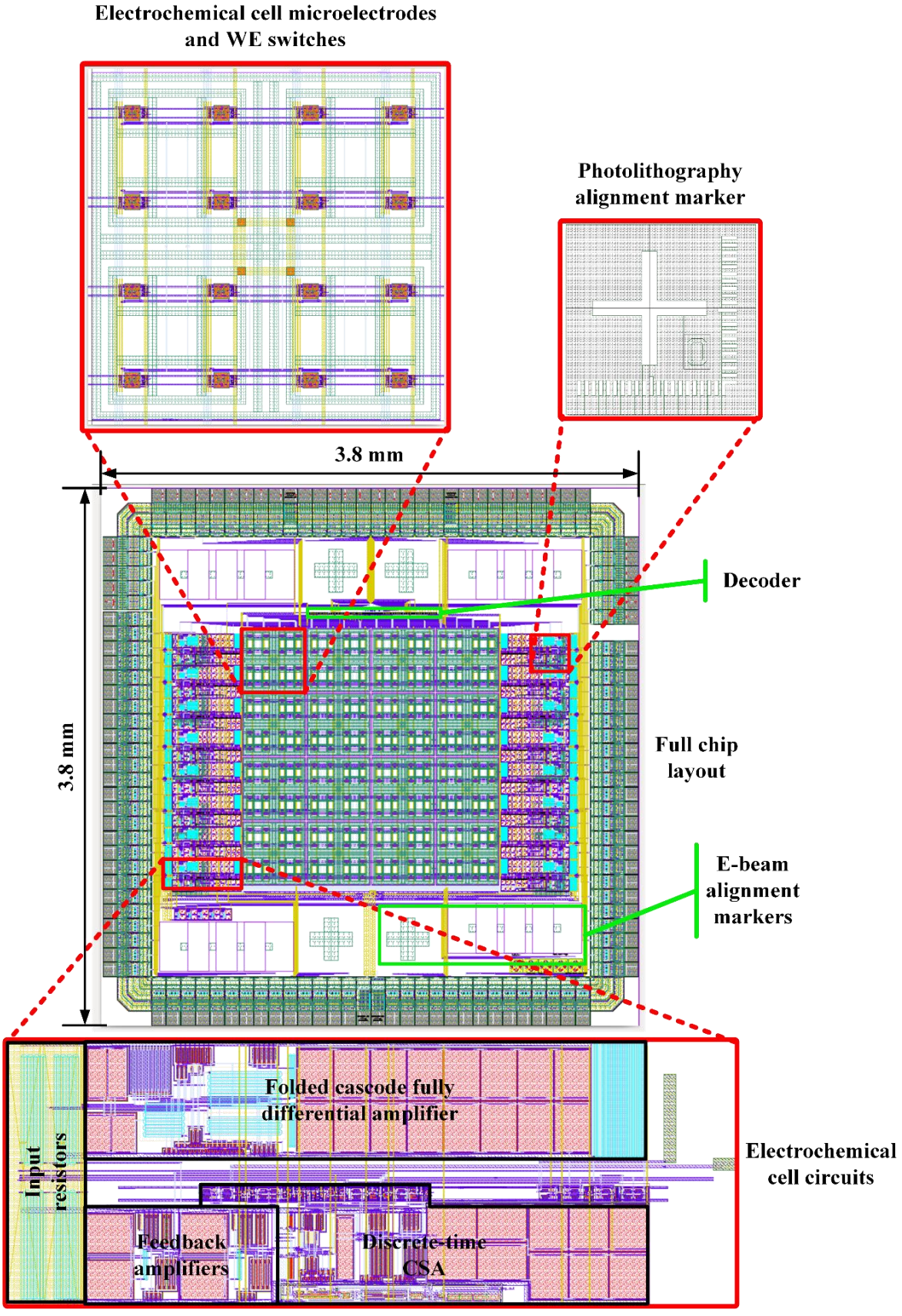

Figure 4.22: Physical layout of the electrochemical cell microarray chip.

error by proximal devices and non-isotropic effects. A measure that was used to prevent major influence by potential mismatch was to group transistors together and join their drains and sources where the design allowed it. To acquire a consistent response from all electrochemical cells, the devices were made as symmetrical as possible.

4.8.2 Microarray Layout

The individual layout designs of circuits and electrodes were placed together to form the electrochemical cell microarray. The design steps that were described in Section 4.2 were followed to make the final chip layout. After the physical design passed the LVS and DRC checks the layout passed several iterations of post-layout simulations to finally produce a GDSII file. The file was sent to Europractice IC and it was outsourced to ams AG for fabrication. The chip components were designed as symmetric as possible, as shown in Figure 4.22. The circuit input and outputs as well as power requirements were connected to bond-pads provided by the ams AG library. The bond-pads' layout design included wiring and electrostatic discharge (ESD) protection circuits so that they could be arranged in a ring structure with the power supply pads ensuring a correct biasing of the ring. The embedded ESD protection is necessary in integrated circuits as they have small capacitors that are susceptible to damage by large electrostatic potentials. The devices are protected by the use of diodes that clamp the external discharge to V_{DD} or V_{SS}. A similar issue occurs at fabrication stages as the gates of MOSFETs collect charged ions and there is a risk of breaking down the gate oxide irreversibly. One of the DRC rules checks for these "antenna" errors at metal tracks connected to MOSFET gates. They were corrected either by changing the total metal layer area connecting to the gate, with buffers in between the track length or with tie-down diodes. However, as it will be described in the next chapter the CMOS die required post-processing plasma etching steps to expose the top metal layer electrodes. These steps required a consideration for the protection of the circuits connected to the electrodes. The transmission gates that were directly connected to the electrodes as switches, acted also as diode connections to V_{SS} and V_{DD}.

In the layout of the microarray connections at the top metal layer were avoided so that the electrodes could occupy that space. This decision led to a space on

top of the electrochemical cell circuits that was used for photolithographic alignment markers necessary for post-processing fabrication, as shown in Figure 4.22. The cleanroom facilities of the James Watt nanofabrication centre (JWNC) [169] at the University of Glasgow provide electron-beam (e-beam) lithography services, hence e-beam alignment markers were also designed at the top metal layer of the layout. No circuits were placed around the markers to prevent misalignment issues by backscattered electrons from other layers of the silicon die.

4.9 Summary

In this chapter Cadence CAD software was used to simulate the electrochemical response of electrode geometries using models described in Chapter 3. Cadence was used to design the circuit diagram and physical layout of the ASIC microarray and to simulate its performance. Electrical models were arranged to construct geometrical shapes of microelectrodes in a chemical solution that were introduced in Cadence. The modelled system provided a unique insight into both the electrochemical behaviour and circuit response to design the microelectrode structure and the driving circuits to match as efficiently as possible. The consistency of the electrical model for electrochemical simulations was investigated and it was found to conform to theoretical expectations. The research conducted in this work indicated that a miniaturised array of independently controlled electrochemical cells in a common liquid sample medium can be realised with the combined use of a coaxial electrode pattern and a fully differential potentiostat. However, a future verification of the simulated results using specialised electrochemical simulation software would be beneficial for a more accurate estimation of the electrochemical response as it would take into account mass transfer phenomena and set more dynamic boundary conditions [172]. The 4 × 4 electrochemical cell microarray comprised of 16 × 16 WEs was designed in the 0.35 µm ams AG technology. Each cell had its own analogue current to voltage conversion and digital ΔΣ modulated output. Another feature of the array was the addition of microelectrode grouping switches for the external control of the on-chip microelectrodes. The ASIC layout integrated the circuits together with a geometrical arrangement in the top metal layer that formed the microelectrode array. A batch of passivated chips was received from ams AG, shown in Figure 4.23. To make the array

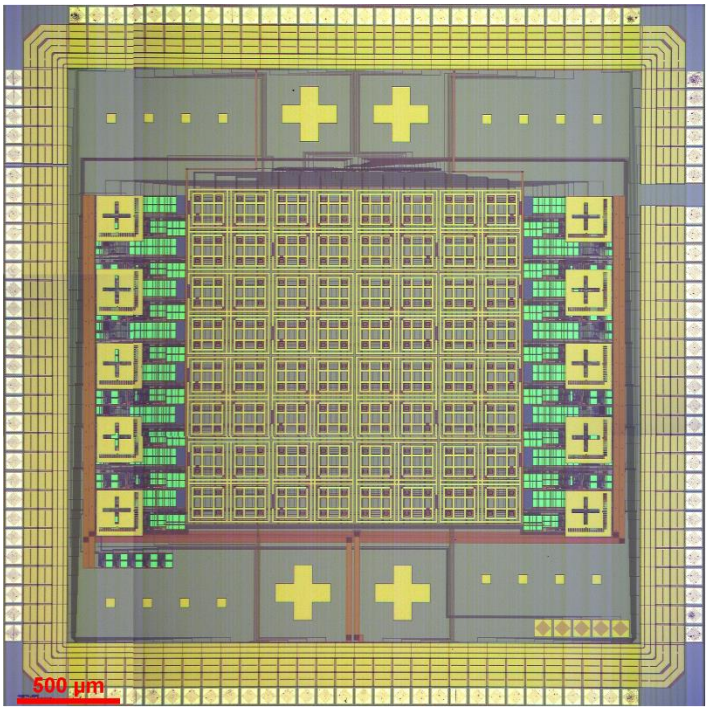

Figure 4.23: Optical micrograph of the fabricated CMOS ASIC electrochemical cell microarray by ams AG.

electrochemically active, the microelectrodes have to be exposed and the chip needs to be prepared for use in a harsh chemical liquid environment which will be presented in the next chapter.

5 Post Processing Fabrication and Packaging

5.1 Introduction

The previous chapter described the simulations and design that led to the fabrication of the CMOS electrochemical cell microarray. This chapter reviews the procedure that was followed to prepare the chip for electrochemical purposes. Post-processing fabrication in a cleanroom facility was required to prepare the microelectrodes on the silicon surface. The chapter starts with a description of the ASIC as it was received from the foundry. Then, the developed fabrication processes that made a biocompatible IC and were first evaluated on test samples are explained. Apart from microelectrodes other points that connect the ASIC to the physical environment are embedded bond-pads. Encapsulation methods that were used to isolate the bond-pad connections make the device effective in a liquid environment are described. Lastly, the Au microelectrode structures that were constructed by the post-processing fabrication steps, presented in this chapter, were introduced to organic contaminants that needed to be cleaned with an electrochemical method.

5.2 Foundry Technology

The microchip was received from the foundry as an unpackaged silicon IC. A cross section of the 0.35 μm 4-metal technology by ams AG [17] is shown in Figure 5.1. The integrated circuits are built on a silicon p-doped substrate. The technology is also comprised of metal-insulator-metal (MIM) and polysilicon capacitor and polysilicon resistor features. The top metal layer of the CMOS chip where the microelectrode structures were designed was made of aluminium. The ASIC was coated by a passivation layer, a common practice in CMOS fabrication to prevent surface contamination and metal corrosion that can lead to degraded performance.

Before the chip's bond-pads were wire bonded to a pin grid array (PGA) package to make a lab-on-a-chip device, its surface needed to be treated to prepare its electrochemical transducer interface. Although the passivation layer was necessary for the ASIC performance, the surface covering the electrodes of the top-metal layer had to be removed to make an electrical connection. The

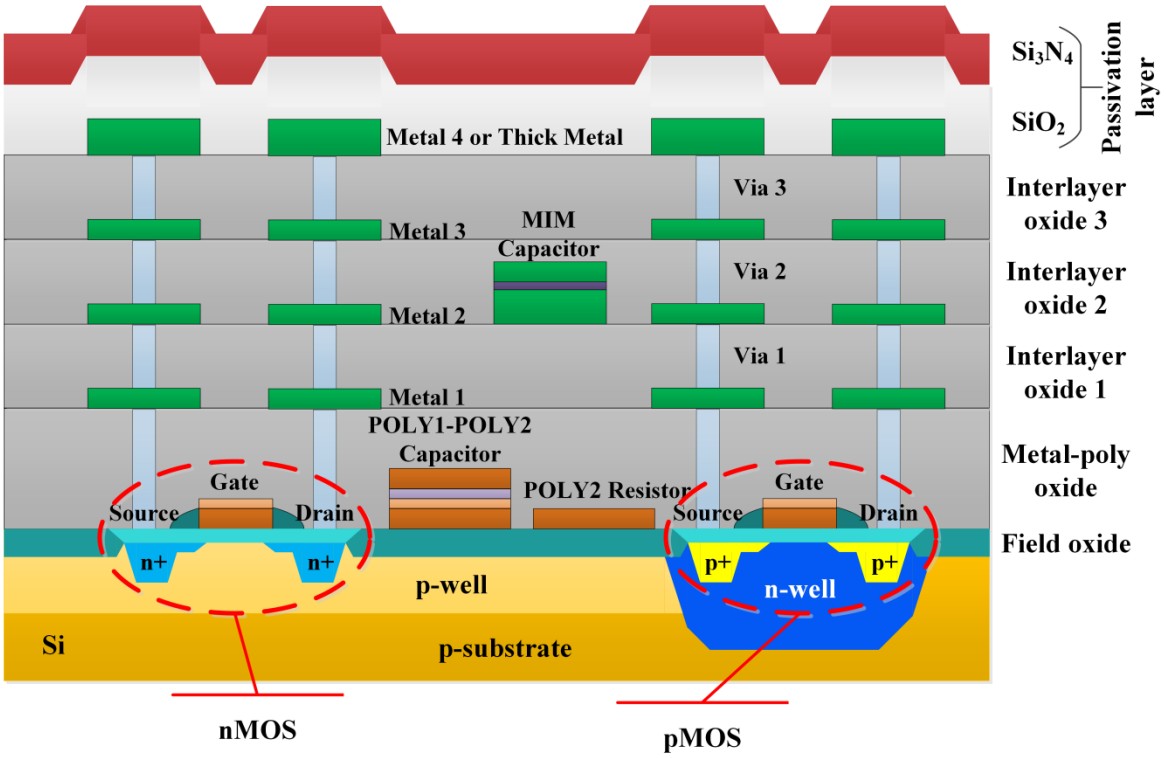

Figure 5.1: Cross-section drawing of the 0.35 μm 4-metal process of ams AG [17].

foundry provided a service for the removal of the passivation layer (used to make bond-pads) but custom post-processing etching offered more options in particular in defining the size of the exposed electrode area. Aluminium is a cheap material with good electrical properties. However it is easily corroded in a chemical environment and it is also toxic for biological samples. A method to cover the aluminium with chemically inert metal layers was also developed, presented in the following sections. Post-processing was performed in the facilities of the James Watt Nanofabrication Centre (JWNC) [169]. The procedure required the use of photolithographic techniques; hence a photomask with all the necessary patterns was designed in L-Edit [173] using as a reference imported GDS files of the microelectrode layout, developed in Cadence. The chrome photomask was fabricated by Compugraphics [174] and ferric oxide copies of that mask that were made by the JWNC staff.

5.3 Test Microelectrodes

Before any post-processing fabrication was performed on the CMOS chips, test samples without electronic circuits which resembled the ASIC's surface were prepared. The development of these samples served many purposes that are presented over this chapter. Purposes the samples served were: to develop

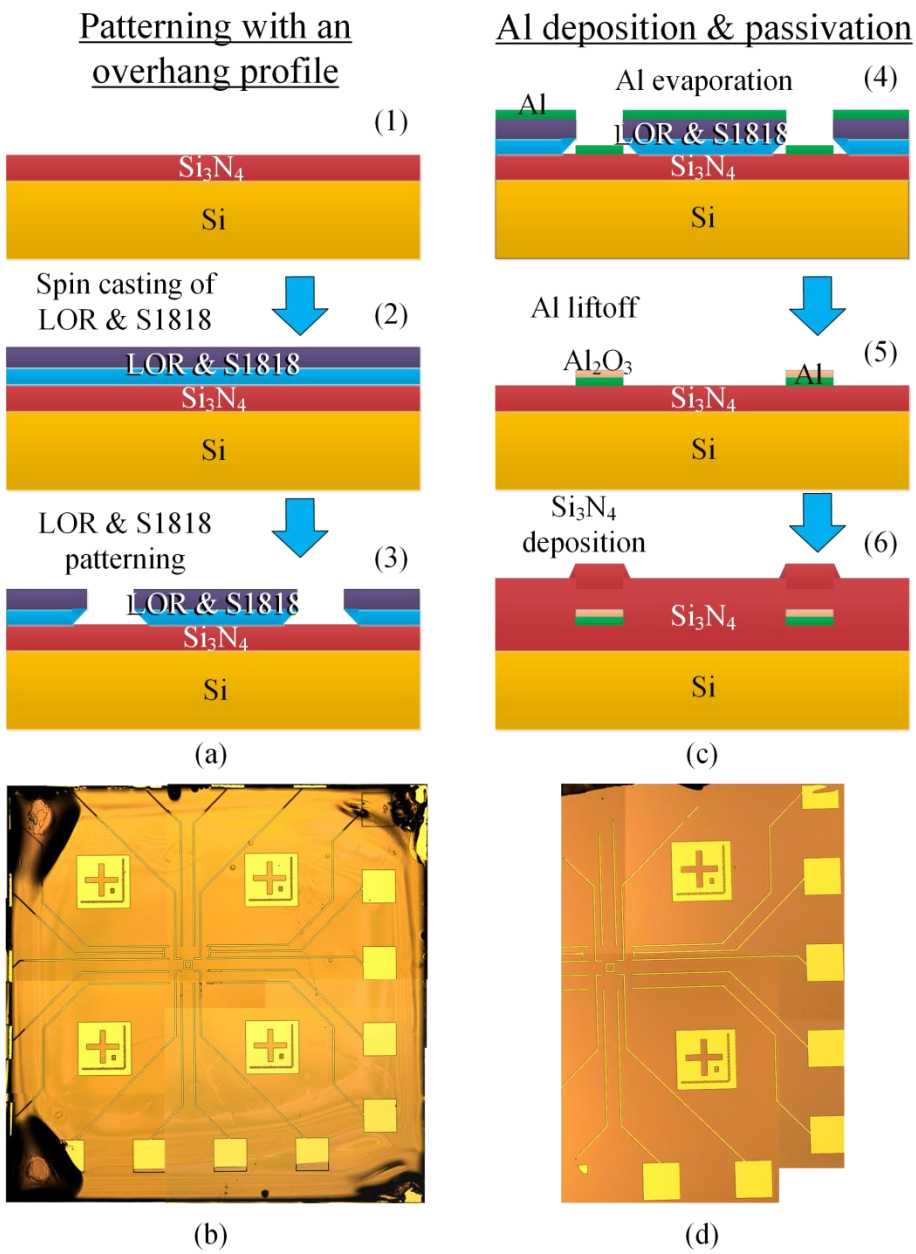

Figure 5.2: Preparation of the test samples that mimicked the CMOS ASIC. The process started with patterning of a positive photoresist with an overhang profile shown in (a) a schematic diagram and (b) an optical micrograph. It continued with the deposition of Al, a lift-off step to form the metal tracks and Si_3N_4 passivation layer deposition shown in (c) a schematic diagram and (d) an optical micrograph.

processes, to test the electrical conductivity, to measure the thickness of electroplated metals and finally to serve as external electrodes used with both a commercial potentiostat and the on-chip circuits to characterise them. The use of test samples without electronic circuits simplified the measurement of the structure's electrical characteristics. Moreover the features on the test sample's surface were simpler than the CMOS chips' multi-layered structure. After the successful processing of these samples using the same recipes as the ones for the ASIC, the test samples exactly mimicked the on-chip microelectrode structure.

Step	Details
Si_3N_4 deposition	Inductively coupled plasma chemical vapour deposition (ICP/CVD) of 1 μm Si_3N_4 with a flow of SiH_4/N_2 at 7/6 sccm, a 100 W power and for a temperature of 35°C the pressure was adjusted at 4.4 mTorr.
Pre-treat	Dehydrate sample in an 180°C oven for 10 minutes
LOR10A Coat	1. Static dispense of LOR10A. 2. Spin cycle – ramp up from 0 to 9000 rpm at 1000 rpm/s and hold for 60 s.
Soft bake	Bake at 150°C for 2 minutes on a hotplate.
S1818 Coat	1. Static dispense of S1818. 2. Spread cycle – ramp up from 0 to 1000 rpm at 250 rpm/s and hold for 5 s. 3. Spin cycle - ramp up from 1000 to 4000 rpm at 2000 rpm/s and hold for 30 s. 4. Edge bead resist removal – ramp up from 4000 rpm to 9000 rpm at 20000 rpm/s and hold for 2 s.
Soft bake	Bake at 115°C for 3 minutes on a hotplate.
Expose	Expose on a Karl Suss MA6 mask aligner for 6 s in vacuum mode.
Develop	Immerse in the Microposit MF-319 developer from MicroChem for 2 minutes and 30 s while agitating every 15 s.
Rinse and dry	Immerse the sample in deionised (DI) water, rinse for 5 minutes and dry with a N_2 gun.
Ash	Place in PlasmaFab barrel asher for 1 minute at 100 W to remove resist residuals.
Metallisation	Deposit metal with required thickness using a Plassys electron evaporation tool.
Lift-off	Immerse the sample in a beaker of Microposit 1165 resist stripper from MicroChem. Place the beaker in a 50°C hot bath for at least 1 hour to let the stripper dissolve the resist bi-layer and leave behind the metal pattern.
Si_3N_4 deposition	500 nm Si_3N_4 using the same method as above

Table 5.1: Liftoff process with a LOR10A and S1818 bi-layer.

The process to develop the passivated test samples that mimicked the CMOS ASIC which was received from the foundry is presented in Figure 5.2. The first step was to deposit 1 μm of Si_3N_4 on a Si wafer using inductively coupled plasma chemical vapour deposition (ICP/CVD) with a flow of SiH_4/N_2 at 7/6 sccm (standard cubic centimetre per minute), Platen power of 100 W and pressure of 4.4 mTorr. This is the standard recipe in the JWNC for Si_3N_4 deposition. The wafer was cleaved into approximately 4 mm × 4 mm samples with a diamond dicing saw (to mimic the 3.8 mm × 3.8 mm CMOS die). The next step was a bi-layer lift-off process that is described in Table 5.1 to selectively pattern the bond-pads and metal tracks made of Al. The sample size was too small to be used with the spinner chucks available at the JWNC, thus they were temporarily bonded on cut 2 cm × 2 cm Si carrier substrates with a 15% Poly(methyl methacrylate) (PMMA) resist [175] (spun from 0 rpm to 2000 rpm at 1000 rpm/s and held for 60 s). The two silicon dies were bonded after a baking step at 154^{o}C for 2 minutes on a hotplate. Note that this bonding step was performed every time a resist is reported to have been spun in this work. The process used S1818 [176], a positive photoresist that after it was spun had an approximate thickness of 1.8 μm and LOR10A [177], a resist based on polydimethylglutarimide with a 1 μm thickness which was used as a sacrificial layer a to create the undercut profile necessary for successful lift-off. The recipe included a resist edge bead removal step to remove the large edge bead that developed for the size of the small silicon ASICs. 50 nm of Al metal were deposited with an electron evaporation tool in high vacuum from Plassys [178]. The last step was a further 500 nm Si_3N_4 deposition using the described recipe to mimic the passivation layer of the CMOS chips. Between the last two steps, a thin layer of Al_2O_3 formed on the surface of the patterned Al metal as it came in contact with an O_2 rich environment, an issue that was also observed in the CMOS processing and is addressed in Section 5.5.

5.4 CMOS Microelectrodes Opening

The microelectrode structure that was part of the top metal layer of the CMOS ASIC had to be exposed from the Si_3N_4 and SiO_2 passivation bi-layer. The first step was to thin the Si_3N_4 layer over the area of the microelectrode array by partial etching, as indicated by a red box in Figure 5.3(a). That layer was not completely removed as it plays a major role in the passivation layer as SiO_2 is

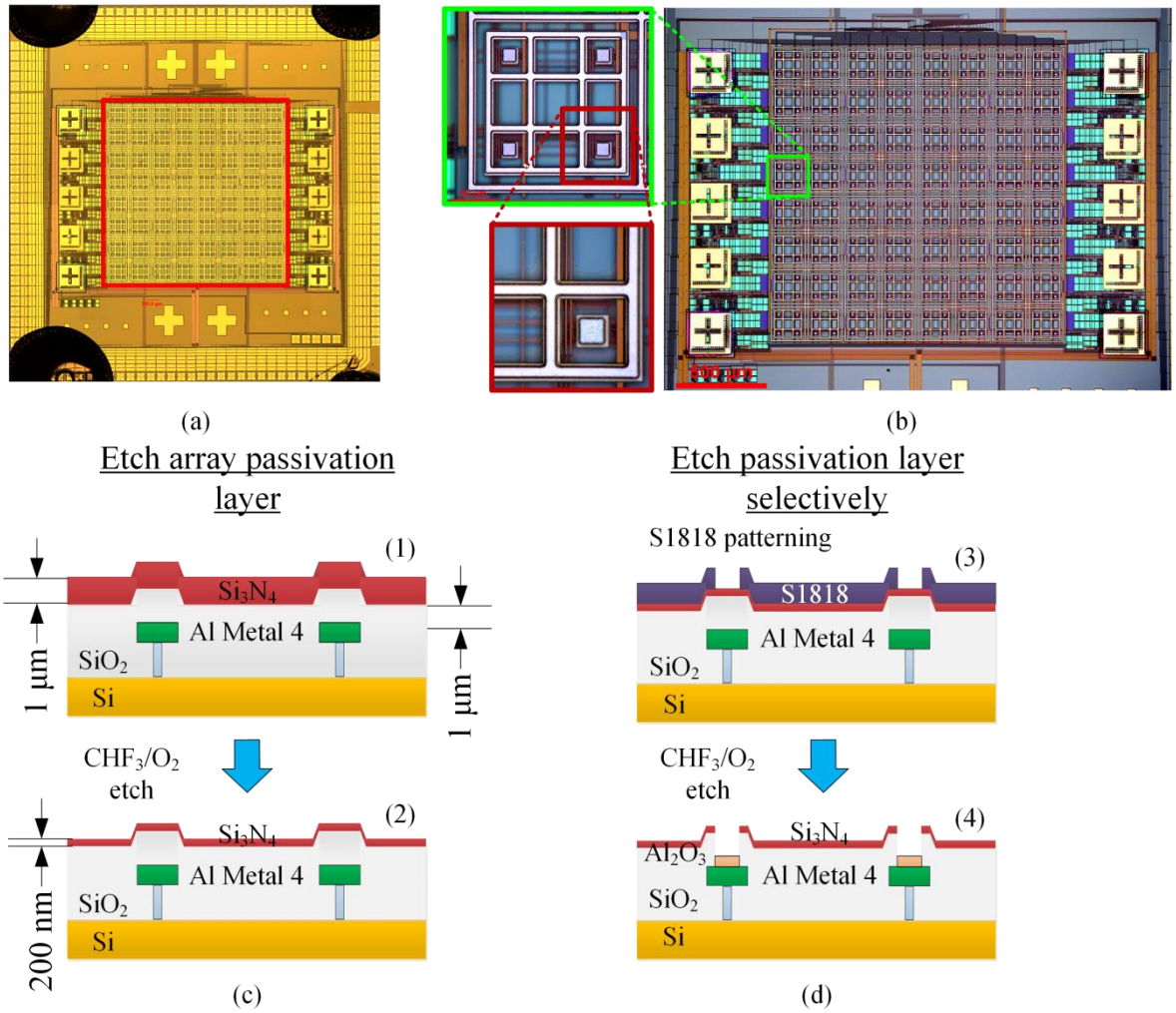

Figure 5.3: Optical micrographs of (a) the passivation layer thinning before the photoresist was removed and (b) the selectively etched chip. (c, d) A schematic diagram of the process [170].

more permeable to water vapours as well as chemicals that were used with the processed chips [175]. The rest of the passivation layer was removed with a width 25% smaller than the 20 µm side length of the square WEs and the 11 µm wide REs and CEs, as shown in Figure 5.3. Etching the electrodes with the desired shape and the existing Al metal were prepared so that the metallisation steps that followed had maximum electrical contact area to the ASIC. The size of the selective etch ensured that the side walls of the Al top metal layer of the integrated circuit were not exposed.

5.4.1 Etch Process

The processing steps that were followed to pattern the chips for both of the etch processes are given in Table 5.2. Both the Si_3N_4 and the SiO_2 layers were removed by the same reactive ion etch process that had a flow of CHF_3/O_2 at 50/5 sccm, using a 500 W power and for a temperature of 20°C the pressure was

Step	Details
Pre-treat	Dehydrate sample in an 180°C oven for 10 minutes
S1818 Coat	1. Static dispense of S1818. 2. Spread cycle – ramp up from 0 to 1000 rpm at 250 rpm/s and hold for 5 s. 3. Spin cycle - ramp up from 1000 to 4000 rpm at 2000 rpm/s and hold for 30 s. 4. Edge bead resist removal – ramp up from 4000 rpm to 9000 rpm at 20000 rpm/s and hold for 2 s.
Soft bake	Bake at 115°C for 3 minutes on a hotplate.
Expose	Expose on a Karl Suss MA6 mask aligner for 4 s in hard mode.
Develop	Immerse in the Microposit MF-319 developer from MicroChem for 1 minutes and 15 s while agitating every 15 s.
Rinse and dry	Immerse the sample in deionised (DI) water, rinse for 5 minutes and dry with a N_2 gun.
Ash	Place in PlasmaFab barrel asher for 1 minute at 100 W to remove resist residuals.
Etch	Reactive ion etch with a flow of CHF_3/O_2 at 50/5 sccm, a 500 W power and for a temperature of 20°C the pressure was adjusted at 55 mTorr. The step is run until a metal is detected to be exposed by the interferometer.

Table 5.2: Patterning process with S1818 for etching

adjusted at 55 mTorr. 800 nm of the 1 µm Si_3N_4 layer was removed in the first passivation thinning etch process (Figure 5.3(c)). The following selective etch process resulted in a step of 1.2 µm from the Al electrode to the surrounding Si_3N_4 and SiO_2, as shown in Figure 5.3(d). The thinning etch process ensured this smaller height of the openings which assisted the patterning of photoresist to evaporate metals, as presented in Section 5.5.1. The CMOS chip size was very small to provide a uniform surface area for the etching process. The process was monitored using an interferometer while it was running. The alignment markers proved as a good reference point for the interferometer. After the Al metal was exposed an additional 10% of the elapsed time was added to the run time to

account for etch non-uniformities and ensure complete removal of SiO_2. The etching process was developed using the test samples, however the mask was slightly different exposing only the ends of the metal tracks for the deposited microelectrode pattern (explained in Section 5.5) to be connected to the bond-pads.

5.4.2 Evaluation

The duration of each etching process was recorded. Before and after each etch step the chips were measured with the Dektak 6M electromechanical system for thick and thin film height measurements. The height difference of features at the surface of the chips was recorded to determine parameters such as etch rate and mask selectivity of the etch. It was found that the etch rate for the Si_3N_4 layer was ≈ 68 nm/min and for the SiO_2 layer was ≈ 30 nm/min. The average etching depth of the Si_3N_4 thinning step was measured at 853 nm. The thinning step uniformity was verified by numerous height measurements on different locations of the CMOS chips.

5.5 Metal Deposition on Al Microelectrodes

Following the etching steps, the next required step, was the metallisation of the exposed Al metal layer with a biocompatible metal. The first batch of post-processed chips were prepared with an Au interface as it is electrochemically inert and it can be modified for biosensing applications (using thiol chemistry) as it was discussed in Section 2.3.

5.5.1 Metal Evaporation

As the side walls of the Al top metal layer were not exposed, metal evaporation on the exposed surfaces was a viable option for a process that would result in only inert surfaces being exposed to an electrochemical environment. The metal was selectively patterned using a photolithographic process with electrode features 2.5 μm wider than the exposed Al layer.

The process used for the deposition of the Au microelectrode structure was detailed in Table 5.1. The process steps are shown in Figure 5.4(a). The test samples did not require thinning of the Si_3N_4 layer. After the electrodes were

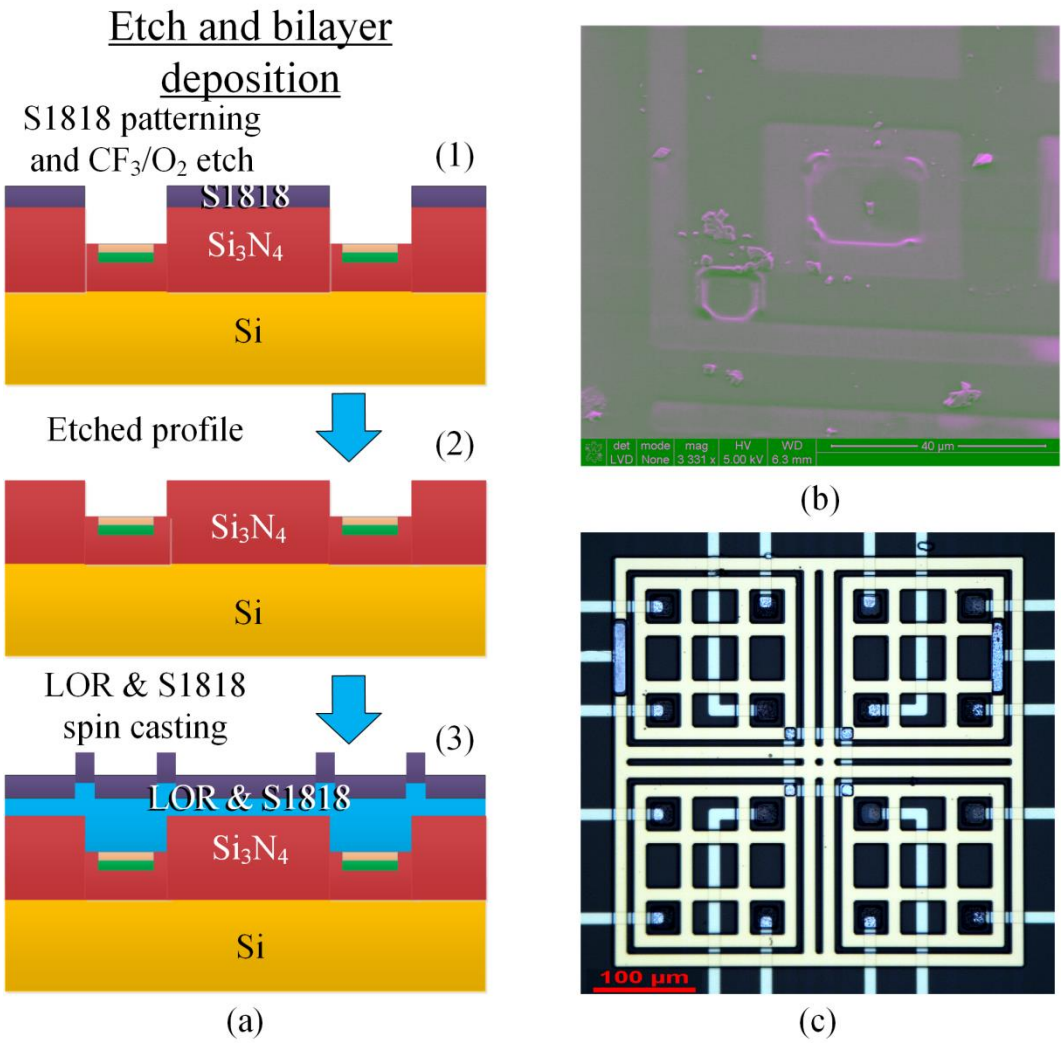

Figure 5.4: Illustration of the LOR10A and S1818 lift-off process problem in (a) a schematic diagram of the process, (b) an SEM image of the sample with the resist layers and (c) an optical micrograph of the resulting metallised test sample.

selectively etched using the process described in Table 5.2, the LOR10A and S1818 resist bi-layer was spun in order to create the lift-off profile. However, LOR10A created a bead at the edge of the trenches, as shown in Figure 5.4(a). The problem was detected by measuring secondary electrons from the covered with resist test sample with an FEI Nova NanoSem 630 scanning electron microscope (SEM) in low vacuum mode, as shown in Figure 5.4(b). After the process was completed Au was not deposited in the trenches of the resulting test microelectrode sample, as shown in Figure 5.4(c). The reason behind this problem is most probably the formation of a thick LOR10A layer in the trenches, which was not fully removed at the development step. Therefore when the Ti/Au stack was deposited, the remaining LOR10A layer prevented the adhesion of the Ti layer in the trenches, as shown in Figure 5.4(c).

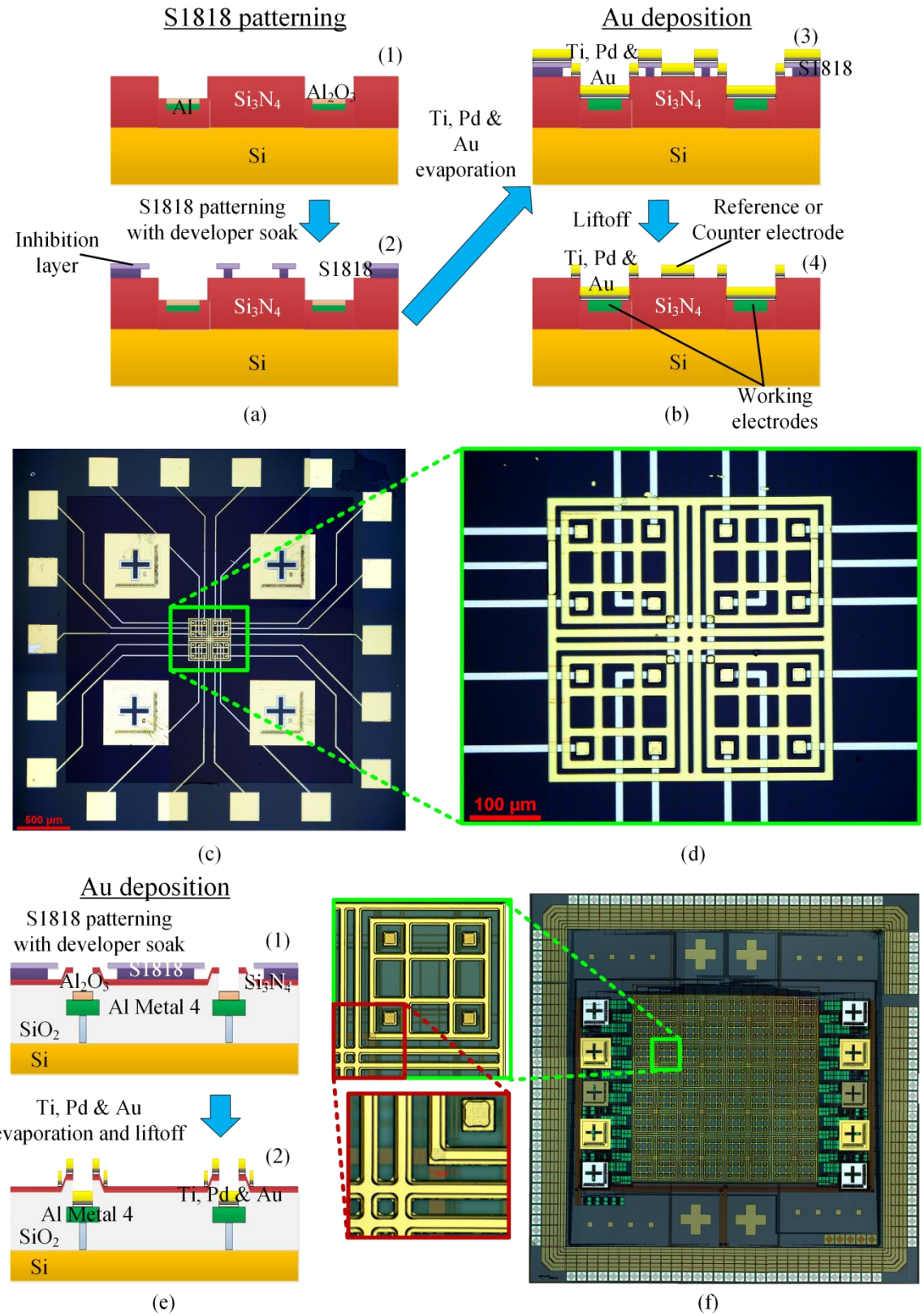

Figure 5.5: Schematic diagram illustrating (a) patterning for metallisation and the overhang profile and (b) a Ti, Pd and Au deposition on the test samples. Optical micrographs of (c) the resulting test sample and (d) a detail of the microelectrodes. (e) Schematic diagram and (f) optical micrographs of the same process on the CMOS chip [170].

Another lift-off process, where LOR10A resist was not used, was developed to selectively pattern the Au layer. As a solution the S1818 photoresist alone could be used to create an undercut profile. An inhibition layer can be created when a

Step	Details
Pre-treat	1. Dehydrate sample in an 180°C oven for 10 minutes. 2. Static dispense of 1-2 drops of MCC 20/80 primer, left to sit for 20 s and then ramp up from 0 to 4000 rpm with a 1000 rpm/s and hold for 5 s.
S1818 Coat	1. Static dispense of S1818. 2. Spread cycle – ramp up from 0 to 1000 rpm at 250 rpm/s and hold for 5 s. 3. Spin cycle - ramp up from 1000 to 4000 rpm at 2000 rpm/s and hold for 30 s. 4. Edge bead resist removal – ramp up from 4000 rpm to 9000 rpm at 20000 rpm/s and hold for 2 s.
Soft bake	Bake at 115°C for 3 minutes on a hotplate.
Developer soak	Immerse in TMAH based Microposit developer concentrate from MicroChem diluted 1:1 with DI water for 1 minute and 40 s.
Expose	Expose on a Karl Suss MA6 mask aligner for 5 s in hard mode.
Develop	Immerse in the Microposit developer concentrate diluted 1:1 with DI water from MicroChem for 1 minutes and 15 s while agitating every 15 s.
Rinse and dry	Immerse the sample in deionised (DI) water, rinse for 5 minutes and dry with a N_2 gun.
Ash	Place in PlasmaFab barrel asher for 1 minute at 100 W to remove resist residuals.
Metallisation	Etch with an in-situ ion beam etching capability for 30 s with a flow of Ar at 12 sccm, a beam voltage and current of 200 V and 10 mA respectively and a pressure of 135 μTorr and deposit metals at the required thickness with a Plassys electron evaporation tool.
Lift-off	Immerse the sample in a beaker of acetone. Place the beaker in a 50°C hot bath for at least 1 hour to let acetone dissolve the resist and leave behind the metal pattern.

Table 5.3: Lift-off process with S1818 and a developer soak step.

tetramethylammonium hydroxide (TMAH) based developer soak step, much like chlorobenzene soak, precedes exposure to ultraviolet light. The inhibition layer decomposes slower than the rest of the exposed photoresist, leading to an overhang profile for lift-off [179], as shown in Figure 5.5(a). The resist had already proven to be compatible with the developed CMOS chips and test samples. The process is explained in Table 5.3. MCC 80/20 primer [180] composed of 80% propylene glycol monomethyl ether acetate and 20% Bis(trimethylsilyl)amine (HMDS) was used prior to resist coating to increase the photoresist adhesion to the silicon surface. A cross sectional schematic diagram shows the lift-off undercut profile shape that is created with the aforementioned recipe in Figure 5.5(a). After patterning a metal tri-layer composed of 20 nm Ti, 50 nm Pd and 200 nm Au was electron evaporated to cover and create a contact with the Al metal as well as form the electrode pattern on the test samples, as shown in Figure 5.5(b). The thin layer of Ti was used for adhesion purposes and Pd was used as a diffusion barrier to prevent an Al-Au intermetallic formation that leads to poor conductivity [181]. The photoresist was dissolved in acetone, the lift-off process resulted in CE and RE structures on the Si3N4 surface and WEs and contacts on the Al metal, as shown in Figure 5.5(b). The resulting test microelectrode sample is presented in Figure 5.5(c) and (d). After the successful fabrication of the test samples the process was repeated on the CMOS chips, as shown in Figure 5.5(e). A resulting CMOS device with Au microelectrodes is presented in Figure 5.5(f).

Part of the developed lift-off process is a step that includes the use of an in-situ Ar etching of the electron evaporating tool before metal evaporation. This step was introduced to remove a thin Al_2O_3 layer that readily forms upon contact of the Al metal layer to environmental air rich in O_2. The phenomenon occurs naturally in CMOS bond-pads but the wire bonding process breaks this thin oxide layer. Test samples with the patterns that have been shown in this chapter were prepared to investigate this process with a procedure described in Figure 5.6(a). A pair of samples was prepared with the processing steps presented in Table 5.1, but the last step which covered the Al metal tracks with a Si_3N_4 insulating layer was not performed. The microelectrode structure was directly evaporated on top of the metal tracks, as shown in Figure 5.6(b), using the Ar etching step prior to depositing the Ti/Au stack in only one of the samples. The Ti-Au

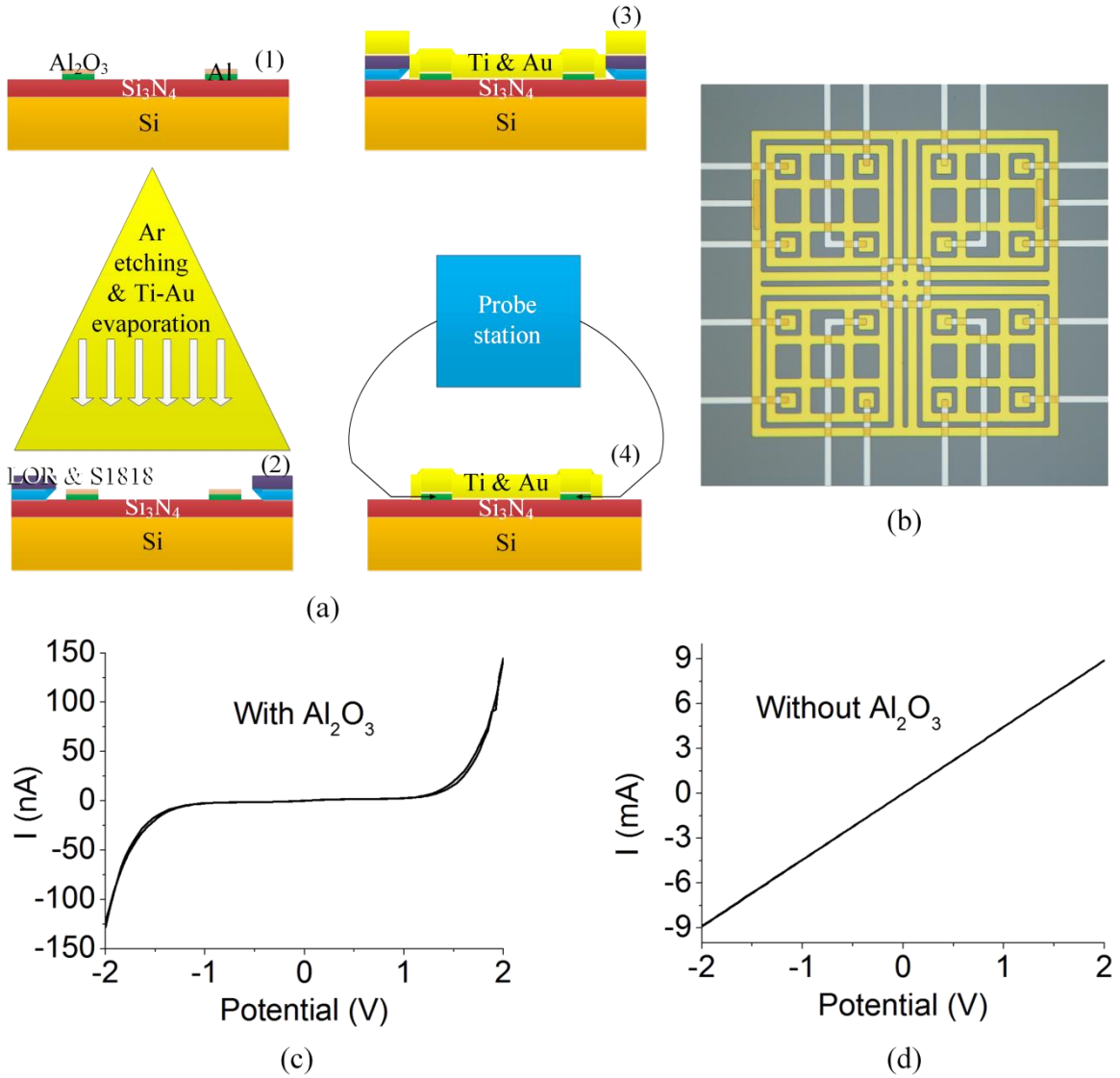

Figure 5.6: (a) Schematic diagram and (b) optical micrograph of a sample to check the electrical response of an Al-Au contact. Current-potential characteristics of (a) a contact with a native Al_2O_3 in between and (b) with the Al_2O_3 removed [170].

(20 nm/200 nm) bi-layer acted as a short circuit between Al tracks. The I-V curve between the same two bond-pads of each sample was then measured on a probe station, as shown in Figure 5.6(c) and (d). The Al_2O_3 layer caused a barrier effect to the electrical conductivity building a metal-insulator-metal structure. The samples with the oxide layer exhibited a diode response with tunnelling currents appearing at roughly 1.5 V. The Ar etching step proved to be efficient in the removal of the degrading performance oxide. Samples where the Ar etching step was performed had a resistance of about 225 Ω. The oxide was measured to break down for a voltage magnitude greater than 1.5 V. Depending on the potential window used in an electrochemical experiment this value may never appear at an electrode interface. Although even at the CMOS power supply

voltage of 3.3 V the oxide layer broke down but the samples exhibited a high resistance of 600 Ω.

5.5.2 Electroplating

Another method complementary to the metal evaporation patterning was to electroplate Au on the metal electrodes. An Au seed layer was required to maintain a uniform electroplating process, thus metal evaporation of Au was necessary prior to electroplating. The method to electroplate electrodes in a packaged chip was evaluated using a test sample prepared with the process presented in Section 5.3 using a stack of Ti-Al-Ti-Pd-Au at 20 nm/100 nm/20 nm/50 nm/200 nm to replicate the structure on the CMOS ASIC instead of Al for the metal tracks, etched to make electrode openings. The sample was wire bonded on a ceramic pin grid array (CPGA) package and an encapsulation process involving wax (described in Section 5.7.2) was used to protect the bond-pads and bonding wires from coming in contact with the electroplating solution. A custom designed printed circuit board (PCB) was used to connect all the electrodes together, as shown in Figure 5.7(a). An Au plating solution that had been warmed in a water bath to 50^{o}C was used to plate the electrodes with a plating current density of 13 μA/mm^{2}. To achieve the required current density using the available current control of the power supply unit that was used, an additional surface area needed to be added to the cathode. A copper wire of the required length connected to the other electrodes was used as a part of the cathode and a Pt wire of a larger surface area was used as the anode, as shown in Figure 5.7(b). The plating solution was agitated manually using a micropipette.

The Au electrode before and after the electroplating process is shown in Figure 5.7(c) and (d). The power supply unit was activated for a duration of 5 minutes. To measure the thickness of plated Au and its roughness an atomic force microscopy (AFM) measurement of the exposed metal was performed before and after the plating process, as shown in Figure 5.7(e) and (f). The thickness was increased by ≈320 nm and as it was expected the surface of the plated metal had an increased mean roughness from 2 nm before to 18 nm after electroplating. The rate of electroplating Au deposition was determined to be ≈64 nm/min.

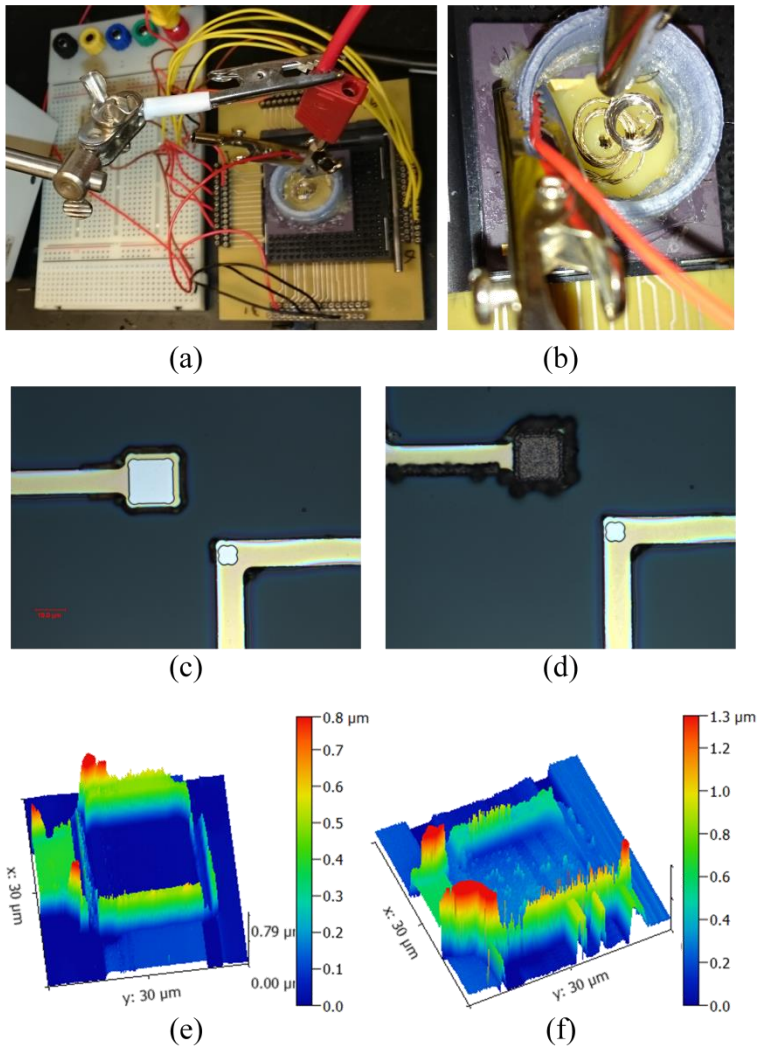

Figure 5.7: Pictures of (a) the electroplating setup and (b) a detail of the packaged chip. An Al contact optical micrograph (c) before and (d) after the electroplating process. AFM measurements of the same contact (e) before and (f) after the electroplating process.

The same process was repeated on a permanently encapsulated CMOS chip on a CPGA package with already prepared microelectrodes with the evaporated metal process. The CEs were connected to the power supply unit while it was operational; using the functionalisation switches capability that was described in Section 4.5.4. The CE_func_{EN} switch was turned on and the cathode was connected at V_{func_CEs}. All conditions were kept the same as in the test sample trial and the CEs were electroplated for 10 minutes. The ASICs prepared with the evaporated metal microelectrodes and the electroplating process are evaluated in the next section.

5.5.3 Evaluation

The metallisation processes were assessed with optical profiling measurements using a Bruker ContourGT optical profiler [182]. This metrology method was

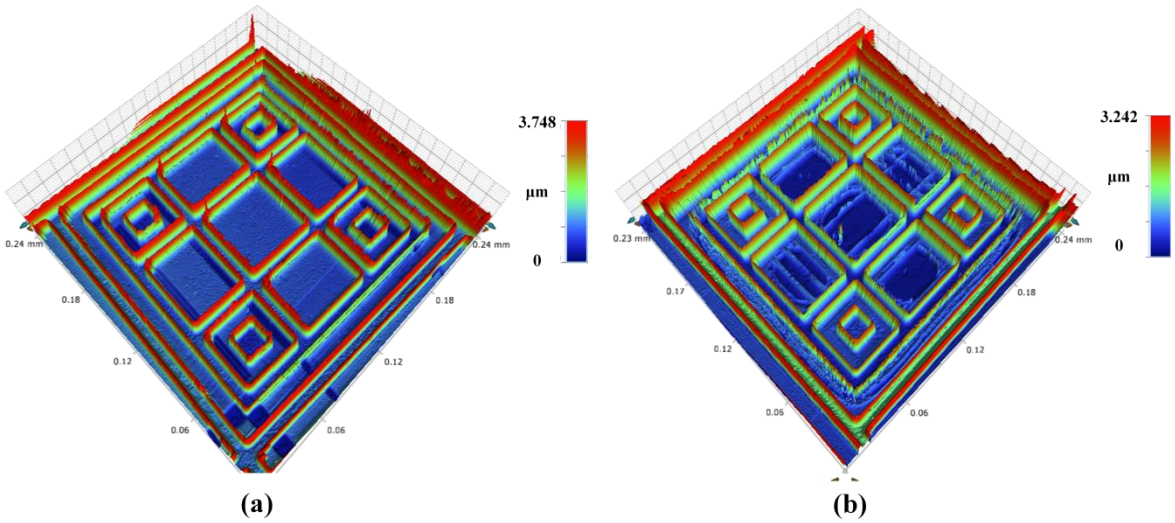

Figure 5.8: 3-D surface detail of the electrochemical cell of (a) the photolithographically processed and (b) the electroplated CMOS chip acquired with an optical profiler.

chosen as it can measure larger areas than a scanning probe microscopy tool (AFM). The CMOS chips were also encapsulated for the electroplating process and they could not be placed in an AFM tool. An optical profile of the photolithographically processed chip is shown in Figure 5.8(a). The measured height difference between the thinned passivation layer where electrodes were not deposited and the electrodes surface was about 100 nm. The height difference between the electrode surface and metallised parts on top of the unetched part of the Al metals was about 1 µm. The values agreed with the schematic representation presented in Figure 5.5(e)(2). An optical profile after the chip was electroplated is shown in Figure 5.8(b). The thickness of the electroplated Au at the CE was measured as a height difference between the CE and the RE electrode surfaces. It was found that it was about 660 nm hence the electroplating rate was 66 nm/min. Electroplating with the embedded functionalisation switches was very similar to the reference test sample measurement. The scale bars from both measurements show an increased range possibly due to lift-off artefacts.

5.6 Post-processing the Electrodes of Electrochemical Cells with Different Materials

After the first batch of processed CMOS chips was prepared a second process was developed to deposit more appropriate metals on each microelectrode hence the CE, RE and WE. Each electrode in a three-electrode system serves a different function. As was explained in Sections 2.3 and 3.2.2 a RE is fabricated

with materials that exhibit behaviour similar to an ideal non-polarisable electrode and Ag is often used as a quasi-reference electrode. A CE is fabricated with electrochemically inert materials for a large potential window to prevent any by-products jeopardising the measurements, Pd is one of these metals. Au is a good option for a WE as it is an inert, biocompatible metal that can be functionalised for biosensing.

After the electrode openings were created with the process described in Section 5.4, the CMOS dies were prepared for metallisation with the S1818 developer soak lift-off process. As a first step a bi-layer of Ti-Pd with a thickness of 20 nm/150 nm was deposited on all microelectrodes. Pd served as the surface material of the CEs and a diffusion barrier for the following evaporated metal layers of the REs and the WEs. Separate photomasks were prepared to create a

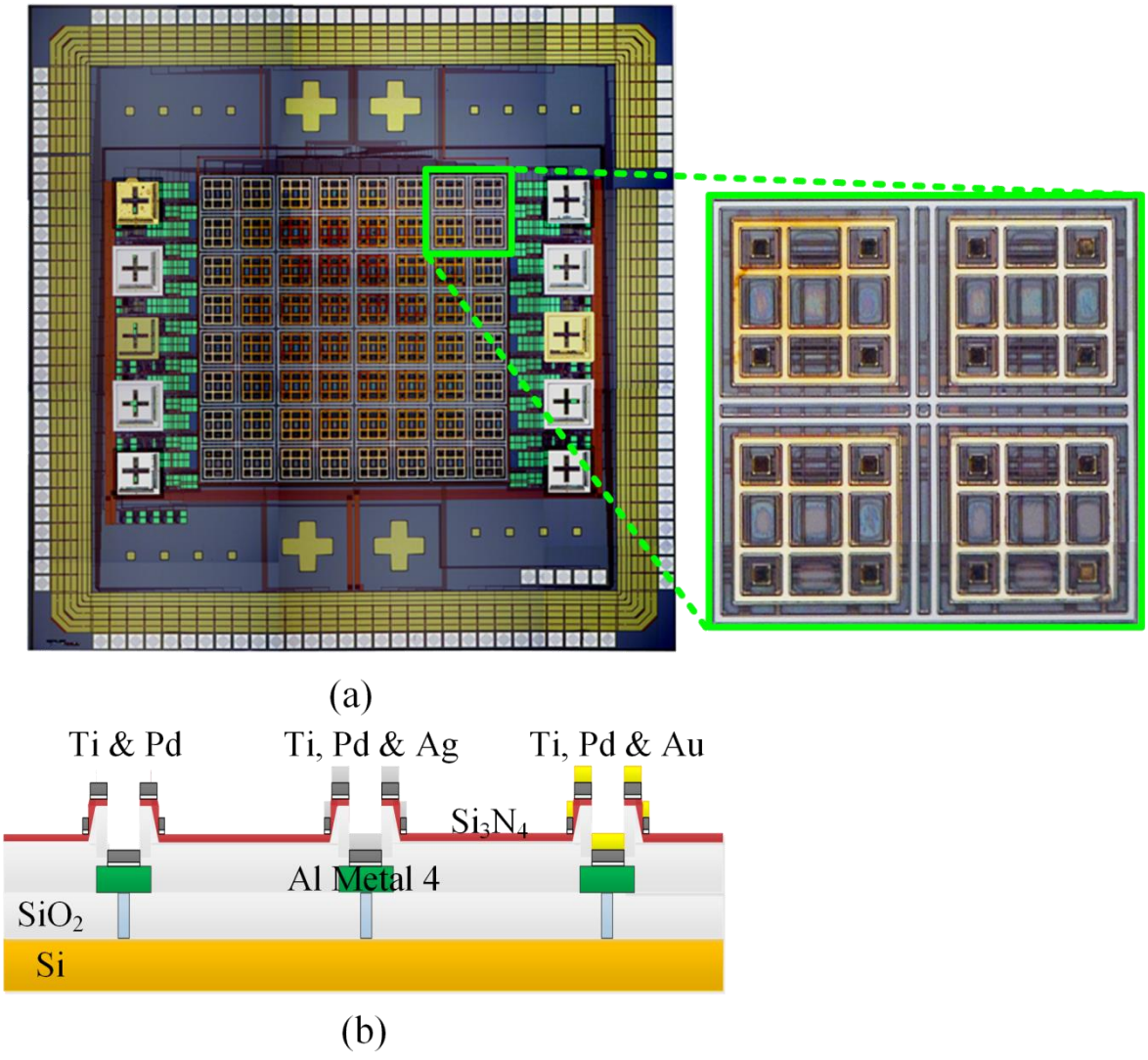

Figure 5.9: (a) Optical micrograph with a detail of an electrochemical cell and (b) a schematic repsentation of the cross-section of a chip prepared with Pd, Ag and Au for the CEs, REs and WEs respectively.

lift-off pattern for the other electrode types (RE and WE) in the array. 200 nm of Au were deposited on the WEs using the Plassys electron evaporation tool [178]. Ag was not supported as a material by the tool so a modified thermal metal evaporator that could use materials introduced by the user was selected for this process. Ag in the form of a wire was placed in the evaporator heating elements ("boats") and 550 nm were deposited on the REs. An optical micrograph and a schematic representation of a cross section of the electrodes is shown in Figure 5.9(a) and (b) respectively. As it can be observed in Figure 5.9(a) the Ag metal of the RE appeared to be discoloured, indicating a change in its molecular structure that was investigated and presented in the next section.

5.6.1 Evaluation

Metal deposition was evaluated by comparing the height between electrodes of

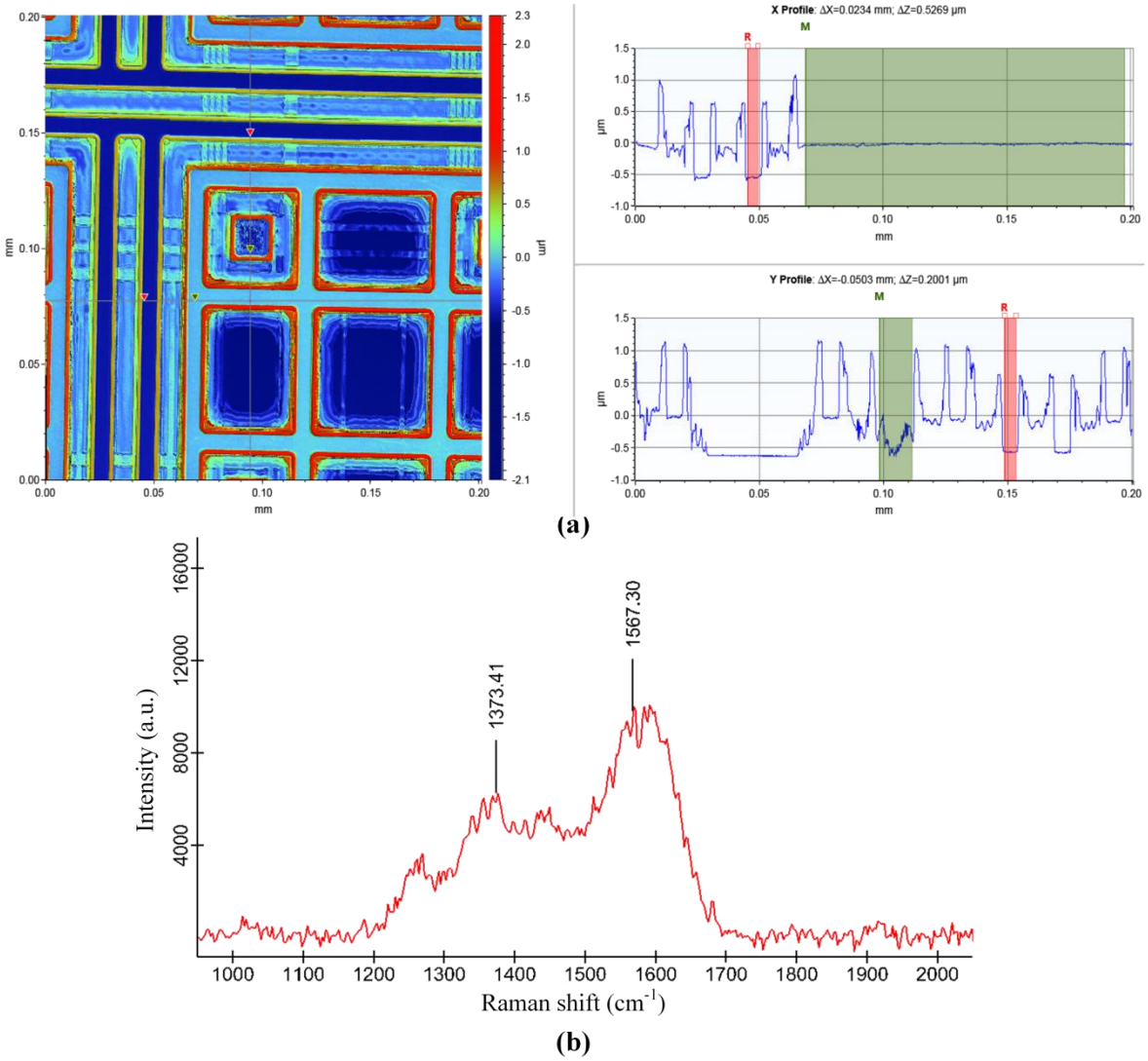

Figure 5.10: Evaluation measurements of a post-processed CMOS chip with Pd, Ag and Au. (a) 3-D surface detail of the chip acquired with an optical profiler and (b) raman spectra of the Ag metal at the RE.

the post-processed chips with optical profiling measurements. As it can be observed in Figure 5.10(a) the height difference between the CE surface and the other microelectrodes was identical to the deposited metals thickness. The quality of the Ag metal was also evaluated using a Raman alpha300 RAS microscope from Witec. The Raman spectra, shown in Figure 5.10(b), was used to record the structural fingerprint of the material that was deposited on the RE. It was found that the resulting spectra has been reported to occur in carbon films containing Ag nanoparticles [183]. The phenomenon's origin was recognised as carbon contamination in the modified evaporator tool.

Although the materials chosen for this batch of CMOS post-processed chips were more suitable for electroanalysis, only the first batch with Au used as a universal material for all the microelectrodes has yet been used in electrochemical experiments. The influence of carbon present in the Ag metal on its standard potential remains to be measured.

5.7 Chip Encapsulation

The bond-pads that were embedded in the design were used to connect the ASIC to external instrumentation. After the CMOS chips underwent post-processing fabrication they were glued with a thermally conductive H74 epoxy from Epoxy Technology [184] and wire bonded in a 144-pin CPGA chip carrier package purchased from Spectrum Semiconductor Materials Inc [185]. The test samples were glued in a smaller 120-pin CPGA package. The packages offered a capability for through-hole pin connections with excellent electrical performance on PCBs. Wire bonding was conducted at the School of Physics and Astronomy of the University of Glasgow, using a Hesse and Knipps Bondjet 710 ultrasonic wire bonding tool [186]. The ceramic package ensured efficient heat dissipation, an important feature for the correct operation of integrated circuits. The package also served as a platform for the chips' encapsulation to turn them into Lab-on-a-Chip devices. As it was explained in Section 2.5.3 the bonding wires and bond-pads need to be insulated and only the active area needs to come in contact with liquids used in electrochemistry. The encapsulation methods used to construct a waterproof container on the CMOS chips are explained in the following sections.

5.7.1 Epoxy and PET-G Encapsulation

The use of chemical solvents such as acetone and acetonitrile were extensively used in the electrochemical experiments of this work thus chemical resistance of the materials used for encapsulation was an important factor in their selection. The encapsulating material used in this method was a chemically resistive 302-3M epoxy from Epoxy Technology [184]. This particular epoxy was also chosen for its viscosity characteristics, as a lower viscosity is required for the material to flow in between the closely spaced bonding wires. The use of a more chemically resistant epoxy (EP42HT-2MED from Masterbond [187]) was also explored but due to poor adhesion to the ceramic package it was not used as part of the encapsulated package. The active area of the ECM chip had to be kept protected from being encapsulated. As explained in Section 2.5.3 polydimethylsiloxane (PDMS) is an elastomer used in microfluidics. After it is cured PDMS exhibits a hydrophobic surface and it develops reversible van der Waals forces with smooth surfaces. These characteristics make it an ideal choice to use a cube of PDMS as an epoxy casting material as it can be temporarily

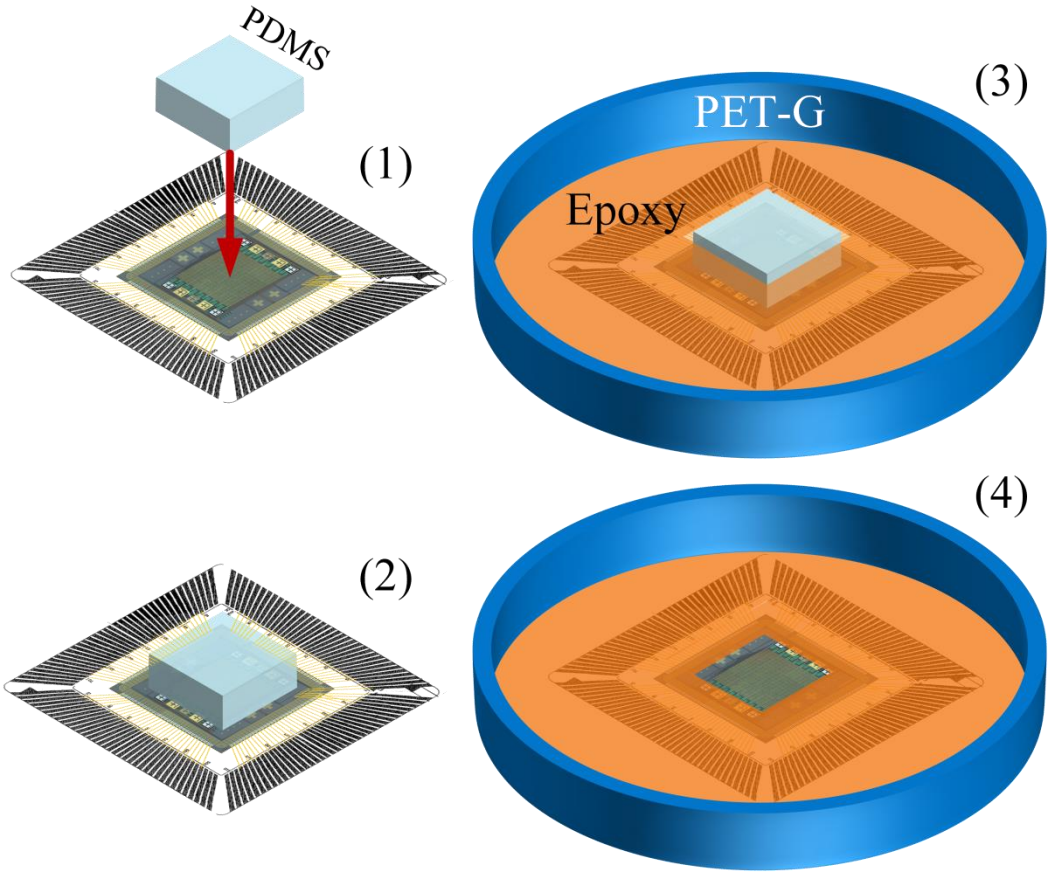

Figure 5.11: Epoxy-PETG encapsulation process using a PDMS cube as a casting material.

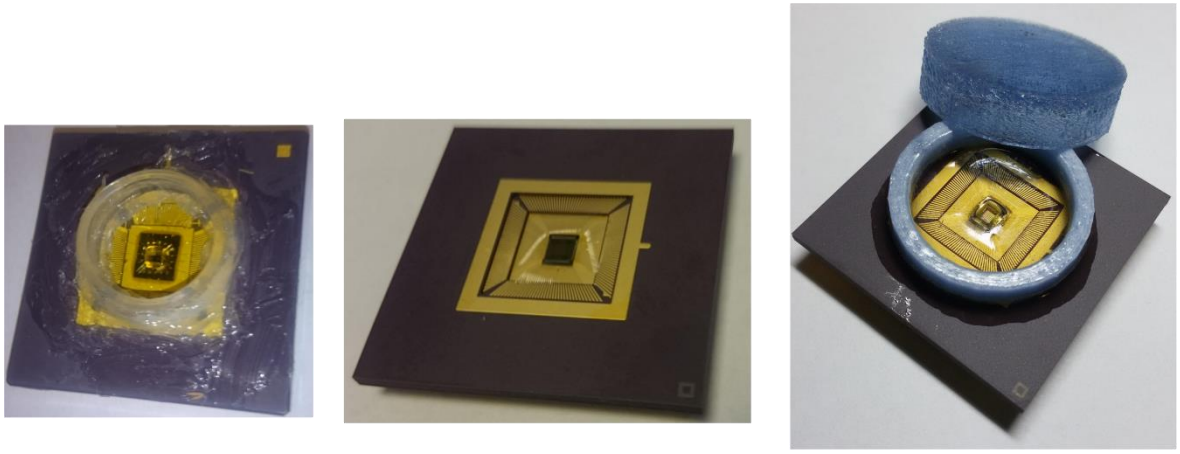

(a) (b) (c)

Figure 5.12: Pictures of (a) an encapsulated test microelectrodes sample, (b) a wire bonded post-processed CMOS ECM on a 144-pin CPGA package and (c) an its encapsulated version with the PET-G tube and lid.

bonded on top of the chip's active area, as shown in Figure 5.11(1-2). A polyethylene terephthalate glycol-modified (PET-G) tube and a lid were designed and 3-D printed in an Ultimaker 2 3-D printer. The material is a polymer of the polyester family that is chemically resistant to common solvents. An off-the shelf polypropylene test tube was cut for the test sample packaging. The tube was glued with the epoxy around the wire bonded chip and contacts. This process created a mould that was subsequently filled with epoxy and left to dry for 24 hours, as shown in Figure 5.11(3) [188]. The package was baked at 65^{o}C for 3 hours as a post-curing step to evaporate any remaining solvents. After curing, the epoxy had a good adhesion to the ceramic package, the gold plated cavity and contacts as well as the silicon die. As a last step the PDMS cube was easily removed as epoxy did not bond on its hydrophobic surface and a permanently encapsulated device with a chamber for chemical solutions to be analysed was created, as shown in Figure 5.11(4). Pictures of the packaged and encapsulated chips are shown in Figure 5.12.

5.7.2 Encapsulation for Electroplating

After the electroplating process that was described in Section 5.5.2 the test sample had to be removed from the encapsulated package and measured in metrology tools. In order to achieve this capability the encapsulation process was altered to include removable non-permanent materials. Epoxies were replaced by wax which melted as the packaged sample was placed on a hotplate at 100^{o}C. The tube was fixed on the package with a silicone sealant from Geocel

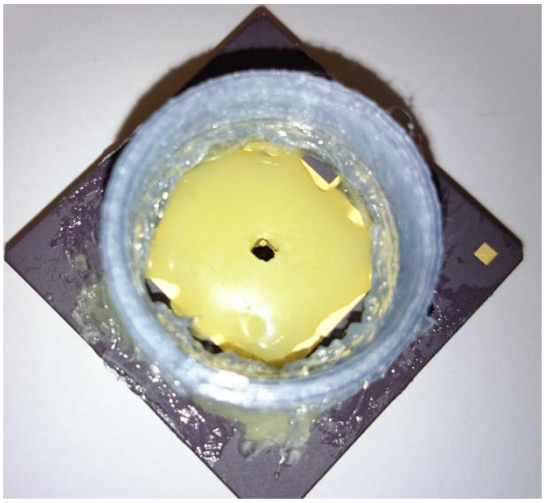

Figure 5.13: Encapsulated package for electroplating.

and could be peeled of after the electroplating process. Another tube was stacked to increase the volume size for efficient pipetting of the electroplating solution, as shown in Figure 5.13. After the electrodes were electroplated, the tubes and wax were peeled off and after some heating the sample was retrieved. It was placed in beakers of acetone, methanol and isopropanol and sonicated for 5 minutes in each solvent to remove any residual wax and debris before it was measured.

5.8 Microelectrode Cleaning

The Au microelectrodes that were prepared and encapsulated with the aforementioned methods on both the ASICs and the test samples required a cleaning step from organic contaminants before they were used for electroanalytical measurements. Au is susceptible to organic impurities with weak bonds on its surface [189] and the use of oxygen plasma steps in the photolithographic processes with tools that have been reported to suffer from carbon contamination in the JWNC increased this effect. Surface contamination of microfabricated microelectrodes has been reported before and cleaning methods have been investigated [190]. One of these methods that was reported to remove most of the contaminants from the Au surface was adopted in this work. A solution of 50 mM KOH and 25% H_2O_2 was poured in the containers of encapsulated chips for 10 minutes. After they were cleaned with DI water, a solution of 50 mM of KOH was used and a linear potential sweep from −200 mV to −1200 mV (vs Ag^+/AgCl) with a 50 mV/s was performed to clean the WEs. A Ag^+/AgCl RE was prepared with a Ag wire electrolysed in 3 M KCl that was used

as an external RE. To perform the electrochemical cleaning step the test sample WEs were all connected together to a potentiostat, the CMOS ECMs were connected and controlled by a setup that was prepared to make up an electroanalytical system that will be described in the next chapter.

5.9 Summary

The CMOS dies that were received from the foundry required an etch of the isolating passivation layer to expose connection points for the microelectrodes. The passivation layer was first thinned to make the trenches that reach the top metal layer of the CMOS chips shallower. This assisted to develop the lift-off profile of photoresists necessary for the next step of metallisation. The deposited metals were inert to harsh electrochemical conditions opposing to the inherent Al metal tracks (shaped at the microelectrode pattern of this work). No contact of liquids to the easily corroded and contaminant Al metal had to be ensured. The openings were made smaller so that only the surface of the top metal layer may be exposed and the evaporated metals pattern was wider to ensure full coverage over the openings. Two batches of post-process fabricated CMOS chips were prepared, the first one (used for all the experimental measurements) had all the microelectrodes made of Au, the second one had each microelectrode type (CE, RE and WE) selectively covered with an appropriate metallic material with suitable characteristics for its operation. However, Au being a material whose behaviour lies between ideal and non-ideal polarisable electrode, it is adequate for use at all microelectrode types.

To develop processes for the CMOS ASIC, test samples that mimicked its structure were prepared. A problem of an Al_2O_3 layer forming upon the Al metal was exposed from the passivation layer was identified with the test samples. The oxide layer blocked the contact between Al and the microelectrode surface and it was solved with an Ar etching step under vacuum before the metal evaporation. An electroplating option was also explored with the test samples and it was verified with the CMOS chips with a resulting Au deposition at a 64 nm/min rate. Last but not least, the test samples were prepared as an external microelectrode array mimicking the structure of an on-chip electrochemical cell. To prepare the CMOS chips and the test samples as Lab-on-a-Chip devices, they were encapsulated with chemically resistant materials with

a chamber open to be filled with chemical solution for analysis. Lastly, the microelectrodes were cleaned with an oxidising and electrochemical method to be prepared as an electroanalytical transducer used in the system presented in the next chapter.

6 Experimental Results

6.1 Introduction

The preparation of the CMOS chips as Lab-on-a-Chip devices suitable for use in an electrochemical environment and the post-processing fabrication of microelectrode test samples was described in the previous chapter. This chapter describes the system that included the Lab-on-a-Chip device to produce independent electrochemical results from each electrochemical cell. The chapter begins with a description of the hardware setup used to build an electrochemical cell microarray (ECM) system. To operate the system and analyse the acquired results, software programs were prepared in Labview from National Instruments (NI) [191]. The chapter continues with an electrical and electrochemical response benchmark of the ASIC's potentiostat. Moreover, the encapsulated chip was used as an electrochemical platform and its analogue and digital readout capabilities were evaluated. In order to assess the chip's electrochemical cell independence, a method to measure the electrochemical cross-talk was devised. All the figures of merit (FOM) are summarised and compared with the state of the art. After the chip was characterised, its capabilities were demonstrated with a set of experiments. First, a novel method to reduce the acquisition time of CV at a defined scan rate is presented. The next experiment demonstrates the capability of the ECM to apply multiple electrochemical methods independently in the same sample media. Lastly, a chemical solution with two analytes was prepared and they were measured simultaneously and independently by separate electrochemical cells in different potential windows. The two last experiments produce independently acquired results that can be correlated to produce new results that determine the composition of an analysed compound as explained in Section 2.7.

6.2 Setup

The ASICs that were prepared as described in Chapter 4 need to be connected to external instrumentation for the input and output signals to be supplied and acquired respectively. The setup may generate the required scanned potentials for an electroanalytical method and process the acquired results to be represented in an *i*-*V* or *i*-*t* diagram. The necessary hardware setup and software

programs that were developed to construct the ECM system are explained in the following sections.

6.2.1 Hardware

6.2.1.1 Commercial reference setup

Initial experiments were performed with a commercial CHI600D potentiostat from CH Instruments [192] that is a standalone instrument with its own acquisition hardware and software, as shown in Figure 6.1. Three wires shown in Figure 6.1 were used as connection points to electrodes according to the colour coding (red-CE, white-RE and green-WE). The commercial potentiostat was used as a reference for the measurements conducted with the ECM system that was developed.

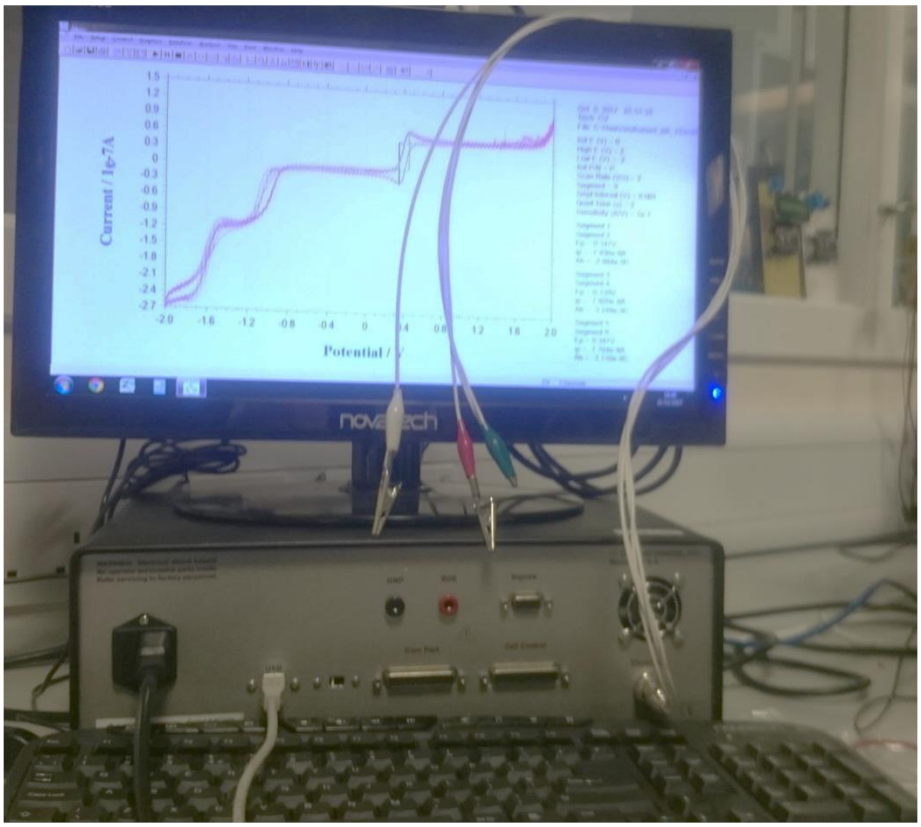

Figure 6.1: The CHI600D potentiostat instrument from CH instruments showing the crocodile clips of the three electrode system [192].

6.2.1.2 ASIC ECM setup

The ECM system is comprised of the encapsulated CMOS ASIC on the 144-pin CPGA package that is housed in a custom designed printed circuit board (PCB).

The PCB was designed so that the chip was connected to the required power supply voltage of 3.3 V and metal tracks connected the required input and output (I/O) pins of the packaged chip to connection cables. The other end of the cables was connected to a PXIe interface system from NI that completed the

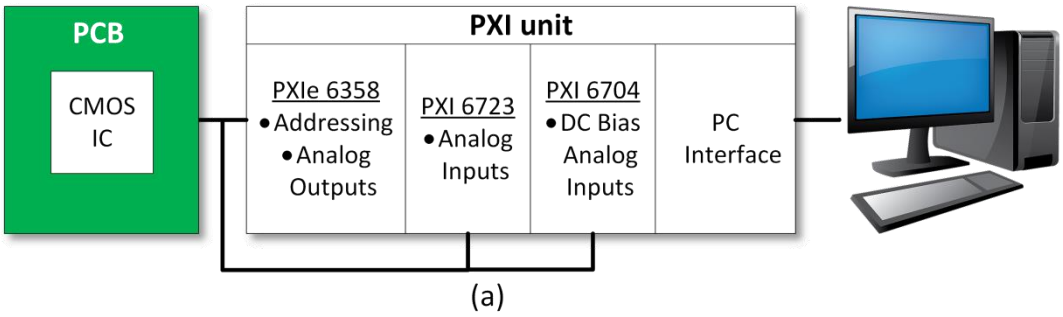

(a)

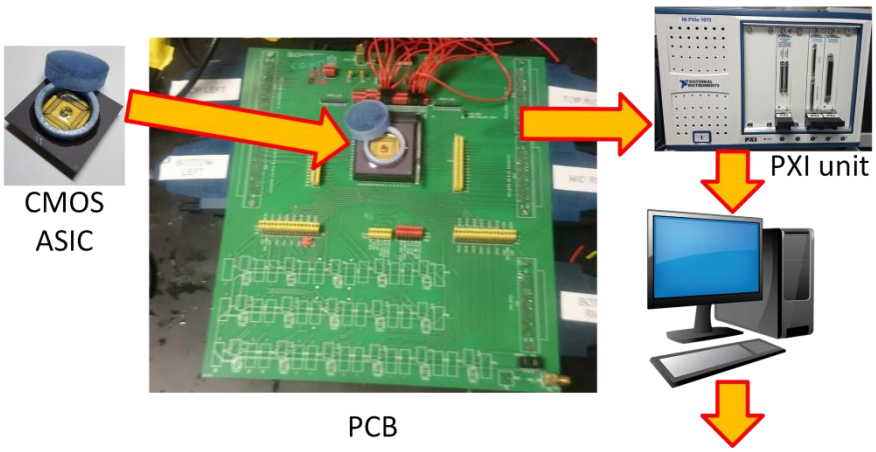

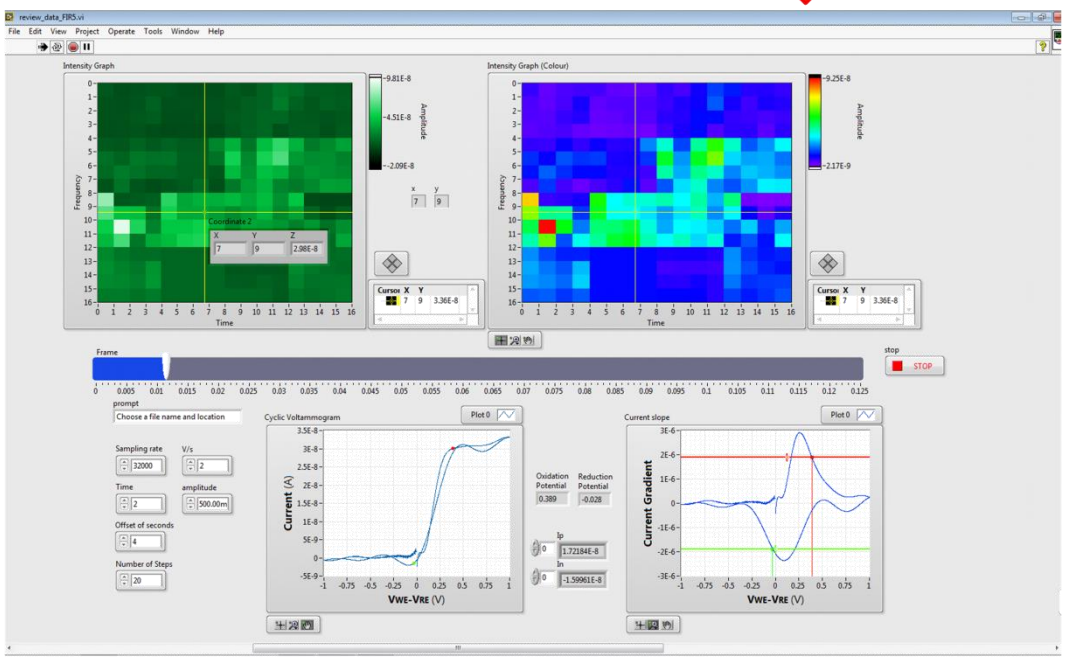

Labview inerfacial software

(b)

Figure 6.2: (a) Schematic representation and (b) pictures describing the electrochemical cell microarray driving and acquisition system.

system with its analogue and digital I/O interface comprised of analogue-to-digital and digital-to-analogue converters (ADCs and DACs), registers, buffers, high speed reference clocks (at 10 MHz and 100MHz) and computer interface.

The PXIe system consists of a PXIe-1073 chassis [193] that contains three cards. The analogue input signals were supplied by a PXI-6723 [194] and a PXI 6704 [195] cards. For the readout of the analogue outputs and the digital I/O a PXIe-6358 [196] card with a 1.25 MS/s/channel capability was used. The system was connected to a personal computer through a PCI-Express-8361 card and it was controlled directly from Labview [191] as NI provided program functions that conditioned the analogue and digital interface circuits. Programs with a graphical user interface (GUI) were prepared to set the bias voltages, generate the driving digital and analogue signals, record and process the output signals as they are described in Section 6.2.2. The system is described with a schematic representation in Figure 6.2(a) and with pictures from the actual components in Figure 6.2(b).

The PCB was designed using the Capture and PCB Editor tools of the Cadence OrCAD software package [197]. The design files were prepared in “drl” (specifying the drilling pattern) and “art” (specifying the photomasks for metal etching, the insulating material soldermask and legend processes) formats and

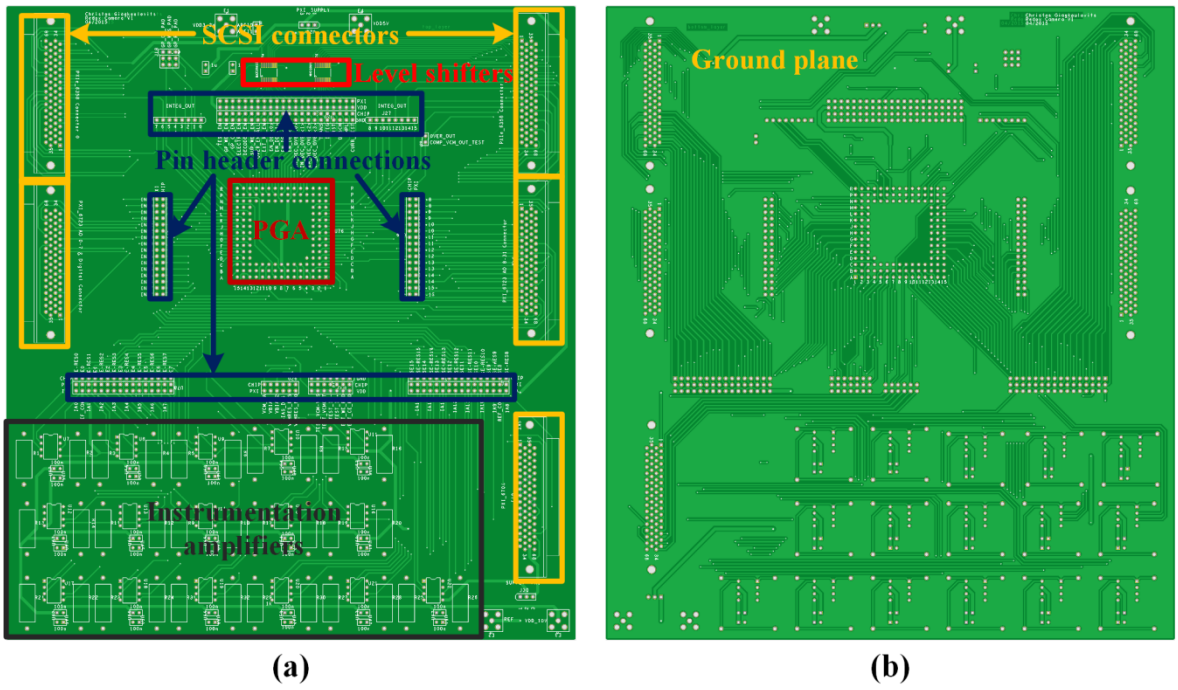

Figure 6.3:Custom designed PCB (a) front and (b) back view pictures extracted from the design files by Eurocircuits [8] with added details of the components.

were sent for fabrication to Eurocircuits [198]. The vendor was chosen to fulfil the requirements for the PCB's size (22.9 cm × 25.4 cm), hole size (a minimum of 550 μm), vias (300 μm) and complexity. The PCB design front and back view are shown in Figure 6.3(a) and (b) respectively. A PGA ZIF 15 × 15 socket was used on the PCB for ease of interchangeability of the packaged chips. The SCSI connectors were used for the interconnections with the PXIe system. The digital inputs supplied by the PXIe-6358 card had a 0 – 5 V voltage range which had to be changed as it was not compatible with the 0 - 3.3 V range of the CMOS ASIC. Two MAX 3001E potential level shifters were used to convert the two voltage ranges. Pin headers were also soldered on the PCB on the signal tracks to change any connection to the CMOS chip according to the experimental needs. The PCB was initially designed with an output signal amplification capability using 16 discrete component INA217 instrumentation amplifiers (IAs) from Texas Instruments [199]. However, the chosen IA's input stage required a large 2 μA input bias current compared to the nA range current detected at the $R_{\text{I to V}}$ output resistors and a suitable replacement has not yet been found. The output was sampled directly from the on-chip output resistors without additional amplification. Lastly, the PCB was designed with a ground plane at the bottom side for screening and 1 μF decoupling capacitors for the 3.3 V and 5 V power supply voltages.

6.2.2 Software

Having the hardware connected to construct the ECM system, a program was developed to control the electrochemical cells with electroanalytical methods, acquire the results and store the raw data in a file. Another set of programs was developed to analyse the raw data measurements and arrange them to be presented in plots and 16 × 16 frames imaging the WE current in the array over the course of electroanalysis. The programs are presented in the next sections.

6.2.2.1 Data Acquisition

A conceptual flowchart of the program that was created to drive the potentiostats and record the analogue voltages and digital pulses is shown in Figure 6.4. A GUI was made to assist the user to select the required electroanalytical method to be run on each electrochemical cell. Analogue and

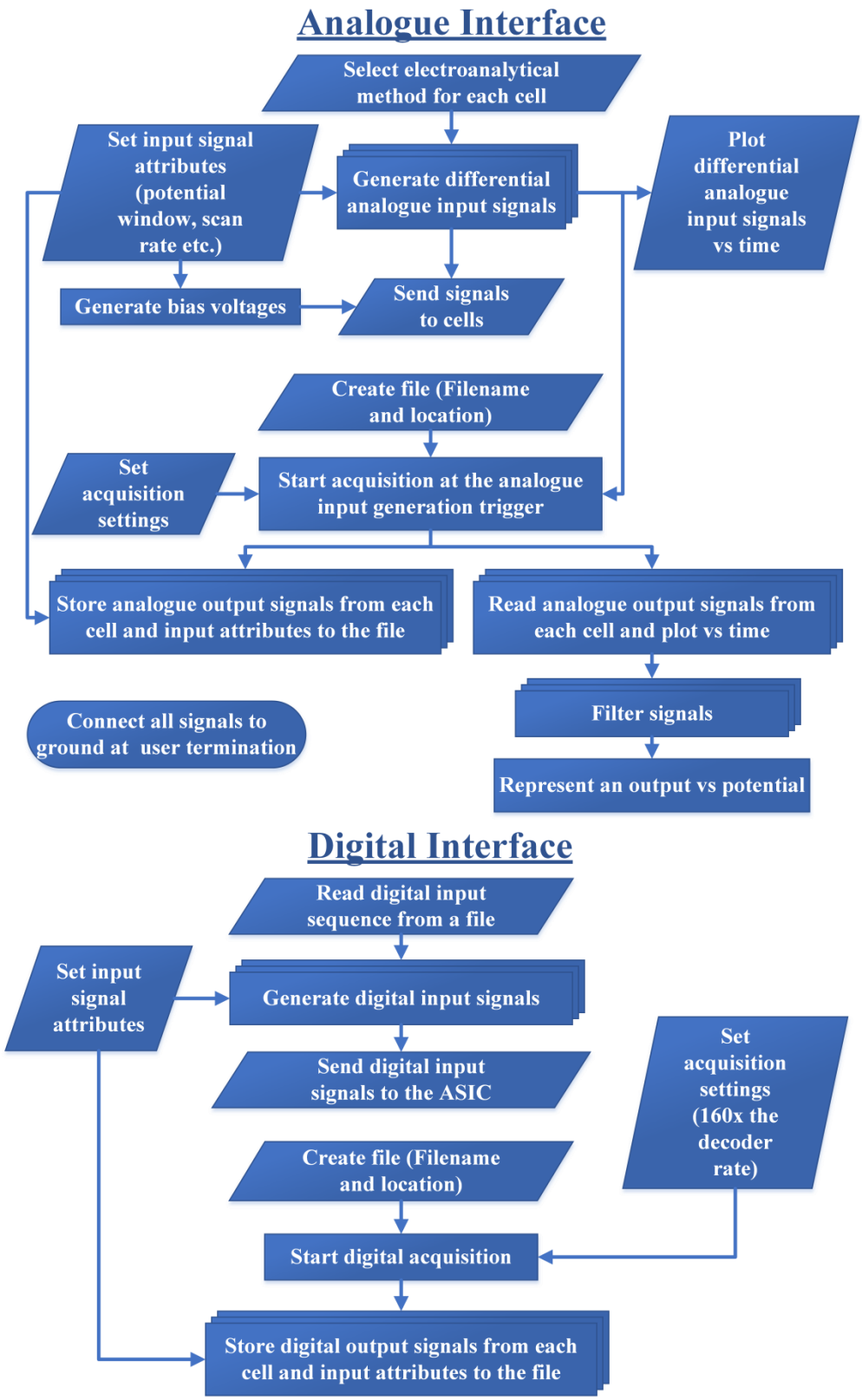

Figure 6.4: Flowchart of the program that controls the analogue and digital interface.

digital input signal attributes were also made available to the user to configure the bias voltages, the decoder rate, the sampling rate, the input signal value and the amplitude, the scan rate and the potential window in voltammetric methods as well as other parameters specific to the selected method. The

analogue input signals were generated according to the user inputs by built in numerical and signal generating functions, “for” loops and a subroutine that was developed to generate a staircase cyclic voltammogram. The digital CSA inputs were programmed to run at a 10 times faster frequency than the decoding signals, both their sequences were sourced from text files. The analogue outputs acquisition started with a trigger at the input signals generation using a sampling rate of 32 kS/s/channel throughout the experimental measurements presented over the next sections. Measurements were conducted at a decoder rate up to 6.4 KHz to multiplex WEs at the analogue output and 51.2 KHz for the digital output (meaning a 8.192 MHz digital sampling rate). The raw analogue output results were plotted in the acquisition software to ensure the correct operation of the ECM while the experiments were conducted. After the end of an electroanalytical measurement, a “stop” pushbutton was selected by the user for all the voltages to be set to ground. These connections prevented any biasing of the integrated circuits that could lead to further uncontrolled electrochemical processes occurring at the microelectrode array.

6.2.2.2 Data Analysis

After the raw data were stored separate data analysis programs for the analogue and digital measurements were used to process the acquired data, demultiplex them and present them in plots and imaging frames.

A flowchart of the analogue analysis program created in Labview is presented in Figure 6.5. Some of the user defined parameters used at the acquisition were sourced from the stored files to represent and demultiplex the WE outputs from each potentiostat output (e.g. the decoder rate). The analogue outputs were recorded as voltage difference on the $R_{\text{I to V}}$ conversion resistors of each potentiostat. These results were converted to current values with a measured resistor size map that was created for every chip as described in Section 6.3.1. Furthermore, impulse noise artefacts originating from the signal generating circuits of the PXIe system needed to be eliminated from the measurements, thus digital non-linear 1D median filtering was applied to the multiplexed data. Options for calculating the mean value per cell and for the whole array were also introduced to the program as in cases of WEs detecting the same process such practices can lead to more accurate results eliminating the need for

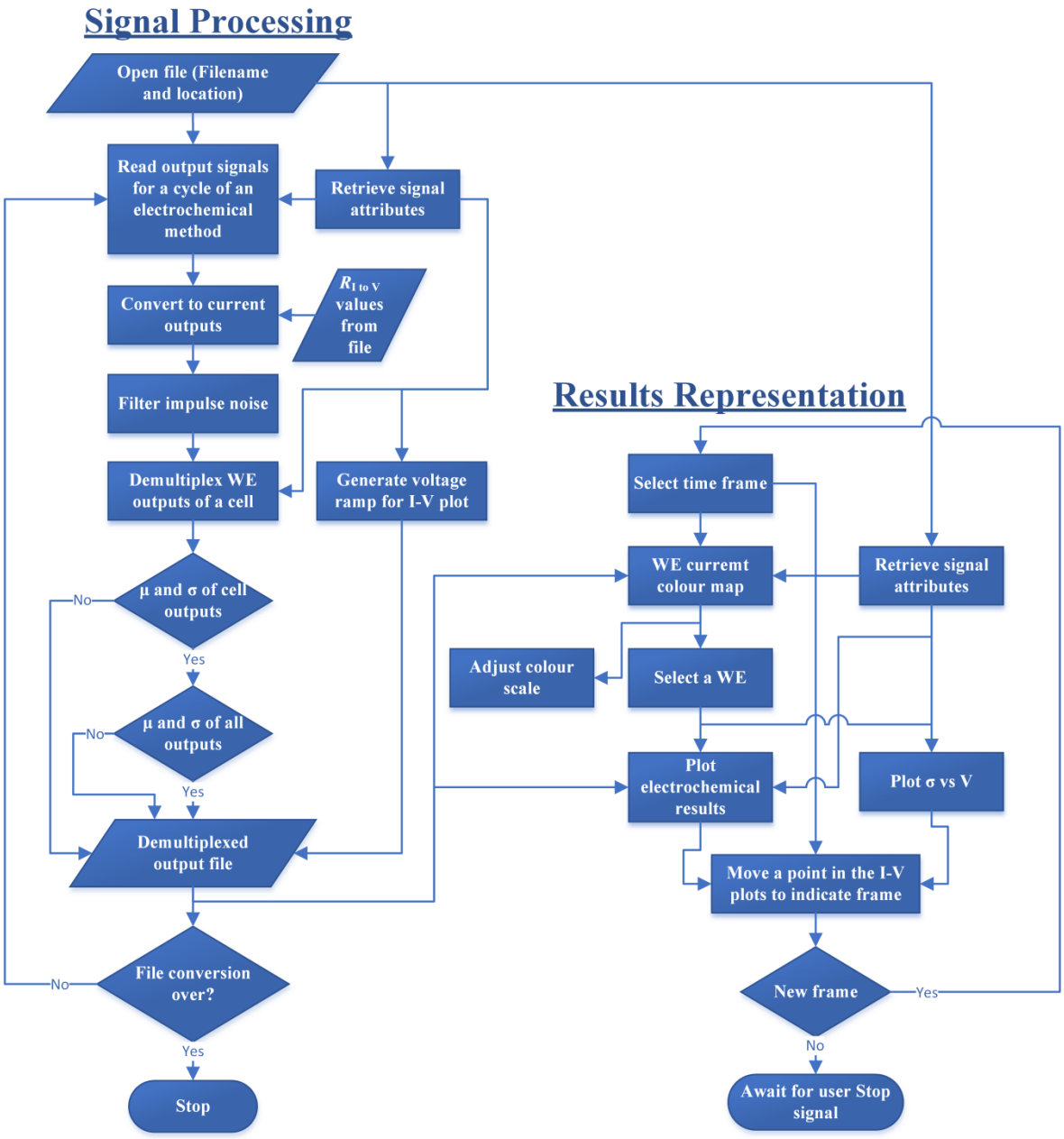

Figure 6.5: Flowchart of the analogue data analysis program.

consecutive measurements (e.g. cycles of a voltammogram). While the signals were conditioned, they were temporarily stored in a file to be read and represented as colour-coded WE current maps at discrete time frames. Selecting a WE in the current map produced its respective results for a cycle of an electroanalytical method where the selected frame belongs to (e.g. a cyclic voltammogram).

A separate program was created in Labview to analyse the digital pulses acquired from the digital CSA presented in Section 4.6, as shown in Figure 6.6. The sampling rate was used to represent the digital waveforms as they were

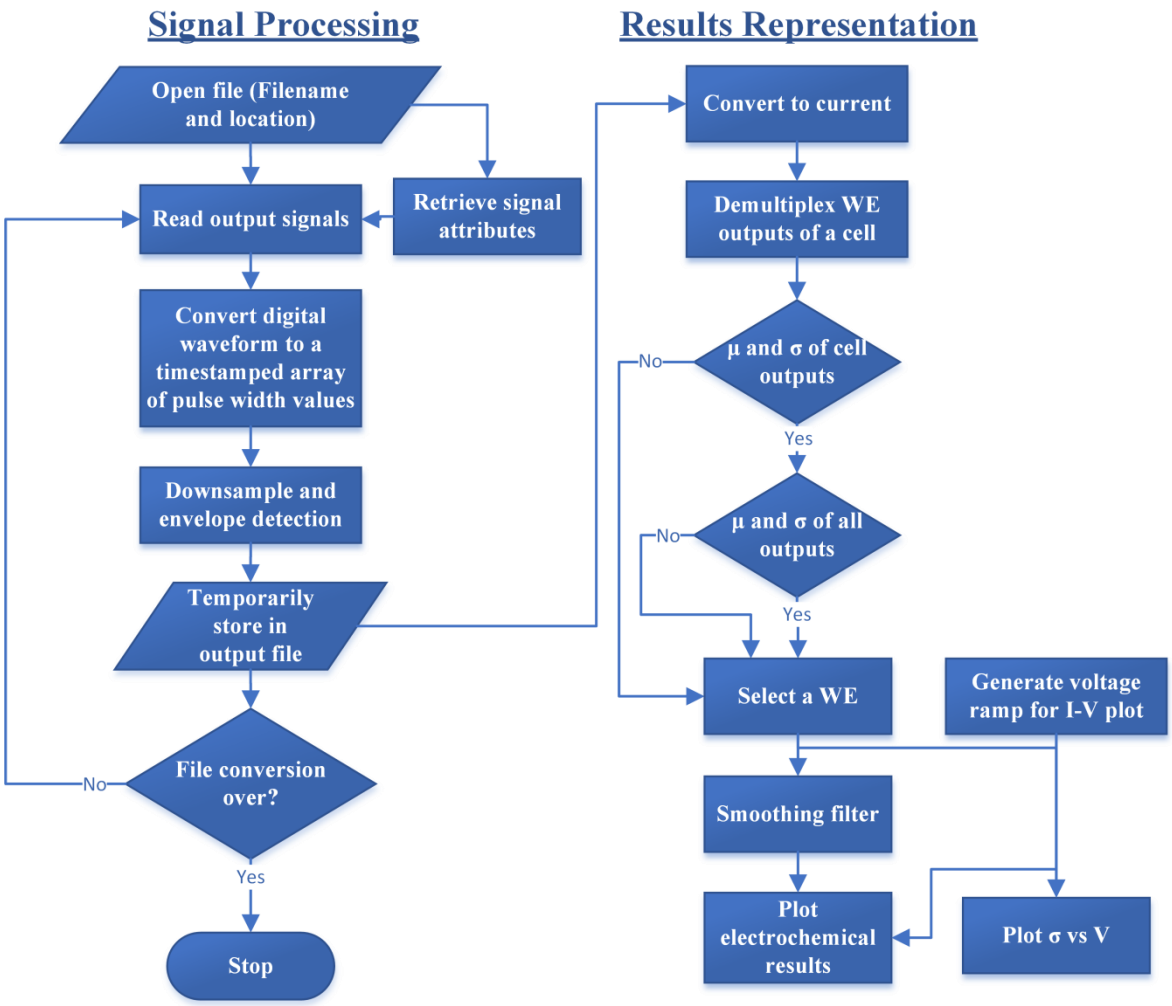

Figure 6.6: Flowchart of the digital data analysis program.

recorded. The samples were converted into a numeric array of pulse width values.

An envelope detection algorithm using a Hilbert conversion of the array was added to the program to demodulate the numeric array to a signal representing the pulse width magnitude. The current source magnitude that discharged the integrating capacitor was used as a reference for the conversion of the demodulated signal to represent current. As for the analogue analysis program the WEs were demultiplexed and averaging functions were made available. Finally, a smoothing filter was used to remove noise artefacts. The Labview programs GUI and block diagram codes that were described in this section are provided in Appendix D.

6.3 Chip Characterisation

The purpose of the built system is to conduct experiments that make use of the independently operated electrochemical cells. A characterisation of the CMOS ASIC connected to the laboratory setup was first conducted to benchmark the integrated circuits' performance and their ability to perform as a potentiostat. Results were obtained by the analogue and digital readouts using the on-chip microelectrodes of the microarray. The cell-to-cell cross-talk was also measured as it is an important aspect for the simultaneous application of different electroanalytical measurements on the separate electrochemical cells.

6.3.1 On-chip Circuits

Before any electrochemistry was applied to the ECM, the on-chip circuits' electrical behaviour was characterised. On-chip electrodes were isolated with integrated switches by the internal circuits test mode that was described in Section 4.7. The nodes of only one potentiostat were connected and fed to analogue pads that were connected to the PCB and accessed through the pin headers. If the load between the CE and the RE is defined as R_1 and between the RE and the WE as R_2, a potentiostat's output at the CE is described by:

$$V_{out} = - V_{in} \frac{R_1 + R_2}{R_2} \tag{6.1}$$

Discrete components of an R_2 = 10 MΩ resistor and a low negligible resistance R_1 = 1 kΩ were used. The values were chosen so that the current that was conducted through the electrode nodes was maintained at the anticipated experimental levels. Using a waveform generator and an Agilent Infiniium 9000 series oscilloscope a differential 2 V_{pp} sinus function was applied at the potentiostat inputs and the gain was measured as a function of the frequency. The frequency response is shown in Figure 6.7(a), the bandwidth at -3 dB was found to be 150 kHz owing to the Miller compensation of the amplifiers. The acquired bandwidth allowed for the use of FSCV at high scan rates up to 18 KV/s if a 4 V potential window was used. The voltage swing of the WE versus the RE capability of the fully differential potentiostat was measured at 5.2 V_{pp} using the same load. The resistor values were changed to find the maximum current that

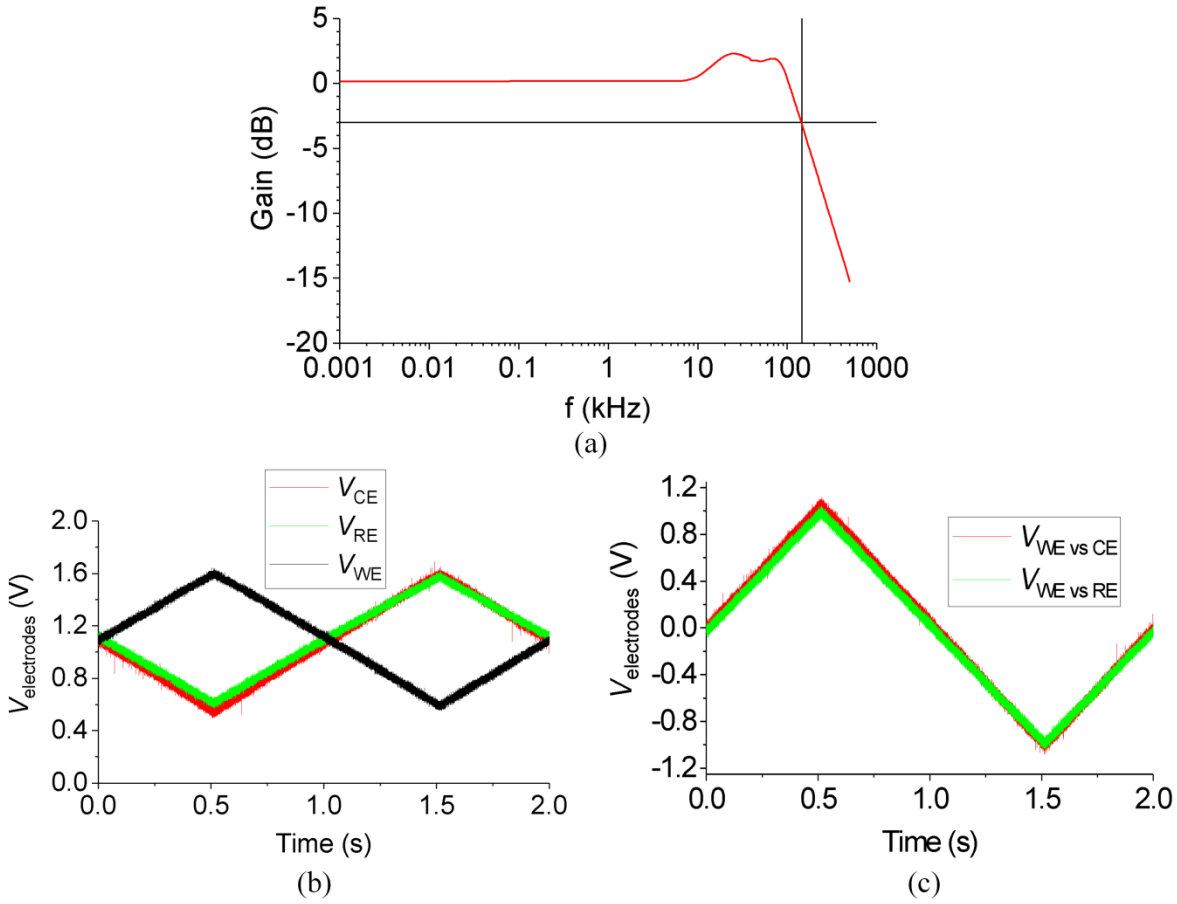

Figure 6.7: (a) Frequency response, (b) electrode potentials and (c) potential differences of the integrated potentiostat connected to external discrete component loads.

could be detected with the on-chip readout system. It was found as I_{max} = 13 µA using the resistor R_2 = 5 kΩ as a load and setting R_1 = 100 Ω and an input signal with a 100 mV differential amplitude.

The external discrete component circuit was changed to an exact replica of the electrochemical circuit equivalent model presented in Section 3.3.4 using the same values as the simplified model used for the electrical simulations. The potentials that appeared at each electrode node were buffered with discrete component LM324-N opamps [200] connected as unity gain amplifiers. The recorded output signals for a 1 V differential triangular input waveform, typical of CV are shown in Figure 6.7(b). Using these readout voltages the potential difference between the WE and RE as well as the WE and the CE are plotted in Figure 6.7(c). The potentiostat exhibits behaviour identical to the simulations. The same load was used to measure the slew rate of the potentiostat which is a FOM that relates to the correct representation of a voltammogram; a 1.09 V/µs value was measured.

Last but not least, the on-chip $R_{I\,to\,V}$ current converting resistors had a reported tolerance of ± 20%. To circumvent measurement variations by the tolerance, a resistor map was made, stored into a file and used by the data analysis software for each chip as described in Section 6.2.2. Using the integrated isolation switches in the characterisation mode that was described in Section 4.7 access to the $R_{I\,to\,V}$ resistors was attained without interference from the internal circuits. An Agilent B2902A Precision Source/Measure Unit was used as a 10 nA reference current source and voltage measurement instrument to derive the resistor values. It should also be noted that the measurements converged to a smaller 5% $R_{I\,to\,V}$ tolerance.

6.3.2 Electrochemical Cell

After the integrated circuits were electrically characterised, the integrated potentiostats were verified to work with a microelectrode array in an electrochemical environment. An encapsulated 4 x 4 WE test sample was prepared as described in Chapter 5 and was used as a microelectrode array to characterise the electrochemical response of the integrated potentiostat against results from a commercial potentiostat. The structure exactly mimicked the one used in the electrochemical cells of the ECM. A well-documented reference analyte was used to verify the operation of the ECM to work as a platform that can govern and record redox reactions. As it was explained in Section 2.4 the ferrocene/ferrocenium couple is an organometallic compound that has been used extensively as a reference substrate with many applications in electroanalytical chemistry. It was used for the characterisation and experimental procedures of this chapter as it exhibits reversible behaviour and distinctive redox current peaks. The oxidation of ferrocene to ferrocenium is described by:

$$Fe\left(C_5H_5\right)_2 \rightleftarrows Fe\left(C_5H_5\right)_2^{+} + e^{-} \tag{6.2}$$

The half-wave potential against a Ag^{+}/AgCl reference electrode in acetonitrile is $E_{1/2}$ = 415 mV [201]. The used chemical solutions were prepared with 98% pure ferrocene and acetonitrile (CH_3CN) of 99+% purity, supplied by ACROS Organics and purchased from Fischer Scientific. The supporting electrolyte was 98% pure

Tetrabutylammonium hexafluorophosphate ($TBAPF_6$) from Sigma Aldrich that was used to enhance the chemical solution conductivity.

The on-chip potentiostat was accessed by using the internal circuits test mode as in the previous section. A simpler version of the analogue acquisition and analysis programs was used for these experiments as only one WE was connected to the potentiostats. A digital smoothing filter was used to supress any noise in the acquired results. A Ag wire that was prepared as a $Ag^+/AgCl$ quasi reference electrode as it was described in Section 5.8 was used externally for the experiments with the test sample. Measurements with the on-chip potentiostat were first conducted, followed by consecutive measurements with the same concentration by the commercial potentiostat mentioned in Section 6.2.1. CV measurements were taken with chemical solutions containing ferrocene at concentrations of 1 mM, 3 mM, 5 mM and 10 mM in acetonitrile with 100 mM $TBAPF_6$. The same configuration was set in both devices to conduct CV, a $\upsilon = 2$ V/s scan rate in a −2 V to 2 V potential window was used. The large potential window was selected to assess the capability of the integrated fully differential potentiostat to operate in potentials greater than the 3.3 V power supply voltage of the CMOS ASIC. The results from the two devices are shown in Figure 6.8. Each time a measurement was completed the test sample was rinsed and cleaned with acetone and isopropanol and dried with a N_2 gun. Measurements carried out with the same microelectrode sample ensured a one-to-one comparison of the acquired results. All the results from both devices demonstrated half-peak potentials $E_{p/2} \approx 400$ mV, which is close to ferrocene's

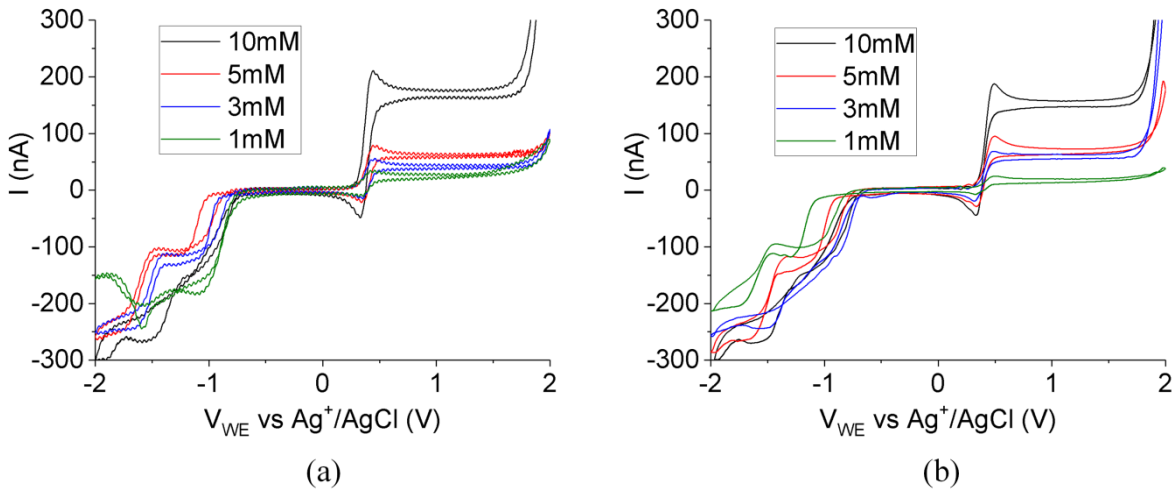

Figure 6.8: Cyclic voltammograms obtained from the test microelectrode samples with (a) the commercial and (b) the on-chip CMOS potentiostat [170].

$E_{1/2}$, an anticipated behaviour. Peaks which are observed close to the limits of the potential window are a consequence of the oxidation and reduction reaction of the solvent and the supporting electrolyte, as background measurements of the chemical solution without ferrocene suggest. In conclusion the results from both devices were almost identical, indicating that the CMOS potentiostat was eligible to be used with the post-processed integrated microelectrodes. The operation of the ECM with the analogue readout is reviewed in the next section.

6.3.3 Microarray Analogue Readout

Having the integrated circuits verified to operate in an electrochemical cell, the next step was to perform measurements using the on-chip microelectrodes post-processed on the CMOS chip and the array of the integrated potentiostats. Measurements were conducted using the described hardware and software setup that was presented in Section 6.2. CV was not a method compatible for WE multiplexing over the course of the measurement as it was described in Section

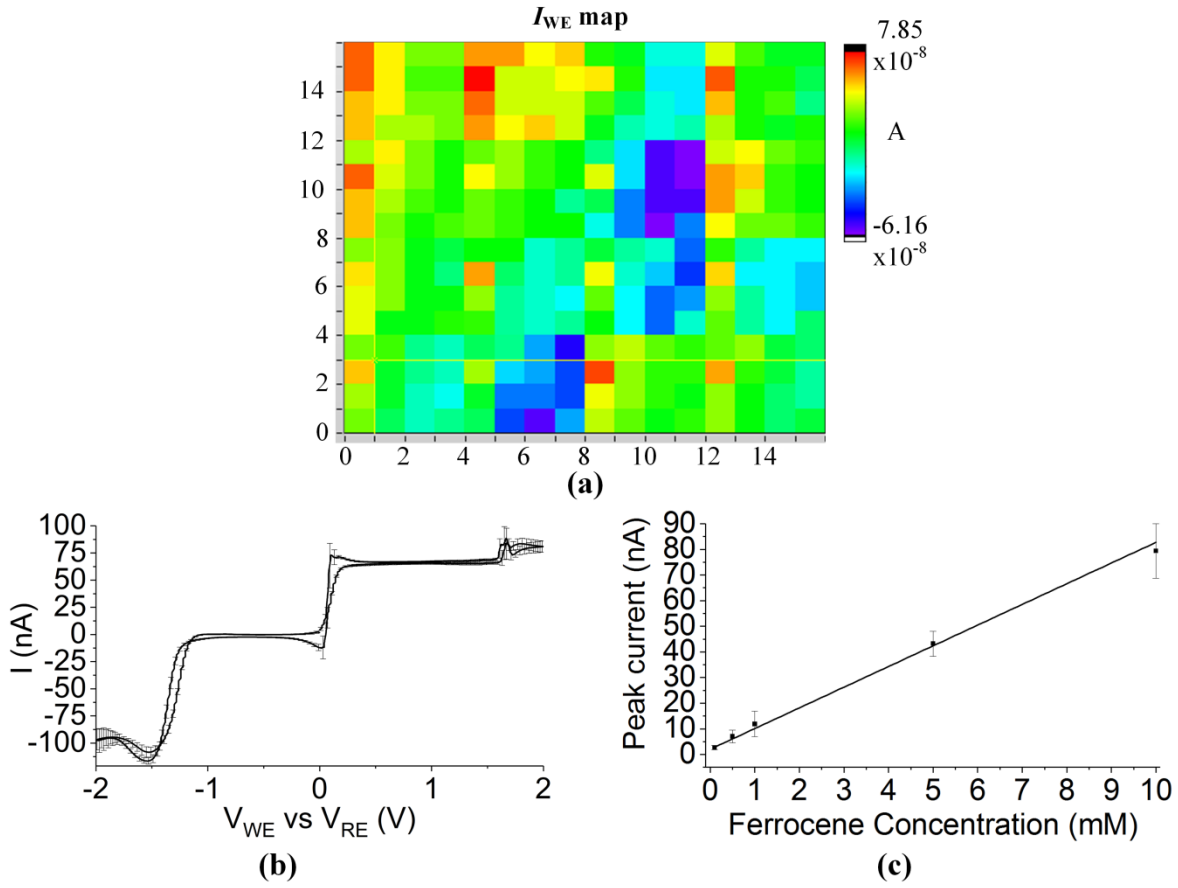

Figure 6.9: Results from the ECM's integrated microelectrodes. (a) WE current map at the oxidiation peak for a 5 mM ferrocene chemical sample and (b) its respective averaged voltammogram. (c) A concentration-averaged peak current plot for several ferrocene concentrations [170].

4.5.3. Therefore staircase voltammetry with a reverse potential scan step was used instead (staircase cyclic voltammetry). The method is comprised of segmented voltage levels with small increments arranged in a waveform that follows the potential scan of CV. WEs from each cell were multiplexed over each voltage level sequentially before its value was changed. After signal processing, the experimental procedure led to 256 simultaneous independent voltammograms that observed the ionic activity over the array at approximately the same time within a very small interval. These measurements were performed at $\upsilon = 2$ V/s, using the same differential input signal on all the independently controlled electrochemical cells with a 10 ms duration per voltage level. The solution exhibited a uniform distribution of the electroactive analyte concentration to its bulk concentration value. This was ensured as the liquid was not disturbed by stirring or shaking. It was also ensured by the use of a supporting electrolyte (TBAPF6) to a much higher concentration than the analyte. Therefore effects of convection and migration can be neglected. Hence, in these experiments the ECM acted as a uniform platform that measured the same reaction. The same chemical solution composition was analysed with ferrocene concentrations varying from 100 μM to 10 mM. The coloured current map at the oxidation peak current for a 5 mM ferrocene solution is shown in Figure 6.9(a). The function to obtain the mean value of all the WEs was used to diminish WE interference and the resulting voltammogram is shown in Figure 6.9(b), taken after 2-3 pre-concentration cycles. As it was explained in the fabrication procedure, in Section 5.5.1, the on-chip REs were covered with Au. The measurement was repeated for other concentrations. The Au on the REs performed as a quasi-reference electrode and this is the reason why the half-peak potential is observed shifted at $E_{p/2} = 75$ mV. The absolute values of the anodic and cathodic peak currents were averaged for each measurement and a linear fit of the concentration-peak current response was extracted, as shown in Figure 6.9(c).

Moreover, measurements with the same experimental procedure were used to measure the quiescent power dissipation. Using the potentiostats to control a real electrochemical environment provided a measure of the actual power dissipation. It was measured at 42.9 mW when a 0 V dc differential potential was connected to the input, while at a high scan rate $\upsilon = 8$ V/s staircase

voltammetry and a ferrocene at the highest detectable limit it was 125.4 mW. The recorded power consumption is considered to originate not only from the power requirements of the integrated circuits but also from the composition of the chemical sample and potential differences among CEs belonging to separate electrochemical cells. Hence, the power dissipation of the ECM is a trade-off to its electrochemical cell isolation feature. The dissipated power values could potentially lead to an elevated temperature in the chemical solution. Such a phenomenon would induce evaporation of the volatile acetonitrile solvent as well as change the diffusion coefficients of the ferrocene/ferrocenium pair due to temperature dependant ion-pairing [202]. However, the temperature of the chemical solution and the chip packaging remained stable before and during the electrochemical experiments, as measurements with an FLIR camera indicated. The temperature stability owed to the careful powerline layout design of the CMOS chip, the use of the heat dissipating ceramic PGA packaging and the heat conductive epoxy as well as the short time periods of tens of seconds each electrochemical experiment required.

6.3.4 Cross-talk

The first measurements that were conducted on the on-chip microelectrodes of the ECM ASIC, presented in the previous section, configured the potentiostats to operate all the electrochemical cells as a uniform platform. As it was mentioned in Section 3.5 cross-talk in MEAs that operate in this manner can be observed as chemical cross-talk by overlapping WE diffusion and electrical cross-talk by the wiring and circuits as well as through a conductive path in the chemical solution. However, the ECM's purpose is to make its electrochemical cells to operate independently with different potential settings. Such measurements in the same chemical solution could potentially lead to increased values of cross-talk compared to regular MEAs, thus a new method was used to characterise the electrochemical cross-talk.

An experiment was devised to characterise the electrochemical cross-talk as a figure of merit (FOM) that included both electrical and chemical aspects. The procedure that was followed with experimental measurements and an algorithm of the program that was created in Matlab (provided in Appendix C.2) are presented in Figure 6.10. The ECM microfluidic package was filled with a

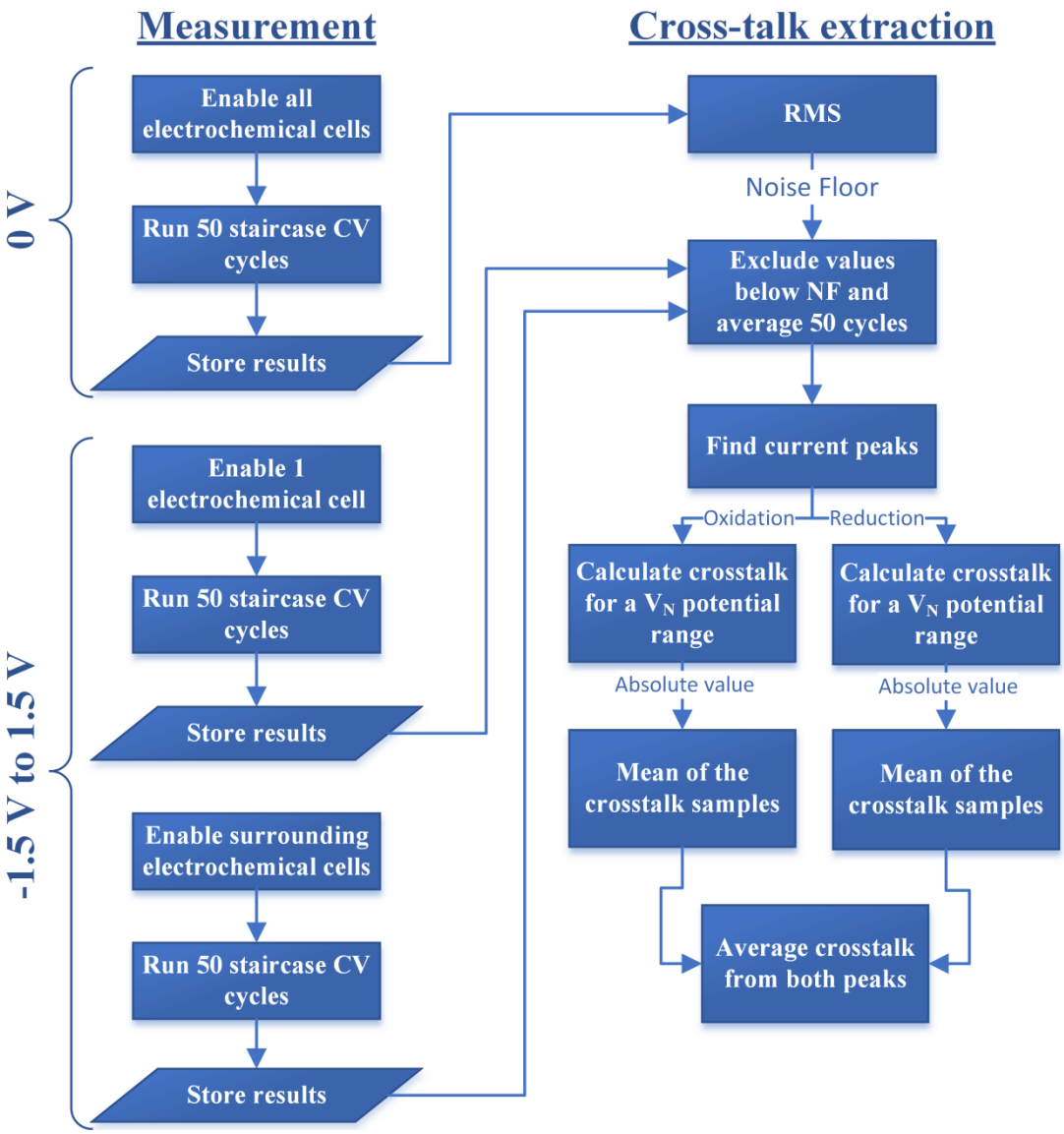

Figure 6.10: Flowchart that describes the measurement procedure and a program created in Matlab to extract the electrochemical cross-talk of the ECM.

chemical solution of the aforementioned composition with 5 mM ferrocene. The first measurement was conducted to determine the noise floor of the device. The potential difference between the WE and the RE was set at 0 V, and any signal that was recorded by the WEs of the array for the duration of 200 s was used for the calculation of the noise floor according to $NF = \overline{rms(I_{cell\_noise}(i))} = 1.0$ nA, where i is a number assigned to distinguish electrochemical cells and $I_{cell\_noise}(i)$ is an already averaged current measurement of cell's WEs acquired by the built-in function of the analogue analysis program. Two further measurements were conducted to obtain the data for the cross-talk calculation. In the first one, the central cell shown in Figure 6.11 (a) was activated with a $\upsilon = 2$ V/s for a −1.5 V to 1.5 V potential window for 50 cycles. An averaged voltammogram for this 50-cycle measurement can be seen in Figure

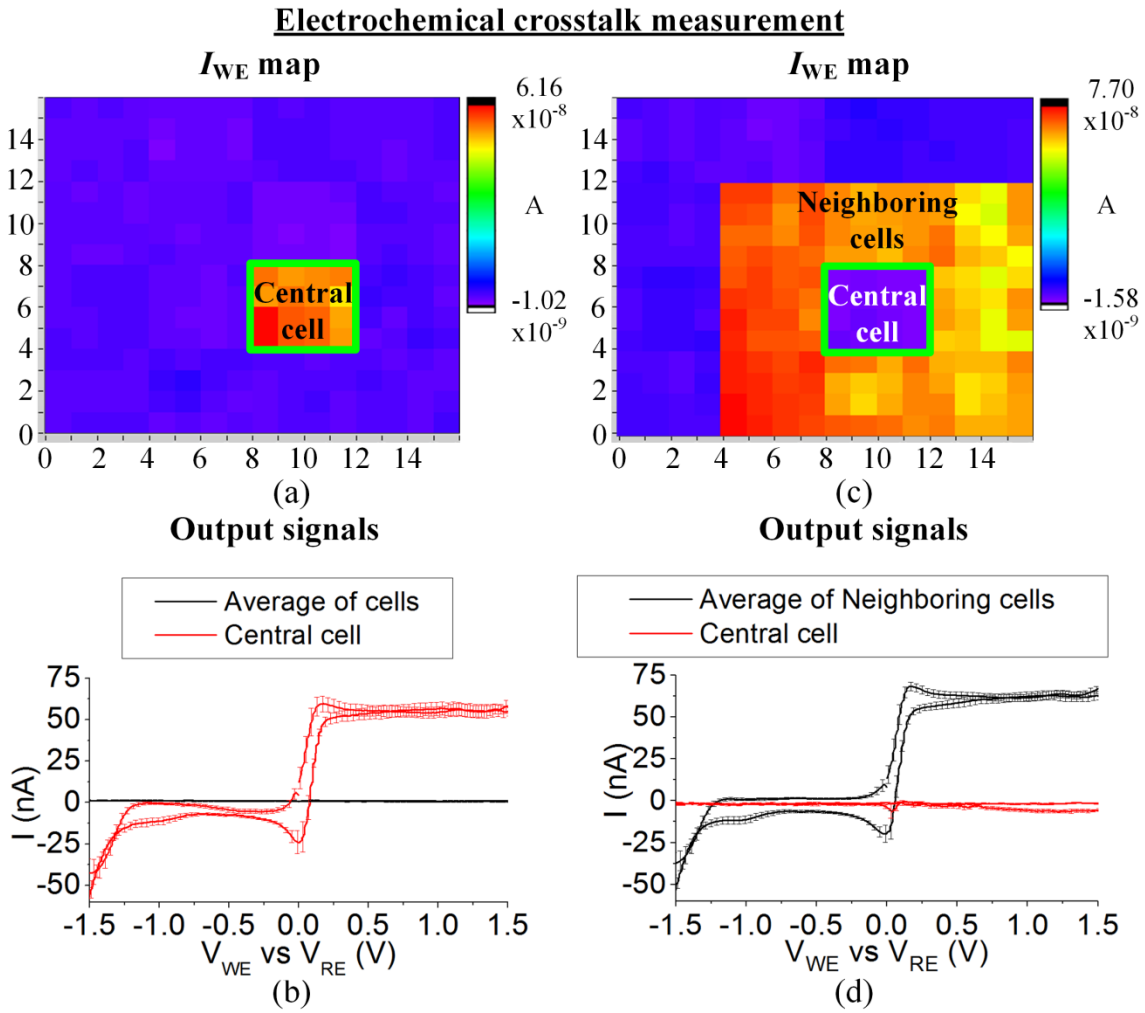

Figure 6.11: Current map at the oxidation peak current of the array's WEs and (b) its respective averaged voltammogram for the 50 cycles of the measurements where the central cell (indicated by a green box) was activated. (c) The WE current map and (d) its respective averaged voltammogram for the 50 cycles of the measurements where the central cell was deactivated [170].

6.11 (b), where the central cell's current magnitude is similar to the one shown in Figure 6.9(b), while the other electrochemical cells recorded current was negligible. A complementary measurement where the central cell is deactivated but the voltammetric method was applied to its neighbouring cells was then recorded, as shown in Figure 6.11(c). The respective voltammogram illustrates a small current being sensed by the central cell's WEs, as shown in Figure 6.11(d). The averaged WE current of the central cell from both measurements was used to calculate the cell-to-cell electrochemical cross-talk, using results obtained by the same transducers. The function that describes the cross-talk calculation as presented in the flowchart of Figure 6.10 is:

$$\text{cross-talk} = \frac{\sum_{V_n = V_{peak}}^{V_N} \left| \frac{\overline{I_{central\_in}}(V_n - V_N/2)}{\overline{I_{central\_ac}}(V_n - V_N/2)} \right|}{N} \quad (6.3)$$

where V_{peak} is the potential at which a current peak is observed, V_N is a range of potential samples around the peak, N is the number of samples, $\overline{I_{central\_ac}}$ and $\overline{I_{central\_in}}$ are averages of WE current results for the 50-cycle measurements of the activated and deactivated central cell respectively. Values of the measurements below the noise floor were excluded. The cross-talk calculation was performed around the current peaks using V_N = 100 mV. The reason was that the current recorded by the deactivated central cell exhibited a maximum around these potentials. The resulting electrochemical cross-talk was calculated at 12%.

Although chemical and electrical cross-talk have been reported in previous studies [71], [124], [139], [159], [161], a measure of an acceptable level for the correct representation of signals has not been investigated yet. The results of a voltammogram are mainly significant in the region around the peaks, where the cross-talk was mostly observed. However, the cross-talk's 12% value cannot substantially alter the shape of a voltammogram to become indistinguishable from its former state. Moreover, a change of this ratio would not be important for the estimation of the chemical solution's concentration, using the plot of Figure 6.9(c), since such small variations may already exist between different sweeps of voltammetry. It is clear from Figure 6.11(a) and (c) that current is sensed to the respective electrochemical cells that were selected in each case, this result is regarded to the circuit and microelectrode structure designs. Even though the cross-talk value that was attained in this study might be adequate for the independent recording of signals, further efforts to minimise this figure must be pursued in the future.

The measured data used for the noise floor calculation was also used for the calculation of other FOMs. The limit of detection (LOD) for the device, expressed in current was:

$$\text{LOD} = \mu_{I_{cell\_noise}} \pm 3.3 \times SD_{I_{cell\_noise}} = 0.9 \pm 0.5 \text{ nA} \quad (6.4)$$

From that value only 8% could be regarded as thermal noise of the $R_{I\,to\,V}$ resistors. The fairly high values of the noise floor and the LOD are regarded to the PXIe system that records the output potentials of the $R_{I\,to\,V}$ resistors with a 291 μV accuracy [203]. Using the noise floor data and the data used to find I_{max} in Section 6.3.1 the signal-to-noise ratio and the dynamic range were calculated as SNR = 83 dB and DR = 75.6 dB.

6.3.5 Comparison to the State-of-the-art

The figures of merit representing the chip's performance obtained over the previous sections were all summarised and compared to the-state-of-the art in Table 6.1. The ECM system was designed with numerous electrochemical cells which can be independently controlled. A CMOS ASIC that was found in the literature was also comprised of a relatively large number of potentiostats [66]. However, that chip demonstrated a two-electrode system by the use of current conveyors which cannot regulate the potential on the microelectrodes as efficiently as a potentiostat in a three-electrode system. Moreover, a configuration with independent potentials was not presented on the 2-electrode current conveyors.

Furthermore, the CMOS ASIC described in this thesis used fully differential potentiostats that demonstrated independent regulation of the electrochemical cell's potential, as it was presented through simulations and experimental results in previous sections. Another advantage of this design was a large V_{WE} vs V_{RE} voltage swing of 5.2 V_{pp}, meaning the range of the potential windows that can be scanned. While the power dissipation recorded in the ECM system was increased compared to other chips, it was necessary for the operation of circuits that were responsible for the recorded bandwidth (which was far greater than the state-of-the-art CMOS MEAs). The wider bandwidth facilitates the use of voltammetric methods at higher scan rates such as FSCV.

As it was shown in the previous chapter the CMOS ASIC can successfully be electroplated with the functionalisation switches. In the case of individual functionalisation of WEs being required, it would be better conducted by the chip's integrated circuits. The large maximum detectable current (I_{max}) assists in monitoring such individual functionalisation processes as well as enabled high

	JSSC-08 [52]	**JMM-11** [44]	**Anal. Chem.-14** [79]	**TBioCAS-13** [66]	**This work**
Electrochemical system type	3-electrode SE[a]	3-electrode SE[a]	3-electrode SE[a]	2-electrode SE[a]	3-electrode FD[a]
Technology	0.25 µm	0.6 µm	0.35 µm	0.35 µm	0.35 µm
Power Supply Voltage	2.5 V	5 V	3.3 V	3.3 V	3.3 V
Die Size	5 x 3 mm^2	6.5 x 3 mm^2	7.5 x 4.8 mm^2	3.8 x 3.1 mm^2	3.79 x 3.79 mm^2
Chip Sensing Area	Not Available	~3 × 3 mm^2	3.2 × 3.2 mm^2	3.15 × 1.9 mm^2	1.81 × 1.81 mm^2
WE size	70 × 70 μm^2 to 100 × 100 μm^2	ø 10 -100 μm^2	ø 25 μm^2 and ø 5 μm^2-50 μm^2	100 µm long bumps	20 × 20 μm^2
WE pitch	Not Available	100 µm	100 µm	200 µm	114 µm
Number of WEs	4 × 4 (16)	24 × 24 (576)	32 × 32 (1024)	16 × 12 (192)	16 × 16 (256)
WEs per readout Channel	1	24	16	1	16
Number of Potentiostats	4	1 (external)	1 (bipotentiostat)	192 (current conveyor)	16
Number of independent E-cells	1	1	1	4 × 24[b]	16
I_{max}	150 nA	5 µA	2 µA or 10 µA	350 nA	13 µA
Limit of Detection (LOD)	550 pA_{rms}	500 pA	100 pA or 1 nA	24 pA	1.4 nA
Readout SNR | Noise Floor	~55 dB @ 40 nA | Not Available	Not Available	73.6 dB @ 1 µA / channel | 540 fA_{rms} to 250 pA_{rms}	70.2 dB @ 300 nA / channel | Not Available	83 dB @ 13 µA / channel | 1.0 nA_{rms}
Cross-talk	Not Available	Not Available	Not Available	Not Available	12 %
Voltage Swing (V_{WE} vs V_{RE})	1.25 V_{pp} (used)	4 V_{pp}	2.8 V_{pp}	2 V_{pp} (simulated)	5.2 V_{pp}
Slew Rate	Not Available	Not Available	0.35 V/µs	13 V/µs	1.09 V/µs
Bandwidth	10 kHz	4 kHz	up to 1 kHz	1 kHz	150 kHz
Max. Sampling Rate	2.5 kS/s/channel	Not Available	1.4 MS/s/channel	1 kS/s	1.25 MS/s/channel
Max. Power dissipation	Not Available	25 ± 5 mW	Not Available	188 µW/channel (36 mW)	125.4 mW

[a]SE stands for single-ended potentiostat and FD stands for fully differential potentiostat.[b]A WE potential setting per 24 current conveyors.

Table 6.1: Comparison table of CMOS amperometric MEA systems [170].

analyte concentration detection at the WEs. Due to this capability the SNR was increased. On the contrary the LOD of the system's analogue output had an increased value compared to the state-of-the-art. However, the LOD of the ECM is adequate to detect ferrocene used as a label in genotyping applications. The "target" oligonucleotide binds and places ferrocene close to the Au WE surface. If FSCV is used, the resulting current peak can be estimated by:

$$I_{peak} = \frac{n^2 F^2 \upsilon A D}{4RTN_A} \tag{6.5}$$

where n is the valence number, F is Faraday's constant, A is the electrode area, D is the coverage density, R is the gas constant, T is the absolute temperature and N_A is Avogadro's number [52]. A 7.5 nA peak current would be observed for a υ = 400 V/s if ferrocene with at least a $D = 3 \times 10^{12}$ cm^{-2} was used, a value significantly higher than the 1.4 nA LOD. The ECM is also eligible to detect H_2O_2 as it was indicated by results from a similar setup with microelectrodes at approximately the same size as the ECM [79]. H_2O_2 is a detectable electroactive by-product of many enzymatic reactions (oxidases) and from measurements of those microelectrodes with glucose it was indicated that if the ECM's WEs are prepared in the same manner they could detect glucose in its physiological range (1.5 mM-50 mM) [204].

One of the most important parameters for the aspects of the ECM that was characterised in this chapter is electrochemical cross-talk. As it was described in Section 6.3.4 it is a new FOM that includes both the electrical and chemical aspects of cross-talk as it was calculated with data from electrochemical measurements. A relevant FOM has not been reported in similar CMOS MEAs. The acquired electrochemical cross-talk value was achieved by several actions taken in the ECM design. The chemical cross-talk within the electrochemical cell was reduced by the WE pitch d = 114 μm ≈ 15.2α, where α is the WE radius (defined by the WE passivation opening size) that approached the proposed $d_{necessary}$ = 24α by the Guo and Linder guidelines that were introduced in Section 3.5.1 [139]. As a reminder, these guidelines were proposed as a measure to prevent the diffusion layers of different WEs to overlap and alter the sigmoidal response of these microelectrodes. Provided that diffusion layers do not overlap,

microelectrodes benefit from high mass transfer that is shown as a sigmoidal response in cyclic voltammetry and properties of the chemical solution may be found by deviations from this response. In this study, the response was very close to a sigmoidal response but further improvements can be performed by a careful selection of the size and distance between microelectrodes. The microelectrode structure that was chosen for the design of the ECM plays a major role on the electrical cross-talk between electrochemical cells. As the simulations of Chapter 3 suggest, the use of the CE rings and the fully-differential potentiostats led to development of isopotential "guarding" regions that protect the sensitive WEs of each cell from leakage currents and protruding neighbouring diffusion layers.

6.3.6 Microarray Digital Readout

Experimental results have been presented using the analogue readout of the CMOS ASIC. As it was described in Sections 4.6 and 6.2.2, the ECM was also prepared with a digital readout method and programs to control it. The readout comprised of an integrating capacitor in a current to frequency (*i* to *F*) converting charge-sensitive amplifier (CSA). The CSA was designed to measure results with electrochemical methods that required both forward and backward potential scans. The input common mode voltage of the amplifier was controlled and the current polarity was sensed with the digital input waveforms to reconfigure the CSA accordingly with the internal circuits, as it was shown in simulation of Section 4.6.

A set of switches disabled the analogue and enabled the digital readout method (Figure 4.16). The CSAs of all the electrochemical cells were controlled with the acquisition program presented in Section 6.2.2 and the recorded output pulse widths represented the current level. To convert the pulse width to current the digital analysis program required the magnitude of the reference current sources used in the discharging cycle (Figure 4.18) as an input variable. To measure the reference current magnitude, the CSA control signals were configured so that the reference current source and sink charged and discharged the capacitor respectively in a cycle. The capacitor's potential output was read with a test output of the chip, and the reference current values were determined. For the

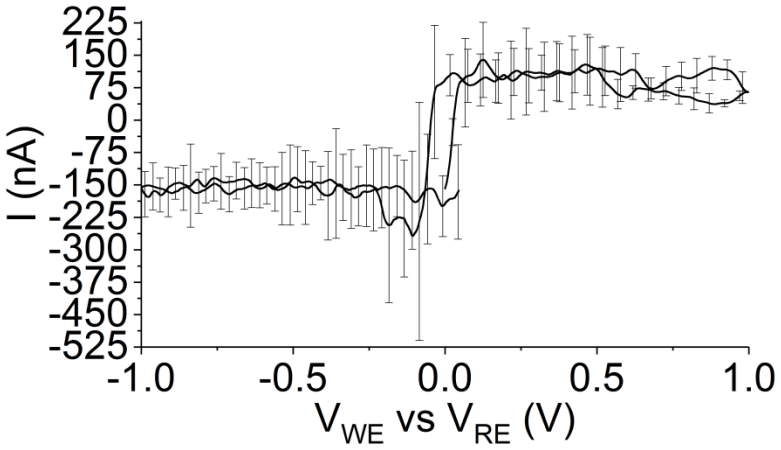

Figure 6.12: Staircase voltammogram acquired with the digital readout.

810 mV biasing potential the reference current source and sink were found to be 129.5 nA and 245.8 nA respectively.

A chemical solution of the aforementioned composition with 5 mM ferrocene was analysed using staircase cyclic voltammetry at 2 V/s in a -1 V to 1 V potential window with a 4.4 ms voltage step duration. The decoder rate was set at 44.8 KHz and the integration and discharging cycles for each WE lasted 4.5 μs and 6.7 μs respectively. The digital analysis program with the averaging function was used and the results are presented in Figure 6.12. As for the analogue readout method, output signals from all 256 WEs of the array were obtained and averaged, the error bars represent the standard deviation of this averaged voltammogram. The digital design of the fabricated chip had a shortcoming, even though the current polarity was sensed by the internal circuits of the CSA it was not connected to an output port. To circumvent this problem and represent polarity in the plot the current values sign was changed according to the control signals sign. However, this method is an approximate representation of current polarity. Therefore, an additional functionality for the polarity of the current needs to be added in a future version of the chip. Due to this uncertainty in the accuracy of the plotted results using the digital readout, the analogue outputs were used for all the subsequent results. A limited amount of data was obtained using the digital readout to extract conclusions about the method's efficiency. Nevertheless, the voltammogram of Figure 6.12 demonstrated a rather increased standard deviation probably from charge injection while switching CSA. Observations suggests a possible need for a correlated double sampling (CDS) circuit to be included in a future iteration of the CMOS chip, as it was presented in Section 2.5.1, to eliminate this noise source.

6.4 Methods Multiplexing

In the previous sections the ECM ASIC was characterised electrically and electrochemically with its FOMs compared to prior work. It was proven that the system can function as an electroanalytical platform of microelectrodes and produce individual voltammograms with a 12% electrochemical cross-talk. As long as the diffusion layer length is smaller than the WE pitch the WE current measurements from their respective electrochemical cells can be considered as independent. Any set of electrochemical methods can be conducted independently and simultaneously in one-pot to separate electrochemical cells to produce results not possible with existing systems. A demonstration of possible experiments that can be conducted with the ECM and illustrate its capabilities with the achieved electrochemical cross-talk are presented over the next sections.

6.4.1 Multiplexed Cyclic Voltammetry

Making use of the ECM's capability for independent voltage control with a low leakage current, a novel technique was developed that uses parallelisation to record voltammograms quicker than their scan rates normally allow. The technique is named multiplexed cyclic voltammetry and it records voltammetric data with a faster equivalent scan rate υ_{eq}.

A conceptual representation that depicts the electrochemical cells with their respective potentiostats controlled at a different $V_{controlled} = V_{WE}$ vs V_{RE} is presented in Figure 6.13(a). For the multiplexed cyclic voltammetry technique the differential input waveform function of CV was split into sections that were resolved over all the electrochemical cells of the ECM, as shown in Figure 6.13(b). Each electrochemical cell was responsible to produce only a section of a voltammogram. In order to maintain mass transfer on the WEs as in normal CV, for every new cycle the waveform function sections were recycled successively over the electrochemical cells. The aforementioned chemical solution with 5 mM of ferrocene was used for analysis, the scan rate was set at $\upsilon = 2$ V/s in a −2 V to 2 V potential window. After some pre-concentration cycles, the WE current map was acquired at the beginning of the first cycle, as shown in Figure 6.13(c). The respective current outputs, averaged for the WEs of each cell with

the analysis program are shown in Figure 6.13(d), the voltammogram was essentially multiplexed at this point. The results represent the response of the electrochemical cells to analyse the chemical solution with different potential settings, a behaviour achieved with the ECM system's architecture. The analogue data analysis program was modified with a step in the results representation section that reconstructs the voltammogram from the independent outputs. The reconstructed voltammograms from the demultiplexed outputs of the array is

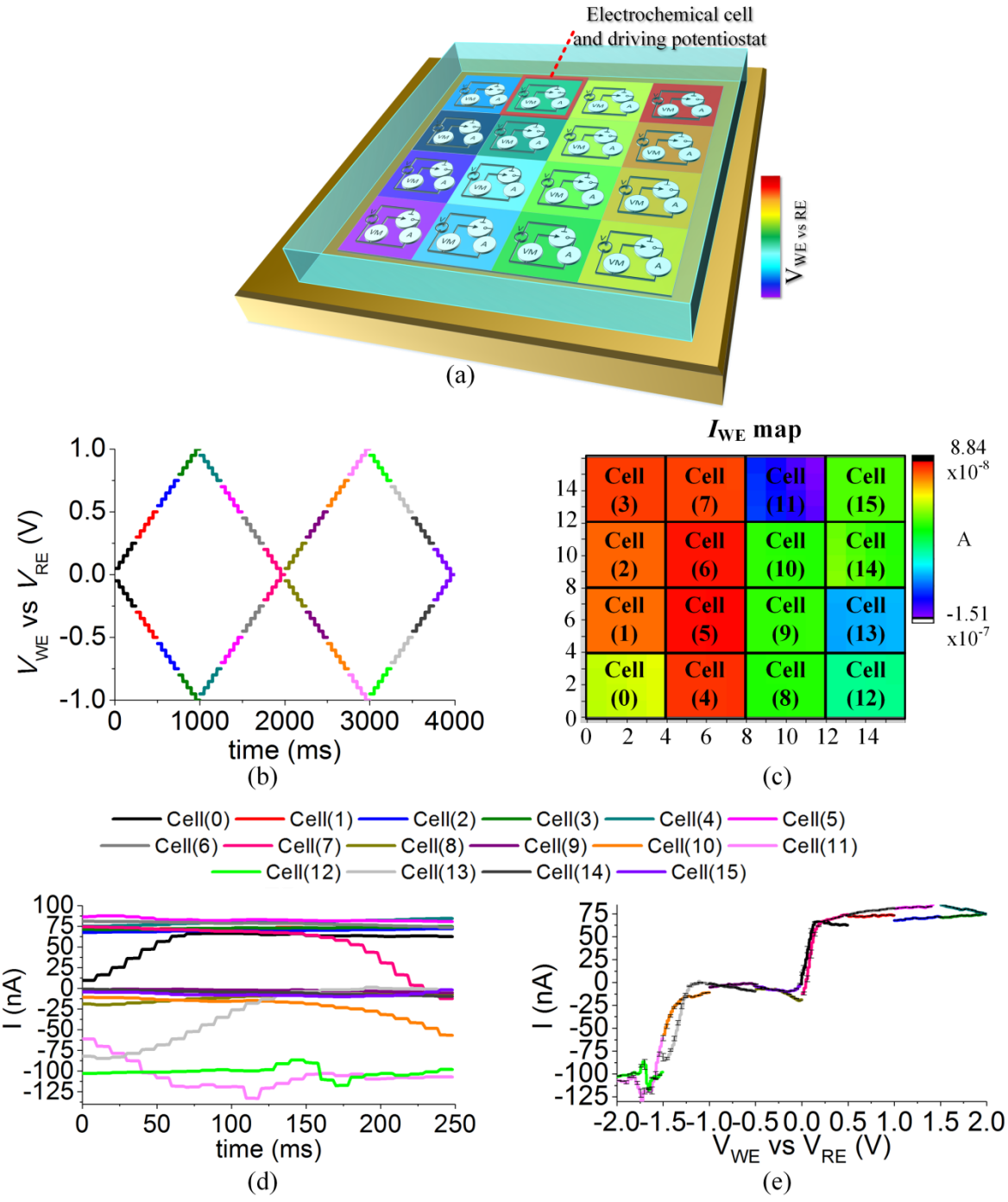

Figure 6.13: (a) Conceptual representation of the ECM configured for multiplexed cyclic voltammetry. (b) $V_{controlled}$ differential input signals of all the cells. (c) WE current map of the electrochemical cells for the multiplexed CV measurement, (d) the respective output signals and (e) their reorganised voltammogram. The plots legends are presented in the middle.

shown in Figure 6.13(e). A slight mismatch can be observed in the reconstructed voltammogram among results from different electrochemical cells. This observation can be regarded to post-processing fabrication variability of the WEs. The results from each electrochemical cell were acquired independently and averaged per each cell's 16 respective WEs. A variability of the size of even one WE can change the magnitude of the averaged voltammogram to cause the observed mismatch. Another justification of the magnitude mismatch can also be the recorded 12% electrochemical cross-talk. Nevertheless, the final reconstructed voltammogram of multiplexed cyclic voltammetry remains a result that can be used competently for electrochemical analysis as the shape, redox peaks and their approximate current magnitude are consistent to Figure 6.9(b) and Figure 6.11(b) and (d).

The scan rate that was applied to each electrochemical cell was $\upsilon_{cell} = \upsilon = 2$ V/s. However, in multiplexed CV the overall acquisition speed is increased and this is measured by an equivalent scan rate according to $\upsilon_{eq} = \upsilon_{cell} \times N_{cells}$, where N_{cells} is the number of electrochemical cells in the array. The recorded voltammogram has a $\upsilon_{eq} = 32$ V/s, which means it was acquired 16 times faster than the scan rate that was applied to the cells $\upsilon_{cell} = 2$ V/s. In a future version of the ECM with more electrochemical cells integrated in the ASIC, the equivalent scan rate could reach the levels used in FSCV. The temporal resolution would be greatly improved for continuous monitoring, while actual low scan rates applied on the microelectrodes ensure a stable diffusion layer and the recording of faradaic currents. The technique can become better than FSCV as in the latter perturbations in the WE potential have been observed and it requires a separate measurement of the background current in order to be removed from the data due to the high scan rates that are used [126], [127].

6.4.2 Voltammetric/Amperometric Methods Multiplexing

A technique that used the ECM's independent cells to improve the acquisition speed of a single electrochemical method was shown in the previous section. In this section the electrochemical cells are organised in columns and each column performs a separate electroanalytical method. The same chemical solution containing 5 mM of ferrocene was used and each method was used to analyse the compound and produce its respective results. Performing multiple

electroanalytical methods in the same fluidic container, results in different analysis representations which when combined with chemometrics can produce new results, as it was explained in Section 2.7.2 (e.g. detect indistinguishable peak currents from different analytes [120]).

The ECM is organised as it is shown in Figure 6.14(a). The first column is configured to run constant potential amperometry, the 2nd staircase cyclic voltammetry, the 3rd differential pulse voltammetry (DPV) and the 4th normal pulse voltammetry (NPV). Functions for each method were introduced in the acquisition program and a slightly modified version of the analogue signal analysis program was developed to sample and represent the current according to the specifications of each method. The mean value of the measurements from WEs of the cells on each column was calculated and plotted for their respective method.

A description of the used electroanalytical methods follows:

6.4.2.1 Constant potential amperometry

Constant potential amperometry is an amperometric technique, simpler than chronoamperometry, which uses a single potential level at a value higher than the anticipated formal potential $E^{0'}$ while the resulting current is measured. In this measurement the potential level was set at 400 mV, experiments presented in the previous sections indicated that the half-peak potential $E_{p/2}$ would appear at a lower magnitude. The resulting *i-t* diagram and an insert of the driving signal are shown in Figure 6.14(b), where a measurement with a 4 mM ferrocene concentration solution was added to show the effect of a change in concentration.

6.4.2.2 Staircase cyclic voltammetry

The staircase cyclic voltammetry method that was described in Section 6.3.3 was used with a scan rate set at υ = 1 V/s. The resulting voltammogram and an insert of the control signal is shown in Figure 6.14(c), where $E_{p/2}$ = 75 mV.

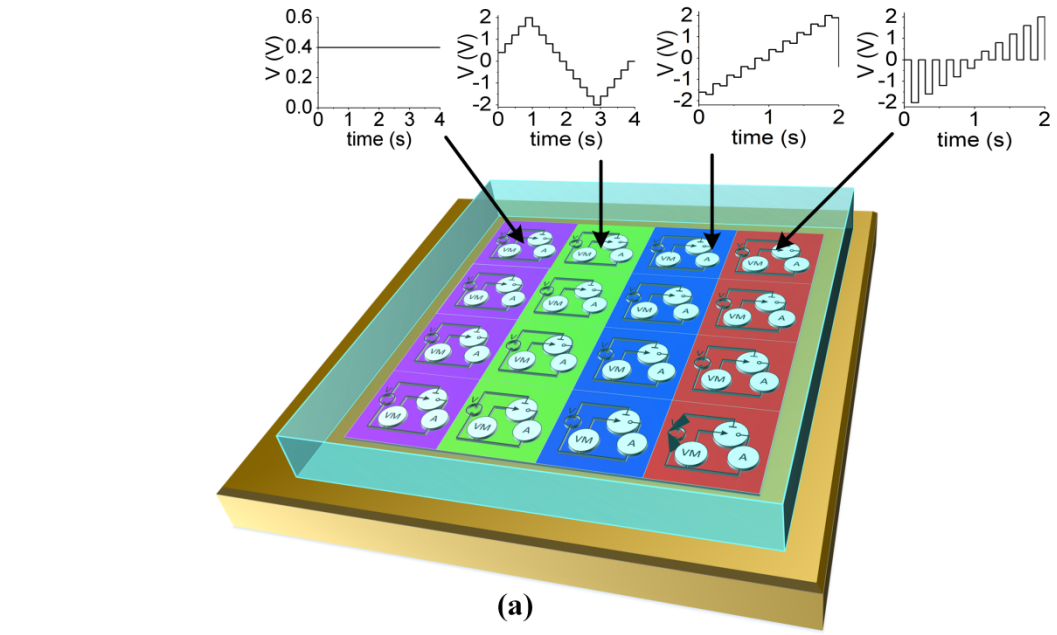

(a)

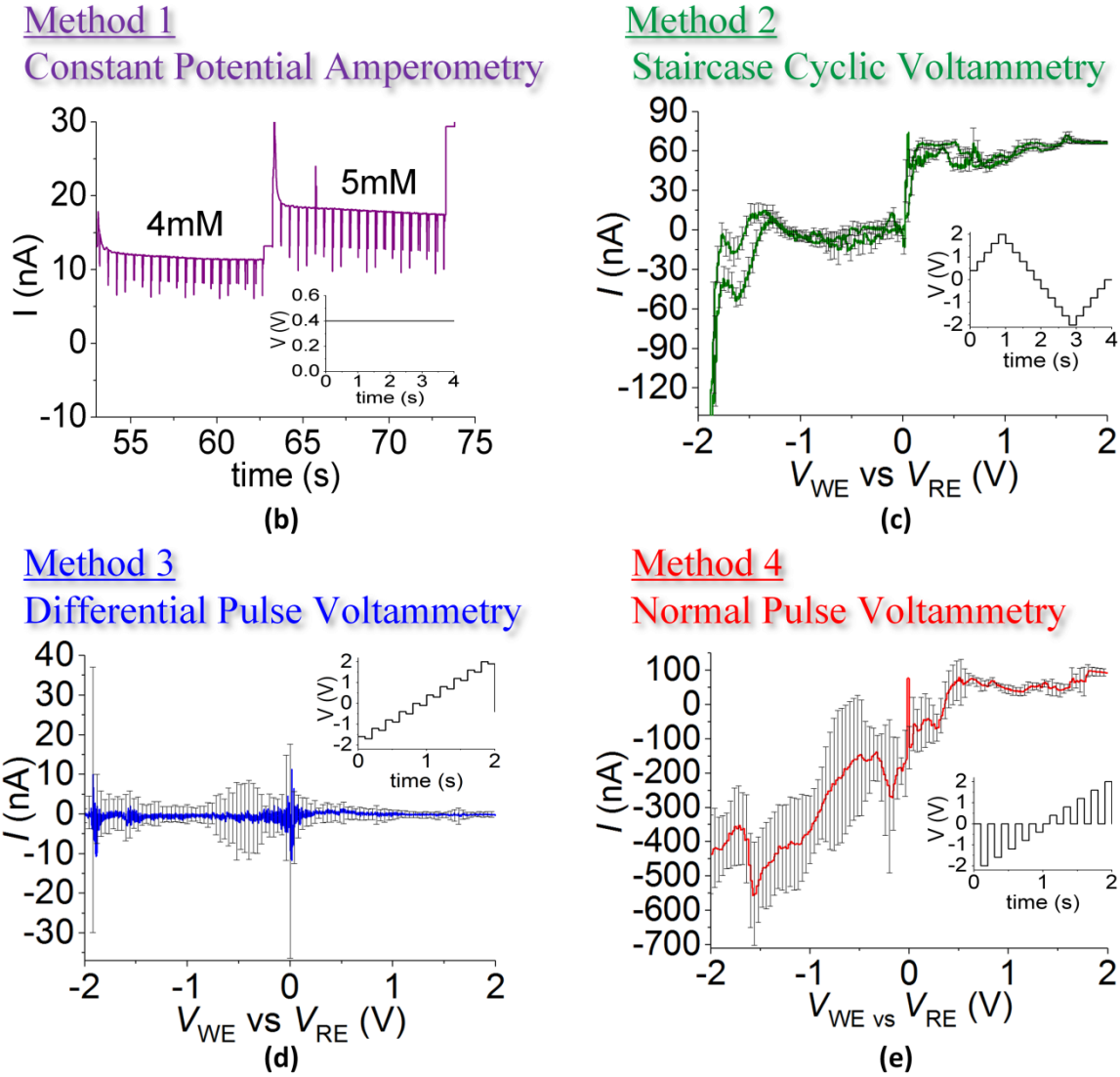

Figure 6.14: Electroanalytical method multiplexing measurement. (a) Conceptual representation of the ECM configured to run multiple electroanalytical methods. Simultaneously acquired results and inserts of the driving signals for (a) constant potential amperometry, (b) Staircase cyclic voltammetry, (c) differential pulse voltammetry and (d) normal pulse voltammetry.

6.4.2.3 Normal pulse voltammetry

NPV is a sampled-current voltammetric method as described in Section 3.4.3. The measurement begins at a base potential set at 0 V where pulses of increasing potential are applied at a set interval interrupted by the base potential, as shown in the insert of Figure 6.14(e). The current is sampled towards the end of the pulse to measure the plateau of Faradaic phenomena and a voltammogram similar to linear scan voltammetry is produced. The settings were selected so that the method results in a $\upsilon = 1$ V/s and each potential increment lasted for 20 ms before the pulse potential was changed. The current response to the NPV pulses arises from the potential step which needs to be applied to each WE. To apply the NPV method on all WEs in the column a 500 ns pulse was repeated 16 times at each voltage level. The voltammogram from the averaged WE measurement is shown in Figure 6.14(e). The peak potential is observed at $E_p = 40$ mV which is very close to the one obtained from staircase voltammetry. The NPV method is used in applications where small concentrations need to be analysed as the pulses lead to higher mass transport [31].

6.4.2.4 Differential pulse voltammetry

DPV is a sampled-current voltammetric method similar to NPV with some differences in the base potential and the sampled current. The base potential is increased in a staircase linear sweep manner with a step height ΔE_s equal to the voltage increment of the pulses, so that a constant voltage change height ΔE is maintained between them, as shown in the insert of Figure 6.14(d). The current is sampled just before each pulse application (i_1) and at the end of the pulse (i_2). The recorded current is a differential measurement of the two currents according to $\Delta i = i_2 - i_1$, where the method takes its name from. The resulting voltammogram is a function of Δi against the base potential. The nature of the differential measurement produces a result that excludes non-Faradaic charging currents and the voltammogram appears as a peaked output at the peak potential. In measurements with the ECM $\Delta E = 100$ mV, $\Delta E_s = 2$ mV and $\upsilon = 1$ V/s. The same 20 ms potential increment duration and 500 ns pulse width as in the NPV was used. The resulting averaged measurement from all the WEs of the column is shown in Figure 6.14(d). The peak potential is observed at $E_p = 20$ mV,

in accordance to the other methods. The reduced contribution by the charging current assists DPV to present results from Faradaic processes with enhanced sensitivity.

The results of Figure 6.14 indicate that different electroanalytical methods can be performed concurrently in the same chemical sample media without a major influence by cross-talk among the electrochemical cells. The chemical composition can be determined by the use of different electrochemical techniques. Their analytical power could potentially be enhanced if they were combined by the use of multivariate analysis, as it was explained in Section 2.7.2. The ECM could become a platform capable of detecting unknown chemical compositions otherwise undetectable by each of the electrochemical methods alone.

6.5 Multiple Analyte Multiplexing

In the previous section the eligibility of the independent electrochemical cells of the ECM to perform different electroanalytical methods simultaneously was proven with one analyte. The electroanalytical methods were rearranged in this measurement to measure the concentrations of two different analytes in the same solution. This experimental technique offers the advantage of parallel sensing, important for continuous monitoring applications [80]. The aim of this measurement is to prove that more than one analytes can be sensed simultaneously, aiming at an automatic identification and detection of the available analytes.

The procedure to automatically configure the electrochemical cells of the ASIC would commence with a staircase cyclic voltammogram for a large potential window to identify the current peaks, corresponding to available analytes in the chemical solution. The next step would be to adjust the ECM settings so that the analytes are detected with a multitude of methods on specific electrochemical cells.

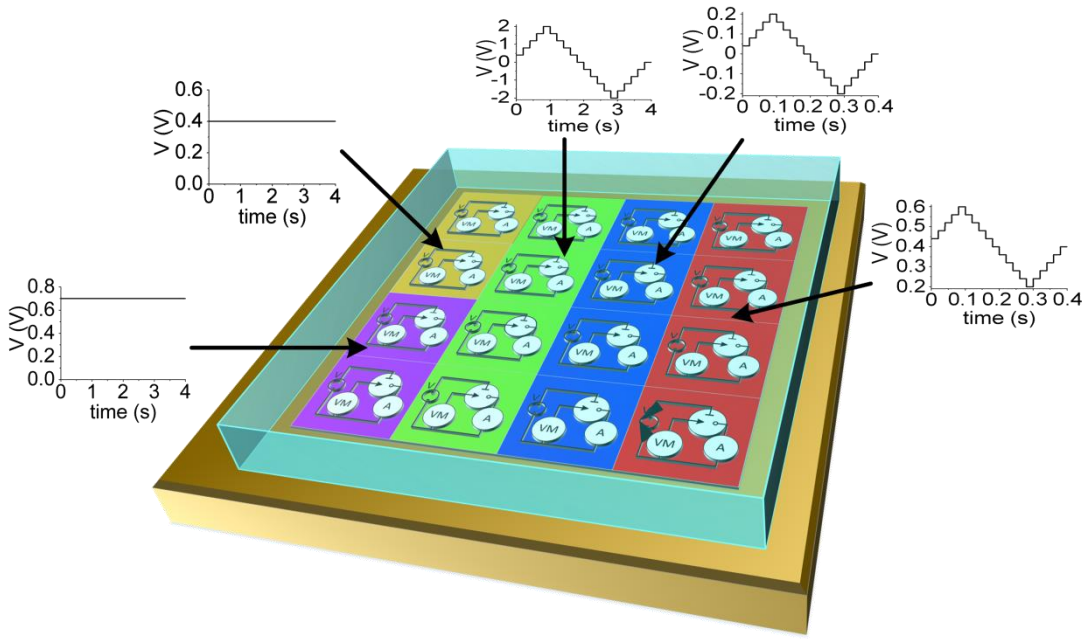

Figure 6.15: Conceptual representation of the ECM electrochemical cells configured to run electroanalytical methods aimed at specific analysis of the chemical species of interest.

In this measurement the steps for the identification and detection were all run manually and simultaneously, as it is shown in Figure 6.15. One column was selected to run staircase CV with υ = 2 V/s in a -2 V to 2 V potential window. Having 1 mM of ferrocene, 1 mM of decamethylferrocene (DmFc) and 100 mM $TBAPF_6$ in acetonitrile, two current peaks were detected, as shown in Figure 6.16(a). Although Au pseudo-REs were used in these measurements, the half-peak potential of Fc^0 was observed higher than in the experimental results of Section 6.3.3, possibly due to a change in electrode kinetics by the introduction of DmFc.

Columns of electrochemical cells were configured to perform staircase cyclic voltammetry at potential windows specific for each analyte. As it was identified from Figure 6.16(a) and the literature, the formal potential of DmFc is approximately 0 V vs Ag^+/AgCl [205], thus a -0.2 V to 0.2 V at potential window with υ = 2 V/s was used in a column of electrochemical cells. The averaged result is shown in Figure 6.16(b), where $E_{p/2}$ = 15 mV. For the detection of Fc^0 a potential window from 0.2 V to 0.6 V was used and the result shown in Figure 6.16(c), exhibited that $E_{p/2}$ = 450 mV. The small potential windows had a 400 ms cycle which assists for the fast detection of analyte concentration changes in continuous monitoring.

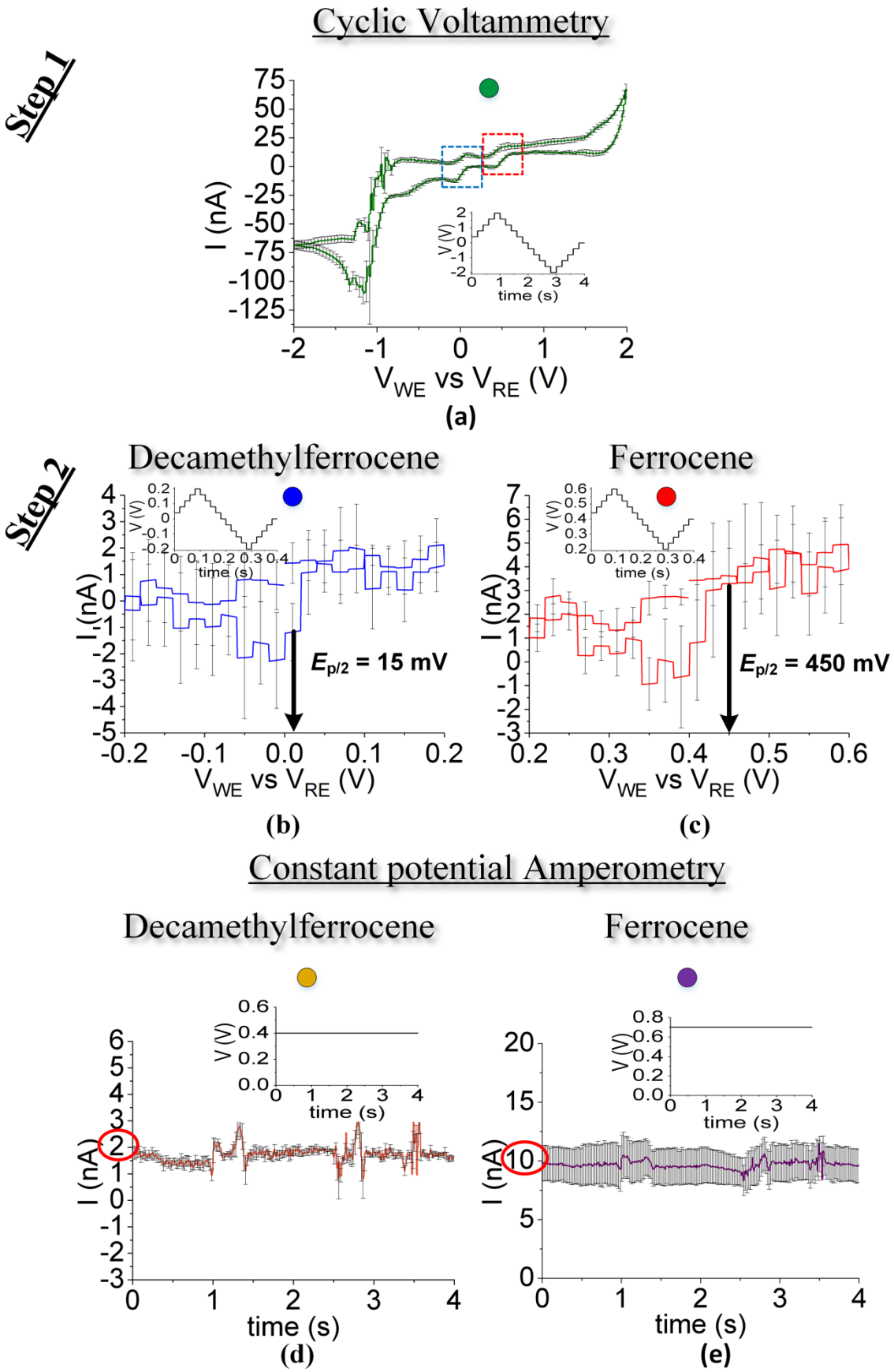

Figure 6.16: Averaged measurements simultaneously performed on the ECM and insets of their respective controlled potentials. (a) Voltammograms of staircase cyclic voltammetry in (a) a large potential window and smaller potential windows arround (b) $E^{0'}_{DmFc}$ and (c) $E^{0'}_{Fc}$. Constant potential amperometry *i-t* diagrams that sensed (d) DmFc and (e) Fc.

Other electrochemical cells were configured for constant potential amperometry at potentials targeted to measure the oxidation current of each analyte. Groups of two electrochemical cells were set at 400 mV and 800 mV to oxidise DmFc and Fc^0 respectively, the averaged result from the WEs of both cells is shown in Figure 6.16(d) and (e). For the 1 mM of DmFc the measured current was 2 nA, while for the 1 mM of Fc^0 it was 10 nA due to the smaller diffusion coefficient of DmFc and a contribution from the latter to the current observed with the 800 mV setting.

The results indicate that the ECM can function as a platform for the simultaneous continuous monitoring of analytes. If a peak detection algorithm is included in software with automated functions the procedure could be run for any set of distinguishable analyte current peaks.

6.6 Summary

In this chapter, the encapsulated CMOS ASIC devices were used as an ECM by their incorporation into a hardware system and the use of dedicated software. The hardware setup with the PXIe system offered increased acquisition speed capabilities and a set of functions to control it directly from Labview. Programs were developed in Labview for data acquisition and signal analysis with some variations for some of the techniques presented in the chapter. The CMOS chip was characterised electrically and electrochemically and after a validation of its operation against a commercial potentiostat its recorded FOMs were compared with the State-of-the-Art. The advantages of the ECM system include multiple independent electrochemical cells, a wide bandwidth, a large potential window range, a large maximum detectable current and a 12% electrochemical cross-talk between electrochemical cells that has not been reported before with CMOS MEA systems.

The ECM's capabilities to control each electrochemical cell independently, to record data from several electrochemical techniques and to detect multiple analytes simultaneously were demonstrated by a set of experimental techniques. First the individual cell control was used to make multiplexed cyclic voltammetry possible, a technique that increases the acquisition speed of CV with parallelisation that can be used for continuous monitoring applications.

Multiple electroanalytical methods were also simultaneously conducted by separate electrochemical cells in the same solution. Lastly, the ECM has shown that it can detect two analytes simultaneously and independently at different sites in the microarray with two different electroanalytical methods.

The 12% electrochemical cross-talk was measured at conditions where electrochemical cells were set with a different potential setting. The effect of cross-talk is regarded to the potential difference between electrochemical cells. When the ECM was used as a platform that monitors electrochemical reactions within the same potential window the analytical result could be considered equivalent to a regular MEA. In cases of different potential settings such as multiplexed cyclic voltammetry or even multiple electrochemical methods being employed on separate groups of electrochemical cells, the cross-talk effect can be observed. However, the impact of the cross-talk on electroanalysis is relative to the anticipated accuracy necessary for a case study. Results shown in Sections 6.4 and 6.5 indicate that they may appear noisier but the redox potential and the shape of e.g. a voltammogram remain intact. The current magnitude, that is significant to estimate the analyte concentration, is affected but the 12% cross-talk value leads to inaccuracy levels that are already inherent in different runs of an electrochemical method.

Using the Au WEs, individual functionalisation of each electrochemical cell to measure a different target compound of interest (e.g. a biomarker) is possible. Combined with the ability to use different potentials and methods, the WEs can be functionalised individually with a versatile range of biosensing elements (described in Sections 2.3 and 2.4) sensed at a different potential level. If the experimental technique presented in the previous section was also used, results from different biomarkers could be sensed with more than one ways and correlated with multivariate analysis. The ECM aims at such an application that would make it a system of enhanced analytical power for a wide range of applications.

7 Conclusion

7.1 Introduction

Electroanalysis has been limited to perform single method measurements at a time and commercial point-of-care diagnostic devices have only been limited to perform them on large scale components. The perspectives of MEAs have yet to be explored to make cost-effective multiple analyses on a portable device using sophisticated disposable test strips such as CMOS chips. This study concerned the simulation, design, fabrication, characterisation and implementation of an integrated ECM system capable of performing multiple simultaneous electroanalytical measurements in the same chemical solution, aiming towards biochemical sensing. The system consisted of a CMOS ASIC comprised of integrated potentiostats and an integrated MEA to make independent electrochemical cells on the silicon substrate.

The main achievements of this study are:

- The development of a simulation technique to co-investigate the design of circuits and electrode structures, taking into account the effect they have on each other, to make independent integrated electrochemical cells.

- The design of an integrated ECM on an unmodified commercial CMOS process, featuring multiple electrochemical cells operated by separate integrated potentiostats. The use of a fully differential potentiostat design made possible the simultaneous operation of electrochemical cells in a single fluidic chamber for the first time.

- A post-processing fabrication process to prepare the CMOS chips to function as MEAs packaged in a waterproof container. A set of integrated switches made the CMOS ASIC a highly reconfigurable system. One of these configurations made possible to electroplate the chip's microelectrodes, bypassing the integrated circuits.

- The characterisation of the CMOS chips circuits as well as their ability to drive custom made microelectrodes compared to a large scale commercial

potentiostat counterpart. Part of the characterisation was an electrochemical cross-talk figure of merit (FOM) was devised to characterise the co-existence of simultaneously operated electrochemical cells.

- The development of measurements that take advantage of the ECM system's concurrent and independent electrochemical method employment. These include a new electrochemical method, named multiplexed cyclic voltammetry, and the simultaneous analysis of different compounds with different electrochemical methods.

The rest of the chapter reviews the major findings and limitations of this research project and presents some suggestions for future work.

7.2 Final Analysis

7.2.1 Electrical Simulation of Electrochemical Cells

The basis of creating a system where a chemical sample is introduced and many measurements by different experimental procedures are performed required an investigation to find the correct combination of circuits and electrode arrangement. To that end electrical CAD software (Cadence) was used to house the simulation of the circuits as well as the electrodes in the chemical environment. The electrical component models used in Cadence are supplied by the CMOS foundry to develop CMOS ASICs. Interpreting the electrochemical environment into an electrical model provided a unique insight for its interaction with the circuits that were sent for fabrication.

A standard potentiostat design was not found eligible to be used in a system of neighbouring electrochemical cells. Thus other designs were investigated and through simulations a fully differential potentiostat's [57] capability to auto-adjust the controlled potentials applied on separate sets of microelectrodes was first explored. That capability enabled neighbouring electrochemical cells to attain individual voltage configurations. The creation of independent electrochemical cells was complemented by a microelectrode arrangement that surrounded the WEs coaxially with a CE ring having the RE arranged between

them which demonstrated an isolating behaviour as the CE rings sank most of the leakage current between cells. A program that was developed in Matlab enabled results obtained by the simulation in Cadence to be depicted as 2-D planes and 3-D volumes of the potential distribution, the electric field intensity and the current density vector. The program created a link between the electrical simulation software and the depiction of electrochemical results in a comprehensive manner. The unified simulation setup's consistency was investigated and it was found to agree with theoretical expectations. However, as a simulation based on the electrical behaviour it does not take into account mass transfer phenomena, thus specialised electrochemical simulation software can be used to verify these results. Last but not least, the electrochemical models were simplified and used for the simulation of the circuits, assisting in their design process which led to an ECM system that successfully operated in an electrochemical environment from the first iteration of the chip.

7.2.2 From Silicon to Integrated MEA

A 4 x 4 ECM containing a 16 x 16 WE MEA was designed in Cadence using the aforementioned circuits and microelectrode structures as a basis. The ASIC was designed using a 0.35 μm CMOS technology from ams AG [17] with models and some existing components provided by the foundry toolkit for Cadence. The ASIC was designed with each of the 16 WE structures connected to their respective potentiostat to make an electrochemical cell. A two-stage fully differential folded cascode operational amplifier with a CMFB stage was used as the control amplifier and two-stage differential amplifiers buffered microelectrode potentials to construct a feedback loop. The amplifiers were designed to multiplex WEs during the run time of an electrochemical method, able to record electrochemical events at approximately the same time (within some ms difference) and achieve a high spatiotemporal resolution in the array rather than the conventional procedure to take measurements from each WE sequentially. Another feature of the ASIC were integrated switches (transmission gates) added in key positions of the circuits to select between different modes of operations as follows: analogue readout mode, digital readout mode, internal circuits test mode, characterisation mode and functionalisation mode. The switches constructed a configurable system that can be used with or without certain internal circuits. A use of the switches (test mode) was to connect an integrated

potentiostat to test outputs and permit a straightforward verification of the system. The CMOS ASIC potentiostat was first characterised with resistive and capacitive loads. As a second stage the integrated as well a commercial potentiostat operated test microelectrode samples fabricated in a cleanroom environment and a one to one verification of the results was demonstrated.

The test microelectrode samples fabrication process was used as a reference for the post-processing fabrication of the CMOS chips. The CMOS chips that were received from the foundry were passivated and the microelectrode structures on the top metal layer were made of Al which is a non-electrochemically compatible metal. The passivation layer of the unprocessed CMOS dies was first thinned over the MEA and then etched on top of the microelectrodes with a smaller width so that the side walls were not exposed as their profile is not easily covered with inert metals. A lift-off process followed to cover the Al microelectrodes with electrochemically inert and biocompatible metals. A phenomenon that was first identified with the test samples was a thin Al_2O_3 layer formation on the CMOS inherent Al metal surface that needed to be etched prior to metal deposition in high vacuum to create a good contact. The lift-off profile was also challenging to create, thus two processes were tried to find the one with S1818 [206] and a TMAH developer soak step to create an inhibition layer for the undercut profile to be created.

The chips were packaged and wire bonded on a 144-PGA ceramic package to dissipate heat and a method that included a PDMS cube to create a mould along with a chemically resistive epoxy and a 3-D-printed PET-G ring were used to form a microfluidic container. The integrated switches were used to isolate the circuits and electroplate an additional layer of Au on the microelectrodes that covered any Al metal that was still exposed. To monitor the electroplating process a microelectrode test sample was used and epoxy was replaced with wax for its encapsulation for the sample to be removed and measured with an AFM tool after electroplating. The process was also verified on a CMOS chip with an optical profiler [182] and a 64-66 nm/s rate was recorded. The use of the integrated switches proved that it is possible for CMOS MEAs with integrated potentiostats to be electroplated or functionalised externally, bypassing the internal circuits.

7.2.3 ECM System Capabilities

The electrochemically ready CMOS chips instrumentation hardware was used to house them and create the ECM system. They were connected to a PXIe system from NI [193]–[196] with a fast 1.25 MS/s/channel acquisition speed for each analogue output and independent control with 16 differential input signals applied to the ASICs through a custom designed PCB. IAs [199] were initially planned to be part of the PCB but they had a large 2 μA input current bias compared to the nA levels normally detected on the $R_{\text{I to V}}$ resistor, thus they could not be used as they consumed too large a current magnitude from the readout nodes. Replacement IAs to be soldered on the designed PCB footprint and connections have not yet been found. Programs specifically for the operation and analysis of results from the ECM systems were developed.

To discover the ECM system's capabilities, a characterisation of its circuits and operation followed. The ECM exhibited a higher number of independent potentiostats than prior work using a three-electrode system. The available potential window range was also one of the largest reported with a CMOS system, owing to the fully-differential design of the potentiostats. A bandwidth significantly higher than other systems was recorded which enables the use of fast techniques (i.e. FSCV) and fast multiplexing. The WEs were multiplexed as mentioned before with a rate up to 51.2 kHz and some input settings were stored along with the results to assist the measurements' analysis. Furthermore, integrated resistors have a tolerance and measurements of current converted to voltage are not deemed reliable. In the ECM system the analogue readout relied on $R_{\text{I to V}}$ on-chip resistor conversion. The integrated switches assisted once more for this problem, used in the characterisation mode, the $R_{\text{I to V}}$ were measured. A resistance map was created for every CMOS chip to ensure an accurate conversion of current. The ECM was operated using staircase cyclic voltammetry with the on-chip microelectrodes and using measurements from several ferrocene concentrations a concentration-peak current plot was extracted showing a linear relation.

The activation of multiple electrochemical cells in the chemical solution required a cross-talk characterisation between the electrochemical cells of the microarray. This FOM was evaluated for the first time as CMOS MEAs have not

previously been characterised in this way. Therefore an experiment was designed for this purpose and the electrochemical cross-talk was found to be 12%. Results from measurements that were conducted later showed that this value was adequate for an independent application of different potential settings simultaneously. The ability of the ECM to perform such measurements is regarded to its design both with fully differential potentiostats and the coaxial microelectrode arrangement. Improvements in the circuit and electrode arrangements can be pursued in the future to further minimise the electrochemical cross-talk.

Apart from the analogue readout method, a digital discrete time current sense amplifier (CSA) ADC circuit was materialised in the CMOS chip. The readout method is suitable for a future integration of the system with a state machine. During characterisation an issue of a lack of current polarity output was identified in the current readout method design. Results obtained with this method were also noisier which was regarded to charge injection and a correlated double sampling (CDS) circuit was deemed as an appropriate solution for a future version of the chip.

7.2.4 Simultaneous Electroanalytical Measurements

The ECM was designed as a system that can offer simultaneous electroanalytical capabilities not previously possible with an aim to be used in diagnostics and biochemical applications. Possible tests for biosensing were explored by a set of analytical methods on chemical compounds that take advantage of simultaneously applied multiple independent analytical settings.

The ECM system's capability to use individual potential settings was first demonstrated with the development of a novel electroanalytical method. The new method makes use of all the 16 electrochemical cells operating in parallel to increase the acquisition speed. Splitting the voltage scan between the cells the speed of a voltammogram is increased while a low scan rate essential for accurate measurements is maintained. The speed can be further increased with any additional electrochemical cell added to future designs to share the potential range. The method can be used for continuous monitoring applications where speed as well as accuracy are important.

Two more experiments were conducted to show how the ECM can be used to sense different compounds of interest (e.g. biomarkers) simultaneously with several electrochemical methods. The first experiment involved the detection of only one chemical compound, namely 5 mM of ferrocene, where several electroanalytical methods were applied to columns of electrochemical cells to concurrently analyse the sample. The methods were constant potential amperometry, staircase cyclic voltammetry, normal and differential pulse voltammetry. The results were represented in the respective format of each method and they all recognised the chemical composition correctly. Compounds can sometimes be sensed by specific electroanalytical methods [207], the experiment showed that a sample can be analysed with many methods to find the one that provides a detectable result.

A second experiment was conducted using two analytes, namely ferrocene and decamethylferrocene with different standard potentials (E^0). The current peaks for the two analytes were identified with staircase CV in a large potential window. Smaller specific potential windows to the analytes' peaks were applied on separate electrochemical cells. In conjunction, constant potential amperometry at two different potential levels was also used at different cells to detect the analyte concentration independently. The experiment was used to prove the eligibility of the system not only to use different electrochemical methods but also sense different biomarkers simultaneously. Such an experimental setting can be used to enhance the detection accuracy and monitor the correlation of chemical compounds in the solution.

The experiments demonstrate the capability of the ECM to make independent measurement and the results were encouraging. The use of these results for accurate diagnostics is possible with approaches that are suggested in the next section.

7.3 Future Work

The focus on this study was on the demonstration of a complete working system, rather than the optimisation of each individual component. Consequently, several areas can now be identified where further research could be used to improve the performance of the ECM system. Moreover, this work combined in

multidisciplinary research can also produce new more accurate diagnostic results; some ideas are presented in this section.

7.3.1 Potential Distribution Measurement

The cross-talk measurement is an important characterisation parameter. However the potential distribution induced by the electrochemical cells in the chemical solution was also a large part of this study through simulations. It would be beneficial for the establishment of the design methodology to isolate electrochemical cells in a chemical solution to measure the potential distribution while an experiment is conducted. Scanning electrochemical potential microscopy (SECPM) is a technique that has been used before to measure the potential of the electrical double layer of an electrode in an electrochemical setup [208]. It is a scanning microscopy technique that uses a small conductive tip to scan potential changes in the chemical solution volume. A bipotentiostat is used and the potential difference between the tip and the WE is measured. A connection that is compatible to the existing electrochemical setup needs to be considered and the technique could possibly measure the potential distribution in the volume of the chemical solution. An alternative is to design a CMOS chip with the existing setup and an ISFET array that measures the potential on top of the passivation layer. A feasibility study has been conducted by the author with microelectrodes microfabricated on top of an existing CMOS ISFET array, as shown in Figure 7.1 [209].

7.3.2 Circuits and Setup Improvement

Improvements could be made to the analogue and the digital readout circuits. As

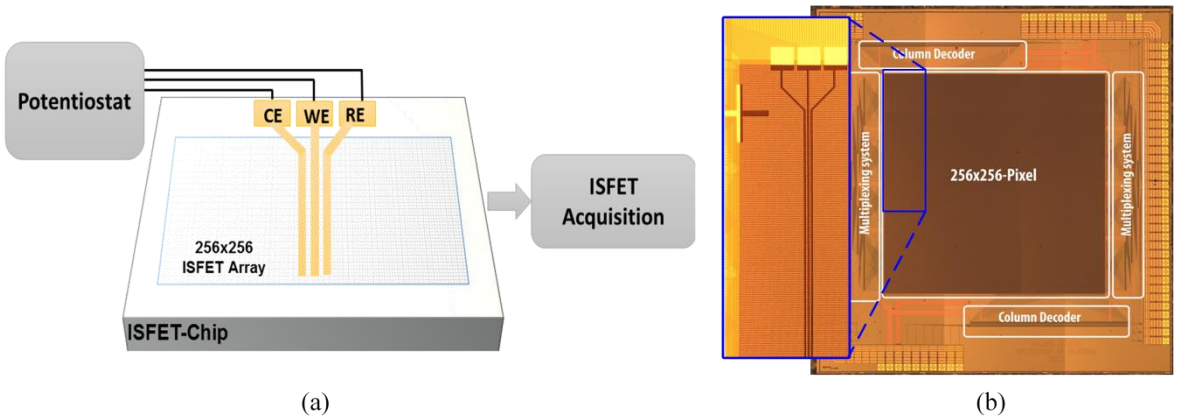

Figure 7.1: (a) A voltammetric and potentiometric electrochemical setup and (b) the ISFET array chip with microelectrodes deposited on top [209].

it was mentioned the chosen IA was not suitable to be used with the readout $R_{I\,to\,V}$ resistors due to a high input bias current. A solution would be to find suitable IAs (preferably with a CMOS based input stage) that fit on the existing PCB. This task has proven to be difficult, thus if an IA with low input bias current is found a new PCB would be necessary to be made. This change would improve the system's LOD and enable detection of lower analyte concentrations. Regarding the digital readout circuit, a current polarity output along the magnitude already provided by the discrete time CSA would make it eligible to be used with voltammetric methods. A correlated double sampling (CDS) approach would also decrease the noise from charge injection found in the discrete time CSA. Considering that the circuit is on-chip, a new CMOS ASIC with a current polarity output and a digital output serialiser (to reduce the large number of bond-pads) would need to be designed. If a circuit to produce the input waveform was embedded the new chip would allow for integration to a smaller PCB and acquisition system. A Point-of-Care (POC) portable device could be constructed to make diagnosis where it is needed. A microarray with more electrochemical cells could be easily designed as the ASIC's design is both modular and scalable.

7.3.3 Microelectrodes Suitability

In terms of post-processing of the CMOS ASIC two steps can be taken to improve the microelectrode array. The first step is to use the already post-processed chips with Pd on the CE and Ag on the RE that are more suitable materials for the electrodes on which they are placed (as was explained in Section 5.6). The RE material could also be further improved by an electrolysing step in the functionalisation mode to prepare an AgCl surface, similar to the method described in Section 5.8. Covering it with an encapsulating layer (e.g. a hydrogel) would also be beneficial to limit degradation of the AgCl layer [43]. The second step would be to reduce the area of every WE. As was described in Section 3.5.1 a guideline for the optimal WE size to pitch to ensure that the individual diffusion layers do not overlap is available in the literature [139]. Although the ratio d/a = 15.2 (where d is the pitch and α is the WE radius) that was attained with the existing process was close to the required value, a reduction of the WE opening to a side length less than 10 μm would achieve the proposed ratio. This change as well as an investigation of more electrode

geometrical arrangements could also assist in reducing the 12% electrochemical cross-talk reported in this work.

7.3.4 Multivariate Analysis

The ECM system is prepared with biocompatible microelectrodes that enable the functionalisation of the MEA with biorecognition elements to construct a tool for parallel cross-referenced diagnosis. The functionalisation part can be adapted to a wide selection of applications [8]. A common target application for MEAs is the detection of biomarkers with trapped enzymes in permiselective polymers as described in Sections 2.3 and 2.4. Having the capability of multiple analyte detection, each electrochemical cell can be functionalised for a different biomarker as has already been demonstrated [105], [108]. Another biofunctionalisation technique compatible with ECM is DNA and RNA oligonucleotide sensing for genotyping and pathogen identification [48], [210]. The Au WE surface can be functionalised with "probe" oligonucleotides to sense hybridised "target" DNA sequences tagged with ferrocene [52], [73] using FSCV. Using other redox labels along ferrocene (e.g. decamethylferrocene) with a different standard potential (E^0) to different oligonucleotides to be sensed in separate electrochemical cells would prevent false reading by cross-hybridisation [52], [73], [211]. Many other multiple analyte techniques are possible as explained in Section 2.7.1. Furthermore, combining the detection of enzymatic biomarkers and DNA/RNA sensing a diagnostic device for the detection of, for example, cancer could be constructed [39].

Cross-referencing the acquired results is the second part that can be used with the ECM system. It was already shown that results from multiple electroanalytical methods are possible to be acquired simultaneously with the system developed in this work. The combination of these measurements and their introduction in statistical analysis programs is used to model the concentration and composition. The models are then used to determine compounds of unknown composition and concentration. This is the principle of multivariate analysis and chemometrics (more details were provided in Section 2.7). The complex data can be used to determine results that are difficult to interpret e.g. overlapping analyte current peaks [120], or otherwise incomprehensible to a trained researcher, e.g. the categorisation of tea

varieties [121]. As it has already been demonstrated the use of multivariate analysis is fully compatible to be integrated in CMOS systems to determine biomarker concentrations in FSCV measurements with interference from pH changes. It was used for continuous monitoring with a feedback system to maintain the dopamine levels in the brain [117]. If it is used with the ECM system it could potentially offer the parallelised measurements as a means to produce diagnostic results that would describe a condition rather than just biomarker concentrations. Another possibility that would further enhance its prospects would be for the ECM system to be integrated with other electrochemical and optical sensors. Multivariate analysis has been shown to work with multiple sensors before [212]. Lastly, a function that would complete the ECM system to be used as a commercial POC device would be to make an automated software that would identify compounds of interest in the biochemical solution. It could also automatically analyse them as a whole and present the final pathological result to the user.

Appendices

A C++ Source Code

A.1 Electrolyte Resistance Mesh

The resistor mesh netlist used to simulate the composition of the electrolyte, made of TBAPF6 in acetonitrile, was produced using the following program (grid2.cpp):

```
// grid2.cpp : Defines the entry point for the console application.
//

#include "stdafx.h"
# include <stdio.h>
# include <stdlib.h>
#include <iostream>
using namespace std;


int _tmain(int argc, _TCHAR* argv[])
{
	FILE *fp;
	int i,size,x,y,z,res;
	cout << "Type cube side size\n";
	cin >> size;
	cout << "Type the unit resistor size in Ohms\n";
	cin >> res;


	fp = fopen("netlist", "w");
	if (fp == NULL) {
		printf("Couldn't open file netlist.txt\n");
	}
	// here is the main code that creates the netlist

	fprintf(fp,
"**********************************************************\n**********  This cube
size is %dx%dx%d
**********\n**********************************************************\n\n",
size,size,size);

	fputs("*.BIPOLAR\n*.RESI =
20\n*.RESVAL\n*.CAPVAL\n*.DIOPERI\n*.DIOAREA\n*.EQUATION\n*.LDD\n*.SCALE
METER\n*.MEGA\n.PARAM\n\n\n.SUBCKT res_grid ", fp);

	i = 0;
	y = 0;
```

```
		for (x = 0; x < size + 1; x++)
		{
		for (z = 0; z < size + 1; z++)
			{
				if (i>7)
				{
					i = 0;
					fprintf(fp, "\n+net<%d%d%d> ", x, y, z);
				}
				else
				fprintf(fp, "net<%d%d%d> ", x, y, z);
				i++;
				}
		}

	fputs("\n*.PININFO ", fp);

	i = 0;
	for (x = 0; x < size + 1; x++)
	{
		for (z = 0; z < size + 1; z++)
		{
			if (i>6)
			{
				i = 0;
				fprintf(fp, "\n*.PININFO net<%d%d%d>:B ", x, y, z);
			}
			else
				fprintf(fp, "net<%d%d%d>:B ", x, y, z);
			i++;
		}
	}

	fputs("\n\n\n*X axis resistors\n", fp);
	for (x = 0; x < size; x++)
	{
		fputs("\n", fp);
		for (y = 0; y < size+1; y++)
		{
			for (z = 0; z < size+1; z++)
			fprintf(fp, "RR%d%d%dx net<%d%d%d> net<%d%d%d> %d $
[RP]\n", x, y, z, x, y, z, x + 1, y, z, res);
		}
	}

	fputs("\n\n\n*Y axis resistors\n", fp);

	for (y = 0; y < size; y++)
	{
		fputs("\n", fp);
		for (x = 0; x < size + 1; x++)
		{
```

```
                        for (z = 0; z < size + 1; z++)
                                fprintf(fp, "RR%d%d%dy net<%d%d%d> net<%d%d%d> %d
$ [RP]\n", x, y, z, x, y, z, x, y + 1, z,res);
                }
        }

        fputs("\n\n\n*Z axis resistors\n", fp);

        for (z = 0; z < size; z++)
        {
                fputs("\n", fp);
                for (x = 0; x < size + 1; x++)
                {
                        for (y = 0; y < size + 1; y++)
                                fprintf(fp, "RR%d%d%dz net<%d%d%d> net<%d%d%d> %d
$ [RP]\n", x, y, z, x, y, z, x, y, z + 1,res);
                }
        }

        fputs("\n.ENDS\n", fp);

        fclose(fp);
        return 0;
}
```

A.2 Electrode Transmission Line Connections

Apart from the electrode-electrolyte connections to the resistor mesh the electrodes' 10×10 μm^2 elements were connected together with a sheet resistance of 40 mΩ/□. The following program (electrode.cpp) was used to make netlists of resistors connecting the appropriate mesh nodes together to construct the electrodes' shapes:

```
// electrode.cpp : Defines the entry point for the console application.
//

#include "stdafx.h"
# include <stdio.h>
# include <stdlib.h>
#include <iostream>
using namespace std;


int _tmain(int argc, _TCHAR* argv[])
{
        FILE *fp;
        int i, j, xorig, xfinal, yorig, yfinal, zorig, zfinal, x, y, z, res =50 ;
        cout << "Type x origin position\n";
        cin >> xorig;
```

```
	cout << "Type x final position\n";
	cin >> xfinal;
	cout << "Type y origin position\n";
	cin >> yorig;
	cout << "Type y final position\n";
	cin >> yfinal;
	cout << "Type z origin position\n";
	cin >> zorig;
	cout << "Type z final position\n";
	cin >> zfinal;



	fp = fopen("elec_netlist", "w");
	if (fp == NULL) {
		printf("Couldn't open file netlist.txt\n");
	}
	// here is the main code that creates the netlist

	fprintf(fp, "*********************************************************************\n***   This
electrode dimensions are x= %d-%d, y= %d-%d, z= %d-%d
***\n*********************************************************************\n\n", xorig, xfinal,
yorig, yfinal, zorig, zfinal);

	fputs("*.BIPOLAR\n*.RESI =
20\n*.RESVAL\n*.CAPVAL\n*.DIOPERI\n*.DIOAREA\n*.EQUATION\n*.LDD\n*.SCALE
METER\n*.MEGA\n.PARAM\n\n\n.SUBCKT electrode ", fp);

	i = 0;
	for (x = xorig; x < xfinal + 1; x++)
	{
		for (y = yorig; y < yfinal + 1; y++)
		{
			for (z = zorig; z < zfinal + 1; z++)
			{
				if (i>7)
				{
					if ((x>=xorig+1) && (x<=xfinal-1) &&
(y>=yorig+1) && (y<=yfinal) && (z>=zorig+1) && (z<=zfinal-1))
						NULL;
					else
					{
						i = 0;
						fprintf(fp, "\n+net<%d%d%d> ", x, y, z);
						i++;
					}
				}
				else
				{
					if ((x >= xorig + 1) && (x <= xfinal - 1) && (y >=
yorig + 1) && (y <= yfinal) && (z >= zorig + 1) && (z <= zfinal - 1))
						NULL;
```

```
                                        else
                                        {
                                                fprintf(fp, "net<%d%d%d> ", x, y, z);
                                                i++;
                                        }
                                }
                        }
                }
        }

        fputs("\n*.PININFO ", fp);

        i = 0;
        for (x = xorig; x < xfinal + 1; x++)
        {
                for (y = yorig; y < yfinal + 1; y++)
                {
                        for (z = zorig; z < zfinal + 1; z++)
                        {
                                if (i>6)
                                {
                                        if ((x >= xorig + 1) && (x <= xfinal - 1) && (y >=
yorig + 1) && (y <= yfinal) && (z >= zorig + 1) && (z <= zfinal - 1))
                                                NULL;
                                        else
                                        {
                                                i = 0;
                                                fprintf(fp, "\n*.PININFO net<%d%d%d>:B
", x, y, z);
                                                i++;
                                        }
                                }
                                else
                                {
                                        if ((x >= xorig + 1) && (x <= xfinal - 1) && (y >=
yorig + 1) && (y <= yfinal) && (z >= zorig + 1) && (z <= zfinal - 1))
                                                NULL;
                                        else
                                        {
                                                fprintf(fp, "net<%d%d%d>:B ", x, y, z);
                                                i++;
                                        }
                                }
                        }
                }
        }

        fputs("\n\n\n*X axis resistors\n", fp);
        for (x = xorig; x < xfinal; x++)
        {
                fputs("\n", fp);
                for (y = yorig; y < yfinal + 1; y++)
```

```
                {
                        for (z = zorig; z < zfinal + 1; z++)
                                fprintf(fp, "RR%d%d%dxe net<%d%d%d> net<%d%d%d>
%d $ [RP]\n", x, y, z, x, y, z, x + 1, y, z, res);
                }
        }

        fputs("\n\n\n*Y axis resistors\n", fp);

        for (y = yorig; y < yfinal; y++)
        {
                fputs("\n", fp);
                for (x = xorig; x < xfinal + 1; x++)
                {
                        for (z = zorig; z < zfinal + 1; z++)
                                fprintf(fp, "RR%d%d%dye net<%d%d%d> net<%d%d%d>
%d $ [RP]\n", x, y, z, x, y, z, x, y + 1, z, res);
                }
        }

        fputs("\n\n\n*Z axis resistors\n", fp);

        for (z = zorig; z < zfinal; z++)
        {
                fputs("\n", fp);
                for (x = xorig; x < xfinal + 1; x++)
                {
                        for (y = yorig; y < yfinal + 1; y++)
                                fprintf(fp, "RR%d%d%dze net<%d%d%d> net<%d%d%d>
%d $ [RP]\n", x, y, z, x, y, z, x, y, z + 1, res);
                }
        }

        fputs("\n.ENDS\n", fp);

        fclose(fp);
        return 0;
}
```

B Cadence Schematics

B.1 Electrochemical Electrical Equivalent

The imported resistor mesh and the electrode-electrolyte interface elements were introduced in circuit diagrams to construct the electrical equivalent of electrode structure geometries in a chemical solution, shown in Figure B.1-B.2.

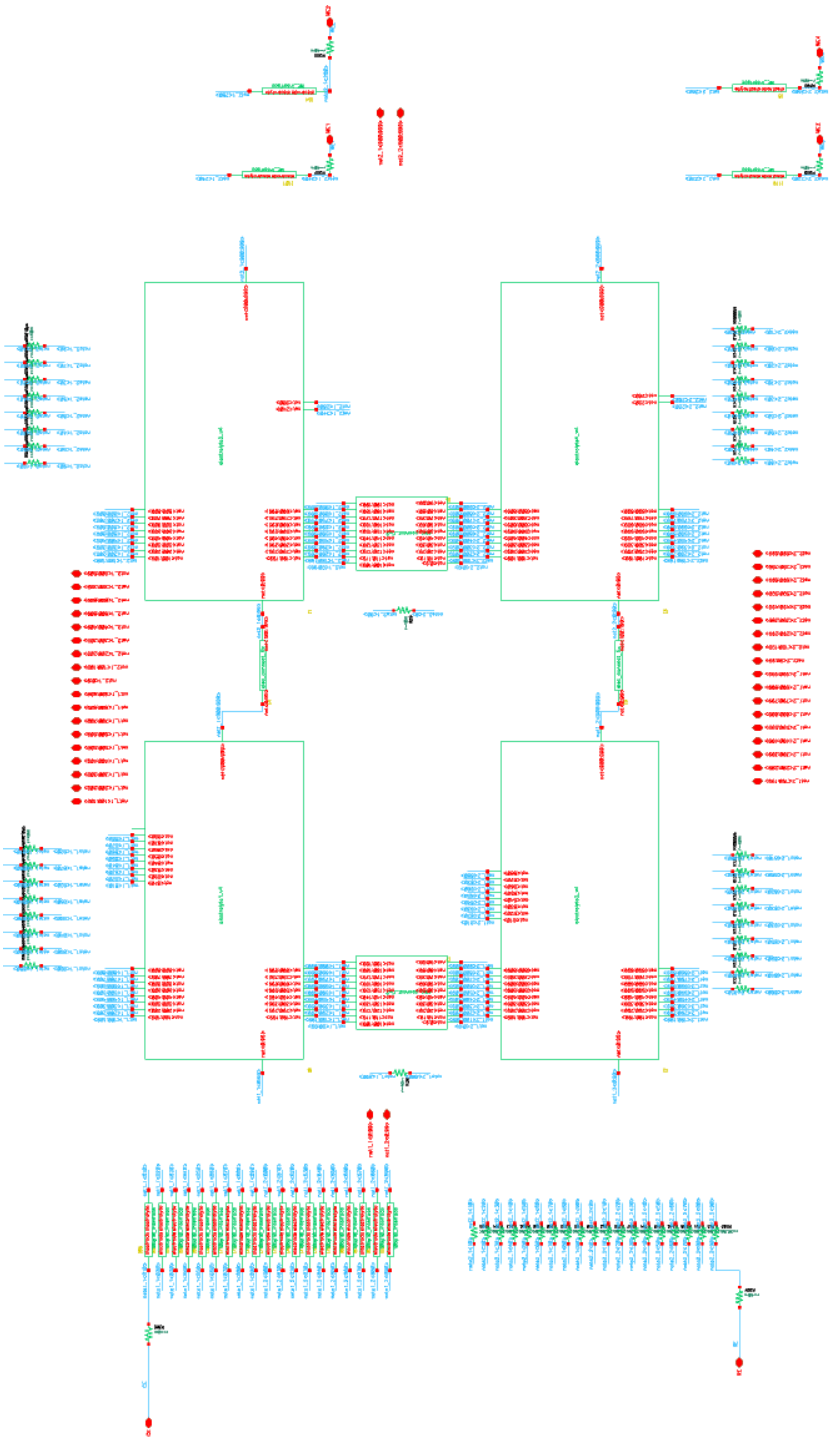

Figure B.1: Electrical equivalent of the conventional microelectrode structure.

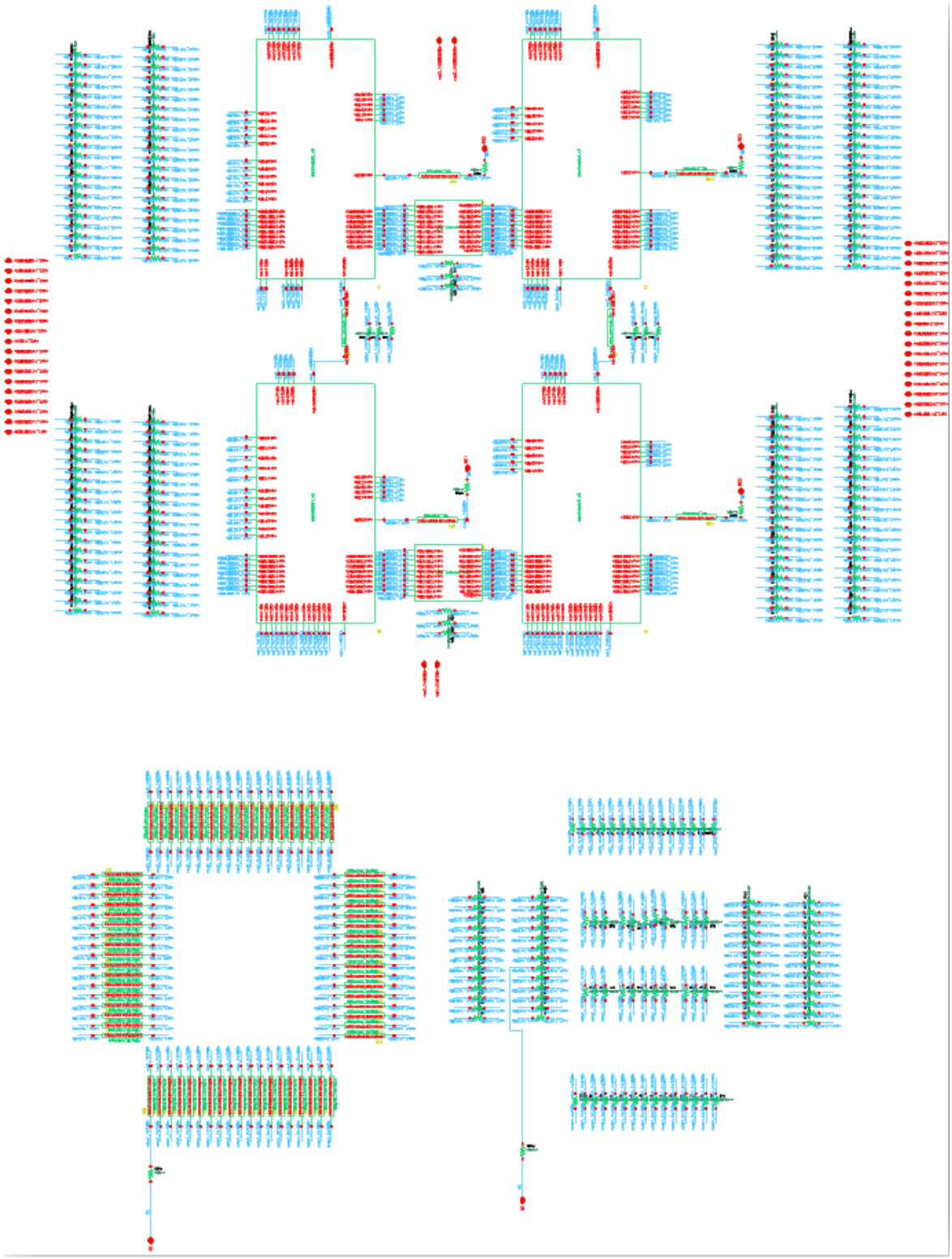

Figure B.2: Electrical equivalent of the coaxial microelectrode structure.

B.2 Electrochemical Cell Test Setup

The electrical equivalent schematic blocks were introduced in fully differential potentiostat setups to make up electrochemical cell simulations, as shown in Figure B.3-B.4.

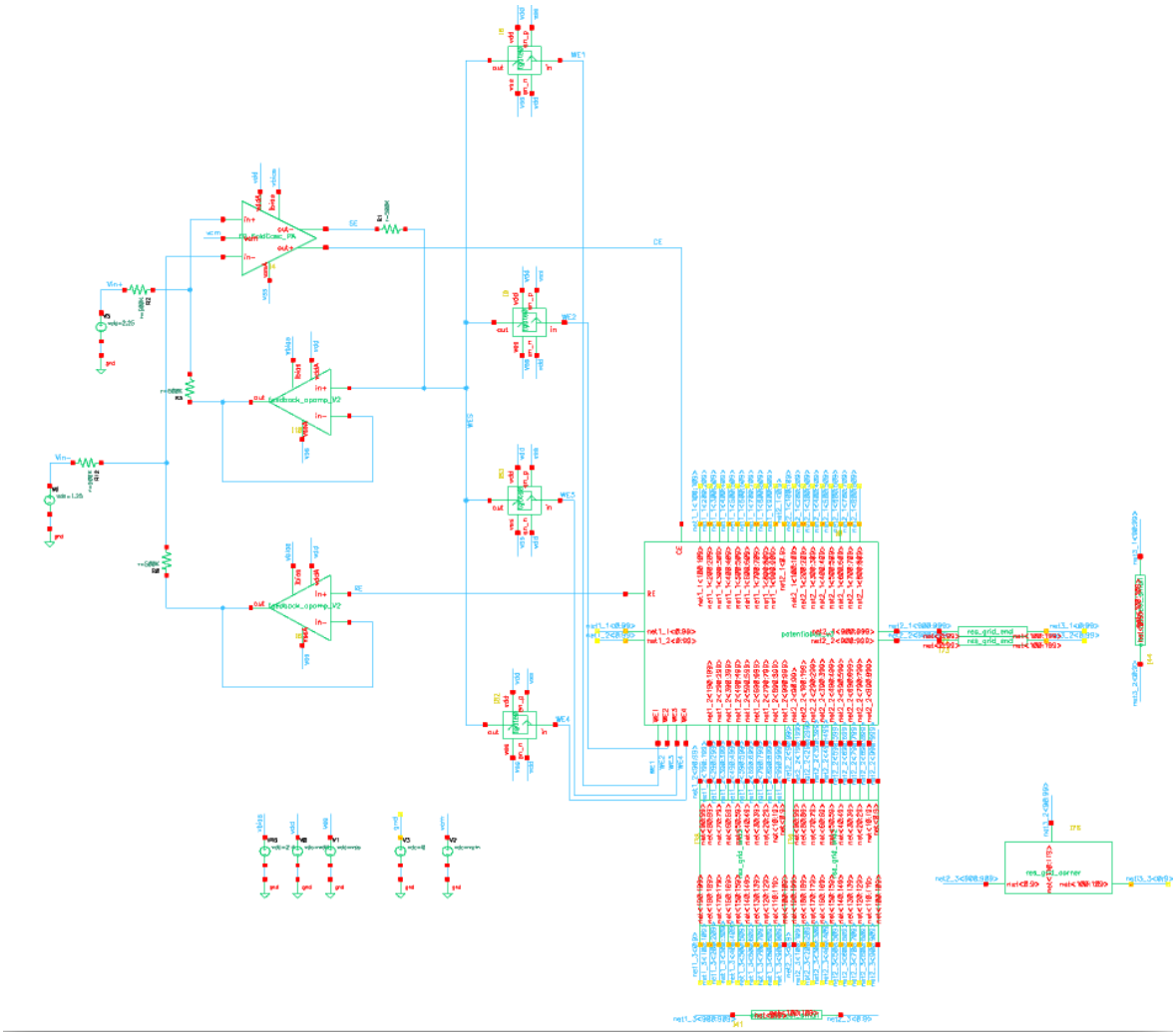

Figure B.3: Simulation setup of a fully differential potentiostat controlling the electrical equivalent of an electrode structure in a chemical solution.

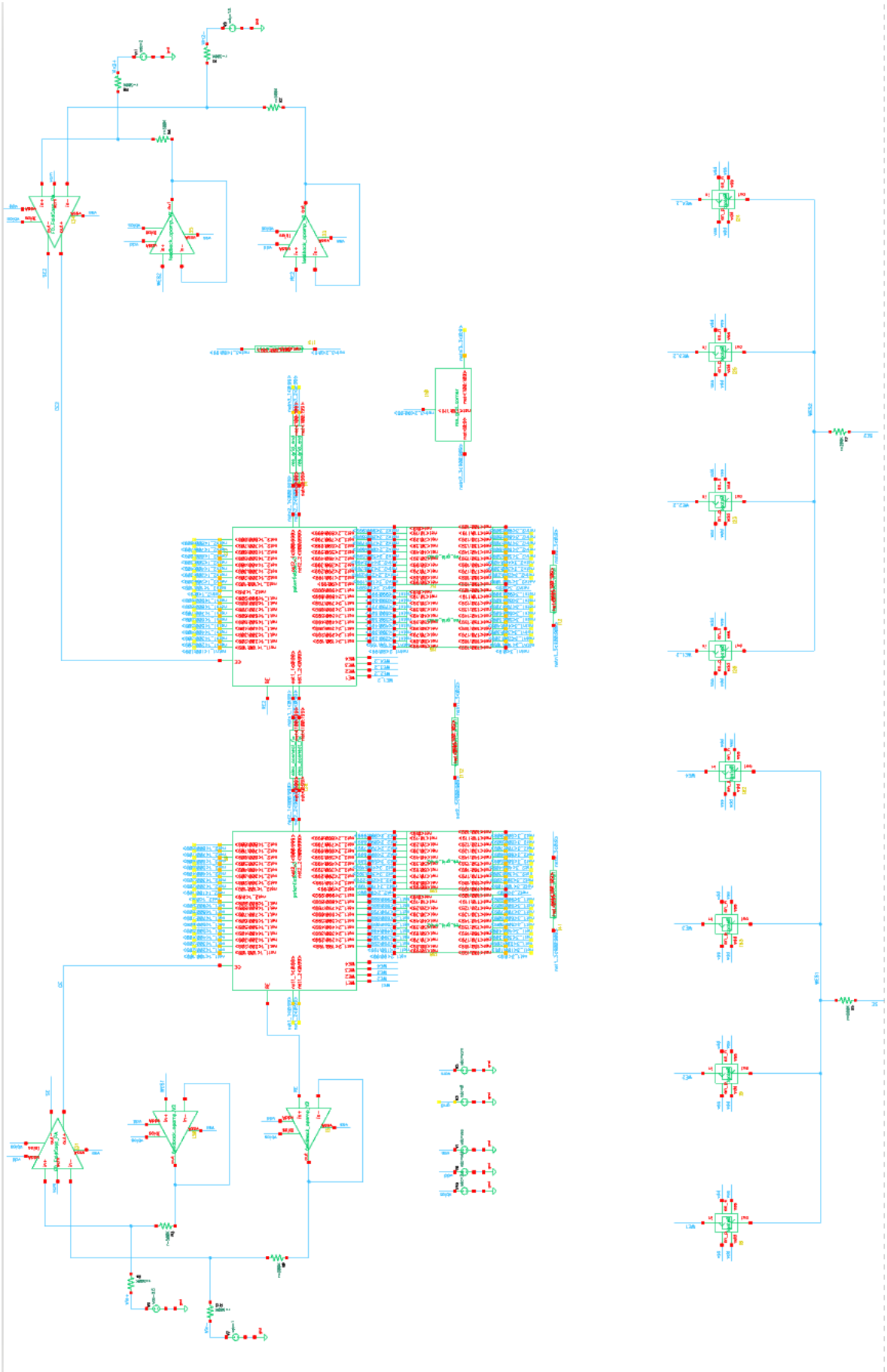

Figure B.4: Simulation setup of two fully differential potentiostats controlling the electrical equivalent of two adjacent electrochemical cells.

B.3 Electrochemical Cell Microarray ASIC Design Overview

Schematic hierarchical blocks containing circuits lower in hierarchy that show how individual circuits of the ASIC are designed as a system are shown in Figure B.3-B.4.

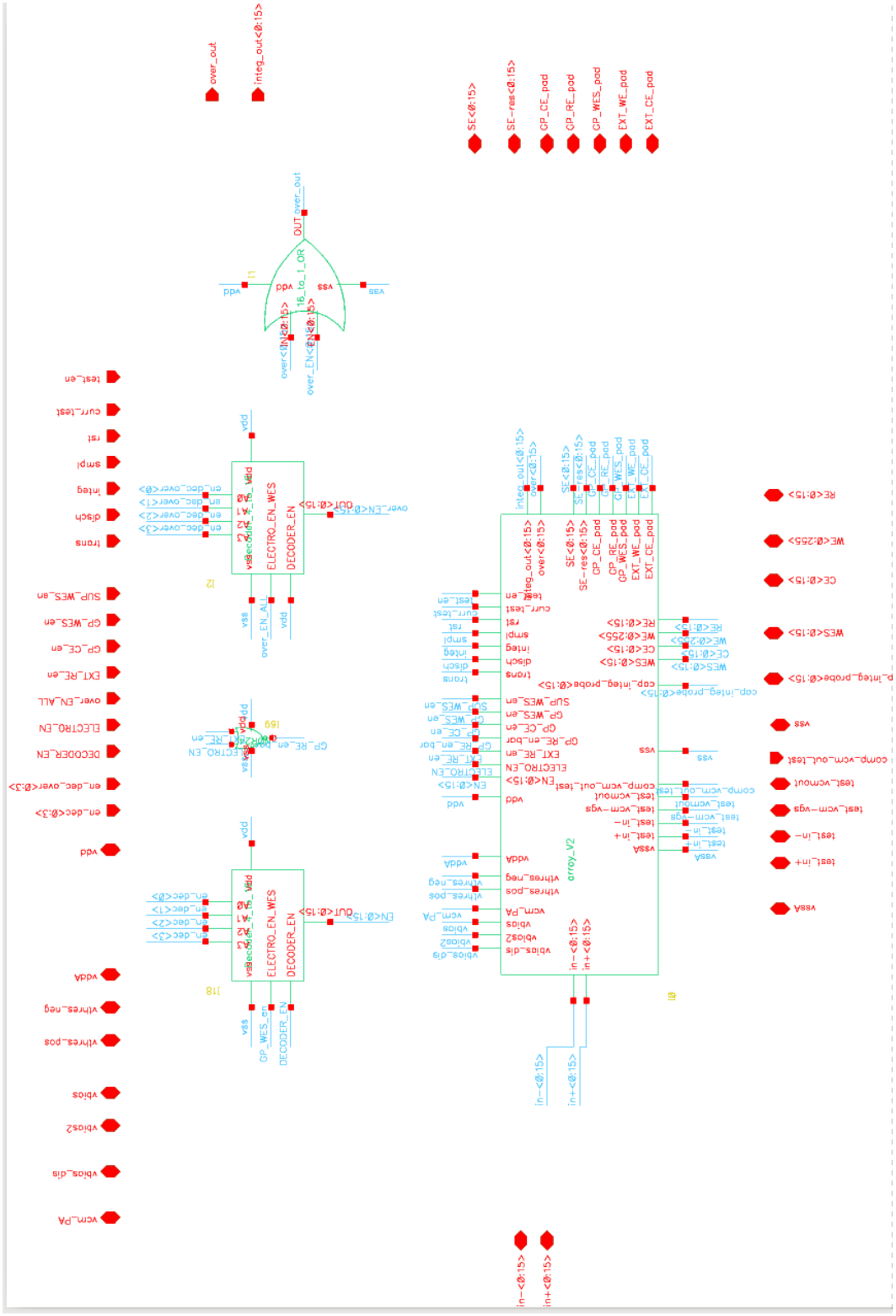

Figure B.5: Schematic circuit diagram of the electrochemical cell microarray.

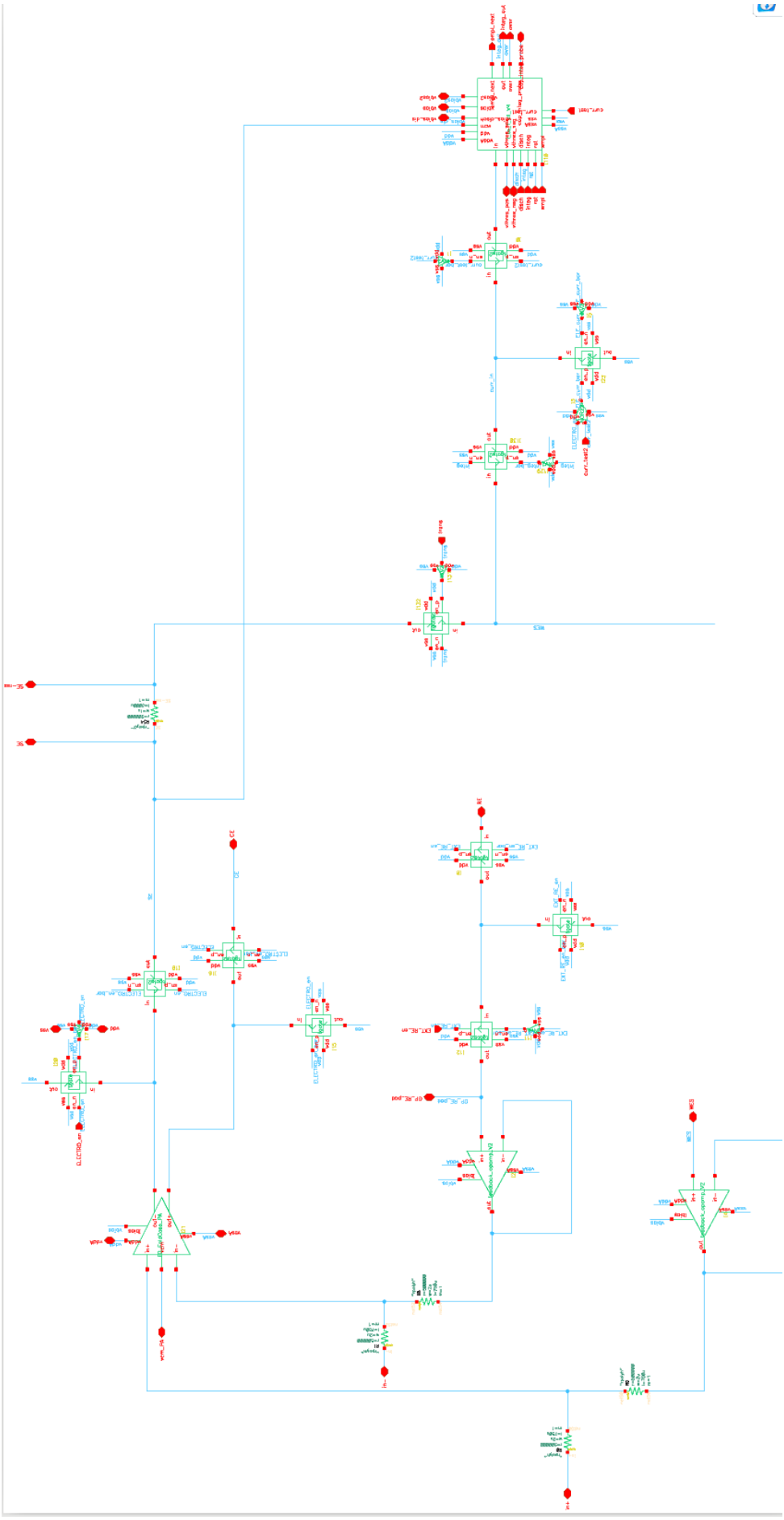

Figure B.6: Schematic circuit diagram of the potentiostat of an electrochemical cell.

C Matlab Source Code

C.1 Simulation Results Representation

C.1.1 Single Fully-differential Electrochemical Cell

C.1.1.1 Potential map

The 2-D and 3-D electrical potential maps along with the current density streamlines of a fully differential electrochemical cell were produced using the following program (voltage_map_FD_v2.m):

```
clear;
close all;
[filename,pathname]=uigetfile('*.dc', 'Pick a file of x,y,z data');
fullpath=[pathname,filename];
imagepath=[pathname,'electrodes.bmp'];
imagepath2=[pathname,'electrodes2.bmp'];

A=imread(imagepath);
A2=imread(imagepath2);
B=255*ones(200,200,3);
B2=255*ones(200,200,3);
B=uint8(B);
B2=uint8(B2);
for i=1:190
    for j=1:190
        for k=1:3
       B(i+5,j+5,k)=A(i,j,k);
       B2(i+5,j+5,k)=A2(i,j,k);
        end
    end
end
xImage = [0 200; 0 200];
yImage = [200 200; 0 0];
zImage = [-30 -30; -30 -30];

figure(25),
image(A)
figure(26),
image(B)

[words, val]=textread(fullpath,'%s %f', 'commentstyle','shell');

chars=char(words);
[length,width]=size(chars);

for l=1:length-1
    for w=1:width
    if chars(l,w)=='<'
        offset(l,1)=w-7;
    end
    end
end

i=1;
```

```
%% Electrolyte voltages
for l=1:length-1
if chars(l,1)=='n' && chars(l,2)=='e' && chars(l,3)=='t' &&
chars(l,4)=='1' && chars(l,5)=='_' && chars(l,6)=='3'
    if chars(l,9+offset(l)) == '>'
    z(i)=str2num(chars(l,8+offset(l)));
    y(i)=0+20;
    x(i)=0;
    v(i)=val(l);
    end
    if chars(l,10+offset(l)) == '>'
    z(i)=str2num(chars(l,9+offset(l)));
    y(i)=str2num(chars(l,8+offset(l)))+20;
    x(i)=0;
    v(i)=val(l);
    end
    if chars(l,11+offset(l)) == '>'
    z(i)=str2num(chars(l,10+offset(l)));
    y(i)=str2num(chars(l,9+offset(l)))+20;
    x(i)=str2num(chars(l,8+offset(l)));
    v(i)=val(l);
    end
    i=i+1;
end
end

for l=1:length-1
if chars(l,1)=='n' && chars(l,2)=='e' && chars(l,3)=='t' &&
chars(l,4)=='2' && chars(l,5)=='_' && chars(l,6)=='3'
    if chars(l,9+offset(l)) == '>'
    z(i)=str2num(chars(l,8+offset(l)));
    y(i)=0+20;
    x(i)=0+10;
    v(i)=val(l);
    end
    if chars(l,10+offset(l)) == '>'
    z(i)=str2num(chars(l,9+offset(l)));
    y(i)=str2num(chars(l,8+offset(l)))+20;
    x(i)=0+10;
    v(i)=val(l);
    end
    if chars(l,11+offset(l)) == '>'
    z(i)=str2num(chars(l,10+offset(l)));
    y(i)=str2num(chars(l,9+offset(l)))+20;
    x(i)=str2num(chars(l,8+offset(l)))+10;
    v(i)=val(l);
    end
    i=i+1;
end
end

for l=1:length-1
if chars(l,1)=='n' && chars(l,2)=='e' && chars(l,3)=='t' &&
chars(l,4)=='i' && chars(l,5)=='3' && chars(l,6)=='_' && chars(l,7)=='3'
    if chars(l,9+offset(l)) == '>'
    z(i)=str2num(chars(l,8+offset(l)));
    y(i)=0+20;
    x(i)=0+20;
    v(i)=val(l);
    end
    if chars(l,10+offset(l)) == '>'
    z(i)=str2num(chars(l,9+offset(l)));
    y(i)=str2num(chars(l,8+offset(l)))+20;
    x(i)=0+20;
```

```
    v(i)=val(l);
    end
    if chars(l,11+offset(l)) == '>'
    z(i)=str2num(chars(l,10+offset(l)));
    y(i)=str2num(chars(l,9+offset(l)))+20;
    x(i)=str2num(chars(l,8+offset(l)))+20;
    v(i)=val(l);
    end
    i=i+1;
end
end

for l=1:length-1
if chars(l,1)=='n' && chars(l,2)=='e' && chars(l,3)=='t' &&
chars(l,4)=='3' && chars(l,5)=='_' && chars(l,6)=='2'
    if chars(l,9+offset(l)) == '>'
    z(i)=str2num(chars(l,8+offset(l)));
    y(i)=0+10;
    x(i)=0+20;
    v(i)=val(l);
    end
    if chars(l,10+offset(l)) == '>'
    z(i)=str2num(chars(l,9+offset(l)));
    y(i)=str2num(chars(l,8+offset(l)))+10;
    x(i)=0+20;
    v(i)=val(l);
    end
    if chars(l,11+offset(l)) == '>'
    z(i)=str2num(chars(l,10+offset(l)));
    y(i)=str2num(chars(l,9+offset(l)))+10;
    x(i)=str2num(chars(l,8+offset(l)))+20;
    v(i)=val(l);
    end
    i=i+1;
end
end

for l=1:length-1
if chars(l,1)=='n' && chars(l,2)=='e' && chars(l,3)=='t' &&
chars(l,4)=='3' && chars(l,5)=='_' && chars(l,6)=='1'
    if chars(l,9+offset(l)) == '>'
    z(i)=str2num(chars(l,8+offset(l)));
    y(i)=0;
    x(i)=0+20;
    v(i)=val(l);
    end
    if chars(l,10+offset(l)) == '>'
    z(i)=str2num(chars(l,9+offset(l)));
    y(i)=str2num(chars(l,8+offset(l)));
    x(i)=0+20;
    v(i)=val(l);
    end
    if chars(l,11+offset(l)) == '>'
    z(i)=str2num(chars(l,10+offset(l)));
    y(i)=str2num(chars(l,9+offset(l)));
    x(i)=str2num(chars(l,8+offset(l)))+20;
    v(i)=val(l);
    end
    i=i+1;
end
end

for l=1:length-1
```

```
if chars(l,1)=='n' && chars(l,2)=='e' && chars(l,3)=='t' &&
chars(l,4)=='1' && chars(l,5)=='_' && chars(l,6)=='1'
    if chars(l,9+offset(l)) == '>'
    z(i)=str2num(chars(l,8+offset(l)));
    y(i)=0;
    x(i)=0;
    v(i)=val(l);
    end
    if chars(l,10+offset(l)) == '>'
    z(i)=str2num(chars(l,9+offset(l)));
    y(i)=str2num(chars(l,8+offset(l)));
    x(i)=0;
    v(i)=val(l);
    end
    if chars(l,11+offset(l)) == '>'
    z(i)=str2num(chars(l,10+offset(l)));
    y(i)=str2num(chars(l,9+offset(l)));
    x(i)=str2num(chars(l,8+offset(l)));
    v(i)=val(l);
    end
    i=i+1;
end
end

for l=1:length-1
if chars(l,1)=='n' && chars(l,2)=='e' && chars(l,3)=='t' &&
chars(l,4)=='1' && chars(l,5)=='_' && chars(l,6)=='2'
    if chars(l,9+offset(l)) == '>'
    z(i)=str2num(chars(l,8+offset(l)));
    y(i)=0+10;
    x(i)=0;
    v(i)=val(l);
    end
    if chars(l,10+offset(l)) == '>'
    z(i)=str2num(chars(l,9+offset(l)));
    y(i)=str2num(chars(l,8+offset(l)))+10;
    x(i)=0;
    v(i)=val(l);
    end
    if chars(l,11+offset(l)) == '>'
    z(i)=str2num(chars(l,10+offset(l)));
    y(i)=str2num(chars(l,9+offset(l)))+10;
    x(i)=str2num(chars(l,8+offset(l)));
    v(i)=val(l);
    end
    i=i+1;
end
end

for l=1:length-1
if chars(l,1)=='n' && chars(l,2)=='e' && chars(l,3)=='t' &&
chars(l,4)=='2' && chars(l,5)=='_' && chars(l,6)=='2'
    if chars(l,9+offset(l)) == '>'
    z(i)=str2num(chars(l,8+offset(l)));
    y(i)=0+10;
    x(i)=0+10;
    v(i)=val(l);
    end
    if chars(l,10+offset(l)) == '>'
    z(i)=str2num(chars(l,9+offset(l)));
    y(i)=str2num(chars(l,8+offset(l)))+10;
    x(i)=0+10;
    v(i)=val(l);
    end
```

```
    if chars(l,11+offset(l)) == '>'
    z(i)=str2num(chars(l,10+offset(l)));
    y(i)=str2num(chars(l,9+offset(l)))+10;
    x(i)=str2num(chars(l,8+offset(l)))+10;
    v(i)=val(l);
    end
    i=i+1;
end
end

for l=1:length-1
if chars(l,1)=='n' && chars(l,2)=='e' && chars(l,3)=='t' &&
chars(l,4)=='2' && chars(l,5)=='_' && chars(l,6)=='1'
    if chars(l,9+offset(l)) == '>'
    z(i)=str2num(chars(l,8+offset(l)));
    y(i)=0;
    x(i)=0+10;
    v(i)=val(l);
    end
    if chars(l,10+offset(l)) == '>'
    z(i)=str2num(chars(l,9+offset(l)));
    y(i)=str2num(chars(l,8+offset(l)));
    x(i)=0+10;
    v(i)=val(l);
    end
    if chars(l,11+offset(l)) == '>'
    z(i)=str2num(chars(l,10+offset(l)));
    y(i)=str2num(chars(l,9+offset(l)));
    x(i)=str2num(chars(l,8+offset(l)))+10;
    v(i)=val(l);
    end
    i=i+1;
end
end

for l=1:length-1
if chars(l,1)=='I' && chars(l,2)=='0' && chars(l,3)=='.' &&
chars(l,4)=='n' && chars(l,5)=='e' && chars(l,6)=='t' && chars(l,7)=='1'
&& chars(l,8)=='_' && chars(l,9)=='1'
    if chars(l,9+offset(l)) == '>'
    z(i)=str2num(chars(l,8+offset(l)));
    y(i)=0;
    x(i)=0;
    v(i)=val(l);
    end
    if chars(l,10+offset(l)) == '>'
    z(i)=str2num(chars(l,9+offset(l)));
    y(i)=str2num(chars(l,8+offset(l)));
    x(i)=0;
    v(i)=val(l);
    end
    if chars(l,11+offset(l)) == '>'
    z(i)=str2num(chars(l,10+offset(l)));
    y(i)=str2num(chars(l,9+offset(l)));
    x(i)=str2num(chars(l,8+offset(l)));
    v(i)=val(l);
    end
    i=i+1;
end
end

for l=1:length-1
```

```
if chars(l,1)=='I' && chars(l,2)=='0' && chars(l,3)=='.' &&
chars(l,4)=='n' && chars(l,5)=='e' && chars(l,6)=='t' && chars(l,7)=='1'
&& chars(l,8)=='_' && chars(l,9)=='2'
    if chars(l,9+offset(l)) == '>'
    z(i)=str2num(chars(l,8+offset(l)));
    y(i)=0+10;
    x(i)=0;
    v(i)=val(l);
    end
    if chars(l,10+offset(l)) == '>'
    z(i)=str2num(chars(l,9+offset(l)));
    y(i)=str2num(chars(l,8+offset(l)))+10;
    x(i)=0;
    v(i)=val(l);
    end
    if chars(l,11+offset(l)) == '>'
    z(i)=str2num(chars(l,10+offset(l)));
    y(i)=str2num(chars(l,9+offset(l)))+10;
    x(i)=str2num(chars(l,8+offset(l)));
    v(i)=val(l);
    end
    i=i+1;
end
end

for l=1:length-1
if chars(l,1)=='I' && chars(l,2)=='0' && chars(l,3)=='.' &&
chars(l,4)=='n' && chars(l,5)=='e' && chars(l,6)=='t' && chars(l,7)=='2'
&& chars(l,8)=='_' && chars(l,9)=='1'
    if chars(l,9+offset(l)) == '>'
    z(i)=str2num(chars(l,8+offset(l)));
    y(i)=0;
    x(i)=0+10;
    v(i)=val(l);
    end
    if chars(l,10+offset(l)) == '>'
    z(i)=str2num(chars(l,9+offset(l)));
    y(i)=str2num(chars(l,8+offset(l)));
    x(i)=0+10;
    v(i)=val(l);
    end
    if chars(l,11+offset(l)) == '>'
    z(i)=str2num(chars(l,10+offset(l)));
    y(i)=str2num(chars(l,9+offset(l)));
    x(i)=str2num(chars(l,8+offset(l)))+10;
    v(i)=val(l);
    end
    i=i+1;
end
end

for l=1:length-1
if chars(l,1)=='I' && chars(l,2)=='0' && chars(l,3)=='.' &&
chars(l,4)=='n' && chars(l,5)=='e' && chars(l,6)=='t' && chars(l,7)=='2'
&& chars(l,8)=='_' && chars(l,9)=='2'
    if chars(l,9+offset(l)) == '>'
    z(i)=str2num(chars(l,8+offset(l)));
    y(i)=0+10;
    x(i)=0+10;
    v(i)=val(l);
    end
    if chars(l,10+offset(l)) == '>'
    z(i)=str2num(chars(l,9+offset(l)));
    y(i)=str2num(chars(l,8+offset(l)))+10;
```

```
    x(i)=0+10;
    v(i)=val(l);
    end
    if chars(l,11+offset(l)) == '>'
    z(i)=str2num(chars(l,10+offset(l)));
    y(i)=str2num(chars(l,9+offset(l)))+10;
    x(i)=str2num(chars(l,8+offset(l)))+10;
    v(i)=val(l);
    end
    i=i+1;
end
end

for l=1:length-1
if chars(l,1)=='I' && chars(l,2)=='0' && chars(l,3)=='.' &&
chars(l,4)=='I' && chars(l,5)=='0' && chars(l,6)=='.' && chars(l,7)=='n'
&& chars(l,8)=='e' && chars(l,9)=='t'
    if chars(l,9+offset(l)) == '>'
    z(i)=str2num(chars(l,8+offset(l)));
    y(i)=0;
    x(i)=0;
    v(i)=val(l);
    end
    if chars(l,10+offset(l)) == '>'
    z(i)=str2num(chars(l,9+offset(l)));
    y(i)=str2num(chars(l,8+offset(l)));
    x(i)=0;
    v(i)=val(l);
    end
    if chars(l,11+offset(l)) == '>'
    z(i)=str2num(chars(l,10+offset(l)));
    y(i)=str2num(chars(l,9+offset(l)));
    x(i)=str2num(chars(l,8+offset(l)));
    v(i)=val(l);
    end
    i=i+1;
end
end

for l=1:length-1
if chars(l,1)=='I' && chars(l,2)=='0' && chars(l,3)=='.' &&
chars(l,4)=='I' && chars(l,5)=='1' && chars(l,6)=='.' && chars(l,7)=='n'
&& chars(l,8)=='e' && chars(l,9)=='t'
    if chars(l,9+offset(l)) == '>'
    z(i)=str2num(chars(l,8+offset(l)));
    y(i)=0;
    x(i)=0+10;
    v(i)=val(l);
    end
    if chars(l,10+offset(l)) == '>'
    z(i)=str2num(chars(l,9+offset(l)));
    y(i)=str2num(chars(l,8+offset(l)));
    x(i)=0+10;
    v(i)=val(l);
    end
    if chars(l,11+offset(l)) == '>'
    z(i)=str2num(chars(l,10+offset(l)));
    y(i)=str2num(chars(l,9+offset(l)));
    x(i)=str2num(chars(l,8+offset(l)))+10;
    v(i)=val(l);
    end
    i=i+1;
end
end
```

```
for l=1:length-1
if chars(l,1)=='I' && chars(l,2)=='0' && chars(l,3)=='.' &&
chars(l,4)=='I' && chars(l,5)=='2' && chars(l,6)=='.' && chars(l,7)=='n'
&& chars(l,8)=='e' && chars(l,9)=='t'
    if chars(l,9+offset(l)) == '>'
    z(i)=str2num(chars(l,8+offset(l)));
    y(i)=0+10;
    x(i)=0;
    v(i)=val(l);
    end
    if chars(l,10+offset(l)) == '>'
    z(i)=str2num(chars(l,9+offset(l)));
    y(i)=str2num(chars(l,8+offset(l)))+10;
    x(i)=0;
    v(i)=val(l);
    end
    if chars(l,11+offset(l)) == '>'
    z(i)=str2num(chars(l,10+offset(l)));
    y(i)=str2num(chars(l,9+offset(l)))+10;
    x(i)=str2num(chars(l,8+offset(l)));
    v(i)=val(l);
    end
    i=i+1;
end
end

for l=1:length-1
if chars(l,1)=='I' && chars(l,2)=='0' && chars(l,3)=='.' &&
chars(l,4)=='I' && chars(l,5)=='3' && chars(l,6)=='.' && chars(l,7)=='n'
&& chars(l,8)=='e' && chars(l,9)=='t'
    if chars(l,9+offset(l)) == '>'
    z(i)=str2num(chars(l,8+offset(l)));
    y(i)=0+10;
    x(i)=0+10;
    v(i)=val(l);
    end
    if chars(l,10+offset(l)) == '>'
    z(i)=str2num(chars(l,9+offset(l)));
    y(i)=str2num(chars(l,8+offset(l)))+10;
    x(i)=0+10;
    v(i)=val(l);
    end
    if chars(l,11+offset(l)) == '>'
    z(i)=str2num(chars(l,10+offset(l)));
    y(i)=str2num(chars(l,9+offset(l)))+10;
    x(i)=str2num(chars(l,8+offset(l)))+10;
    v(i)=val(l);
    end
    i=i+1;
end
end

%% Electrodes
i=1;
for l=1:length-1
if chars(l,1)=='I' && chars(l,2)=='0' && chars(l,3)=='.' &&
chars(l,4)=='n' && chars(l,5)=='e' && chars(l,6)=='t' && chars(l,7)=='e'
&& chars(l,8)=='1' && chars(l,9)=='_' && chars(l,10)=='1'
    if chars(l,9+offset(l)) == '>'
    ze(i)=str2num(chars(l,8+offset(l)));
    ye(i)=0;
    xe(i)=0;
    ve(i)=val(l);
```

```
    end
    if chars(l,10+offset(l)) == '>'
    ze(i)=str2num(chars(l,9+offset(l)));
    ye(i)=str2num(chars(l,8+offset(l)));
    xe(i)=0;
    ve(i)=val(l);
    end
    if chars(l,11+offset(l)) == '>'
    ze(i)=str2num(chars(l,10+offset(l)));
    ye(i)=str2num(chars(l,9+offset(l)));
    xe(i)=str2num(chars(l,8+offset(l)));
    ve(i)=val(l);
    end
    i=i+1;
end
end

for l=1:length-1
if chars(l,1)=='I' && chars(l,2)=='0' && chars(l,3)=='.' &&
chars(l,4)=='n' && chars(l,5)=='e' && chars(l,6)=='t' && chars(l,7)=='e'
&& chars(l,8)=='1' && chars(l,9)=='_' && chars(l,10)=='2'
    if chars(l,9+offset(l)) == '>'
    ze(i)=str2num(chars(l,8+offset(l)));
    ye(i)=0+10;
    xe(i)=0;
    ve(i)=val(l);
    end
    if chars(l,10+offset(l)) == '>'
    ze(i)=str2num(chars(l,9+offset(l)));
    ye(i)=str2num(chars(l,8+offset(l)))+10;
    xe(i)=0;
    ve(i)=val(l);
    end
    if chars(l,11+offset(l)) == '>'
    ze(i)=str2num(chars(l,10+offset(l)));
    ye(i)=str2num(chars(l,9+offset(l)))+10;
    xe(i)=str2num(chars(l,8+offset(l)));
    ve(i)=val(l);
    end
    i=i+1;
end
end

for l=1:length-1
if chars(l,1)=='I' && chars(l,2)=='0' && chars(l,3)=='.' &&
chars(l,4)=='n' && chars(l,5)=='e' && chars(l,6)=='t' && chars(l,7)=='e'
&& chars(l,8)=='2' && chars(l,9)=='_' && chars(l,10)=='1'
    if chars(l,9+offset(l)) == '>'
    ze(i)=str2num(chars(l,8+offset(l)));
    ye(i)=0;
    xe(i)=0+10;
    ve(i)=val(l);
    end
    if chars(l,10+offset(l)) == '>'
    ze(i)=str2num(chars(l,9+offset(l)));
    ye(i)=str2num(chars(l,8+offset(l)));
    xe(i)=0+10;
    ve(i)=val(l);
    end
    if chars(l,11+offset(l)) == '>'
    ze(i)=str2num(chars(l,10+offset(l)));
    ye(i)=str2num(chars(l,9+offset(l)));
    xe(i)=str2num(chars(l,8+offset(l)))+10;
    ve(i)=val(l);
```

```
    end
    i=i+1;
end
end

for l=1:length-1
if chars(l,1)=='I' && chars(l,2)=='0' && chars(l,3)=='.' &&
chars(l,4)=='n' && chars(l,5)=='e' && chars(l,6)=='t' && chars(l,7)=='e'
&& chars(l,8)=='2' && chars(l,9)=='_' && chars(l,10)=='2'
    if chars(l,9+offset(l)) == '>'
    ze(i)=str2num(chars(l,8+offset(l)));
    ye(i)=0+10;
    xe(i)=0+10;
    ve(i)=val(l);
    end
    if chars(l,10+offset(l)) == '>'
    ze(i)=str2num(chars(l,9+offset(l)));
    ye(i)=str2num(chars(l,8+offset(l)))+10;
    xe(i)=0+10;
    ve(i)=val(l);
    end
    if chars(l,11+offset(l)) == '>'
    ze(i)=str2num(chars(l,10+offset(l)));
    ye(i)=str2num(chars(l,9+offset(l)))+10;
    xe(i)=str2num(chars(l,8+offset(l)))+10;
    ve(i)=val(l);
    end
    i=i+1;
end
end

%% Output
for l=1:length-1
if chars(l,1)=='W' && chars(l,2)=='E' && chars(l,3)=='S'
    VWES=val(l);
end
end

v(1,:)=v(1,:)-VWES;

%Voltage in 3D co-ordinates
for i=1:4410
      vsort(y(1,i)+1,x(1,i)+1,z(1,i)+1)=v(1,i);
end

% Electric field in 3D co-ordinates
[Ex,Ey,Ez]=gradient(vsort);
Ex=-Ex*0.00001;
Ey=-Ey*0.00001;
Ez=-Ez*0.00001;
% X-Y as a matrix
 x2=[0:20; 0:20; 0:20; 0:20; 0:20; 0:20; 0:20; 0:20; 0:20; 0:20; 0:20;
0:20; 0:20; 0:20; 0:20; 0:20; 0:20; 0:20; 0:20; 0:20; 0:20; ];
 y2=x2';
 % electrodes  dots
 [xel yel]=size(xe);
dots=ones(1,yel);
dots=dots*(0.1);

% 3D co-ordinates matrix
for i=1:21
    for j=1:21
        for k=1:10
```

```
        x4(i,j,k)=x2(i,j);
        end
    end
end
for i=1:21
    for j=1:21
        for k=1:10
        y4(i,j,k)=y2(i,j);
        end
    end
end
z4=zeros(21,21,10);
for i=1:21
    for j=1:21
        for k=1:10
       z4(i,j,k)=k-1;
        end
    end
end

%% Figures
% Electrodes 2D
figure, image(B2);
set(gca,'YDir','normal')
hold on
scatter(10*xe,10*ye, 100, 'MarkerEdgeColor','k', 'Markerfacecolor', 'w');
axis([0,200,0,200])
ax=gca;
set(ax, 'FontName', 'Times New Roman', 'Fontsize', 30);
xlabel('x (\mum)','interpreter','Tex'); ylabel('y
(\mum)','interpreter','Tex');
axpos=get(ax, 'position');
axpos(3)=0.82*axpos(3);
set(ax,'position', axpos);
hold off

% Contour 2D
for a=1:10
    Ex2(:,:,a)=kron(10*Ex(:,:,a),ones(10));
    Ey2(:,:,a)=kron(10*Ey(:,:,a),ones(10));
    Ez2(:,:,a)=kron(10*Ez(:,:,a),ones(10));
end

Ix=Ex*1.6443;
Iy=Ey*1.6443;
Iz=Ez*1.6443;

figure
for a=1:10
  figure(a+1), contourf(10*x2,10*y2,vsort(:,:,a))
    ax=gca;
  colormap(hot);
set(ax, 'FontName', 'Times New Roman', 'Fontsize', 30);
xlabel('x (\mum)','interpreter','Tex'); ylabel('y
(\mum)','interpreter','Tex');
c=colorbar;
set(c, 'FontName', 'Times New Roman', 'Fontsize', 30);
 ylabel(c,'V')
hold on
scatter(10*xe,10*ye, 100,'MarkerEdgeColor','k', 'Markerfacecolor', 'w');
s1=streamslice(10*x2,10*y2,Ix(:,:,a),Iy(:,:,a),0.3,'arrowsmode');
set(s1, 'LineWidth',1.5, 'Color', 'b')
```

```
quiver(10*x2(1:2:end,1:2:end),10*y2(1:2:end,1:2:end),Ix(1:2:end,1:2:end,a
),Iy(1:2:end,1:2:end,a), 1.5, 'LineWidth',1.5, 'Color', 'b','EraseMode',
'background')
hold off
end

% Electrodes 3D
 figure,surf(xImage,yImage,zImage,...    %# Plot the surface
     'CData',B,...
     'FaceColor','texturemap');
hold on
scatter3(10*xe,10*ye,dots,100,'MarkerEdgeColor','k','Markerfacecolor',
'w');
axis([0,200,0,200,-30,90])
daspect([1,1,1])
ax=gca;
set(ax, 'FontName', 'Times New Roman', 'Fontsize', 30, 'XTick', [0 100
200], 'YTick', [0 100 200], 'ZTick', [0 40 80]);
xlabel('x (\mum)','interpreter','Tex'); ylabel('y
(\mum)','interpreter','Tex');zlabel('z (\mum)','interpreter','Tex');
grid on;
hold off
%Contour 3D
figure,contourslice(10*x4,10*y4,10*z4,vsort,[40:10:60,140:10:160],[40:10:
60,140:10:160],0:10:90,10)
colormap(jet)
ax=gca;
set(ax,  'FontName', 'Times New Roman', 'Fontsize', 15, 'ZTick', [0 20 40
60 80]);
axis([0,200,0,200,-30,90])
daspect([1,1,1])
box on

%3D volume
vrange=vsort(:,:,2:10);
minv=min(vrange(:));
maxv=max(vrange(:));
for i=1:9
    hold on
p1 = patch(isocaps(10*x4(11-i:1:11+i,11-i:1:11+i,1:i+1),10*y4(11-
i:1:11+i,11-i:1:11+i,1:i+1),10*z4(11-i:1:11+i,11-
i:1:11+i,1:i+1),vsort(11-i:1:11+i,11-
i:1:11+i,1:i+1),minv),'FaceColor','interp',...
'EdgeColor','none');
grid on;
colormap(jet(1000));
caxis([minv maxv])
alpha(1-0.05*i)
hold on
end
    hold on
p1 =
patch(isocaps(10*x4(1:1:21,1:1:21,1:10),10*y4(1:1:21,1:1:21,1:10),10*z4(1
:1:21,1:1:21,1:10),vsort(1:1:21,1:1:21,1:10),minv),'FaceColor','interp',.
..
'EdgeColor','none');
xlabel('x (\mum)','interpreter','Tex'); ylabel('y
(\mum)','interpreter','Tex');zlabel('z (\mum)','interpreter','Tex');
grid on;
colormap(jet(1000));
caxis([minv maxv])
c=colorbar;
set(c,  'FontName', 'Times New Roman', 'Fontsize', 15,  'YTick', [minv
maxv]);
```

```
ylabel(c,'V')
alpha(0.14)
hold on
surf(xImage,yImage,zImage,...    %# Plot the surface
     'CData',B,...
     'FaceColor','texturemap');
scatter3(10*xe,10*ye,dots, 100,'MarkerEdgeColor','k', 'Markerfacecolor',
'w');
hold off

figure
ax=gca;
set(ax, 'FontName', 'Times New Roman', 'Fontsize', 33,'ZTick', [0 30 60
90]);
axis([0,200,0,200,-30,90])
box off
%3D volume
[sx sy sz] = meshgrid(0:50:210,0:50:210,0:30:90);
for i=1:9
    hold on
p1 = patch(isocaps(10*x4(11-i:1:11+i,11-i:1:11+i,1:i+1),10*y4(11-
i:1:11+i,11-i:1:11+i,1:i+1),10*z4(11-i:1:11+i,11-
i:1:11+i,1:i+1),vsort(11-i:1:11+i,11-
i:1:11+i,1:i+1),minv),'FaceColor','interp',...
'EdgeColor','none');
grid on;
colormap(jet(1000));
caxis([minv maxv])
alpha(1-0.1*i)
hold on
end

    hold on
p1 =
patch(isocaps(10*x4(1:1:21,1:1:21,1:10),10*y4(1:1:21,1:1:21,1:10),10*z4(1
:1:21,1:1:21,1:10),vsort(1:1:21,1:1:21,1:10),minv),'FaceColor','interp',.
..
'EdgeColor','none');
xlabel('x (\mum)','interpreter','Tex'); ylabel('y
(\mum)','interpreter','Tex');zlabel('z (\mum)','interpreter','Tex');
grid on;
colormap(jet(1000));
caxis([minv maxv])
alpha(0.14)
hold on
surf(xImage,yImage,zImage,...    %# Plot the surface
     'CData',B,...
     'FaceColor','texturemap');
scatter3(10*xe,10*ye,dots, 100,'MarkerEdgeColor','k','Markerfacecolor',
'w');
hold on

XYZ=stream3(10*x4(1:1:end,1:1:end,:),10*y4(1:1:end,1:1:end,:),10*z4(1:1:e
nd,1:1:end,:),Ix(1:1:end,1:1:end,:),Iy(1:1:end,1:1:end,:),Iz(1:1:end,1:1:
end,:),sx,sy,sz);
s1=streamline(XYZ);
set(s1, 'LineWidth',1.5, 'Color', 'k')
quiver3(10*x4(1:3:end,1:3:end,:),10*y4(1:3:end,1:3:end,:),10*z4(1:3:end,1
:3:end,:),Ix(1:3:end,1:3:end,:),Iy(1:3:end,1:3:end,:),Iz(1:3:end,1:3:end,
:),10,'LineWidth',1.5, 'Color', 'k')
```

C.1.1.2 Electric field intensity map

The 2D and 3-D electric field intensity maps were produced using the following program (field_map.m):

```
clear;
close all;
[filename,pathname]=uigetfile('*.dc', 'Pick a file of x,y,z data');
fullpath=[pathname,filename];
imagepath=[pathname,'electrodes.bmp'];
imagepath2=[pathname,'electrodes2.bmp'];

A=imread(imagepath);
A2=imread(imagepath2);
B=255*ones(200,200,3);
B2=255*ones(200,200,3);
B=uint8(B);
B2=uint8(B2);
for i=1:190
    for j=1:190
        for k=1:3
       B(i+5,j+5,k)=A(i,j,k);
       B2(i+5,j+5,k)=A2(i,j,k);
        end
    end
end
xImage = [0 200; 0 200];
yImage = [200 200; 0 0];
zImage = [-30 -30; -30 -30];

figure(58),
image(A)
figure(59),
image(B)

[words, val]=textread(fullpath,'%s %f', 'commentstyle','shell');

chars=char(words);
[length,width]=size(chars);

for l=1:length-1
    for w=1:width
    if chars(l,w)=='<'
        offset(l,1)=w-7;
    end
    end
end

i=1;
%% Electrolyte voltages
for l=1:length-1
if chars(l,1)=='n' && chars(l,2)=='e' && chars(l,3)=='t' &&
chars(l,4)=='1' && chars(l,5)=='_' && chars(l,6)=='3'
    if chars(l,9+offset(l)) == '>'
    z(i)=str2num(chars(l,8+offset(l)));
    y(i)=0+20;
    x(i)=0;
    v(i)=val(l);
    end
    if chars(l,10+offset(l)) == '>'
```

```
    z(i)=str2num(chars(l,9+offset(l)));
    y(i)=str2num(chars(l,8+offset(l)))+20;
    x(i)=0;
    v(i)=val(l);
    end
    if chars(l,11+offset(l)) == '>'
    z(i)=str2num(chars(l,10+offset(l)));
    y(i)=str2num(chars(l,9+offset(l)))+20;
    x(i)=str2num(chars(l,8+offset(l)));
    v(i)=val(l);
    end
    i=i+1;
end
end

for l=1:length-1
if chars(l,1)=='n' && chars(l,2)=='e' && chars(l,3)=='t' &&
chars(l,4)=='2' && chars(l,5)=='_' && chars(l,6)=='3'
    if chars(l,9+offset(l)) == '>'
    z(i)=str2num(chars(l,8+offset(l)));
    y(i)=0+20;
    x(i)=0+10;
    v(i)=val(l);
    end
    if chars(l,10+offset(l)) == '>'
    z(i)=str2num(chars(l,9+offset(l)));
    y(i)=str2num(chars(l,8+offset(l)))+20;
    x(i)=0+10;
    v(i)=val(l);
    end
    if chars(l,11+offset(l)) == '>'
    z(i)=str2num(chars(l,10+offset(l)));
    y(i)=str2num(chars(l,9+offset(l)))+20;
    x(i)=str2num(chars(l,8+offset(l)))+10;
    v(i)=val(l);
    end
    i=i+1;
end
end

for l=1:length-1
if chars(l,1)=='n' && chars(l,2)=='e' && chars(l,3)=='t' &&
chars(l,4)=='i' && chars(l,5)=='3' && chars(l,6)=='_' && chars(l,7)=='3'
    if chars(l,9+offset(l)) == '>'
    z(i)=str2num(chars(l,8+offset(l)));
    y(i)=0+20;
    x(i)=0+20;
    v(i)=val(l);
    end
    if chars(l,10+offset(l)) == '>'
    z(i)=str2num(chars(l,9+offset(l)));
    y(i)=str2num(chars(l,8+offset(l)))+20;
    x(i)=0+20;
    v(i)=val(l);
    end
    if chars(l,11+offset(l)) == '>'
    z(i)=str2num(chars(l,10+offset(l)));
    y(i)=str2num(chars(l,9+offset(l)))+20;
    x(i)=str2num(chars(l,8+offset(l)))+20;
    v(i)=val(l);
    end
    i=i+1;
end
end
```

```
for l=1:length-1
if chars(l,1)=='n' && chars(l,2)=='e' && chars(l,3)=='t' &&
chars(l,4)=='3' && chars(l,5)=='_' && chars(l,6)=='2'
    if chars(l,9+offset(l)) == '>'
    z(i)=str2num(chars(l,8+offset(l)));
    y(i)=0+10;
    x(i)=0+20;
    v(i)=val(l);
    end
    if chars(l,10+offset(l)) == '>'
    z(i)=str2num(chars(l,9+offset(l)));
    y(i)=str2num(chars(l,8+offset(l)))+10;
    x(i)=0+20;
    v(i)=val(l);
    end
    if chars(l,11+offset(l)) == '>'
    z(i)=str2num(chars(l,10+offset(l)));
    y(i)=str2num(chars(l,9+offset(l)))+10;
    x(i)=str2num(chars(l,8+offset(l)))+20;
    v(i)=val(l);
    end
    i=i+1;
end
end

for l=1:length-1
if chars(l,1)=='n' && chars(l,2)=='e' && chars(l,3)=='t' &&
chars(l,4)=='3' && chars(l,5)=='_' && chars(l,6)=='1'
    if chars(l,9+offset(l)) == '>'
    z(i)=str2num(chars(l,8+offset(l)));
    y(i)=0;
    x(i)=0+20;
    v(i)=val(l);
    end
    if chars(l,10+offset(l)) == '>'
    z(i)=str2num(chars(l,9+offset(l)));
    y(i)=str2num(chars(l,8+offset(l)));
    x(i)=0+20;
    v(i)=val(l);
    end
    if chars(l,11+offset(l)) == '>'
    z(i)=str2num(chars(l,10+offset(l)));
    y(i)=str2num(chars(l,9+offset(l)));
    x(i)=str2num(chars(l,8+offset(l)))+20;
    v(i)=val(l);
    end
    i=i+1;
end
end

for l=1:length-1
if chars(l,1)=='n' && chars(l,2)=='e' && chars(l,3)=='t' &&
chars(l,4)=='1' && chars(l,5)=='_' && chars(l,6)=='1'
    if chars(l,9+offset(l)) == '>'
    z(i)=str2num(chars(l,8+offset(l)));
    y(i)=0;
    x(i)=0;
    v(i)=val(l);
    end
    if chars(l,10+offset(l)) == '>'
    z(i)=str2num(chars(l,9+offset(l)));
    y(i)=str2num(chars(l,8+offset(l)));
    x(i)=0;
```

```
    v(i)=val(l);
    end
    if chars(l,11+offset(l)) == '>'
    z(i)=str2num(chars(l,10+offset(l)));
    y(i)=str2num(chars(l,9+offset(l)));
    x(i)=str2num(chars(l,8+offset(l)));
    v(i)=val(l);
    end
    i=i+1;
end
end
for l=1:length-1
if chars(l,1)=='n' && chars(l,2)=='e' && chars(l,3)=='t' &&
chars(l,4)=='1' && chars(l,5)=='_' && chars(l,6)=='2'
    if chars(l,9+offset(l)) == '>'
    z(i)=str2num(chars(l,8+offset(l)));
    y(i)=0+10;
    x(i)=0;
    v(i)=val(l);
    end
    if chars(l,10+offset(l)) == '>'
    z(i)=str2num(chars(l,9+offset(l)));
    y(i)=str2num(chars(l,8+offset(l)))+10;
    x(i)=0;
    v(i)=val(l);
    end
    if chars(l,11+offset(l)) == '>'
    z(i)=str2num(chars(l,10+offset(l)));
    y(i)=str2num(chars(l,9+offset(l)))+10;
    x(i)=str2num(chars(l,8+offset(l)));
    v(i)=val(l);
    end
    i=i+1;
end
end

for l=1:length-1
if chars(l,1)=='n' && chars(l,2)=='e' && chars(l,3)=='t' &&
chars(l,4)=='2' && chars(l,5)=='_' && chars(l,6)=='2'
    if chars(l,9+offset(l)) == '>'
    z(i)=str2num(chars(l,8+offset(l)));
    y(i)=0+10;
    x(i)=0+10;
    v(i)=val(l);
    end
    if chars(l,10+offset(l)) == '>'
    z(i)=str2num(chars(l,9+offset(l)));
    y(i)=str2num(chars(l,8+offset(l)))+10;
    x(i)=0+10;
    v(i)=val(l);
    end
    if chars(l,11+offset(l)) == '>'
    z(i)=str2num(chars(l,10+offset(l)));
    y(i)=str2num(chars(l,9+offset(l)))+10;
    x(i)=str2num(chars(l,8+offset(l)))+10;
    v(i)=val(l);
    end
    i=i+1;
end
end

for l=1:length-1
if chars(l,1)=='n' && chars(l,2)=='e' && chars(l,3)=='t' &&
chars(l,4)=='2' && chars(l,5)=='_' && chars(l,6)=='1'
```

```
    if chars(l,9+offset(l)) == '>'
    z(i)=str2num(chars(l,8+offset(l)));
    y(i)=0;
    x(i)=0+10;
    v(i)=val(l);
    end
    if chars(l,10+offset(l)) == '>'
    z(i)=str2num(chars(l,9+offset(l)));
    y(i)=str2num(chars(l,8+offset(l)));
    x(i)=0+10;
    v(i)=val(l);
    end
    if chars(l,11+offset(l)) == '>'
    z(i)=str2num(chars(l,10+offset(l)));
    y(i)=str2num(chars(l,9+offset(l)));
    x(i)=str2num(chars(l,8+offset(l)))+10;
    v(i)=val(l);
    end
    i=i+1;
end
end

for l=1:length-1
if chars(l,1)=='I' && chars(l,2)=='0' && chars(l,3)=='.' &&
chars(l,4)=='n' && chars(l,5)=='e' && chars(l,6)=='t' && chars(l,7)=='1'
&& chars(l,8)=='_' && chars(l,9)=='1'
    if chars(l,9+offset(l)) == '>'
    z(i)=str2num(chars(l,8+offset(l)));
    y(i)=0;
    x(i)=0;
    v(i)=val(l);
    end
    if chars(l,10+offset(l)) == '>'
    z(i)=str2num(chars(l,9+offset(l)));
    y(i)=str2num(chars(l,8+offset(l)));
    x(i)=0;
    v(i)=val(l);
    end
    if chars(l,11+offset(l)) == '>'
    z(i)=str2num(chars(l,10+offset(l)));
    y(i)=str2num(chars(l,9+offset(l)));
    x(i)=str2num(chars(l,8+offset(l)));
    v(i)=val(l);
    end
    i=i+1;
end
end

for l=1:length-1
if chars(l,1)=='I' && chars(l,2)=='0' && chars(l,3)=='.' &&
chars(l,4)=='n' && chars(l,5)=='e' && chars(l,6)=='t' && chars(l,7)=='1'
&& chars(l,8)=='_' && chars(l,9)=='2'
    if chars(l,9+offset(l)) == '>'
    z(i)=str2num(chars(l,8+offset(l)));
    y(i)=0+10;
    x(i)=0;
    v(i)=val(l);
    end
    if chars(l,10+offset(l)) == '>'
    z(i)=str2num(chars(l,9+offset(l)));
    y(i)=str2num(chars(l,8+offset(l)))+10;
    x(i)=0;
    v(i)=val(l);
    end
```

```
    if chars(l,11+offset(l)) == '>'
    z(i)=str2num(chars(l,10+offset(l)));
    y(i)=str2num(chars(l,9+offset(l)))+10;
    x(i)=str2num(chars(l,8+offset(l)));
    v(i)=val(l);
    end
    i=i+1;
end
end

for l=1:length-1
if chars(l,1)=='I' && chars(l,2)=='0' && chars(l,3)=='.' &&
chars(l,4)=='n' && chars(l,5)=='e' && chars(l,6)=='t' && chars(l,7)=='2'
&& chars(l,8)=='_' && chars(l,9)=='1'
    if chars(l,9+offset(l)) == '>'
    z(i)=str2num(chars(l,8+offset(l)));
    y(i)=0;
    x(i)=0+10;
    v(i)=val(l);
    end
    if chars(l,10+offset(l)) == '>'
    z(i)=str2num(chars(l,9+offset(l)));
    y(i)=str2num(chars(l,8+offset(l)));
    x(i)=0+10;
    v(i)=val(l);
    end
    if chars(l,11+offset(l)) == '>'
    z(i)=str2num(chars(l,10+offset(l)));
    y(i)=str2num(chars(l,9+offset(l)));
    x(i)=str2num(chars(l,8+offset(l)))+10;
    v(i)=val(l);
    end
    i=i+1;
end
end

for l=1:length-1
if chars(l,1)=='I' && chars(l,2)=='0' && chars(l,3)=='.' &&
chars(l,4)=='n' && chars(l,5)=='e' && chars(l,6)=='t' && chars(l,7)=='2'
&& chars(l,8)=='_' && chars(l,9)=='2'
    if chars(l,9+offset(l)) == '>'
    z(i)=str2num(chars(l,8+offset(l)));
    y(i)=0+10;
    x(i)=0+10;
    v(i)=val(l);
    end
    if chars(l,10+offset(l)) == '>'
    z(i)=str2num(chars(l,9+offset(l)));
    y(i)=str2num(chars(l,8+offset(l)))+10;
    x(i)=0+10;
    v(i)=val(l);
    end
    if chars(l,11+offset(l)) == '>'
    z(i)=str2num(chars(l,10+offset(l)));
    y(i)=str2num(chars(l,9+offset(l)))+10;
    x(i)=str2num(chars(l,8+offset(l)))+10;
    v(i)=val(l);
    end
    i=i+1;
end
end

for l=1:length-1
```

```
if chars(l,1)=='I' && chars(l,2)=='0' && chars(l,3)=='.' &&
chars(l,4)=='I' && chars(l,5)=='0' && chars(l,6)=='.' && chars(l,7)=='n'
&& chars(l,8)=='e' && chars(l,9)=='t'
    if chars(l,9+offset(l)) == '>'
    z(i)=str2num(chars(l,8+offset(l)));
    y(i)=0;
    x(i)=0;
    v(i)=val(l);
    end
    if chars(l,10+offset(l)) == '>'
    z(i)=str2num(chars(l,9+offset(l)));
    y(i)=str2num(chars(l,8+offset(l)));
    x(i)=0;
    v(i)=val(l);
    end
    if chars(l,11+offset(l)) == '>'
    z(i)=str2num(chars(l,10+offset(l)));
    y(i)=str2num(chars(l,9+offset(l)));
    x(i)=str2num(chars(l,8+offset(l)));
    v(i)=val(l);
    end
    i=i+1;
end
end

for l=1:length-1
if chars(l,1)=='I' && chars(l,2)=='0' && chars(l,3)=='.' &&
chars(l,4)=='I' && chars(l,5)=='1' && chars(l,6)=='.' && chars(l,7)=='n'
&& chars(l,8)=='e' && chars(l,9)=='t'
    if chars(l,9+offset(l)) == '>'
    z(i)=str2num(chars(l,8+offset(l)));
    y(i)=0;
    x(i)=0+10;
    v(i)=val(l);
    end
    if chars(l,10+offset(l)) == '>'
    z(i)=str2num(chars(l,9+offset(l)));
    y(i)=str2num(chars(l,8+offset(l)));
    x(i)=0+10;
    v(i)=val(l);
    end
    if chars(l,11+offset(l)) == '>'
    z(i)=str2num(chars(l,10+offset(l)));
    y(i)=str2num(chars(l,9+offset(l)));
    x(i)=str2num(chars(l,8+offset(l)))+10;
    v(i)=val(l);
    end
    i=i+1;
end
end

for l=1:length-1
if chars(l,1)=='I' && chars(l,2)=='0' && chars(l,3)=='.' &&
chars(l,4)=='I' && chars(l,5)=='2' && chars(l,6)=='.' && chars(l,7)=='n'
&& chars(l,8)=='e' && chars(l,9)=='t'
    if chars(l,9+offset(l)) == '>'
    z(i)=str2num(chars(l,8+offset(l)));
    y(i)=0+10;
    x(i)=0;
    v(i)=val(l);
    end
    if chars(l,10+offset(l)) == '>'
    z(i)=str2num(chars(l,9+offset(l)));
    y(i)=str2num(chars(l,8+offset(l)))+10;
```

```
    x(i)=0;
    v(i)=val(l);
    end
    if chars(l,11+offset(l)) == '>'
    z(i)=str2num(chars(l,10+offset(l)));
    y(i)=str2num(chars(l,9+offset(l)))+10;
    x(i)=str2num(chars(l,8+offset(l)));
    v(i)=val(l);
    end
    i=i+1;
end
end
for l=1:length-1
if chars(l,1)=='I' && chars(l,2)=='0' && chars(l,3)=='.' &&
chars(l,4)=='I' && chars(l,5)=='3' && chars(l,6)=='.' && chars(l,7)=='n'
&& chars(l,8)=='e' && chars(l,9)=='t'
    if chars(l,9+offset(l)) == '>'
    z(i)=str2num(chars(l,8+offset(l)));
    y(i)=0+10;
    x(i)=0+10;
    v(i)=val(l);
    end
    if chars(l,10+offset(l)) == '>'
    z(i)=str2num(chars(l,9+offset(l)));
    y(i)=str2num(chars(l,8+offset(l)))+10;
    x(i)=0+10;
    v(i)=val(l);
    end
    if chars(l,11+offset(l)) == '>'
    z(i)=str2num(chars(l,10+offset(l)));
    y(i)=str2num(chars(l,9+offset(l)))+10;
    x(i)=str2num(chars(l,8+offset(l)))+10;
    v(i)=val(l);
    end
    i=i+1;
end
end

%% Electrodes
i=1;
for l=1:length-1
if chars(l,1)=='I' && chars(l,2)=='0' && chars(l,3)=='.' &&
chars(l,4)=='n' && chars(l,5)=='e' && chars(l,6)=='t' && chars(l,7)=='e'
&& chars(l,8)=='1' && chars(l,9)=='_' && chars(l,10)=='1'
    if chars(l,9+offset(l)) == '>'
    ze(i)=str2num(chars(l,8+offset(l)));
    ye(i)=0;
    xe(i)=0;
    ve(i)=val(l);
    end
    if chars(l,10+offset(l)) == '>'
    ze(i)=str2num(chars(l,9+offset(l)));
    ye(i)=str2num(chars(l,8+offset(l)));
    xe(i)=0;
    ve(i)=val(l);
    end
    if chars(l,11+offset(l)) == '>'
    ze(i)=str2num(chars(l,10+offset(l)));
    ye(i)=str2num(chars(l,9+offset(l)));
    xe(i)=str2num(chars(l,8+offset(l)));
    ve(i)=val(l);
    end
    i=i+1;
end
```

```
end

for l=1:length-1
if chars(l,1)=='I' && chars(l,2)=='0' && chars(l,3)=='.' &&
chars(l,4)=='n' && chars(l,5)=='e' && chars(l,6)=='t' && chars(l,7)=='e'
&& chars(l,8)=='1' && chars(l,9)=='_' && chars(l,10)=='2'
    if chars(l,9+offset(l)) == '>'
    ze(i)=str2num(chars(l,8+offset(l)));
    ye(i)=0+10;
    xe(i)=0;
    ve(i)=val(l);
    end
    if chars(l,10+offset(l)) == '>'
    ze(i)=str2num(chars(l,9+offset(l)));
    ye(i)=str2num(chars(l,8+offset(l)))+10;
    xe(i)=0;
    ve(i)=val(l);
    end
    if chars(l,11+offset(l)) == '>'
    ze(i)=str2num(chars(l,10+offset(l)));
    ye(i)=str2num(chars(l,9+offset(l)))+10;
    xe(i)=str2num(chars(l,8+offset(l)));
    ve(i)=val(l);
    end
    i=i+1;
end
end

for l=1:length-1
if chars(l,1)=='I' && chars(l,2)=='0' && chars(l,3)=='.' &&
chars(l,4)=='n' && chars(l,5)=='e' && chars(l,6)=='t' && chars(l,7)=='e'
&& chars(l,8)=='2' && chars(l,9)=='_' && chars(l,10)=='1'
    if chars(l,9+offset(l)) == '>'
    ze(i)=str2num(chars(l,8+offset(l)));
    ye(i)=0;
    xe(i)=0+10;
    ve(i)=val(l);
    end
    if chars(l,10+offset(l)) == '>'
    ze(i)=str2num(chars(l,9+offset(l)));
    ye(i)=str2num(chars(l,8+offset(l)));
    xe(i)=0+10;
    ve(i)=val(l);
    end
    if chars(l,11+offset(l)) == '>'
    ze(i)=str2num(chars(l,10+offset(l)));
    ye(i)=str2num(chars(l,9+offset(l)));
    xe(i)=str2num(chars(l,8+offset(l)))+10;
    ve(i)=val(l);
    end
    i=i+1;
end
end

for l=1:length-1
if chars(l,1)=='I' && chars(l,2)=='0' && chars(l,3)=='.' &&
chars(l,4)=='n' && chars(l,5)=='e' && chars(l,6)=='t' && chars(l,7)=='e'
&& chars(l,8)=='2' && chars(l,9)=='_' && chars(l,10)=='2'
    if chars(l,9+offset(l)) == '>'
    ze(i)=str2num(chars(l,8+offset(l)));
    ye(i)=0+10;
    xe(i)=0+10;
    ve(i)=val(l);
    end
```

```
    if chars(l,10+offset(l)) == '>'
    ze(i)=str2num(chars(l,9+offset(l)));
    ye(i)=str2num(chars(l,8+offset(l)))+10;
    xe(i)=0+10;
    ve(i)=val(l);
    end
    if chars(l,11+offset(l)) == '>'
    ze(i)=str2num(chars(l,10+offset(l)));
    ye(i)=str2num(chars(l,9+offset(l)))+10;
    xe(i)=str2num(chars(l,8+offset(l)))+10;
    ve(i)=val(l);
    end
    i=i+1;
end
end

%% Output
for l=1:length-1
if chars(l,1)=='W' && chars(l,2)=='E' && chars(l,3)=='S'
    VWES=val(l);
end
end

v(1,:)=v(1,:)-VWES;

%Voltage in 3D co-ordinates
for i=1:4410
      vsort(y(1,i)+1,x(1,i)+1,z(1,i)+1)=v(1,i);
end
% Electric field in 3D co-ordinates
[Ex,Ey,Ez]=gradient(vsort);
Ex=-Ex*0.00001;
Ey=-Ey*0.00001;
Ez=-Ez*0.00001;
 E2D = sqrt(Ex.^2+Ey.^2);
 E3D = sqrt(Ex.^2+Ey.^2+Ez.^2);
% X-Y as a matrix
 x2=[0:20; 0:20; 0:20; 0:20; 0:20; 0:20; 0:20; 0:20; 0:20; 0:20; 0:20;
0:20; 0:20; 0:20; 0:20; 0:20; 0:20; 0:20; 0:20; 0:20; 0:20; ];
 y2=x2';
 x2zlin=0:1:20;
 z2lin=0:1:9;
 [x2z,z2]=meshgrid(x2zlin,z2lin);
 % electrodes  dots
 [xel yel]=size(xe);
dots=ones(1,yel);
dots=dots*0.01;
% 3D co-ordinates matrix
for i=1:21
    for j=1:21
        for k=1:10
        x4(i,j,k)=x2(i,j);
        end
    end
end
for i=1:21
    for j=1:21
        for k=1:10
        y4(i,j,k)=y2(i,j);
        end
    end
end
z4=zeros(21,21,10);
for i=1:21
```

```
    for j=1:21
        for k=1:10
       z4(i,j,k)=k-1;
        end
    end
end

%% Figures
% Electrodes 2D
figure, scatter(10*xe,10*ye, 100, 'MarkerEdgeColor','k',
'Markerfacecolor', 'w');
axis([0,200,0,200])
ax=gca;
set(ax, 'FontName', 'Times New Roman', 'Fontsize', 30);
xlabel('x (\mum)','interpreter','Tex'); ylabel('y
(\mum)','interpreter','Tex');
axpos=get(ax, 'position');
axpos(3)=0.82*axpos(3);
set(ax,'position', axpos);

% Contour 2D
for a=1:10
    Exuseless(:,:,a)=kron(10*Ex(:,:,a),ones(10));
    Eyuseless(:,:,a)=kron(10*Ey(:,:,a),ones(10));
    Ezuseless(:,:,a)=kron(10*Ez(:,:,a),ones(10));
end

%% XY
figure
for a=1:10
  figure(a+1), contourf(10*x2,10*y2,E3D(:,:,a))
    ax=gca;
  colormap(jet);
set(ax, 'FontName', 'Times New Roman', 'Fontsize', 30);
xlabel('x (\mum)','interpreter','Tex'); ylabel('y
(\mum)','interpreter','Tex');
c=colorbar;
set(c, 'FontName', 'Times New Roman', 'Fontsize', 30);
  ylabel(c,'$$\frac{V}{m}$$','interpreter','latex','Rotation',0)
hold on
scatter(10*xe,10*ye, 100,'MarkerEdgeColor','k', 'Markerfacecolor', 'w');
s1=streamslice(10*x2,10*y2,Ex(:,:,a),Ey(:,:,a),0.3,'arrowsmode');
set(s1, 'LineWidth',1.5, 'Color', 'm')
quiver(10*x2(1:2:end,1:2:end),10*y2(1:2:end,1:2:end),Ex(1:2:end,1:2:end,a
),Ey(1:2:end,1:2:end,a), 1.5, 'LineWidth',1.5, 'Color', 'm','EraseMode',
'background')
hold off
end

%% XZ
for i=1:21
E2Dtemp(:,:)=E3D(i,:,:);
ZE3D(:,:,i)=E2Dtemp';

Extemp(:,:)=Ex(i,:,:);
Ex2(:,:,i)=Extemp';

Eytemp(:,:)=Ey(i,:,:);
Ey2(:,:,i)=Eytemp';

Eztemp(:,:)=Ez(i,:,:);
Ez2(:,:,i)=Eztemp';
end
```

```
figure
for a=1:21
  figure(a+11), contourf(10*x2z,10*z2,ZE3D(:,:,a))
    ax=gca;
  colormap(jet);
set(ax, 'FontName', 'Times New Roman', 'Fontsize', 30);
xlabel('x (\mum)','interpreter','Tex'); ylabel('z
(\mum)','interpreter','Tex');
c=colorbar;
 set(c, 'FontName', 'Times New Roman', 'Fontsize', 30);
 ylabel(c,'$$\frac{V}{m}$$','interpreter','latex','Rotation',0)

hold on
[lengthe,widthe]=size(ye);
xe2=30*ones(widthe,21);
ze2=30*ones(widthe,21);
j=1;
for i=1:widthe
    if ye(i)==a-1
        xe2(j,a)=xe(i);
        ze2(j,a)=ze(i);
        j=j+1;
    end
end

scatter(10*xe2(:,a),10*ze2(:,a), 100,'MarkerEdgeColor','k',
'Markerfacecolor', 'w');
s1=streamslice(10*x2z,10*z2,Ex2(:,:,a),Ez2(:,:,a),0.3,'arrowsmode');
set(s1, 'LineWidth',1.5, 'Color', 'm')
quiver(10*x2z(1:2:end,1:2:end),10*z2(1:2:end,1:2:end),Ex2(1:2:end,1:2:end
,a),Ez2(1:2:end,1:2:end,a), 1.5, 'LineWidth',1.5, 'Color',
'm','EraseMode', 'background')
hold off
end

%% YZ
for i=1:21
E2Dtemp(:,:)=E3D(:,i,:);
ZE3D2(:,:,i)=E2Dtemp';

Extemp(:,:)=Ex(:,i,:);
Ex3(:,:,i)=Extemp';

Eytemp(:,:)=Ey(:,i,:);
Ey3(:,:,i)=Eytemp';

Eztemp(:,:)=Ez(:,i,:);
Ez3(:,:,i)=Eztemp';
end
figure
for a=1:21
  figure(a+32), contourf(10*x2z,10*z2,ZE3D2(:,:,a))
    ax=gca;
  colormap(jet);
set(ax, 'FontName', 'Times New Roman', 'Fontsize', 30);
xlabel('y (\mum)','interpreter','Tex'); ylabel('z
(\mum)','interpreter','Tex');
set(c, 'FontName', 'Times New Roman', 'Fontsize', 30);
 ylabel(c,'$$\frac{V}{m}$$','interpreter','latex','Rotation',0)
hold on
[lengthe,widthe]=size(xe);
ye3=30*ones(widthe,21);
ze3=30*ones(widthe,21);
```

```
j=1;
for i=1:widthe
    if xe(i)==a-1
        ye3(j,a)=ye(i);
        ze3(j,a)=ze(i);
        j=j+1;
    end
end

scatter(10*ye3(:,a),10*ze3(:,a), 100,'MarkerEdgeColor','k',
'Markerfacecolor', 'w');
s1=streamslice(10*x2z,10*z2,Ey3(:,:,a),Ez3(:,:,a),0.3,'arrowsmode');
set(s1, 'LineWidth',1.5, 'Color', 'm')
quiver(10*x2z(1:2:end,1:2:end),10*z2(1:2:end,1:2:end),Ey3(1:2:end,1:2:end
,a),Ez3(1:2:end,1:2:end,a), 1.5, 'LineWidth',1.5, 'Color',
'm','EraseMode', 'background')
hold off
end

%% 3D
% Electrodes 3D
 figure,surf(xImage,yImage,zImage,...    %# Plot the surface
     'CData',B,...
     'FaceColor','texturemap');
hold on
scatter3(10*xe,10*ye,dots,100,'MarkerEdgeColor','k','Markerfacecolor',
'w');
axis([0,200,0,200,-30,90])
daspect([1,1,1])
ax=gca;
set(ax, 'FontName', 'Times New Roman', 'Fontsize', 30, 'XTick', [0 100
200], 'YTick', [0 100 200], 'ZTick', [0 40 80]);
xlabel('x (\mum)','interpreter','Tex'); ylabel('y
(\mum)','interpreter','Tex');zlabel('z (\mum)','interpreter','Tex');
grid on;
hold off

%Contour 3D
figure,
contourslice(10*x4,10*y4,10*z4,E3D,[40:10:60,140:10:160],[40:10:60,140:10
:160],0:10:90,10)
colormap(jet)
ax=gca;
set(ax,  'FontName', 'Times New Roman', 'Fontsize', 15);
axis([0,200,0,200,-30,90])
daspect([1,1,1])
box on

%3D volume
E3Drange=E3D(:,:,1:10);
minE=min(E3Drange(:));
maxE=max(E3Drange(:));
for i=1:9
    hold on
p1 = patch(isocaps(10*x4(11-i:1:11+i,11-i:1:11+i,1:i+1),10*y4(11-
i:1:11+i,11-i:1:11+i,1:i+1),10*z4(11-i:1:11+i,11-i:1:11+i,1:i+1),E3D(11-
i:1:11+i,11-i:1:11+i,1:i+1),min(E3D(:))),'FaceColor','interp',...
'EdgeColor','none');
grid on;
colormap(jet(1000));
caxis([minE maxE])
alpha(1-0.05*i)
hold on
end
```

```
    hold on
p1 =
patch(isocaps(10*x4(1:1:21,1:1:21,1:10),10*y4(1:1:21,1:1:21,1:10),10*z4(1
:1:21,1:1:21,1:10),E3D(1:1:21,1:1:21,1:10),min(E3D(:))),'FaceColor','inte
rp',...
'EdgeColor','none');
xlabel('x (\mum)','interpreter','Tex'); ylabel('y
(\mum)','interpreter','Tex');zlabel('z (\mum)','interpreter','Tex');
grid on;
colormap(jet(1000));
caxis([minE maxE])
c=colorbar;
set(c,  'FontName', 'Times New Roman', 'Fontsize', 15);
ylabel(c,'$$\frac{V}{m}$$','interpreter','latex','Rotation',0)
alpha(0.1)
hold on
surf(xImage,yImage,zImage,...    %# Plot the surface
     'CData',B,...
     'FaceColor','texturemap');
scatter3(10*xe,10*ye,dots, 100,'MarkerEdgeColor','k', 'Markerfacecolor',
'w');
hold off

figure
ax=gca;
set(ax, 'FontName', 'Times New Roman', 'Fontsize', 15);
axis([0,200,0,200,-30,90])
box on
%3D volume
[sx sy sz] = meshgrid(0:50:210,0:50:210,0:30:90);
for i=1:9
    hold on
p1 = patch(isocaps(10*x4(11-i:1:11+i,11-i:1:11+i,1:i+1),10*y4(11-
i:1:11+i,11-i:1:11+i,1:i+1),10*z4(11-i:1:11+i,11-i:1:11+i,1:i+1),E3D(11-
i:1:11+i,11-i:1:11+i,1:i+1),min(E3D(:))),...
'FaceColor','interp','EdgeColor','none');
grid on;
colormap(jet(1000));
caxis([minE maxE])
alpha(1-0.1*i)
hold on
end
    hold on
p2 =
patch(isocaps(10*x4(1:1:21,1:1:21,1:10),10*y4(1:1:21,1:1:21,1:10),10*z4(1
:1:21,1:1:21,1:10),E3D(1:1:21,1:1:21,1:10),min(E3D(:))),...
'FaceColor','interp','EdgeColor','none');
xlabel('x (\mum)','interpreter','Tex'); ylabel('y
(\mum)','interpreter','Tex');zlabel('z (\mum)','interpreter','Tex');
grid on;
colormap(jet(1000));
caxis([minE maxE])
c=colorbar;
set(c, 'FontName', 'Times New Roman', 'Fontsize', 15);
ylabel(c,'$$\frac{V}{m}$$','interpreter','latex','Rotation',0)
alpha(0.15)
hold on
surf(xImage,yImage,zImage,...    %# Plot the surface
     'CData',B,...
     'FaceColor','texturemap');
scatter3(10*xe,10*ye,dots, 100,'MarkerEdgeColor','k','Markerfacecolor',
'w');
hold on
```

```
XYZ=stream3(10*x4(1:1:end,1:1:end,:),10*y4(1:1:end,1:1:end,:),10*z4(1:1:e
nd,1:1:end,:),Ex(1:1:end,1:1:end,:),Ey(1:1:end,1:1:end,:),Ez(1:1:end,1:1:
end,:),sx,sy,sz);
s1=streamline(XYZ);
set(s1, 'LineWidth',1.5, 'Color', 'k')
quiver3(10*x4(1:3:end,1:3:end),10*y4(1:3:end,1:3:end),10*z4(1:3:end,1:3:e
nd),Ex(1:3:end,1:3:end),Ey(1:3:end,1:3:end),Ez(1:3:end,1:3:end),10,'LineW
idth',1.5, 'Color', 'k')
hold off

%% 3D slices
figure, slice(10*x4,10*y4,10*z4,E3D,50,150,0)
colormap(jet)
ax=gca;
set(ax,  'FontName', 'Times New Roman', 'Fontsize', 15);
axis([0,200,0,200,-30,90])
daspect([1,1,1])
box on
view(3)
axis on;
grid on;
shading interp;
hold on
scatter3(10*xe,10*ye,dots, 100,'MarkerEdgeColor','k', 'Markerfacecolor',
'w');
surf(xImage,yImage,zImage,...    %# Plot the surface
     'CData',B,...
     'FaceColor','texturemap');
[sx2 sy2 sz2] = meshgrid(50,150,0);
s2=streamslice(10*x4(1:1:end,1:1:end,:),10*y4(1:1:end,1:1:end,:),10*z4(1:
1:end,1:1:end,:),Ex(1:1:end,1:1:end,:),Ey(1:1:end,1:1:end,:),Ez(1:1:end,1
:1:end,:),sx2,sy2,sz2,0.5);
set(s2, 'LineWidth',1.5, 'Color', 'm')
set(ax, 'FontName', 'Times New Roman', 'Fontsize', 30, 'XTick', [0 100
200], 'YTick', [0 100 200], 'ZTick', [0 40 80]);
xlabel('x (\mum)','interpreter','Tex'); ylabel('y
(\mum)','interpreter','Tex');zlabel('z (\mum)','interpreter','Tex');
grid on;
colormap(jet(1000));
caxis([minE maxE])
%c=colorbar;
set(c, 'FontName', 'Times New Roman', 'Fontsize', 15);
ylabel(c,'$$\frac{V}{m}$$','interpreter','latex','Rotation',0)
```

C.1.2 Adjacent Fully-differential Electrochemical Cells

C.1.2.1 Potential map

The 2-D and 3-D electrical potential maps along with the current density streamlines of fully differential electrochemical cells at different potential settings and placed side-by-side were produced using the following program (voltage_map_cells_FD_v4.m):

```
clear;
close all;
[filename,pathname]=uigetfile('*.dc', 'Pick a file of x,y,z data');
fullpath=[pathname,filename];
imagepath=[pathname,'electrodes.bmp'];
imagepath2=[pathname,'electrodes2.bmp'];

A=imread(imagepath);
A2=imread(imagepath2);
B=255*ones(200,200,3);
B2=255*ones(200,200,3);
B=uint8(B);
B2=uint8(B2);
for i=1:190
    for j=1:190
        for k=1:3
       B(i+5,j+5,k)=A(i,j,k);
       B2(i+5,j+5,k)=A2(i,j,k);
        end
    end
end
xImage = [0 200; 0 200];
yImage = [200 200; 0 0];
zImage = [-30 -30; -30 -30];

figure(73),
image(A)
figure(74),
image(B)

[words, val]=textread(fullpath,'%s %f', 'commentstyle','shell');

chars=char(words);
[length,width]=size(chars);

for l=1:length-1
    for w=1:width
    if chars(l,w)=='<'
        offset(l,1)=w-7;
    end
    end
end

i=1;
%% Electrolyte voltages cell 1
for l=1:length-1
if chars(l,1)=='n' && chars(l,2)=='e' && chars(l,3)=='t' &&
chars(l,4)=='1' && chars(l,5)=='_' && chars(l,6)=='3'
    if chars(l,9+offset(l)) == '>'
```

```
    z(i)=str2num(chars(l,8+offset(l)));
    y(i)=0+20;
    x(i)=0;
    v(i)=val(l);
    end
    if chars(l,10+offset(l)) == '>'
    z(i)=str2num(chars(l,9+offset(l)));
    y(i)=str2num(chars(l,8+offset(l)))+20;
    x(i)=0;
    v(i)=val(l);
    end
    if chars(l,11+offset(l)) == '>'
    z(i)=str2num(chars(l,10+offset(l)));
    y(i)=str2num(chars(l,9+offset(l)))+20;
    x(i)=str2num(chars(l,8+offset(l)));
    v(i)=val(l);
    end
    i=i+1;
end
end

for l=1:length-1
if chars(l,1)=='n' && chars(l,2)=='e' && chars(l,3)=='t' &&
chars(l,4)=='2' && chars(l,5)=='_' && chars(l,6)=='3'
    if chars(l,9+offset(l)) == '>'
    z(i)=str2num(chars(l,8+offset(l)));
    y(i)=0+20;
    x(i)=0+10;
    v(i)=val(l);
    end
    if chars(l,10+offset(l)) == '>'
    z(i)=str2num(chars(l,9+offset(l)));
    y(i)=str2num(chars(l,8+offset(l)))+20;
    x(i)=0+10;
    v(i)=val(l);
    end
    if chars(l,11+offset(l)) == '>'
    z(i)=str2num(chars(l,10+offset(l)));
    y(i)=str2num(chars(l,9+offset(l)))+20;
    x(i)=str2num(chars(l,8+offset(l)))+10;
    v(i)=val(l);
    end
    i=i+1;
end
end

for l=1:length-1
if chars(l,1)=='n' && chars(l,2)=='e' && chars(l,3)=='t' &&
chars(l,4)=='1' && chars(l,5)=='_' && chars(l,6)=='1'
    if chars(l,9+offset(l)) == '>'
    z(i)=str2num(chars(l,8+offset(l)));
    y(i)=0;
    x(i)=0;
    v(i)=val(l);
    end
    if chars(l,10+offset(l)) == '>'
    z(i)=str2num(chars(l,9+offset(l)));
    y(i)=str2num(chars(l,8+offset(l)));
    x(i)=0;
    v(i)=val(l);
    end
    if chars(l,11+offset(l)) == '>'
    z(i)=str2num(chars(l,10+offset(l)));
    y(i)=str2num(chars(l,9+offset(l)));
```

```
    x(i)=str2num(chars(l,8+offset(l)));
    v(i)=val(l);
    end
    i=i+1;
end
end

for l=1:length-1
if chars(l,1)=='n' && chars(l,2)=='e' && chars(l,3)=='t' &&
chars(l,4)=='1' && chars(l,5)=='_' && chars(l,6)=='2'
    if chars(l,9+offset(l)) == '>'
    z(i)=str2num(chars(l,8+offset(l)));
    y(i)=0+10;
    x(i)=0;
    v(i)=val(l);
    end
    if chars(l,10+offset(l)) == '>'
    z(i)=str2num(chars(l,9+offset(l)));
    y(i)=str2num(chars(l,8+offset(l)))+10;
    x(i)=0;
    v(i)=val(l);
    end
    if chars(l,11+offset(l)) == '>'
    z(i)=str2num(chars(l,10+offset(l)));
    y(i)=str2num(chars(l,9+offset(l)))+10;
    x(i)=str2num(chars(l,8+offset(l)));
    v(i)=val(l);
    end
    i=i+1;
end
end

for l=1:length-1
if chars(l,1)=='n' && chars(l,2)=='e' && chars(l,3)=='t' &&
chars(l,4)=='2' && chars(l,5)=='_' && chars(l,6)=='2'
    if chars(l,9+offset(l)) == '>'
    z(i)=str2num(chars(l,8+offset(l)));
    y(i)=0+10;
    x(i)=0+10;
    v(i)=val(l);
    end
    if chars(l,10+offset(l)) == '>'
    z(i)=str2num(chars(l,9+offset(l)));
    y(i)=str2num(chars(l,8+offset(l)))+10;
    x(i)=0+10;
    v(i)=val(l);
    end
    if chars(l,11+offset(l)) == '>'
    z(i)=str2num(chars(l,10+offset(l)));
    y(i)=str2num(chars(l,9+offset(l)))+10;
    x(i)=str2num(chars(l,8+offset(l)))+10;
    v(i)=val(l);
    end
    i=i+1;
end
end

for l=1:length-1
if chars(l,1)=='n' && chars(l,2)=='e' && chars(l,3)=='t' &&
chars(l,4)=='2' && chars(l,5)=='_' && chars(l,6)=='1'
    if chars(l,9+offset(l)) == '>'
    z(i)=str2num(chars(l,8+offset(l)));
    y(i)=0;
    x(i)=0+10;
```

```
    v(i)=val(l);
    end
    if chars(l,10+offset(l)) == '>'
    z(i)=str2num(chars(l,9+offset(l)));
    y(i)=str2num(chars(l,8+offset(l)));
    x(i)=0+10;
    v(i)=val(l);
    end
    if chars(l,11+offset(l)) == '>'
    z(i)=str2num(chars(l,10+offset(l)));
    y(i)=str2num(chars(l,9+offset(l)));
    x(i)=str2num(chars(l,8+offset(l)))+10;
    v(i)=val(l);
    end
    i=i+1;
end
end

for l=1:length-1
if chars(l,1)=='I' && chars(l,2)=='0' && chars(l,3)=='.' &&
chars(l,4)=='n' && chars(l,5)=='e' && chars(l,6)=='t' && chars(l,7)=='1'
&& chars(l,8)=='_' && chars(l,9)=='1'
    if chars(l,9+offset(l)) == '>'
    z(i)=str2num(chars(l,8+offset(l)));
    y(i)=0;
    x(i)=0;
    v(i)=val(l);
    end
    if chars(l,10+offset(l)) == '>'
    z(i)=str2num(chars(l,9+offset(l)));
    y(i)=str2num(chars(l,8+offset(l)));
    x(i)=0;
    v(i)=val(l);
    end
    if chars(l,11+offset(l)) == '>'
    z(i)=str2num(chars(l,10+offset(l)));
    y(i)=str2num(chars(l,9+offset(l)));
    x(i)=str2num(chars(l,8+offset(l)));
    v(i)=val(l);
    end
    i=i+1;
end
end

for l=1:length-1
if chars(l,1)=='I' && chars(l,2)=='0' && chars(l,3)=='.' &&
chars(l,4)=='n' && chars(l,5)=='e' && chars(l,6)=='t' && chars(l,7)=='1'
&& chars(l,8)=='_' && chars(l,9)=='2'
    if chars(l,9+offset(l)) == '>'
    z(i)=str2num(chars(l,8+offset(l)));
    y(i)=0+10;
    x(i)=0;
    v(i)=val(l);
    end
    if chars(l,10+offset(l)) == '>'
    z(i)=str2num(chars(l,9+offset(l)));
    y(i)=str2num(chars(l,8+offset(l)))+10;
    x(i)=0;
    v(i)=val(l);
    end
    if chars(l,11+offset(l)) == '>'
    z(i)=str2num(chars(l,10+offset(l)));
    y(i)=str2num(chars(l,9+offset(l)))+10;
    x(i)=str2num(chars(l,8+offset(l)));
```

```
    v(i)=val(l);
    end
    i=i+1;
end
end

for l=1:length-1
if chars(l,1)=='I' && chars(l,2)=='0' && chars(l,3)=='.' &&
chars(l,4)=='n' && chars(l,5)=='e' && chars(l,6)=='t' && chars(l,7)=='2'
&& chars(l,8)=='_' && chars(l,9)=='1'
    if chars(l,9+offset(l)) == '>'
    z(i)=str2num(chars(l,8+offset(l)));
    y(i)=0;
    x(i)=0+10;
    v(i)=val(l);
    end
    if chars(l,10+offset(l)) == '>'
    z(i)=str2num(chars(l,9+offset(l)));
    y(i)=str2num(chars(l,8+offset(l)));
    x(i)=0+10;
    v(i)=val(l);
    end
    if chars(l,11+offset(l)) == '>'
    z(i)=str2num(chars(l,10+offset(l)));
    y(i)=str2num(chars(l,9+offset(l)));
    x(i)=str2num(chars(l,8+offset(l)))+10;
    v(i)=val(l);
    end
    i=i+1;
end
end

for l=1:length-1
if chars(l,1)=='I' && chars(l,2)=='0' && chars(l,3)=='.' &&
chars(l,4)=='n' && chars(l,5)=='e' && chars(l,6)=='t' && chars(l,7)=='2'
&& chars(l,8)=='_' && chars(l,9)=='2'
    if chars(l,9+offset(l)) == '>'
    z(i)=str2num(chars(l,8+offset(l)));
    y(i)=0+10;
    x(i)=0+10;
    v(i)=val(l);
    end
    if chars(l,10+offset(l)) == '>'
    z(i)=str2num(chars(l,9+offset(l)));
    y(i)=str2num(chars(l,8+offset(l)))+10;
    x(i)=0+10;
    v(i)=val(l);
    end
    if chars(l,11+offset(l)) == '>'
    z(i)=str2num(chars(l,10+offset(l)));
    y(i)=str2num(chars(l,9+offset(l)))+10;
    x(i)=str2num(chars(l,8+offset(l)))+10;
    v(i)=val(l);
    end
    i=i+1;
end
end

for l=1:length-1
if chars(l,1)=='I' && chars(l,2)=='0' && chars(l,3)=='.' &&
chars(l,4)=='I' && chars(l,5)=='0' && chars(l,6)=='.' && chars(l,7)=='n'
&& chars(l,8)=='e' && chars(l,9)=='t'
    if chars(l,9+offset(l)) == '>'
    z(i)=str2num(chars(l,8+offset(l)));
```

```
    y(i)=0;
    x(i)=0;
    v(i)=val(l);
    end
    if chars(l,10+offset(l)) == '>'
    z(i)=str2num(chars(l,9+offset(l)));
    y(i)=str2num(chars(l,8+offset(l)));
    x(i)=0;
    v(i)=val(l);
    end
    if chars(l,11+offset(l)) == '>'
    z(i)=str2num(chars(l,10+offset(l)));
    y(i)=str2num(chars(l,9+offset(l)));
    x(i)=str2num(chars(l,8+offset(l)));
    v(i)=val(l);
    end
    i=i+1;
end
end

for l=1:length-1
if chars(l,1)=='I' && chars(l,2)=='0' && chars(l,3)=='.' &&
chars(l,4)=='I' && chars(l,5)=='1' && chars(l,6)=='.' && chars(l,7)=='n'
&& chars(l,8)=='e' && chars(l,9)=='t'
    if chars(l,9+offset(l)) == '>'
    z(i)=str2num(chars(l,8+offset(l)));
    y(i)=0;
    x(i)=0+10;
    v(i)=val(l);
    end
    if chars(l,10+offset(l)) == '>'
    z(i)=str2num(chars(l,9+offset(l)));
    y(i)=str2num(chars(l,8+offset(l)));
    x(i)=0+10;
    v(i)=val(l);
    end
    if chars(l,11+offset(l)) == '>'
    z(i)=str2num(chars(l,10+offset(l)));
    y(i)=str2num(chars(l,9+offset(l)));
    x(i)=str2num(chars(l,8+offset(l)))+10;
    v(i)=val(l);
    end
    i=i+1;
end
end

for l=1:length-1
if chars(l,1)=='I' && chars(l,2)=='0' && chars(l,3)=='.' &&
chars(l,4)=='I' && chars(l,5)=='2' && chars(l,6)=='.' && chars(l,7)=='n'
&& chars(l,8)=='e' && chars(l,9)=='t'
    if chars(l,9+offset(l)) == '>'
    z(i)=str2num(chars(l,8+offset(l)));
    y(i)=0+10;
    x(i)=0;
    v(i)=val(l);
    end
    if chars(l,10+offset(l)) == '>'
    z(i)=str2num(chars(l,9+offset(l)));
    y(i)=str2num(chars(l,8+offset(l)))+10;
    x(i)=0;
    v(i)=val(l);
    end
    if chars(l,11+offset(l)) == '>'
    z(i)=str2num(chars(l,10+offset(l)));
```

```
    y(i)=str2num(chars(l,9+offset(l)))+10;
    x(i)=str2num(chars(l,8+offset(l)));
    v(i)=val(l);
    end
    i=i+1;
end
end

for l=1:length-1
if chars(l,1)=='I' && chars(l,2)=='0' && chars(l,3)=='.' &&
chars(l,4)=='I' && chars(l,5)=='3' && chars(l,6)=='.' && chars(l,7)=='n'
&& chars(l,8)=='e' && chars(l,9)=='t'
    if chars(l,9+offset(l)) == '>'
    z(i)=str2num(chars(l,8+offset(l)));
    y(i)=0+10;
    x(i)=0+10;
    v(i)=val(l);
    end
    if chars(l,10+offset(l)) == '>'
    z(i)=str2num(chars(l,9+offset(l)));
    y(i)=str2num(chars(l,8+offset(l)))+10;
    x(i)=0+10;
    v(i)=val(l);
    end
    if chars(l,11+offset(l)) == '>'
    z(i)=str2num(chars(l,10+offset(l)));
    y(i)=str2num(chars(l,9+offset(l)))+10;
    x(i)=str2num(chars(l,8+offset(l)))+10;
    v(i)=val(l);
    end
    i=i+1;
end
end

%% Electrolyte voltages cell 2
for l=1:length-1
if chars(l,1)=='n' && chars(l,2)=='e' && chars(l,3)=='t' &&
chars(l,4)=='n' && chars(l,5)=='1' && chars(l,6)=='_' && chars(l,7)=='3'
    if chars(l,9+offset(l)) == '>'
    z(i)=str2num(chars(l,8+offset(l)));
    y(i)=0+20;
    x(i)=20;
    v(i)=val(l);
    end
    if chars(l,10+offset(l)) == '>'
    z(i)=str2num(chars(l,9+offset(l)));
    y(i)=str2num(chars(l,8+offset(l)))+20;
    x(i)=20;
    v(i)=val(l);
    end
    if chars(l,11+offset(l)) == '>'
    z(i)=str2num(chars(l,10+offset(l)));
    y(i)=str2num(chars(l,9+offset(l)))+20;
    x(i)=str2num(chars(l,8+offset(l)))+20;
    v(i)=val(l);
    end
    i=i+1;
end
end

for l=1:length-1
if chars(l,1)=='n' && chars(l,2)=='e' && chars(l,3)=='t' &&
chars(l,4)=='n' && chars(l,5)=='2' && chars(l,6)=='_' && chars(l,7)=='3'
    if chars(l,9+offset(l)) == '>'
```

```
    z(i)=str2num(chars(l,8+offset(l)));
    y(i)=0+20;
    x(i)=0+30;
    v(i)=val(l);
    end
    if chars(l,10+offset(l)) == '>'
    z(i)=str2num(chars(l,9+offset(l)));
    y(i)=str2num(chars(l,8+offset(l)))+20;
    x(i)=0+30;
    v(i)=val(l);
    end
    if chars(l,11+offset(l)) == '>'
    z(i)=str2num(chars(l,10+offset(l)));
    y(i)=str2num(chars(l,9+offset(l)))+20;
    x(i)=str2num(chars(l,8+offset(l)))+30;
    v(i)=val(l);
    end
    i=i+1;
end
end

for l=1:length-1
if chars(l,1)=='n' && chars(l,2)=='e' && chars(l,3)=='t' &&
chars(l,4)=='n' && chars(l,5)=='1' && chars(l,6)=='_' && chars(l,7)=='1'
    if chars(l,9+offset(l)) == '>'
    z(i)=str2num(chars(l,8+offset(l)));
    y(i)=0;
    x(i)=20;
    v(i)=val(l);
    end
    if chars(l,10+offset(l)) == '>'
    z(i)=str2num(chars(l,9+offset(l)));
    y(i)=str2num(chars(l,8+offset(l)));
    x(i)=20;
    v(i)=val(l);
    end
    if chars(l,11+offset(l)) == '>'
    z(i)=str2num(chars(l,10+offset(l)));
    y(i)=str2num(chars(l,9+offset(l)));
    x(i)=str2num(chars(l,8+offset(l)))+20;
    v(i)=val(l);
    end
    i=i+1;
end
end

for l=1:length-1
if chars(l,1)=='n' && chars(l,2)=='e' && chars(l,3)=='t' &&
chars(l,4)=='n' && chars(l,5)=='1' && chars(l,6)=='_' && chars(l,7)=='2'
    if chars(l,9+offset(l)) == '>'
    z(i)=str2num(chars(l,8+offset(l)));
    y(i)=0+10;
    x(i)=20;
    v(i)=val(l);
    end
    if chars(l,10+offset(l)) == '>'
    z(i)=str2num(chars(l,9+offset(l)));
    y(i)=str2num(chars(l,8+offset(l)))+10;
    x(i)=20;
    v(i)=val(l);
    end
    if chars(l,11+offset(l)) == '>'
    z(i)=str2num(chars(l,10+offset(l)));
    y(i)=str2num(chars(l,9+offset(l)))+10;
```

```
    x(i)=str2num(chars(l,8+offset(l)))+20;
    v(i)=val(l);
    end
    i=i+1;
end
end

for l=1:length-1
if chars(l,1)=='n' && chars(l,2)=='e' && chars(l,3)=='t' &&
chars(l,4)=='n' && chars(l,5)=='2' && chars(l,6)=='_' && chars(l,7)=='2'
    if chars(l,9+offset(l)) == '>'
    z(i)=str2num(chars(l,8+offset(l)));
    y(i)=0+10;
    x(i)=0+30;
    v(i)=val(l);
    end
    if chars(l,10+offset(l)) == '>'
    z(i)=str2num(chars(l,9+offset(l)));
    y(i)=str2num(chars(l,8+offset(l)))+10;
    x(i)=0+30;
    v(i)=val(l);
    end
    if chars(l,11+offset(l)) == '>'
    z(i)=str2num(chars(l,10+offset(l)));
    y(i)=str2num(chars(l,9+offset(l)))+10;
    x(i)=str2num(chars(l,8+offset(l)))+30;
    v(i)=val(l);
    end
    i=i+1;
end
end

for l=1:length-1
if chars(l,1)=='n' && chars(l,2)=='e' && chars(l,3)=='t' &&
chars(l,4)=='n' && chars(l,5)=='2' && chars(l,6)=='_' && chars(l,7)=='1'
    if chars(l,9+offset(l)) == '>'
    z(i)=str2num(chars(l,8+offset(l)));
    y(i)=0;
    x(i)=0+30;
    v(i)=val(l);
    end
    if chars(l,10+offset(l)) == '>'
    z(i)=str2num(chars(l,9+offset(l)));
    y(i)=str2num(chars(l,8+offset(l)));
    x(i)=0+30;
    v(i)=val(l);
    end
    if chars(l,11+offset(l)) == '>'
    z(i)=str2num(chars(l,10+offset(l)));
    y(i)=str2num(chars(l,9+offset(l)));
    x(i)=str2num(chars(l,8+offset(l)))+30;
    v(i)=val(l);
    end
    i=i+1;
end
end

for l=1:length-1
if chars(l,1)=='I' && chars(l,2)=='2' && chars(l,3)=='7' &&
chars(l,4)=='.' && chars(l,5)=='n' && chars(l,6)=='e' && chars(l,7)=='t'
&& chars(l,8)=='1' && chars(l,9)=='_' && chars(l,10)=='1'
    if chars(l,9+offset(l)) == '>'
    z(i)=str2num(chars(l,8+offset(l)));
    y(i)=0;
```

```
    x(i)=20;
    v(i)=val(l);
    end
    if chars(l,10+offset(l)) == '>'
    z(i)=str2num(chars(l,9+offset(l)));
    y(i)=str2num(chars(l,8+offset(l)));
    x(i)=20;
    v(i)=val(l);
    end
    if chars(l,11+offset(l)) == '>'
    z(i)=str2num(chars(l,10+offset(l)));
    y(i)=str2num(chars(l,9+offset(l)));
    x(i)=str2num(chars(l,8+offset(l)))+20;
    v(i)=val(l);
    end
    i=i+1;
end
end

for l=1:length-1
if chars(l,1)=='I' && chars(l,2)=='2' && chars(l,3)=='7' &&
chars(l,4)=='.' && chars(l,5)=='n' && chars(l,6)=='e' && chars(l,7)=='t'
&& chars(l,8)=='1' && chars(l,9)=='_' && chars(l,10)=='2'
    if chars(l,9+offset(l)) == '>'
    z(i)=str2num(chars(l,8+offset(l)));
    y(i)=0+10;
    x(i)=20;
    v(i)=val(l);
    end
    if chars(l,10+offset(l)) == '>'
    z(i)=str2num(chars(l,9+offset(l)));
    y(i)=str2num(chars(l,8+offset(l)))+10;
    x(i)=20;
    v(i)=val(l);
    end
    if chars(l,11+offset(l)) == '>'
    z(i)=str2num(chars(l,10+offset(l)));
    y(i)=str2num(chars(l,9+offset(l)))+10;
    x(i)=str2num(chars(l,8+offset(l)))+20;
    v(i)=val(l);
    end
    i=i+1;
end
end

for l=1:length-1
if chars(l,1)=='I' && chars(l,2)=='2' && chars(l,3)=='7' &&
chars(l,4)=='.' && chars(l,5)=='n' && chars(l,6)=='e' && chars(l,7)=='t'
&& chars(l,8)=='2' && chars(l,9)=='_' && chars(l,10)=='1'
    if chars(l,9+offset(l)) == '>'
    z(i)=str2num(chars(l,8+offset(l)));
    y(i)=0;
    x(i)=0+30;
    v(i)=val(l);
    end
    if chars(l,10+offset(l)) == '>'
    z(i)=str2num(chars(l,9+offset(l)));
    y(i)=str2num(chars(l,8+offset(l)));
    x(i)=0+30;
    v(i)=val(l);
    end
    if chars(l,11+offset(l)) == '>'
    z(i)=str2num(chars(l,10+offset(l)));
    y(i)=str2num(chars(l,9+offset(l)));
```

```
    x(i)=str2num(chars(l,8+offset(l)))+30;
    v(i)=val(l);
    end
    i=i+1;
end
end

for l=1:length-1
if chars(l,1)=='I' && chars(l,2)=='2' && chars(l,3)=='7' &&
chars(l,4)=='.' && chars(l,5)=='n' && chars(l,6)=='e' && chars(l,7)=='t'
&& chars(l,8)=='2' && chars(l,9)=='_' && chars(l,10)=='2'
    if chars(l,9+offset(l)) == '>'
    z(i)=str2num(chars(l,8+offset(l)));
    y(i)=0+10;
    x(i)=0+30;
    v(i)=val(l);
    end
    if chars(l,10+offset(l)) == '>'
    z(i)=str2num(chars(l,9+offset(l)));
    y(i)=str2num(chars(l,8+offset(l)))+10;
    x(i)=0+30;
    v(i)=val(l);
    end
    if chars(l,11+offset(l)) == '>'
    z(i)=str2num(chars(l,10+offset(l)));
    y(i)=str2num(chars(l,9+offset(l)))+10;
    x(i)=str2num(chars(l,8+offset(l)))+30;
    v(i)=val(l);
    end
    i=i+1;
end
end

for l=1:length-1
if chars(l,1)=='I' && chars(l,2)=='2' && chars(l,3)=='7' &&
chars(l,4)=='.' && chars(l,5)=='I' && chars(l,6)=='0' && chars(l,7)=='.'
&& chars(l,8)=='n' && chars(l,9)=='e' && chars(l,10)=='t'
    if chars(l,9+offset(l)) == '>'
    z(i)=str2num(chars(l,8+offset(l)));
    y(i)=0;
    x(i)=20;
    v(i)=val(l);
    end
    if chars(l,10+offset(l)) == '>'
    z(i)=str2num(chars(l,9+offset(l)));
    y(i)=str2num(chars(l,8+offset(l)));
    x(i)=20;
    v(i)=val(l);
    end
    if chars(l,11+offset(l)) == '>'
    z(i)=str2num(chars(l,10+offset(l)));
    y(i)=str2num(chars(l,9+offset(l)));
    x(i)=str2num(chars(l,8+offset(l)))+20;
    v(i)=val(l);
    end
    i=i+1;
end
end

for l=1:length-1
if chars(l,1)=='I' && chars(l,2)=='2' && chars(l,3)=='7' &&
chars(l,4)=='.' && chars(l,5)=='I' && chars(l,6)=='1' && chars(l,7)=='.'
&& chars(l,8)=='n' && chars(l,9)=='e' && chars(l,10)=='t'
    if chars(l,9+offset(l)) == '>'
```

```
    z(i)=str2num(chars(l,8+offset(l)));
    y(i)=0;
    x(i)=0+30;
    v(i)=val(l);
    end
    if chars(l,10+offset(l)) == '>'
    z(i)=str2num(chars(l,9+offset(l)));
    y(i)=str2num(chars(l,8+offset(l)));
    x(i)=0+30;
    v(i)=val(l);
    end
    if chars(l,11+offset(l)) == '>'
    z(i)=str2num(chars(l,10+offset(l)));
    y(i)=str2num(chars(l,9+offset(l)));
    x(i)=str2num(chars(l,8+offset(l)))+30;
    v(i)=val(l);
    end
    i=i+1;
end
end

for l=1:length-1
if chars(l,1)=='I' && chars(l,2)=='2' && chars(l,3)=='7' &&
chars(l,4)=='.' && chars(l,5)=='I' && chars(l,6)=='2' && chars(l,7)=='.'
&& chars(l,8)=='n' && chars(l,9)=='e' && chars(l,10)=='t'
    if chars(l,9+offset(l)) == '>'
    z(i)=str2num(chars(l,8+offset(l)));
    y(i)=0+10;
    x(i)=0+20;
    v(i)=val(l);
    end
    if chars(l,10+offset(l)) == '>'
    z(i)=str2num(chars(l,9+offset(l)));
    y(i)=str2num(chars(l,8+offset(l)))+10;
    x(i)=20;
    v(i)=val(l);
    end
    if chars(l,11+offset(l)) == '>'
    z(i)=str2num(chars(l,10+offset(l)));
    y(i)=str2num(chars(l,9+offset(l)))+10;
    x(i)=str2num(chars(l,8+offset(l)))+20;
    v(i)=val(l);
    end
    i=i+1;
end
end

for l=1:length-1
if chars(l,1)=='I' && chars(l,2)=='2' && chars(l,3)=='7' &&
chars(l,4)=='.' && chars(l,5)=='I' && chars(l,6)=='3' && chars(l,7)=='.'
&& chars(l,8)=='n' && chars(l,9)=='e' && chars(l,10)=='t'
    if chars(l,9+offset(l)) == '>'
    z(i)=str2num(chars(l,8+offset(l)));
    y(i)=0+10;
    x(i)=0+30;
    v(i)=val(l);
    end
    if chars(l,10+offset(l)) == '>'
    z(i)=str2num(chars(l,9+offset(l)));
    y(i)=str2num(chars(l,8+offset(l)))+10;
    x(i)=0+30;
    v(i)=val(l);
    end
    if chars(l,11+offset(l)) == '>'
```

```
    z(i)=str2num(chars(l,10+offset(l)));
    y(i)=str2num(chars(l,9+offset(l)))+10;
    x(i)=str2num(chars(l,8+offset(l)))+30;
    v(i)=val(l);
    end
    i=i+1;
end
end

for l=1:length-1
if chars(l,1)=='n' && chars(l,2)=='e' && chars(l,3)=='t' &&
chars(l,4)=='n' && chars(l,5)=='i' && chars(l,6)=='3' && chars(l,7)=='_'
&& chars(l,8)=='3'
    if chars(l,9+offset(l)) == '>'
    z(i)=str2num(chars(l,8+offset(l)));
    y(i)=0+20;
    x(i)=0+40;
    v(i)=val(l);
    end
    if chars(l,10+offset(l)) == '>'
    z(i)=str2num(chars(l,9+offset(l)));
    y(i)=str2num(chars(l,8+offset(l)))+20;
    x(i)=0+40;
    v(i)=val(l);
    end
    if chars(l,11+offset(l)) == '>'
    z(i)=str2num(chars(l,10+offset(l)));
    y(i)=str2num(chars(l,9+offset(l)))+20;
    x(i)=str2num(chars(l,8+offset(l)))+40;
    v(i)=val(l);
    end
    i=i+1;
end
end

for l=1:length-1
if chars(l,1)=='n' && chars(l,2)=='e' && chars(l,3)=='t' &&
chars(l,4)=='n' && chars(l,5)=='3' && chars(l,6)=='_' && chars(l,7)=='2'
    if chars(l,9+offset(l)) == '>'
    z(i)=str2num(chars(l,8+offset(l)));
    y(i)=0+10;
    x(i)=0+40;
    v(i)=val(l);
    end
    if chars(l,10+offset(l)) == '>'
    z(i)=str2num(chars(l,9+offset(l)));
    y(i)=str2num(chars(l,8+offset(l)))+10;
    x(i)=0+40;
    v(i)=val(l);
    end
    if chars(l,11+offset(l)) == '>'
    z(i)=str2num(chars(l,10+offset(l)));
    y(i)=str2num(chars(l,9+offset(l)))+10;
    x(i)=str2num(chars(l,8+offset(l)))+40;
    v(i)=val(l);
    end
    i=i+1;
end
end

for l=1:length-1
if chars(l,1)=='n' && chars(l,2)=='e' && chars(l,3)=='t' &&
chars(l,4)=='n' && chars(l,5)=='3' && chars(l,6)=='_' && chars(l,7)=='1'
    if chars(l,9+offset(l)) == '>'
```

```
    z(i)=str2num(chars(l,8+offset(l)));
    y(i)=0;
    x(i)=0+40;
    v(i)=val(l);
    end
    if chars(l,10+offset(l)) == '>'
    z(i)=str2num(chars(l,9+offset(l)));
    y(i)=str2num(chars(l,8+offset(l)));
    x(i)=0+40;
    v(i)=val(l);
    end
    if chars(l,11+offset(l)) == '>'
    z(i)=str2num(chars(l,10+offset(l)));
    y(i)=str2num(chars(l,9+offset(l)));
    x(i)=str2num(chars(l,8+offset(l)))+40;
    v(i)=val(l);
    end
    i=i+1;
end
end

%% Electrodes cell 1
i=1;
for l=1:length-1
if chars(l,1)=='I' && chars(l,2)=='0' && chars(l,3)=='.' &&
chars(l,4)=='n' && chars(l,5)=='e' && chars(l,6)=='t' && chars(l,7)=='e'
&& chars(l,8)=='1' && chars(l,9)=='_' && chars(l,10)=='1'
    if chars(l,9+offset(l)) == '>'
    ze(i)=str2num(chars(l,8+offset(l)));
    ye(i)=0;
    xe(i)=0;
    ve(i)=val(l);
    end
    if chars(l,10+offset(l)) == '>'
    ze(i)=str2num(chars(l,9+offset(l)));
    ye(i)=str2num(chars(l,8+offset(l)));
    xe(i)=0;
    ve(i)=val(l);
    end
    if chars(l,11+offset(l)) == '>'
    ze(i)=str2num(chars(l,10+offset(l)));
    ye(i)=str2num(chars(l,9+offset(l)));
    xe(i)=str2num(chars(l,8+offset(l)));
    ve(i)=val(l);
    end
    i=i+1;
end
end

for l=1:length-1
if chars(l,1)=='I' && chars(l,2)=='0' && chars(l,3)=='.' &&
chars(l,4)=='n' && chars(l,5)=='e' && chars(l,6)=='t' && chars(l,7)=='e'
&& chars(l,8)=='1' && chars(l,9)=='_' && chars(l,10)=='2'
    if chars(l,9+offset(l)) == '>'
    ze(i)=str2num(chars(l,8+offset(l)));
    ye(i)=0+10;
    xe(i)=0;
    ve(i)=val(l);
    end
    if chars(l,10+offset(l)) == '>'
    ze(i)=str2num(chars(l,9+offset(l)));
    ye(i)=str2num(chars(l,8+offset(l)))+10;
    xe(i)=0;
    ve(i)=val(l);
```

```
    end
    if chars(l,11+offset(l)) == '>'
    ze(i)=str2num(chars(l,10+offset(l)));
    ye(i)=str2num(chars(l,9+offset(l)))+10;
    xe(i)=str2num(chars(l,8+offset(l)));
    ve(i)=val(l);
    end
    i=i+1;
end
end

for l=1:length-1
if chars(l,1)=='I' && chars(l,2)=='0' && chars(l,3)=='.' &&
chars(l,4)=='n' && chars(l,5)=='e' && chars(l,6)=='t' && chars(l,7)=='e'
&& chars(l,8)=='2' && chars(l,9)=='_' && chars(l,10)=='1'
    if chars(l,9+offset(l)) == '>'
    ze(i)=str2num(chars(l,8+offset(l)));
    ye(i)=0;
    xe(i)=0+10;
    ve(i)=val(l);
    end
    if chars(l,10+offset(l)) == '>'
    ze(i)=str2num(chars(l,9+offset(l)));
    ye(i)=str2num(chars(l,8+offset(l)));
    xe(i)=0+10;
    ve(i)=val(l);
    end
    if chars(l,11+offset(l)) == '>'
    ze(i)=str2num(chars(l,10+offset(l)));
    ye(i)=str2num(chars(l,9+offset(l)));
    xe(i)=str2num(chars(l,8+offset(l)))+10;
    ve(i)=val(l);
    end
    i=i+1;
end
end

for l=1:length-1
if chars(l,1)=='I' && chars(l,2)=='0' && chars(l,3)=='.' &&
chars(l,4)=='n' && chars(l,5)=='e' && chars(l,6)=='t' && chars(l,7)=='e'
&& chars(l,8)=='2' && chars(l,9)=='_' && chars(l,10)=='2'
    if chars(l,9+offset(l)) == '>'
    ze(i)=str2num(chars(l,8+offset(l)));
    ye(i)=0+10;
    xe(i)=0+10;
    ve(i)=val(l);
    end
    if chars(l,10+offset(l)) == '>'
    ze(i)=str2num(chars(l,9+offset(l)));
    ye(i)=str2num(chars(l,8+offset(l)))+10;
    xe(i)=0+10;
    ve(i)=val(l);
    end
    if chars(l,11+offset(l)) == '>'
    ze(i)=str2num(chars(l,10+offset(l)));
    ye(i)=str2num(chars(l,9+offset(l)))+10;
    xe(i)=str2num(chars(l,8+offset(l)))+10;
    ve(i)=val(l);
    end
    i=i+1;
end
end

%% Output
```

```
for l=1:length-1
if chars(l,1)=='W' && chars(l,2)=='E' && chars(l,3)=='S' &&
chars(l,4)=='1'
    VWES1=val(l);
end
if chars(l,1)=='W' && chars(l,2)=='E' && chars(l,3)=='S' &&
chars(l,4)=='2'
    VWES2=val(l);
end
end

%Voltage in 3D co-ordinates
for i=1:8610
      vsort2(y(1,i)+1,x(1,i)+1,z(1,i)+1)=v(1,i);
end

for picture=1:2;
    if picture==1
        vsort=vsort2(:,1:21,:)-VWES1;
        offset2=0;
        picmap=autumn;
    end
    if picture==2
        vsort=vsort2(:,21:41,:)-VWES2;
        offset2=36;
        picmap=cool;
    end
% Electric field in 3D co-ordinates
[Ex,Ey,Ez]=gradient(vsort);
Ex=-Ex*0.00001;
Ey=-Ey*0.00001;
Ez=-Ez*0.00001;
% X-Y as a matrix
 x2=[0:20; 0:20; 0:20; 0:20; 0:20; 0:20; 0:20; 0:20; 0:20; 0:20; 0:20;
0:20; 0:20; 0:20; 0:20; 0:20; 0:20; 0:20; 0:20; 0:20; 0:20; ];
 y2=x2';
  x2zlin=0:1:20;
 z2lin=0:1:9;
 [x2z,z2]=meshgrid(x2zlin,z2lin);
 % electrodes  dots
 [xel yel]=size(xe);
dots=ones(1,yel);
dots=dots*(0.1);
% 3D co-ordinates matrix
for i=1:21
    for j=1:21
        for k=1:10
        x4(i,j,k)=x2(i,j);
        end
    end
end
for i=1:21
    for j=1:21
        for k=1:10
        y4(i,j,k)=y2(i,j);
        end
    end
end
z4=zeros(21,21,10);
for i=1:21
    for j=1:21
        for k=1:10
       z4(i,j,k)=k-1;
        end
```

```
    end
end

%% Figures
% Electrodes 2D
figure, image(B2);
hFig = figure(offset2+1);
set(hFig, 'Position', [700 300 620 475])
set(gca,'YDir','normal')
hold on
scatter(10*xe,10*ye, 100, 'MarkerEdgeColor','k', 'Markerfacecolor', 'w');
axis([0,200,0,200])
ax=gca;
set(ax, 'FontName', 'Times New Roman', 'Fontsize', 30);
xlabel('x (\mum)','interpreter','Tex'); ylabel('y
(\mum)','interpreter','Tex');
axpos=get(ax, 'position');
axpos(3)=0.8*axpos(3);
set(ax,'position', axpos);
hold off

% Contour 2D
for a=1:10
    Ex2(:,:,a)=kron(10*Ex(:,:,a),ones(10));
    Ey2(:,:,a)=kron(10*Ey(:,:,a),ones(10));
    Ez2(:,:,a)=kron(10*Ez(:,:,a),ones(10));
end

Ix=Ex*1.6443;
Iy=Ey*1.6443;
Iz=Ez*1.6443;

%% XY
figure
for a=1:10
  figure(offset2+a+1), contourf(10*x2,10*y2,vsort(:,:,a))
  hFig = figure(offset2+a+1);
  set(hFig, 'Position', [700 300 620 475])
    ax=gca;
  colormap(picmap);
set(ax, 'FontName', 'Times New Roman', 'Fontsize', 30);
xlabel('x (\mum)','interpreter','Tex'); ylabel('y
(\mum)','interpreter','Tex');
c=colorbar;
set(c, 'FontName', 'Times New Roman', 'Fontsize', 30);
 ylabel(c,'V')

hold on
scatter(10*xe,10*ye, 100,'MarkerEdgeColor','k', 'Markerfacecolor', 'w');
s1=streamslice(10*x2,10*y2,Ix(:,:,a),Iy(:,:,a),0.3,'arrowsmode');
set(s1, 'LineWidth',1.5, 'Color', 'k')
quiver(10*x2(1:2:end,1:2:end),10*y2(1:2:end,1:2:end),Ix(1:2:end,1:2:end,a
),Iy(1:2:end,1:2:end,a), 1.5, 'LineWidth',1.5, 'Color', 'k','EraseMode',
'background')
hold off
end

for i=1:21
vsorttemp(:,:)=vsort(i,:,:);
vsort3(:,:,i)=vsorttemp';

Ixtemp(:,:)=Ix(i,:,:);
Ix3(:,:,i)=Ixtemp';
```

```
Iytemp(:,:)=Iy(i,:,:);
Iy3(:,:,i)=Iytemp';

Iztemp(:,:)=Iz(i,:,:);
Iz3(:,:,i)=Iztemp';
end
%% XZ
figure
for a=1:21
  figure(offset2+a+11), contourf(10*x2z,10*z2,vsort3(:,:,a))
  hFig = figure(offset2+a+11);
  set(hFig, 'Position', [700 300 620 475])
    ax=gca;
  colormap(picmap);
set(ax, 'FontName', 'Times New Roman', 'Fontsize', 30);
xlabel('x (\mum)','interpreter','Tex'); ylabel('z
(\mum)','interpreter','Tex');
c=colorbar;
set(c, 'FontName', 'Times New Roman', 'Fontsize', 30);
 ylabel(c,'A')

hold on
[lengthe,widthe]=size(ye);
xe2=30*ones(widthe,21);
ze2=30*ones(widthe,21);
j=1;
for i=1:widthe
    if ye(i)==a-1
        xe2(j,a)=xe(i);
        ze2(j,a)=ze(i);
        j=j+1;
    end
end

scatter(10*xe2(:,a),10*ze2(:,a), 100,'MarkerEdgeColor','k',
'Markerfacecolor', 'w');
s1=streamslice(10*x2z,10*z2,Ix3(:,:,a),Iz3(:,:,a),0.3,'arrowsmode');
set(s1, 'LineWidth',1.5, 'Color', 'k')
quiver(10*x2z(1:2:end,1:2:end),10*z2(1:2:end,1:2:end),Ix3(1:2:end,1:2:end
,a),Iz3(1:2:end,1:2:end,a), 1.5, 'LineWidth',1.5, 'Color',
'k','EraseMode', 'background')
hold off
end

% Electrodes 3D
 figure,surf(xImage,yImage,zImage,...    %# Plot the surface
     'CData',B,...
     'FaceColor','texturemap');
hold on
scatter3(10*xe,10*ye,dots,100,'MarkerEdgeColor','k','Markerfacecolor',
'w');
axis([0,200,0,200,-30,90])
daspect([1,1,1])
ax=gca;
set(ax, 'FontName', 'Times New Roman', 'Fontsize', 30, 'XTick', [0 100
200], 'YTick', [0 100 200], 'ZTick', [0 40 80]);
xlabel('x (\mum)','interpreter','Tex'); ylabel('y
(\mum)','interpreter','Tex');zlabel('z (\mum)','interpreter','Tex');
grid on;
hold off
%Contour 3D
figure,contourslice(10*x4,10*y4,10*z4,vsort,[40:10:60,140:10:160],[40:10:
60,140:10:160],0:10:90,10)
```

```
colormap(picmap)
ax=gca;
set(ax,  'FontName', 'Times New Roman', 'Fontsize', 15, 'ZTick', [0 20 40
60 80]);
axis([0,200,0,200,-30,90])
daspect([1,1,1])
box on

%3D volume
vrange=vsort(:,:,2:10);
minv=min(vrange(:));
maxv=max(vrange(:));
for i=1:9
    hold on
p1 = patch(isocaps(10*x4(11-i:1:11+i,11-i:1:11+i,1:i+1),10*y4(11-
i:1:11+i,11-i:1:11+i,1:i+1),10*z4(11-i:1:11+i,11-
i:1:11+i,1:i+1),vsort(11-i:1:11+i,11-
i:1:11+i,1:i+1),minv),'FaceColor','interp',...
'EdgeColor','none');
grid on;
colormap(picmap);
caxis([minv maxv])
alpha(1-0.05*i)
hold on
end

    hold on
p1 =
patch(isocaps(10*x4(1:1:21,1:1:21,1:10),10*y4(1:1:21,1:1:21,1:10),10*z4(1
:1:21,1:1:21,1:10),vsort(1:1:21,1:1:21,1:10),minv),'FaceColor','interp',.
..
'EdgeColor','none');
xlabel('x (\mum)','interpreter','Tex'); ylabel('y
(\mum)','interpreter','Tex');zlabel('z (\mum)','interpreter','Tex');
grid on;
colormap(picmap);
caxis([minv maxv])
c=colorbar;
set(c,  'FontName', 'Times New Roman', 'Fontsize', 15,  'YTick', [minv
maxv]);
ylabel(c,'V')
alpha(0.1)
hold on
surf(xImage,yImage,zImage,...    %# Plot the surface
     'CData',B,...
     'FaceColor','texturemap');
scatter3(10*xe,10*ye,dots, 100,'MarkerEdgeColor','k', 'Markerfacecolor',
'w');
hold off

figure
ax=gca;
set(ax, 'FontName', 'Times New Roman', 'Fontsize', 30,'ZTick', [0 30 60
90]);
axis([0,200,0,200,-30,90])
box on
%3D volume
[sx sy sz] = meshgrid(0:50:210,0:50:210,0:30:90);
for i=1:9
    hold on
p1 = patch(isocaps(10*x4(11-i:1:11+i,11-i:1:11+i,1:i+1),10*y4(11-
i:1:11+i,11-i:1:11+i,1:i+1),10*z4(11-i:1:11+i,11-
i:1:11+i,1:i+1),vsort(11-i:1:11+i,11-
i:1:11+i,1:i+1),minv),'FaceColor','interp',...
```

```
'EdgeColor','none');
grid on;
colormap(picmap);
caxis([minv maxv])
alpha(1-0.1*i)
hold on
end

    hold on
p1 =
patch(isocaps(10*x4(1:1:21,1:1:21,1:10),10*y4(1:1:21,1:1:21,1:10),10*z4(1
:1:21,1:1:21,1:10),vsort(1:1:21,1:1:21,1:10),minv),'FaceColor','interp',.
..
'EdgeColor','none');
xlabel('x (\mum)','interpreter','Tex'); ylabel('y
(\mum)','interpreter','Tex');zlabel('z (\mum)','interpreter','Tex');
grid on;
colormap(picmap);
caxis([minv maxv])
alpha(0.14)
hold on
surf(xImage,yImage,zImage,...    %# Plot the surface
     'CData',B,...
     'FaceColor','texturemap');
scatter3(10*xe,10*ye,dots, 100,'MarkerEdgeColor','k','Markerfacecolor',
'w');
hold on

XYZ=stream3(10*x4(1:1:end,1:1:end,:),10*y4(1:1:end,1:1:end,:),10*z4(1:1:e
nd,1:1:end,:),Ix(1:1:end,1:1:end,:),Iy(1:1:end,1:1:end,:),Iz(1:1:end,1:1:
end,:),sx,sy,sz);
s1=streamline(XYZ);
set(s1, 'LineWidth',1.5, 'Color', 'k')

quiver3(10*x4(1:3:end,1:3:end,:),10*y4(1:3:end,1:3:end,:),10*z4(1:3:end,1
:3:end,:),Ix(1:3:end,1:3:end,:),Iy(1:3:end,1:3:end,:),Iz(1:3:end,1:3:end,
:),10,'LineWidth',1.5, 'Color', 'k')

%% 3D slices
vrange2=vsort(:,:,:);
minv2=min(vrange2(:));
maxv2=max(vrange2(:));
if picture==1
figure, slice(10*x4,10*y4,10*z4,vsort,120,160,0)
colormap(picmap)
ax=gca;
set(ax,  'FontName', 'Times New Roman', 'Fontsize', 28,'ZTick', [0 30 60
90]);
axis([0,200,0,200,-30,90])
daspect([1,1,1])
box on
view([-30,25])
axis on;
grid on;
shading interp;
hold on
scatter3(10*xe,10*ye,dots, 100,'MarkerEdgeColor','k', 'Markerfacecolor',
'w');
surf(xImage,yImage,zImage,...    %# Plot the surface
     'CData',B,...
     'FaceColor','texturemap');
[sx2 sy2 sz2] = meshgrid(120,160,0);
```

```
s2=streamslice(10*x4(1:1:end,1:1:end,:),10*y4(1:1:end,1:1:end,:),10*z4(1:
1:end,1:1:end,:),Ix(1:1:end,1:1:end,:),Iy(1:1:end,1:1:end,:),Iz(1:1:end,1
:1:end,:),sx2,sy2,sz2,0.5);
set(s2, 'LineWidth',1.5, 'Color', 'k')
xlabel('x (\mum)','interpreter','Tex'); ylabel('y
(\mum)','interpreter','Tex');zlabel('z (\mum)','interpreter','Tex');
grid on;
colormap(picmap);
caxis([minv2 maxv2])
set(c, 'FontName', 'Times New Roman', 'Fontsize', 28, 'YTick', [minv2
maxv2]);
  ylabel(c,'A')
hold off
end

if picture==2
   figure, slice(200+10*x4,10*y4,10*z4,vsort,320,160,0)
colormap(picmap)
ax=gca;
set(ax,  'FontName', 'Times New Roman', 'Fontsize', 28,'ZTick', [0 30 60
90]);
axis([200,400,0,200,-30,90])
daspect([1,1,1])
box on
view([-30,25])
axis on;
grid on;
shading interp;
hold on
scatter3(200+10*xe,10*ye,dots, 100,'MarkerEdgeColor','k',
'Markerfacecolor', 'w');
surf(200+xImage,yImage,zImage,...    %# Plot the surface
     'CData',B,...
     'FaceColor','texturemap');
[sx2 sy2 sz2] = meshgrid(320,160,0);
s2=streamslice(200+10*x4(1:1:end,1:1:end,:),10*y4(1:1:end,1:1:end,:),10*z
4(1:1:end,1:1:end,:),Ix(1:1:end,1:1:end,:),Iy(1:1:end,1:1:end,:),Iz(1:1:e
nd,1:1:end,:),sx2,sy2,sz2,0.5);
set(s2, 'LineWidth',1.5, 'Color', 'k')
set(ax,'YTickLabel',[],'ZTickLabel',[],'XTick',[200:100:400])
grid on;
colormap(picmap);
caxis([minv2 maxv2])
set(c, 'FontName', 'Times New Roman', 'Fontsize', 28,'YTick', [minv2
maxv2]);
  ylabel(c,'A')
hold off

end
end
```

C.2 Cross-talk Calculation

C.2.1 Import Data

The data from the 50 cycles of staircase voltammetry as well as the 200 s measurement of the current at $V_{controlled}$ = 0 V were imported and averaged using the following program (averaging.m):

```
close all;

[filename,pathname]=uigetfile('*.xlsx', 'Pick a file of electrochemical
data');
fullpath=[pathname,filename];
varname=strrep(filename,'.xlsx','');
var_string=[varname,'(qqq,m,mm-64)=signal((m+(qqq-1)*8000),1);'];
prompt = 'What is the background noise level? ';
limit = input(prompt)

for mm=65:1:80
   g=char(mm,58,mm);
   gg=g';
   hh='Analog Demuxed';
   evalin('base',sprintf('signal=xlsread(fullpath,hh,gg);'));

[r,c]=size(signal);
b=mod(r,8000);      %remainder after division

num1=(r-b)/8000;    %number of samples per each pixel

for qqq=1:1:num1
    for m=1:1:8000
     evalin('base',sprintf(var_string));
    end
end

end

varname_2=[varname,'_2'];
eval([varname_2 ' = mean(' varname '(1:50,:,:));'])

varname_3=[varname,'_window'];
j=1;
for i=1:1:8000
   evalin('base',sprintf(['if
abs(',varname_2,'(1,i,10))>limit\n',varname_3,'(1,j) =
',varname_2,'(1,i,10);\nelse\n',varname_3,'(1,j)=0;\nend']));
   j=j+1;
end

varname_4=[varname,'_window_sf'];
eval([varname_4 ' = round(' varname_3 ',10);'])
```

C.2.2 Noise and Cross-talk Calculation

The noise floor, limit of detection and cross-talk were calculated with the following program (crosstalk_calc.m):

```
clear Background_window_serial noise_lvl_window noise_floor_window
mean_noise_window std_noise_window y1 y2 x1 x2 crosstalk_peaks_ox
crosstalk_peaks_red crosstalk_peaks

%Noise
Background__v2_sf=round(Background_v2,10);
for i=1:1:50
Background_window_serial(1+(8000*(i-
1)):8000*i,:)=Background_v2_sf(i,:,:);
End

noise_lvl_window=rms(Background_window_serial,1);
noise_floor_window=mean(noise_lvl_window)
mean_noise_window=mean(mean(Background_window_serial))
std_noise_window=3.3*mean(std(Background_window_serial))

%Cross-talk

[y1,x1]=max(One_cell_window_sf);
[y2,x2]=min(One_cell_window_sf);

crosstalk_peaks_ox=abs(Surrounding_window_sf(1,x1-
50:x1+50)./One_cell_window_sf(1,x1-50:x1+50));

crosstalk_peaks_red=abs(Surrounding_window_sf(1,x2-
50:x2+50)./One_cell_window_sf(1,x2-50:x2+50));

crosstalk_peaks=(mean(crosstalk_peaks_red)+mean(crosstalk_peaks_ox))/2
```

D Graphical Programming Code

The graphical programming code made of block diagrams of Labview from National Instruments was used to make the control and acquisition program, the analog readout analysis program and the digital readout analysis program. Part of the control and acquisition program that generates input waveforms for different electroanalytical methods on each cell is shown in Figure D.1. The first part of the analogue readout program that converts, filters, demultiplexes and takes the average and standard deviation of cells or the whole WE array is shown in Figure D.2. Lastly, the part of the digital readout analysis program that converts the readout data from the discrete time digital CSA to a downsampled timestamped array and performs envelope detection is shown in Figure D.3.

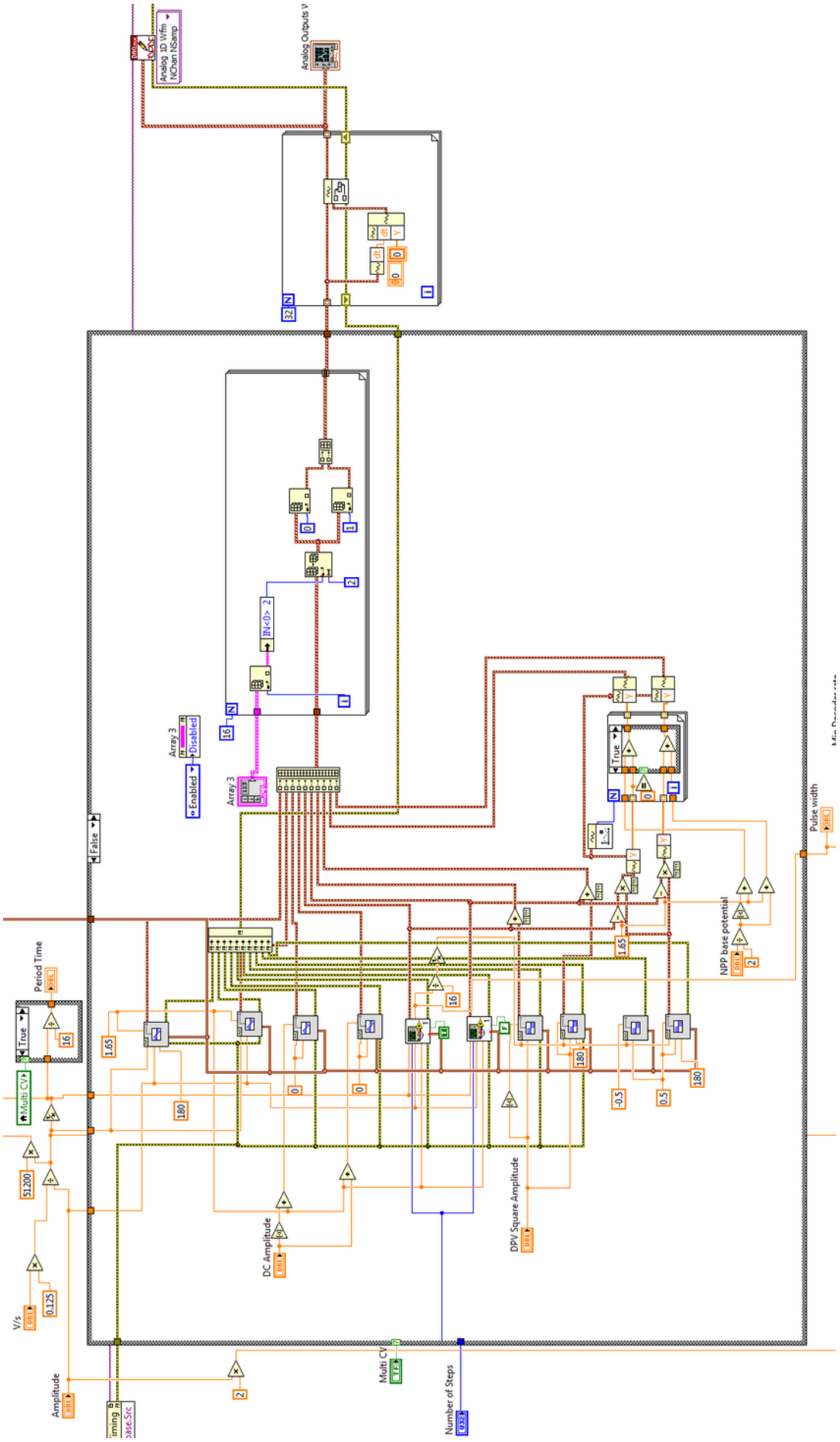

Figure D.1: Detail of electroanalytical driving signal generation part of the Labview program created for the control and acquisition of signals of the ECM.

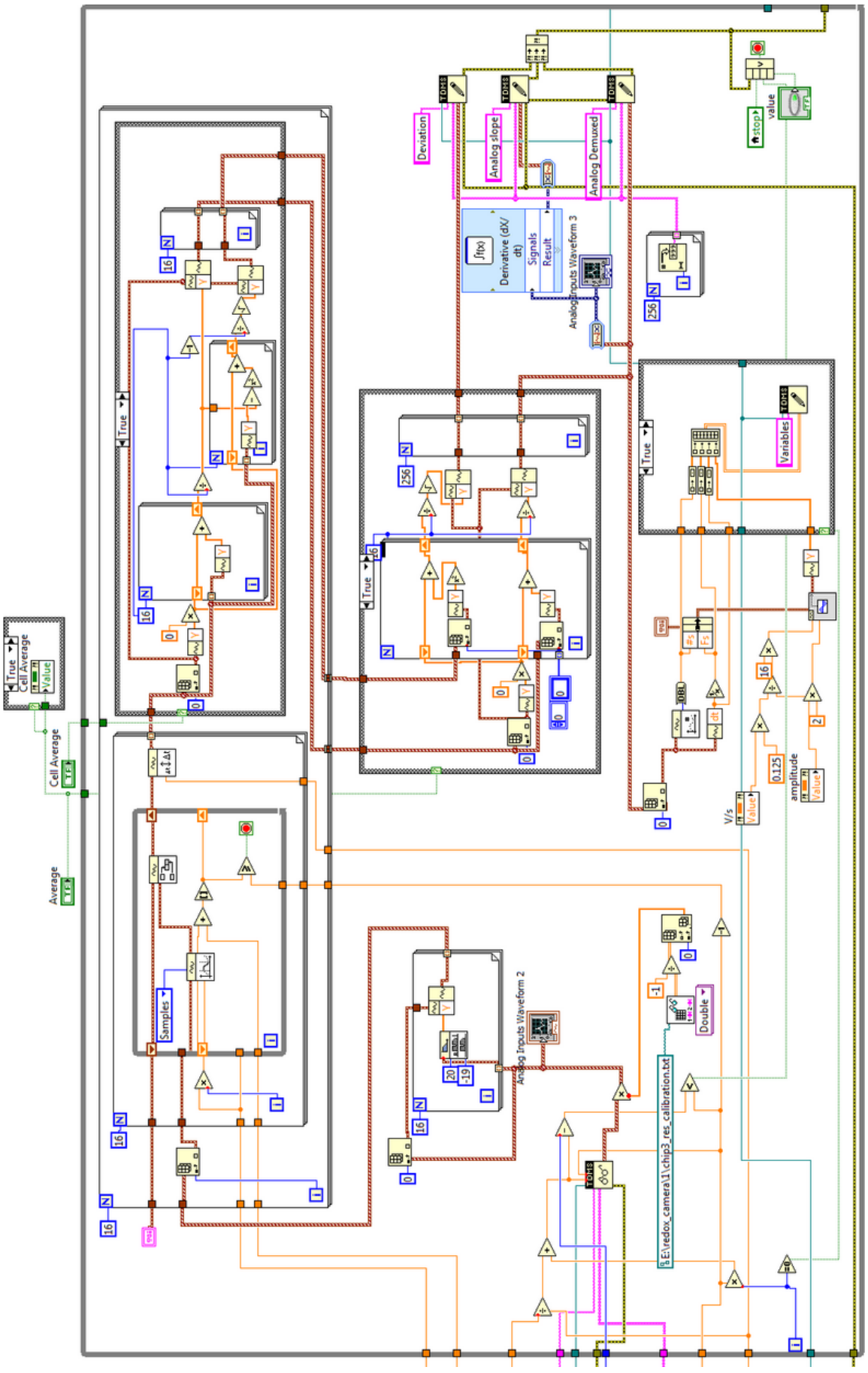

Figure D.2: Detail of the conversion and analysis of WE outputs part of the Labview program created for the analysis of signals acquired from the analogue readout.

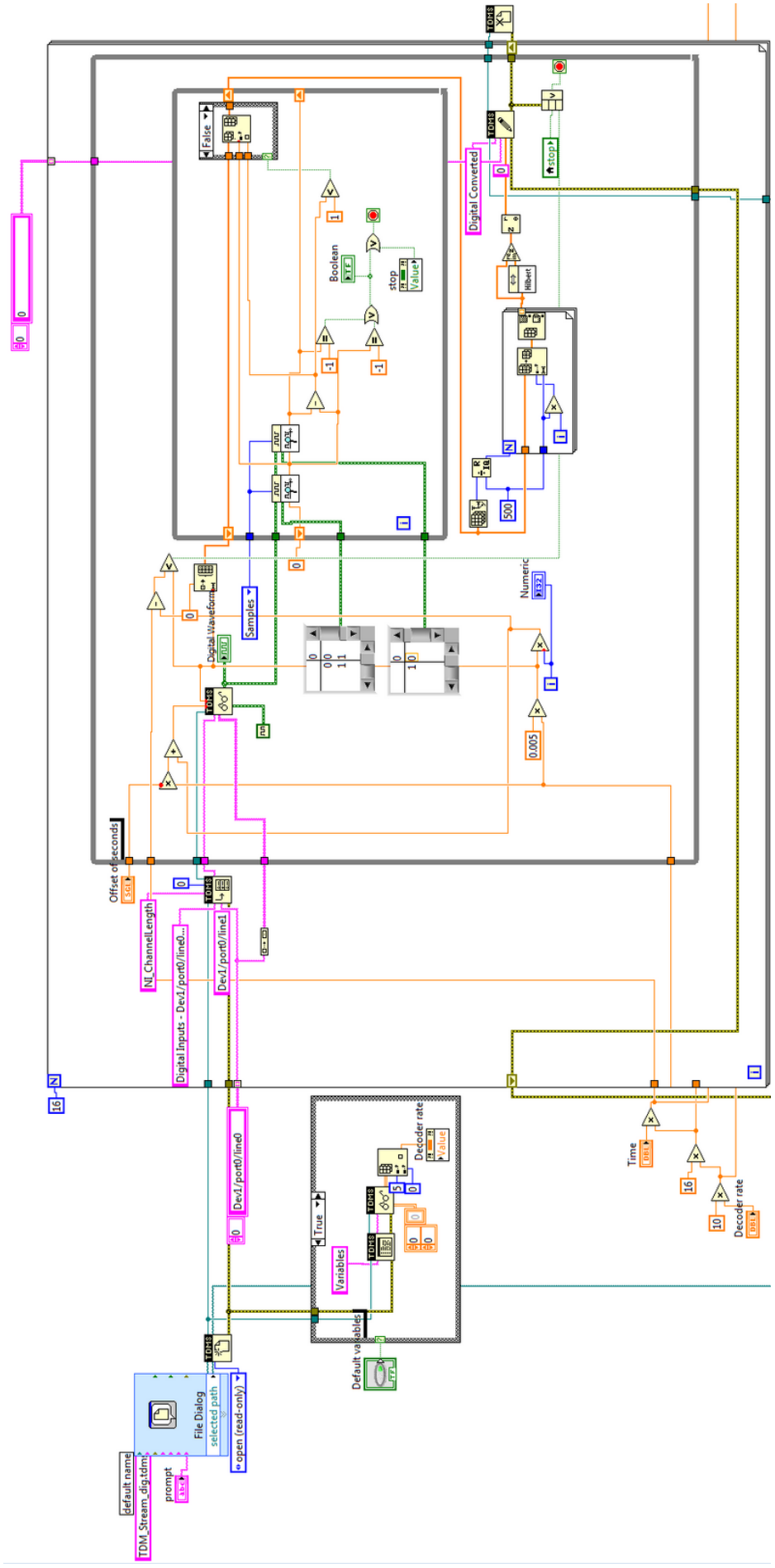

Figure D.3: Detail of the conversion of WE outputs part of the Labview program created for the analysis of signals acquired from the digital readout.

Bibliography

[1] A. Volta and J. Banks, “I. On the electricity excited by the mere contact of conducting substances of different kinds,” *Philos. Mag. Ser. 1*, vol. 7, no. 28, pp. 289–311, Sep. 1800.

[2] J. T. Stock, “Electrochemistry in retrospect,” in *Electrochemistry, Past and Present*, 1989, pp. 1–17.

[3] E. Yoo and S. Lee, “Glucose biosensors: an overview of use in clinical practice,” *Sensors*, vol. 10, no. 5, pp. 4558–4576, May 2010.

[4] J. M. Rothberg *et al.*, “An integrated semiconductor device enabling non-optical genome sequencing,” *Nature*, vol. 475, no. 7356, pp. 348–352, Jul. 2011.

[5] Y. Vlasov and A. Legin, “Non-selective chemical sensors in analytical chemistry: from ‘electronic nose’ to ‘electronic tongue,’” *Fresenius. J. Anal. Chem.*, vol. 361, no. 3, pp. 255–260, Jun. 1998.

[6] M. Wawerla, A. Stolle, B. Schalch, and H. Eisgruber, “Impedance microbiology: application in food hygiene,” *J. Food Prot.*, vol. 12, no. 12, pp. 1488–1496, 1999.

[7] J. Heinze, “Ultramicroelectrodes in electrochemistry,” *Angew. Chemie Int. Ed. English*, vol. 32, no. 9, pp. 1268–1288, Sep. 1993.

[8] O. Ordeig, J. del Campo, F. X. Muñoz, C. E. Banks, and R. G. Compton, “Electroanalysis utilizing amperometric microdisk electrode arrays,” *Electroanalysis*, vol. 19, no. 19–20, pp. 1973–1986, Oct. 2007.

[9] M. D. Serruya, N. G. Hatsopoulos, L. Paninski, M. R. Fellows, and J. P. Donoghue, “Brain-machine interface: Instant neural control of a movement signal,” *Nature*, vol. 416, no. 6877, pp. 141–142, 2002.

[10] E. M. Maynard, C. T. Nordhausen, and R. A. Normann, “The Utah intracortical electrode array: A recording structure for potential brain-

computer interfaces," *Electroencephalogr. Clin. Neurophysiol.*, vol. 102, no. 3, pp. 228–239, Mar. 1997.

[11] A. E. Grumet, J. L. Wyatt, and J. F. Rizzo, "Multi-electrode stimulation and recording in the isolated retina," *J. Neurosci. Methods*, vol. 101, no. 1, pp. 31–42, 2000.

[12] W. Aspray, "The Intel 4004 microprocessor: what constituted invention?," *IEEE Ann. Hist. Comput.*, vol. 19, no. 3, pp. 4–15, 1997.

[13] B. Razavi, *Design of Analog CMOS Integrated Circuits*, 1st ed. New York, NY, USA: McGraw-Hill, Inc., 2001.

[14] I. L. Jones, P. Livi, M. K. Lewandowska, M. Fiscella, B. Roscic, and A. Hierlemann, "The potential of microelectrode arrays and microelectronics for biomedical research and diagnostics," *Anal. Bioanal. Chem.*, vol. 399, no. 7, pp. 2313–2329, Mar. 2011.

[15] Y. H. Ghallab and Y. Ismail, "CMOS based Lab-on-a-Chip: applications, challenges and future trends," *IEEE Circuits Syst. Mag.*, vol. 14, no. 2, pp. 27–47, 2014.

[16] E. Richards, C. Bessant, and S. Saini, "Multivariate data analysis in electroanalytical chemistry," *Electroanalysis*, vol. 14, no. 22, pp. 1533–1542, 2002.

[17] "0.35µm CMOS C35 process parameters." ams AG, 2014.

[18] G. W. A. Kahlbaum and F. V Darbishire, "The letters of Faraday and Schönbein, 1836–1862," *Swabe, Bale, Williams Norgate, London, 5a*, vol. 304, p. 302, 1899.

[19] L. Galvani and G. Aldini, *De viribus electricitatis in motu musculari comentarius cum Joannis Aldini dissertatione et notis; Accesserunt epistolae ad animalis electricitatis theoriam pertinentes*. Apud Societatem Typographicam, 1792.

[20] E. G. Wollish and C. W. Pifer, “Potentiometric titration of salts of organic bases in acetic acid,” vol. 300, no. 98, pp. 300–306, 1951.

[21] A. J. Bard, Ed., *Encyclopedia of Electrochemistry*. Weinheim, Germany: Wiley-VCH Verlag GmbH & Co. KGaA, 2007.

[22] P. R. Unwin, “Introduction to electroanalytical techniques and instrumentation,” *Encycl. Electrochem.*

[23] D. A. Skoog, F. J. Holler, and S. R. Crouch, *Principles of instrumental analysis*. Cengage learning, 2017.

[24] G. Eisenman, “Glass electrodes for hydrogen and other cations,” 1967.

[25] J. W. Ross, J. H. Riseman, and J. a. Krueger, “Potentiometric gas sensing electrodes,” *Pure Appl. Chem.*, vol. 36, no. 4, pp. 473–487, Jan. 1973.

[26] M. Mascini and G. Marrazza, “Enzyme biosensors based on gas electrodes,” in *Enzyme and Microbial Biosensors: Techniques and Protocols*, A. Mulchandani and K. R. Rogers, Eds. Totowa, NJ: Humana Press, 1998, pp. 23–34.

[27] E. Bakker and M. E. Meyerhoff, “Ion-selective electrodes for measurements in biological fluids,” *Encycl. Electrochem.*

[28] P. Bergveld, “Thirty years of ISFETOLOGY: What happened in the past 30 years and what may happen in the next 30 years,” *Sensors Actuators B Chem.*, vol. 88, no. 1, pp. 1–20, Jan. 2003.

[29] B. Nemeth *et al.*, “Real-time ion-flux imaging in the growth of micrometer-scale structures and membranes,” *Adv. Mater.*, vol. 24, no. 9, pp. 1238–1242, Mar. 2012.

[30] P. B. Luppa, L. J. Sokoll, and D. W. Chan, “Immunosensors--principles and applications to clinical chemistry,” *Clin. Chim. Acta.*, vol. 314, no. 1–2, pp. 1–26, 2001.

[31] A. Bard and L. Faulkner, *Electrochemical methods: Fundamentals and applications*. John Wiley & Sons, Inc, 2001.

[32] M. K. Zachek, J. Park, P. Takmakov, R. M. Wightman, and G. S. McCarty, "Microfabricated FSCV-compatible microelectrode array for real-time monitoring of heterogeneous dopamine release," *Analyst*, vol. 135, no. 7, p. 1556, 2010.

[33] L. C. Clark, "The control and monitoring of blood and tissue oxygen," *Trans. Amer. Soc. Anat. Int. Org*, vol. 2, pp. 41–48, 1956.

[34] J. W. Severinghaus and P. B. Astrup, "History of blood gas analysis. V. Oxygen measurement," *J. Clin. Monit.*, vol. 2, no. 3, pp. 174–189, 1986.

[35] S. R. Mikkelsen, "Electrochemistry in bioanalysis," *Encycl. Electrochem.*

[36] L. C. Clark and C. Lyons, "Electrode systems for continuous monitoring in cardiovascular surgery," *Ann. N. Y. Acad. Sci.*, vol. 102, no. 1, pp. 29–45, 1962.

[37] A. Chaubey and B. D. Malhotra, "Mediated biosensors," *Biosens. Bioelectron.*, vol. 17, no. 6–7, pp. 441–456, Jun. 2002.

[38] D. Grieshaber, R. MacKenzie, J. Vörös, and E. Reimhult, "Electrochemical biosensors - sensor principles and architectures," *Sensors*, vol. 8, no. 3, pp. 1400–1458, Mar. 2008.

[39] J. Wang, "Electrochemical biosensors: Towards point-of-care cancer diagnostics," *Biosens. Bioelectron.*, vol. 21, no. 10, pp. 1887–1892, Apr. 2006.

[40] P. Ciosek and W. Wróblewski, "Sensor arrays for liquid sensing – electronic tongue systems," *Analyst*, vol. 132, no. 10, p. 963, 2007.

[41] M. Sohbati and C. Toumazou, "Dimension and Shape Effects on the ISFET Performance," *IEEE Sens. J.*, vol. 15, no. 3, pp. 1670–1679, Mar. 2015.

[42] T. J. Smith and K. J. Stevenson, “4 - Reference Electrodes,” in *Handbook of Electrochemistry*, C. G. B. T.-H. of E. Zoski, Ed. Amsterdam: Elsevier, 2007, pp. 73–110.

[43] H. Li, X. Liu, L. Li, X. Mu, R. Genov, and A. Mason, “CMOS electrochemical instrumentation for biosensor microsystems: A review,” *Sensors*, vol. 17, no. 1, p. 74, Dec. 2016.

[44] J. Rothe, M. K. Lewandowska, F. Heer, O. Frey, and A. Hierlemann, “Multi-target electrochemical biosensing enabled by integrated CMOS electronics,” *J. Micromechanics Microengineering*, vol. 21, no. 5, p. 54010, 2011.

[45] M. Gerard, A. Chaubey, and B. D. Malhotra, “Application of conducting polymers to biosensors,” *Biosens. Bioelectron.*, vol. 17, no. 5, pp. 345–359, 2002.

[46] M. E. Spira and A. Hai, “Multi-electrode array technologies for neuroscience and cardiology,” *Nat. Nanotechnol.*, vol. 8, no. 2, pp. 83–94, Feb. 2013.

[47] M. A. L. Nicolelis and M. A. Lebedev, “Principles of neural ensemble physiology underlying the operation of brain–machine interfaces,” *Nat. Rev. Neurosci.*, vol. 10, no. 7, pp. 530–540, Jul. 2009.

[48] B. Elsholz *et al.*, “Automated detection and quantitation of bacterial RNA by using electrical microarrays,” *Anal. Chem.*, vol. 78, no. 14, pp. 4794–4802, 2006.

[49] G. Wilkinson, M. Rosenblum, M. C. Whiting, and R. B. Woodward, “The structure of iron bis-cyclopentadienyl,” *J. Am. Chem. Soc.*, vol. 74, no. 8, pp. 2125–2126, Apr. 1952.

[50] W. E. Geiger, “Organometallic electrochemistry: Origins, development, and future,” *Organometallics*, vol. 26, no. 24, pp. 5738–5765, Nov. 2007.

[51] F. Lucarelli, S. Tombelli, M. Minunni, G. Marrazza, and M. Mascini, “Electrochemical and piezoelectric DNA biosensors for hybridisation detection,” *Anal. Chim. Acta*, vol. 609, no. 2, pp. 139–159, Feb. 2008.

[52] P. M. Levine, P. Gong, R. Levicky, and K. L. Shepard, “Active CMOS sensor array for electrochemical biomolecular detection,” *IEEE J. Solid-State Circuits*, vol. 43, no. 8, pp. 1859–1871, Aug. 2008.

[53] D. Kahng, “Electric field controlled semiconductor device.” Google Patents, 27-Aug-1963.

[54] F. Wanlass and C. Sah, “Nanowatt logic using field-effect metal-oxide semiconductor triodes,” *Dig. IEEE Int. Solid-State Circuits Conf.*, pp. 32–33, 1963.

[55] G. Moore, “The role of Fairchild in silicon technology in the early days of ‘Silicon Valley,’” *Proc. IEEE*, vol. 86, no. 1, pp. 53–62, 1998.

[56] G. E. Moore, “Cramming more components onto integrated circuits,” *Proc. IEEE*, vol. 86, no. 1, pp. 82–85, Jan. 1998.

[57] S. M. Martin, F. H. Gebara, T. D. Strong, and R. B. Brown, “A fully differential potentiostat,” *IEEE Sens. J.*, vol. 9, no. 2, pp. 135–142, Feb. 2009.

[58] S. Martin, F. Gebara, T. D. Strong, and R. B. Brown, “A low-voltage, chemical sensor interface for systems-on-chip: the fully-differential potentiostat,” in *2004 IEEE International Symposium on Circuits and Systems (IEEE Cat. No.04CH37512)*, 2004, vol. 4, no. 3, p. IV-892-5.

[59] M. M. Ahmadi and G. A. Jullien, “A very low power CMOS potentiostat for bioimplantable applications,” in *Fifth International Workshop on System-on-Chip for Real-Time Applications (IWSOC’05)*, 2005, vol. 2005, pp. 184–189.

[60] W. S. Wang, W. T. Kuo, H. Y. Huang, and C. H. Luo, “Wide dynamic range

CMOS potentiostat for amperometric chemical sensor," *Sensors*, vol. 10, no. 3, pp. 1782–1797, Jan. 2010.

[61] X. Zhu and C. H. Ahn, "On-chip electrochemical analysis system using nanoelectrodes and bioelectronic CMOS chip," *IEEE Sens. J.*, vol. 6, no. 5, pp. 1280–1286, Oct. 2006.

[62] S. Ayers, K. D. Gillis, M. Lindau, and B. A. Minch, "Design of a CMOS potentiostat circuit for electrochemical detector arrays," *IEEE Trans. Circuits Syst. I Regul. Pap.*, vol. 54, no. 4, pp. 736–744, 2007.

[63] R. Hintsche, J. Albers, H. Bernt, and A. Eder, "Multiplexing of microelectrode arrays in voltammetric measurements," *Electroanalysis*, vol. 12, no. 9, pp. 660–665, May 2000.

[64] M. Crescentini, M. Bennati, M. Carminati, and M. Tartagni, "Noise limits of CMOS current interfaces for biosensors: A review," *IEEE Trans. Biomed. Circuits Syst.*, vol. 8, no. 2, pp. 278–292, 2014.

[65] G. Ferrari, F. Gozzini, A. Molari, and M. Sampietro, "Transimpedance amplifier for high sensitivity current measurements on nanodevices," *IEEE J. Solid-State Circuits*, vol. 44, no. 5, pp. 1609–1616, May 2009.

[66] M. H. Nazari, H. Mazhab-Jafari, Lian Leng, A. Guenther, and R. Genov, "CMOS neurotransmitter microarray: 96-channel integrated potentiostat with on-die microsensors," *IEEE Trans. Biomed. Circuits Syst.*, vol. 7, no. 3, pp. 338–348, Jun. 2013.

[67] Jichun Zhang, Yue Huang, N. Trombly, Chao Yang, and A. Mason, "Electrochemical array microsystem with integrated potentiostat," in *IEEE Sensors, 2005.*, 2005, pp. 385–388.

[68] R. G. Kakerow, H. Kappert, E. Spiegel, and Y. Manoli, "Low-power single-chip CMOS potentiostat," *Proc. Int. Solid-State Sensors Actuators Conf. - TRANSDUCERS '95*, vol. 1, pp. 142–145, 1995.

[69] H. M. Jafari and R. Genov, “Chopper-stabilized bidirectional current acquisition circuits for electrochemical amperometric biosensors,” *IEEE Trans. Circuits Syst. I Regul. Pap.*, vol. 60, no. 5, pp. 1149–1157, 2013.

[70] S. H. S. Hwang, C. N. LaFratta, V. Agarwal, X. Y. X. Yu, D. R. Walt, and S. Sonkusale, “CMOS microelectrode array for electrochemical Lab-on-a-Chip applications,” *IEEE Sens. J.*, vol. 9, no. 6, pp. 609–615, 2009.

[71] T. Kuno, K. Niitsu, and K. Nakazato, “Amperometric electrochemical sensor array for on-chip simultaneous imaging,” *Jpn. J. Appl. Phys.*, vol. 53, no. 4S, p. 04EL01, Jan. 2014.

[72] J. B. Wydallis *et al.*, “Spatiotemporal norepinephrine mapping using a high-density CMOS microelectrode array,” *Lab Chip*, vol. 15, no. 20, pp. 4075–4082, 2015.

[73] P. M. Levine, P. Gong, R. Levicky, and K. L. Shepard, “Real-time, multiplexed electrochemical DNA detection using an active complementary metal-oxide-semiconductor biosensor array with integrated sensor electronics,” *Biosens. Bioelectron.*, vol. 24, no. 7, pp. 1995–2001, Mar. 2009.

[74] D. L. Bellin *et al.*, “Integrated circuit-based electrochemical sensor for spatially resolved detection of redox-active metabolites in biofilms,” *Nat. Commun.*, vol. 5, p. 3256, 2014.

[75] D. L. Bellin, H. Sakhtah, Y. Zhang, A. Price-Whelan, L. E. P. Dietrich, and K. L. Shepard, “Electrochemical camera chip for simultaneous imaging of multiple metabolites in biofilms,” *Nat. Commun.*, vol. 7, p. 10535; 10.1038/ncomms10535, 2016.

[76] L. Li, X. Liu, W. A. Qureshi, and A. J. Mason, “CMOS amperometric instrumentation and packaging for biosensor array applications,” *IEEE Trans. Biomed. Circuits Syst.*, vol. 5, no. 5, pp. 439–448, 2011.

[77] M. Schienle *et al.*, “A fully electronic DNA sensor with 128 positions and in-

pixel A/D conversion," *IEEE J. Solid-State Circuits*, vol. 39, no. 12, pp. 2438–2445, 2004.

[78] A. L. Ghindilis *et al.*, "CombiMatrix oligonucleotide arrays: Genotyping and gene expression assays employing electrochemical detection," *Biosens. Bioelectron.*, vol. 22, no. 9–10, pp. 1853–1860, Apr. 2007.

[79] J. Rothe, O. Frey, A. Stettler, Y. Chen, and A. Hierlemann, "Fully integrated CMOS microsystem for electrochemical measurements on 32 × 32 working electrodes at 90 frames per second.," *Anal. Chem.*, vol. 86, no. 13, pp. 6425–6432, Jul. 2014.

[80] P. M. Misun, J. Rothe, Y. R. F. Schmid, A. Hierlemann, and O. Frey, "Multi-analyte biosensor interface for real-time monitoring of 3D microtissue spheroids in hanging-drop networks," *Microsystems Nanoeng.*, vol. 2, no. October 2015, p. 16022, 2016.

[81] G. Massicotte, S. Carrara, G. Di Micheli, and M. Sawan, "A CMOS amperometric system for multi-neurotransmitter detection," *IEEE Trans. Biomed. Circuits Syst.*, vol. 10, no. 3, pp. 731–741, Jun. 2016.

[82] U. Frey *et al.*, "Switch-matrix-based high-density microelectrode array in CMOS technology," *IEEE J. Solid-State Circuits*, vol. 45, no. 2, pp. 467–482, 2010.

[83] X. J. Huang, A. M. O'Mahony, and R. G. Compton, "Microelectrode arrays for electrochemistry: Approaches to fabrication," *Small*, vol. 5, no. 7, pp. 776–788, 2009.

[84] T. Datta-Chaudhuri, P. Abshire, and E. Smela, "Packaging commercial CMOS chips for lab on a chip integration," *Lab Chip*, vol. 14, no. 10, p. 1753, 2014.

[85] Lin Li and A. J. Mason, "Post-CMOS parylene packaging for on-chip biosensor arrays," in *2010 IEEE Sensors*, 2010, pp. 1613–1616.

[86] T. Prodromakis, K. Michelakis, T. Zoumpoulidis, R. Dekker, and C. Toumazou, “Biocompatible encapsulation of CMOS based chemical sensors,” in *2009 IEEE Sensors*, 2009, pp. 791–794.

[87] J. Blain Christen and A. G. Andreou, “Design, fabrication, and testing of a hybrid CMOS/PDMS microsystem for cell culture and incubation,” *IEEE Trans. Biomed. Circuits Syst.*, vol. 1, no. 1, pp. 3–18, Mar. 2007.

[88] A. H. D. Graham, C. R. Bowen, S. M. Surguy, J. Robbins, and J. Taylor, “New prototype assembly methods for biosensor integrated circuits,” *Med. Eng. Phys.*, vol. 33, no. 8, pp. 973–979, Oct. 2011.

[89] C. D. Chin, V. Linder, and S. K. Sia, “Lab-on-a-chip devices for global health: Past studies and future opportunities,” *Lab Chip*, vol. 7, no. 1, pp. 41–57, 2007.

[90] B. Eversmann *et al.*, “A 128 x 128 cmos biosensor array for extracellular recording of neural activity,” *IEEE J. Solid-State Circuits*, vol. 38, no. 12, pp. 2306–2317, Dec. 2003.

[91] A. D. Weston and L. Hood, “Systems biology, proteomics, and the future of health care: toward predictive, preventative, and personalized medicine,” *J. Proteome Res.*, vol. 3, no. 2, pp. 179–196, Apr. 2004.

[92] R. Kaddurah-Daouk, B. S. Kristal, and R. M. Weinshilboum, “Metabolomics: A global biochemical approach to drug response and disease,” *Annu. Rev. Pharmacol. Toxicol.*, vol. 48, no. 1, pp. 653–683, Feb. 2008.

[93] K. A. Erickson and P. Wilding, “Evaluation of a novel point-of-care system, the i-STAT portable clinical analyzer.,” *Clin. Chem.*, vol. 39, no. 2, p. 283 LP-287, Feb. 1993.

[94] I. R. Lauks, H. J. Wieck, M. P. Zelin, and P. Blyskal, “Disposable sensing device for real time fluid analysis.” Google Patents, 17-Mar-1992.

[95] M. E. Lewis, G. R. Chambers, M. D. Deweese, and W. H. Ames,

"Multichemistry measuring device and test strips," 10-Aug-2004.

[96] S. N. Cozzette *et al.*, "Process for the manufacture of wholly microfabricated biosensors." Google Patents, 17-Nov-1998.

[97] "I-STAT handheld," 2017. [Online]. Available: https://www.pointofcare.abbott/int/en/offerings/istat/istat-handheld.

[98] A. DePalma, "Nanogen patents new method for detecting nucleic acid hybridization," 2000. [Online]. Available: https://www.drugdiscoveryonline.com/doc/nanogen-patents-new-method-for-detecting-nucl-0001.

[99] R. P. Ekins, "Multi-analyte immunoassay," *J. Pharm. Biomed. Anal.*, vol. 7, no. 2, pp. 155–168, Jan. 1989.

[100] M. B. Miller and Y.-W. Tang, "Basic concepts of microarrays and potential applications in clinical microbiology," *Clin. Microbiol. Rev.*, vol. 22, no. 4, pp. 611–633, Oct. 2009.

[101] X. Yu, N. Schneiderhan-Marra, and T. O. Joos, "Protein microarrays for personalized medicine," *Clin. Chem.*, vol. 56, no. 3, pp. 376–387, 2010.

[102] M.-Y. Lee, C. B. Park, J. S. Dordick, and D. S. Clark, "Metabolizing enzyme toxicology assay chip (MetaChip) for high-throughput microscale toxicity analyses," *Proc. Natl. Acad. Sci.*, vol. 102, no. 4, pp. 983–987, Jan. 2005.

[103] D. Keen-Kim, W. W. Grody, and C. S. Richards, "Microelectronic array system for molecular diagnostic genotyping: Nanogen NanoChip ® 400 and Molecular Biology Workstation," *Expert Rev. Mol. Diagn.*, vol. 6, no. 3, pp. 287–294, May 2006.

[104] M. Esteban, C. Ariño, and J. M. Díaz-Cruz, "Chemometrics in electroanalytical chemistry," *Crit. Rev. Anal. Chem.*, vol. 36, no. 3–4, pp. 295–313, 2006.

[105] Y. Lin, P. Yu, J. Hao, Y. Wang, T. Ohsaka, and L. Mao, "Continuous and

simultaneous electrochemical measurements of glucose, lactate, and ascorbate in rat brain following brain ischemia," *Anal. Chem.*, vol. 86, no. 8, pp. 3895–3901, 2014.

[106] Y. Lee and J. Kim, "Simultaneous electrochemical detection of nitric oxide and carbon monoxide generated from mouse kidney organ tissues," *Anal. Chem.*, vol. 79, no. 20, pp. 7669–7675, Oct. 2007.

[107] J. Castillo *et al.*, "Simultaneous detection of the release of glutamate and nitric oxide from adherently growing cells using an array of glutamate and nitric oxide selective electrodes," *Biosens. Bioelectron.*, vol. 20, no. 8 SPEC. ISS., pp. 1559–1565, 2005.

[108] T. T. C. Tseng and H. G. Monbouquette, "Implantable microprobe with arrayed microsensors for combined amperometric monitoring of the neurotransmitters, glutamate and dopamine," *J. Electroanal. Chem.*, vol. 682, pp. 141–146, 2012.

[109] A. Abbaspour and A. Noori, "A cyclodextrin host-guest recognition approach to an electrochemical sensor for simultaneous quantification of serotonin and dopamine," *Biosens. Bioelectron.*, vol. 26, no. 12, pp. 4674–4680, 2011.

[110] R. N. Goyal and S. Bishnoi, "Simultaneous determination of epinephrine and norepinephrine in human blood plasma and urine samples using nanotubes modified edge plane pyrolytic graphite electrode," *Talanta*, vol. 84, no. 1, pp. 78–83, 2011.

[111] G. P. Keeley *et al.*, "Simultaneous electrochemical determination of dopamine and paracetamol based on thin pyrolytic carbon films," *Anal. Methods*, vol. 4, no. 7, p. 2048, 2012.

[112] J. Park, P. Takmakov, and R. M. Wightman, "In vivo comparison of norepinephrine and dopamine release in rat brain by simultaneous measurements with fast-scan cyclic voltammetry," *J. Neurochem.*, vol. 119, no. 5, pp. 932–944, Dec. 2011.

[113] M. Esteban, C. Ariño, and J. M. Díaz-Cruz, “Chemometrics for the analysis of voltammetric data,” *TrAC - Trends Anal. Chem.*, vol. 25, no. 1, pp. 86–92, 2006.

[114] C. Krantz-Rülcker, M. Stenberg, F. Winquist, and I. Lundström, “Electronic tongues for environmental monitoring based on sensor arrays and pattern recognition: A review,” *Anal. Chim. Acta*, vol. 426, no. 2, pp. 217–226, 2001.

[115] Y. Ni, Y. Wang, and S. Kokot, “Differential pulse stripping voltammetric determination of paracetamol and phenobarbital in pharmaceuticals assisted by chemometrics,” *Anal. Lett.*, vol. 37, no. February 2013, pp. 3219–3235, 2004.

[116] Y. Ni, S. Li, and S. Kokot, “Simultaneous determination of three synthetic glucocorticoids by differential pulse stripping voltammetry with the aid of chemometrics,” *Anal. Lett.*, vol. 41, no. 11, pp. 2058–2076, 2008.

[117] B. Bozorgzadeh, D. R. Schuweiler, M. J. Bobak, P. A. Garris, and P. Mohseni, “Neurochemostat: A neural interface SoC with integrated chemometrics for closed-loop regulation of brain dopamine,” *IEEE Trans. Biomed. Circuits Syst.*, vol. 10, no. 3, pp. 654–667, 2016.

[118] B. S. Grabarić, Z. Grabarić, R. Tauler, M. Esteban, and E. Casassas, “Application of multivariate curve resolution to the voltammetric data Factor analysis ambiguities in the study of weak consecutive complexation of metal ion with ligand,” *Anal. Chim. Acta*, vol. 341, no. 2–3, pp. 105–120, Apr. 1997.

[119] M. Fernández, C. Ariño, J. M. Díaz-Cruz, R. Tauler, and M. Esteban, “Soft modelling approach applied to voltammetric data: study of electrochemically labile metal–glycine complexes,” *J. Electroanal. Chem.*, vol. 505, no. 1–2, pp. 44–53, Jun. 2001.

[120] E. Cukrowska, L. Trnková, R. Kizek, and J. Havel, “Use of artificial neural networks for the evaluation of electrochemical signals of adenine and

cytosine in mixtures interfered with hydrogen evolution," *J. Electroanal. Chem.*, vol. 503, no. 1–2, pp. 117–124, Apr. 2001.

[121] P. Ivarsson, S. Holmin, N.-E. Höjer, C. Krantz-Rülcker, and F. Winquist, "Discrimination of tea by means of a voltammetric electronic tongue and different applied waveforms," *Sensors Actuators B Chem.*, vol. 76, no. 1–3, pp. 449–454, Jun. 2001.

[122] M. K. Zachek, P. Takmakov, B. Moody, R. M. Wightman, and G. S. McCarty, "Simultaneous decoupled detection of dopamine and oxygen using pyrolyzed carbon microarrays and fast-scan cyclic voltammetry," *Anal. Chem.*, vol. 81, no. 15, pp. 6258–6265, Aug. 2009.

[123] M. P. Marsh, J. E. Koehne, R. J. Andrews, M. Meyyappan, K. E. Bennet, and K. H. Lee, "Carbon nanofiber multiplexed array and wireless instantaneous neurotransmitter concentration sensor for simultaneous detection of dissolved oxygen and dopamine," *Biomed. Eng. Lett.*, vol. 2, no. 4, pp. 271–277, Dec. 2012.

[124] D. C. Kirkpatrick, C. J. McKinney, P. B. Manis, and R. M. Wightman, "Expanding neurochemical investigations with multi-modal recording: simultaneous fast-scan cyclic voltammetry, iontophoresis, and patch clamp measurements," *Analyst*, vol. 141, no. 16, pp. 4902–4911, 2016.

[125] H. Cheng, T. Xiao, D. Wang, J. Hao, P. Yu, and L. Mao, "Simultaneous in vivo ascorbate and electrophysiological recordings in rat brain following ischemia/reperfusion," *J. Electroanal. Chem.*, vol. 781, pp. 90–96, 2016.

[126] D. L. Robinson, A. Hermans, A. T. Seipel, and R. M. Wightman, "Monitoring rapid chemical communication in the brain," *Chem. Rev.*, vol. 108, no. 7, pp. 2554–2584, Jul. 2008.

[127] D. O. Wipf, E. W. Kristensen, M. R. Deakin, and R. M. Wightman, "Fast-scan cyclic voltammetry as a method to measure rapid heterogeneous electron-transfer kinetics," *Anal. Chem.*, vol. 60, no. 4, pp. 306–310, Feb. 1988.

[128] A. Mujezinovic, S. Martinez, A. Muharemovic, and I. Turkovic, “Application of the coupled BEM / FEM method for calculation of cathodic protection system parameters,” vol. 5, no. 5, pp. 659–666, 2017.

[129] J. Horno, C. F. González-Fernández, A. Hayas, and F. González-Caballero, “Simulation of concentration polarization in electrokinetic processes by network thermodynamic methods,” *Biophys. J.*, vol. 55, no. 3, pp. 527–535, Mar. 1989.

[130] D. Britz and J. Strutwolf, *Digital Simulation in Electrochemistry*, vol. 44, no. 8. Cham: Springer International Publishing, 2016.

[131] B. A. Coles, R. G. Compton, C. M. A. Brett, and A. M. C. F. O. Brett, “Ohmic distortion of current-potential curves at wall-jet electrodes,” *J. Electroanal. Chem.*, vol. 381, no. 1–2, pp. 99–104, 1995.

[132] B. A. Cales, R. G. Compton, J. P. Larsen, and R. Anthony Spackman, “Ohmic distortion of mass transport and of current-voltage curves at a channel electrode,” *Electroanalysis*, vol. 8, no. 10, pp. 913–917, Oct. 1996.

[133] A. Hung, D. Zhou, R. Greenberg, and J. W. Judy, “Dynamic electrochemical simulation of micromachined electrodes for neural-stimulation systems,” in *First International IEEE EMBS Conference on Neural Engineering, 2003. Conference Proceedings.*, 2003, vol. 2003-Janua, pp. 200–203.

[134] A. Manzin, C. Boveri, P. P. Capra, F. Durbiano, and O. Bottauscio, “Experimental and numerical characterization of an electrode-matrix cell for electrochemical measurements,” *Sensors Actuators B Chem.*, vol. 138, no. 1, pp. 326–335, Apr. 2009.

[135] N. H. Lovell, S. Dokos, E. Cheng, and G. J. Suaning, “Simulation of parallel current injection for use in a vision prosthesis,” in *Conference Proceedings. 2nd International IEEE EMBS Conference on Neural Engineering, 2005.*, 2005, vol. c, pp. 458–461.

[136] G. Khalili Moghaddam, N. H. Lovell, R. G. H. Wilke, G. J. Suaning, and S. Dokos, “Performance optimization of current focusing and virtual electrode strategies in retinal implants,” *Comput. Methods Programs Biomed.*, vol. 117, no. 2, pp. 334–342, 2014.

[137] T. Flores, G. Goetz, X. Lei, and D. Palanker, “Optimization of return electrodes in neurostimulating arrays,” *J. Neural Eng.*, vol. 13, no. 3, p. 36010, Jun. 2016.

[138] T. J. Davies and R. G. Compton, “The cyclic and linear sweep voltammetry of regular and random arrays of microdisc electrodes: Theory,” *J. Electroanal. Chem.*, vol. 585, no. 1, pp. 63–82, Nov. 2005.

[139] J. Guo and E. Lindner, “Cyclic voltammograms at coplanar and shallow recessed microdisk electrode arrays: Guidelines for design and experiment,” *Anal. Chem.*, vol. 81, no. 1, pp. 130–138, Jan. 2009.

[140] J. Hasegawa, S. Uno, and K. Nakazato, “Amperometric electrochemical sensor array for on-chip simultaneous imaging: Circuit and microelectrode design considerations,” *Jpn. J. Appl. Phys.*, vol. 50, no. 4, p. 04DL03, Apr. 2011.

[141] O. A. Petrii and G. A. Tsirlina, “Electrode potentials,” in *Encyclopedia of Electrochemistry*, Wiley-VCH Verlag GmbH & Co. KGaA, 2007.

[142] D. Tang, J. Lu, L. Zhuang, and P. Liu, “Calculations of the exchange current density for hydrogen electrode reactions: A short review and a new equation,” *J. Electroanal. Chem.*, vol. 644, no. 2, pp. 144–149, Jun. 2010.

[143] E. J. Calvo, “The current–potential relationship,” in *Encyclopedia of Electrochemistry*, Wiley-VCH Verlag GmbH & Co. KGaA, 2007.

[144] J. E. B. Randles, “Kinetics of rapid electrode reactions,” *Discuss. Faraday Soc.*, vol. 1, p. 11, 1947.

[145] H. Helmholtz, “Studien über electrische grenzschichten,” *Ann. der Phys.*

und Chemie, vol. 243, no. 7, pp. 337–382, 1879.

[146] J. Perrin, "Mécanisme de l'électrisation de contact et solutions colloïdales," *J. Chim. Phys.*, vol. 2, pp. 601–651, May 1904.

[147] M. Gouy, "Sur la constitution de la charge électrique à la surface d'un électrolyte," *J. Phys. Théorique Appliquée*, vol. 9, no. 1, pp. 457–468, 1910.

[148] D. L. Chapman, "A contribution to the theory of electrocapillarity," *Philos. Mag. Ser. 6*, vol. 25, no. 148, pp. 475–481, Apr. 1913.

[149] O. Stern, "Zur theorie der elektrolytischen doppelschicht," *Zeitschrift fur Elektrochemie*, vol. 30, pp. 508–516, 1924.

[150] D. Borkholder, "Cell based biosensors using microelectrodes," Stanford University, 1998.

[151] J. P. Diard, B. Le Gorrec, and C. Montella, "Diffusion impedances," *Handbook of Electrochemical Impedance Spectroscopy*. Hosted by Bio-Logic, Oct-2017.

[152] J. Newman, "Resistance for flow of current to a disk," *J. Electrochem. Soc.*, vol. 113, no. 5, p. 501, 1966.

[153] D. A. Stenger and T. M. McKenna, *Enabling Technologies for Cultured Neural Networks*. Academic Press, 1994.

[154] J. O. Howell, W. G. Kuhr, R. E. Ensman, and R. Mark Wightman, "Background subtraction for rapid scan voltammetry," *J. Electroanal. Chem. Interfacial Electrochem.*, vol. 209, no. 1, pp. 77–90, Sep. 1986.

[155] A. J. Bard, M. Stratmann, and P. R. Unwin, "Encyclopedia of electrochemistry: Instrumentation and electroanalytical chemistry; Volume 3." Wiley-VCH, 2003.

[156] A. Molina, J. Gonzalez, E. Laborda, Q. Li, and R. G. Compton,

"Electrochemical behavior of two-electron redox processes by differential pulse techniques at microelectrodes," pp. 1070–1079, 2012.

[157] Y. Ding, L. Zhou, H. B. Halsall, and W. R. Heineman, "Feasibility studies of simultaneous multianalyte amperometric immunoassay based on spatial resolution," *J. Pharm. Biomed. Anal.*, vol. 19, no. 1–2, pp. 153–161, 1999.

[158] G. S. Wilson and R. Gifford, "Biosensors for real-time in vivo measurements," *Biosens. Bioelectron.*, vol. 20, no. 12, pp. 2388–2403, 2005.

[159] B. Zhang, K. L. Adams, S. J. Luber, D. J. Eves, M. L. Heien, and A. G. Ewing, "Spatially and temporally resolved single-cell exocytosis utilizing individually addressable carbon microelectrode arrays," *Anal. Chem.*, vol. 80, no. 5, pp. 1394–1400, Mar. 2008.

[160] E. P. Anderson, J. S. Daniels, N. Pourmand, and T. H. Lee, "Crosstalk in integrated microarrays with current sensing," *IEEE Trans. Circuits Syst. I Regul. Pap.*, vol. 55, no. 11, pp. 3756–3762, Dec. 2008.

[161] P. Yu and G. S. Wilson, "An independently addressable microbiosensor array: What are the limits of sensing element density?," *Faraday Discuss.*, vol. 116, no. 116, pp. 305–317, 2000.

[162] "Cadence custom IC / analog / RF design." [Online]. Available: https://www.cadence.com/content/cadence-www/global/en_US/home/tools/custom-ic-analog-rf-design.html. [Accessed: 11-Dec-2017].

[163] J. M. Rabaey, "The SPICE page." [Online]. Available: https://bwrcs.eecs.berkeley.edu/Classes/IcBook/SPICE/.

[164] "COMSOL Multiphysics." [Online]. Available: https://uk.comsol.com/models/electrochemistry-module. [Accessed: 17-Sep-2018].

[165] J. Bisquert, G. Garcia-Belmonte, F. Fabregat-Santiago, N. S. Ferriols, P. Bogdanoff, and E. C. Pereira, “Doubling exponent models for the analysis of porous film electrodes by impedance. Relaxation of TiO_2 nanoporous in aqueous solution,” *J. Phys. Chem. B*, vol. 104, no. 10, pp. 2287–2298, 2000.

[166] K. Gong, Q. Fang, S. Gu, S. F. Y. Li, and Y. Yan, “Nonaqueous redox-flow batteries: organic solvents, supporting electrolytes, and redox pairs,” *Energy Environ. Sci.*, vol. 8, no. 12, pp. 3515–3530, 2015.

[167] E. Laviron, “General expression of the linear potential sweep voltammogram in the case of diffusionless electrochemical systems,” *J. Electroanal. Chem. Interfacial Electrochem.*, vol. 101, no. 1, pp. 19–28, Jul. 1979.

[168] E. R. S. Arthur A. Maryott, *Table of Dielectric Constants of Pure Liquids*. National Bureau of Standards Circular 514, 1951.

[169] “James Watt nanofabrication centre.” [Online]. Available: http://www.jwnc.gla.ac.uk/. [Accessed: 29-Jan-2018].

[170] C. Giagkoulovits *et al.*, “A 16 x 16 CMOS amperometric microelectrode array for simultaneous electrochemical measurements,” *IEEE Trans. Circuits Syst. I Regul. Pap.*, pp. 1–11, 2018.

[171] J. Z. J. Zhang, N. Trombly, and a. Mason, “A low noise readout circuit for integrated electrochemical biosensor arrays,” *Proc. IEEE Sensors, 2004.*, pp. 36–39, 2004.

[172] E. J. F. Dickinson, H. Ekström, and E. Fontes, “COMSOL Multiphysics®: Finite element software for electrochemical analysis. A mini-review,” *Electrochem. commun.*, vol. 40, pp. 71–74, 2014.

[173] “Tanner L-Edit IC layout.” [Online]. Available: https://www.mentor.com/tannereda/l-edit. [Accessed: 14-Jan-2018].

[174] “Compugraphics the experts behind the mask.” [Online]. Available: https://www.compugraphics-photomasks.com/. [Accessed: 14-Jan-2018].

[175] “NANO PMMA and copolymer.”

[176] “Microposit® S1800® series photo resists.” [Online]. Available: http://cmnst.ncku.edu.tw/ezfiles/23/1023/img/127/s1800seriesDataSheet.pdf.

[177] “LOR and PMGI resists.” [Online]. Available: http://microchem.com/pdf/PMGI-Resists-data-sheetV-rhcedit-102206.pdf.

[178] “Plassys.” [Online]. Available: https://plassys.com/. [Accessed: 29-Jan-2018].

[179] R. Redd, M. A. Spak, J. P. Sagan, O. P. Lehar, and R. R. Dammel, “Lithographic process for high-resolution metal lift-off,” in *Conference on Advances in Resist Technology and Processing XVI*, 1999, vol. 3678, no. March, pp. 641–651.

[180] “MCC primer 80/20.” [Online]. Available: http://www.microchem.com/pdf/Rev.1-MCC Primer 80-20.pdf.

[181] J. A. Cunningham, “Expanded contacts and interconnexions to monolithic silicon integrated circuits,” *Solid. State. Electron.*, vol. 8, no. 9, pp. 735–738, Sep. 1965.

[182] Bruker, “Contour GT-X 3D optical profiler.” [Online]. Available: https://www.bruker.com/products/surface-and-dimensional-analysis/3d-optical-microscopes/contourgt-x/overview.html. [Accessed: 29-Jan-2018].

[183] X. Yan, T. Xu, S. Xu, X. Wang, and S. Yang, “Fabrication of polymer-converted carbon films containing Ag, Pd nanoparticles,” *Nanotechnology*, vol. 15, no. 12, pp. 1759–1762, Dec. 2004.

[184] “Epoxy Technology.” [Online]. Available: http://www.epotek.com/site/.

[185] “Spectrum semiconductor materials, Inc.” [Online]. Available: http://www.spectrum-semi.com/.

[186] “Bondjet BJ653.” [Online]. Available: http://www.hesse-mechatronics.com/en/fully-automatic-heavy-wire-bonder/bondjet-bj653/. [Accessed: 29-Jan-2018].

[187] “EP42HT-2Med product information.” [Online]. Available: https://www.masterbond.com/tds/ep42ht-2med. [Accessed: 17-Jan-2018].

[188] B. C. Cheah *et al.*, “An integrated circuit for chip-based analysis of enzyme kinetics and metabolite quantification,” *IEEE Trans. Biomed. Circuits Syst.*, vol. 10, no. 3, pp. 721–730, Jun. 2016.

[189] J. Kang and P. A. Rowntree, “Gold film surface preparation for self-assembled monolayer studies,” *Langmuir*, vol. 23, no. 2, pp. 509–516, 2007.

[190] L. M. Fischer *et al.*, “Gold cleaning methods for electrochemical detection applications,” *Microelectron. Eng.*, vol. 86, no. 4–6, pp. 1282–1285, Apr. 2009.

[191] “Labview.” [Online]. Available: http://www.ni.com/en-gb/shop/labview.html. [Accessed: 20-Jan-2018].

[192] “Model 600E series electrochemical analyzer/workstation.” [Online]. Available: http://www.chinstruments.com/chi600.shtml. [Accessed: 21-Jan-2018].

[193] “NI PXIe-1073 user manual.” National Instruments Corporation, 2011.

[194] “NI 6722/6723 device specifications.” National Instruments Corporation, 2017.

[195] “NI 6703/6704 specifications.” National Instruments Corporation, 2012.

[196] “NI 6358 device specifications.” National Instruments Corporation, 2016.

[197] “Cadence OrCAD.” [Online]. Available: http://www.orcad.com/. [Accessed: 21-Jan-2018].

[198] “Eurocircuits.” [Online]. Available: https://www.eurocircuits.com/. [Accessed: 21-Jan-2018].

[199] Texas Instruments, “INA217 Low-noise, low-distortion instrumentation amplifier replacement for SSM2017,” no. 1. 2015.

[200] Texas Instruments, “LMx24-N , LM2902-N low-power , quad-operational amplifiers,” 2015.

[201] N. G. Tsierkezos and U. Ritter, “Electrochemical impedance spectroscopy and cyclic voltammetry of ferrocene in acetonitrile/acetone system,” *J. Appl. Electrochem.*, vol. 40, no. 2, pp. 409–417, Feb. 2010.

[202] Y. Wang, E. I. Rogers, and R. G. Compton, “The measurement of the diffusion coefficients of ferrocene and ferrocenium and their temperature dependence in acetonitrile using double potential step microdisk electrode chronoamperometry,” *J. Electroanal. Chem.*, vol. 648, no. 1, pp. 15–19, Sep. 2010.

[203] “NI X series multifunction data acquisition.” National Instruments Corporation, pp. 1–18, 2014.

[204] S. Unser, I. Campbell, D. Jana, and L. Sagle, “Direct glucose sensing in the physiological range through plasmonic nanoparticle formation,” *Analyst*, vol. 140, no. 2, pp. 590–599, 2015.

[205] I. Noviandri *et al.*, “The decamethylferrocenium/decamethylferrocene Redox couple: A superior redox standard to the ferrocenium/ferrocene redox couple for studying solvent effects on the thermodynamics of electron transfer,” *J. Phys. Chem. B*, vol. 103, no. 32, pp. 6713–6722, 1999.

[206] “Microposit® S1800® series photo resists.” .

[207] G. Hussain and D. S. Silvester, “Comparison of Voltammetric Techniques for Ammonia Sensing in Ionic Liquids,” *Electroanalysis*, vol. 30, no. 1, pp. 75–83, Nov. 2017.

[208] M. Herpich, J. Friedl, and U. Stimming, “Scanning electrochemical potential microscopy (SECPM) and electrochemical STM (EC-STM),” C. S. S. R. Kumar, Ed. Berlin, Heidelberg: Springer Berlin Heidelberg, 2015, pp. 1–67.

[209] C. Giagkoulovits *et al.*, “Hybrid amperometric and potentiometric sensing based on a CMOS ISFET array,” in *2017 IEEE SENSORS*, 2017, pp. 1–3.

[210] G. C. King, D. A. Di Giusto, W. A. Wlassoff, S. Giesebrecht, E. Flening, and G. D. Tyrelle, “Proofreading genotyping assays and electrochemical detection of SNPs,” *Hum. Mutat.*, vol. 23, no. 5, pp. 420–425, 2004.

[211] X. Feng *et al.*, “Ratiometric biosensor array for multiplexed detection of microRNAs based on electrochemiluminescence coupled with cyclic voltammetry,” *Biosens. Bioelectron.*, vol. 75, pp. 308–314, 2016.

[212] M. Gutiérrez *et al.*, “Application of an e-tongue to the analysis of monovarietal and blends of white wines,” *Sensors*, vol. 11, no. 12, pp. 4840–4857, May 2011.